Thermodynamic properties of deep eutectic solvents and organic solutes at different temperatures for separation of close boiling mixtures

Submitted in fulfilment of the requirements for the degree of Master of Applied Science in Chemistry, Durban University of Technology

Rosemary Balungile Gasa

19952410

August 2025

PREFACE

I, Rosemary Balungile Gasa, declare that:

- The research work reported in this thesis, except where indicated is my original work.
- This work has not been submitted for any degree or examination at any other university.
- This work does not contain other author's information, data, or graphs, unless specifically stated.

Signed:

Rosemary Balungile Gasa Date: 11 August 2025

Signed:

Prof. N. Deenadayalu (Supervisor) Date: 11 August 2025

Signed:

Dr. B. Kabane (Co-supervisor) Date: 11 August 2025

DEDICATION

I dedicate this research work to

My husband Bonginkosi Gasa,

My children Siphesihle, Aphiwe and Usiphile Gasa,

My sisters Jabulile, Nokulunga, Sizakele Ngcobo and Malehu Fuze,

and

especially my late grandmother Elizabeth Ngcobo,

My late parents Themba (father) and Ntombi Ngcobo (mother)

My late daughter Nosipho Angel Gasa

ACKNOWLEDGEMENTS

I would like to articulate my heartfelt gratitude to:

- Lord God almighty for granting me the strength and perseverance through good and challenging times in my life.
- Prof. N. Deenadayalu and Dr. B. Kabane for their dedicated supervision and unwavering support throughout this research work. Their guidance, expertise and encouragement have been invaluable in all aspects of this research work as well as my personal growth.
- Department of Chemistry, Durban University of Technology (DUT) for financial support and for providing facilities to conduct this study.

Special thanks are given to:

- Durban University of Technology laboratory staff Miss. S. Zungu (ML Sultan Campus), Mrs. M. Xhakaza (Steve Biko Campus), Dr. K. Matshetshe (Mintek) for the experimental support.

Lastly, I would like to convey my appreciation and sincere gratitude to:

- My family for the emotional, practical and esteem support which has made a significant difference in pursuing this degree.

PUBLICATIONS

Research Outputs

1. **Gasa, B**., Kabane, B., Deenadayalu, N., Gumede, N. and Singauke, L., 2024. Experimental and computational insight in molecular interactions of imidazolium based deep eutectic solvent with alcohols (C1 and C2). Journal of Molecular liquids, 414: 126088 (https://doi.org/10.1016/j.molliq.2024.126088).

2. **Gasa, B**., Kabane, B. and Deenadayalu, N., 2024. Thermodynamic evaluation of intermolecular interaction selectivity in separation of binary mixtures based on the activity coefficients at infinite dilution. Journal of Chemical Thermodynamics and Thermal Analysis, 17: 100151 (https://doi.org/10.1016/j.ctta.2024.100151).

3. **Gasa, B**., Kabane, B., Deenadayalu, N., Yadaf, S., Prajapat, A., Singh, P. and Bahadur, I., 2025. Molecular dynamic insight into imidazolium based deep eutectic solvent comprising carboxylic acids (C2 and C3): Experimental and DFT approach. Journal of Molecular Liquids, available online: 127134 (https://doi.org/10.1016/j.molliq.2025.127134).

Book Chapter

1. **Gasa**, **B**., Kabane, B., Deenadayalu, N. Rasool, M., Ahmad, M., Siddiqui, N.A. and Bahadur, I., 2025. Deep Eutectic Solvents. Chater 7 - Physicochemical properties of DESs through experimental techniques. Science Direct, 2025, pages (107-121), (https://doi.org/10.1016/B978-0-443-21962-7.00008-0)

ABSTRACT

The environmental impact of volatile organic compounds coupled with its cost, stability, performance, turnability and versatility of conventional solvents and its effectiveness in the separation of close boiling point mixtures led to the growing interest in separation studies of deep eutectic solvents (DESs). DES have advantages over conventional solvents because of its distinctive properties such as thermal stability, easy and inexpensive methods to synthesise, low toxicity levels and biodegradability. DESs are recognized as possible alternatives to ionic liquids for diverse applications in the chemical industry for example in product development. The understanding of physical properties and intermolecular interactions is crucial for researchers and engineers to design more efficient and environmentally friendly processes for the separation of complex mixtures containing volatile organic solvents.

This study focuses on the thermophysical and thermodynamic properties of deep eutectic solvents, categorized as type (III), for extraction or separation purposes. Conventional organic solvents, which are currently utilized in industrial processes for extraction or separation purposes are not environmentally friendly. The DESs were synthesized at 1:3 mole ratio of hydrogen bond acceptor (HBA) and hydrogen bond donor (HBD).

The classified type (III) deep eutectic solvents under this study were:

- DES1: 1-butyl-3-methylimidazolium chloride + ethylene glycol [BMIM]Cl: EG].

- DES2: 1-butyl-2,3-dimethylimidazolium chloride + ethylene glycol [BDMIM]Cl: EG].

The physical properties namely: densities, ρ, speed of sound, u, and refractive indices, n_D, for the binary mixtures [BMIM]Cl: EG + methanol or ethanol, and [BDMIM]Cl: DEG + acetic acid or propanoic acid were experimentally measured over the entire range of mole fraction, x_{DES} = (0-1) at T = (293.15, 298.15, 303.15, 308.15, and 313.15) K and at atmospheric pressure. The measurements were conducted using an Anton Paar DSA 5000M and Anton Paar Abbermat 3200 refractometer. From the experimental data, excess thermophysical properties including excess molar volumes,

V_m^{E}, isentropic compressibilities, k_s, change in isentropic compressibilities, Δk_s, intermolecular free length, L_f, and change in refractive indices, Δn_D, were calculated from the densities, speed of sound and refractive indices, respectively. The investigated properties of the deep eutectic solvent binary mixtures gave an insight into the types of molecular interactions in 1-butylmethylimidazolium chloride + ethylene glycol with methanol or ethanol or 1-butyl-2,3-dimethyl imidazolium chloride + ethylene glycol with acetic acid or propanoic acid at different experimental temperatures. The excess molar volumes, densities and refractive indices data was correlated with the application of the Lorentz-Lorenz equation.

Density functional theory (DFT) was used to simulate the intermolecular interaction of deep eutectic [BDMIM]Cl: EG] + acetic acid or propanoic acid as well as [BMIM]Cl: EG] + methanol or ethanol binary mixtures. DFT calculations were employed to ascertain some physiochemical descriptors such as chemical potential (μ), electronegativity (χ), hardness (η), the global electrophilicity index (ω) and softness (S).

The activity coefficients at infinite dilution (γ_{13}^{∞}) of the selected deep eutectic solvents with volatile organic solutes were also determined at different temperatures.

The deep eutectic solvents used for the determination of the γ_{13}^{∞} were:

- DES3: Tetrabutylammonium acetate with ethylene glycol, [TBN]AcO: EG].

- DES4: Tetrabutylammonium acetate with diethylene glycol [TBN] AcO: DEG] .

The activity coefficients at infinite dilution was used as a pre-screening tool for the selection of possible entrainers and was calculated from retention data obtained from gas liquid chromatography (GLC) data. The GLC was operated at the temperature range of T = (313.15 – 353.15) K and at 10 K interval. Thermodynamic properties such as excess enthalpies at infinite dilution, $\Delta H_1^{\mathrm{E},\infty}$, excess Gibbs free energies at infinite dilution, $\Delta G_1^{\mathrm{E},\infty}$, and excess entropy at infinite dilution, $\Delta S_1^{\mathrm{E},\infty}$, were computed from the activity coefficient at infinite dilution to further explain the types of intermolecular interactions between the solutes and the investigated DESs. Selectivity at infinite

dilution $\left(S_{ij}^{\infty}\right)$, and capacity at infinite dilution $\left(k_{ij}^{\infty}\right)$ values were determined to evaluate the separation potential of the DESs.

The data obtained from the spectroscopic techniques Fourier transform infrared (FTIR spectroscopy and nuclear magnetic resonance spectroscopy (NMR) were used to validate the formation of DESs and the types of interactions arising between the HBD and HBA. Furthermore, evaluation of thermal stability for the prepared deep eutectic solvents was determined using differential scanning calorimetry (DSC)/ thermogravimetric analysis (TGA).

TABLE OF CONTENTS

LIST OF FIGURES

LIST OF TABLES

ABBREVIATIONS

DESs	: Deep eutectic solvents
ILs	: Ionic liquids
LLE	: Liquid-liquid extraction
[BDMIM] Cl	: 1-butyl - 2,3 – dimethyl imidazolium chloride
[BMIM] Cl	: 1-methyl-3-imidazolium chloride
[TBN] AcO	: Tetrabutyl ammonium acetate
EG	: Ethylene glycol
DEG	: Diethylene glycol
VOCs	: Volatile organic solvents
He	: Helium
GLC	: Gas liquid chromatography
FTIR	: Fourier transform infrared
NMR	: Nuclear magnetic resonance
TCD	: Thermal conductivity detector
TGA	: Thermogravimetric analysis
HBD	: Hydrogen bond donor
HBA	: Hydrogen bond acceptor
HOMO	: Highest occupied molecular orbital
LOMO	: Lowest occupied molecular orbital
NBO	: Natural bond orbital

DFT	: Density functional theory
NCI	: Non-covalent interactions
RDG	: Reduced density gradient.
ELF	: Electron localization function
PBF	: Poisson Boltzmann finite
BSSE	: Basic set superposition error
SPE	: Single point energy

LIST OF SYMBOLS

x_1 : Mole fraction of the 1st component - DES

x_2 : Mole fraction of the 2nd component – methanol, ethanol, acetic acid, propanoic acid

ρ : Density

n : Refractive index

u : Speed of sound

K : Kelvin

V_m^{E} : Excess molar volume

L_f : Intermolecular free length

k_s : Isentropic compressibility

Δk_s : Deviation in isentropic compressibility

Δn : Deviation of refractive index

R : Molar refraction

γ_{13}^{∞} : Activity coefficients at infinite dilution

$\Delta H_{ij}^{\mathrm{E},\infty}$: Excess partial molar enthalpy at infinite dilution

$\Delta G_{ij}^{\mathrm{E},\infty}$: Excess Gibbs free energy at infinite dilution

$\Delta S_{ij}^{\mathrm{E},\infty}$: Excess Entropy at infinite dilution

ω : Acentric factor

S_{ij}^{∞} : Selectivity at infinite dilution

k_j^{∞} : Capacity at infinite dilution

μ : Chemical function

χ : Electronegativity

η : Hardness

ω : Global electrophilicity index

S : Softness

CHAPTER 1

INTRODUCTION

1.1 Background

Separation processes are essential in various industries and scientific fields for purification, resource recovery, environmental protection, product manufacturing and analytical purposes (Li and Zong 2023). Knowledge of thermodynamic equilibria comprising of deep eutectic solvents is a crucial and vital tool to comprehend the driving factors in separation and industrial processes, the deep eutectic solvent possesses qualities of greener solvents with low toxicity, non-volatility, biodegradability and stability in solvents. This includes organic synthesis, electrochemistry, extraction mediums (Nakhle and Kfoury 2021, Ruesgas-Ramón and Figueroa-Espinoza 2017, Lin and Zhang 2021, Habila and Alabdulkarem 2020, Kurtulbas and Pekel 2020), biotechnology and biodiesel synthesis (Troter and Todorović 2016). In addition, DES can be used as a solvent in biological assays or enzymes reactions (Liu et al. 2018), in biocatalysis (Yang *et al.* 2018, Arriaga *et al.* 2019), as well as pharmaceutical industry as excipients for increasing the solubility of hydrophobic drugs (Golgoun *et al.* 2020).

For liquid-liquid extraction (LLE) and azeotropic distillation, deep eutectic solvents have become a viable ecological acceptable substitute for both ionic liquids and traditional organic solvents (Shishov *et al*. 2020; Shekaari *et al*. 2020; Smink *et al*. 2020; Zante *et al*. 2020). DES have more applications in chemical separations, and in addition, they are less expensive when compared to the ionic liquids and favour the green approach to chemical processing as they are mostly derived from non-toxic and renewable bio-resources (Hansen et al. 2020; Ramon and Guillena, 2020). Deep eutectic solvents are energy efficient and can be tailored to selectively extract specific components based on their chemical properties and can be used as entrainers in azeotropic distillation to break the azeotrope and facilitate the separation.

Different techniques including membrane distillation and specialized processes including pressure swing distillation, heteroazeotropic rectification, and extractive distillation, have been developed to separate azeotropic mixtures (Chen et al. 2005.,

Madhi et al. 2015). During an extractive distillation, an entrainer is introduced to the mixture to be separated to remove the azeotropic point and enable separation of the close boiling mixture, the entrainer's requirement is to modify the relative volatilities of the mixture's constituent parts through various interactions. The cost of an optimized process design using an average entrainer could be significantly higher than that of an average design using an optimal entrainer. In this case the choice of the entrainer is critical (Laroche et. al. 1991). When using the conventional solvents as entrainers, large amounts are normally required (entrainer/feed mass ratio up to 5-8) which are not easy to recover with simple distillation. Extractive distillation using ionic liquids (ILs) is also feasible (Lei *et al.* 2013, Lei *et al.* 2014). Ionic liquids were extensively studied as entrainers, however, many aspects of ILs have been brought into question due to costly production, as well as possible toxicity and biodegradability. Deep eutectic solvents are a class of solvents that can be used in extractive distillation. DESs usage for extractive distillation was first introduced in 2014 by Rodríguez *et al.* (2015). In terms of the energy consumption, the latter is preferred during the extraction process as it is easy to recover the entrainer. In addition, solvent loss and emissions are reduced.

Selecting an appropriate solvent in organic synthesis is essential due to its specific properties. Solvents are a major source of waste, DESs are highly valuable as alternatives solvents as they are non-toxic and non-hazardous and additionally DESs can serve other functions namely as catalysts and reactants. DESs have been used for several applications in electrochemistry and are the most extensively researched application of metal deposition incorporating metal ions into a solution (Abbott et *al*. 2022). DESs are known for their high conductivity compared to non-aqueous solvents, and their ability to solubilise metals ions even without water are of critical importance, (Hartley *et al.* 2014). DESs have also been used in electro polishing to reduce surface roughness of metal through controlled dissolution. This process enhances the optical reflectivity of the metal surface, (Zang *et al.* 2012). Metal oxides typically require acidic or basic solutions for solubilization and cannot be dissolved by molecular solvents.

Deep eutectic solvents are synthesized from a Bronsted or Lewis acid or base, which consists of various cationic or anionic components (Lee *et al.* 2020). An essential step in the designing and refining processes for chemical separations is understanding

DESs thermodynamic properties physical parameters, activity coefficient at infinite dilution as well as selectivity and capacity including phase equilibria data which play a crucial role in the separation of mixtures – particular in processes like distillation, extraction and crystallization (Countinho *et al.* 2017).

Within the complex composition of crude oil, asphaltenes are the most difficult components to handle due to their molecular structures, which add significant challenges to oil processing operations. These compounds, identified as the densest and most popular components of crude oil, tend to aggregate, creating formidable challenges for fluid flow for the extraction and refinement of crude oil. Such aggregation can cause significant operational challenges, such as reactor clogging and reduce efficiency in oil production, thereby increasing both economic and safety concerns (Mullins *et al.* 1998, Sheu *et al.* 2002 and Boublia *et al.* 2023). The aggregation behaviour of asphaltene has been confirmed through empirical and theoretical modelling. Historically, non-polar solvents have been used to induce asphaltene precipitation, making it easier to separate them from vacuum distillation residues. The alternative separation technique depends on the molecular weight of the asphaltenes and the physical properties of the resulting oil, (Mullins *et al.* 2007). Although this method is found to be effective, the use of conventional solvents presents substantial environmental and health risks, emphasizing the need for greener chemical practices, (Paiva et al. 2014). DESs contributes less to environmental waste and are more cost-effective, DESs are regarded as a specialized subset of ionic liquids and have been extensively used in separation studies and liquid-liquid extraction, (Li *et al.* 2019). Analytical models like COSMO-SAC, have been utilized to examine the intermolecular interactions within the DESs, focusing particularly on the hydrogen bonding abilities, (Qi *et al.* 2023). DESs have demonstrated promising potential in chemically enhanced oil recovery and accommodating asphaltenes. Molecular dynamics simulations have deepened the understanding of asphaltene aggregation and their interactions with solvents. (Headen *et al.* 2017) and provided an understanding of the molecular behaviour of asphaltenes in various solvent environments, as well as, providing insights into the size and structure of asphaltene clusters.

Sustainable living entails recognizing how our choices affect the environment and ensuring that these choices support the well-being of current and future generations. Transitioning to sustainable production and process methods can contribute to eliminate harmful impacts which are pollution and climate change. The deep eutectic solvents are environmentally friendly alternatives to traditional harsh organic solvents. The deep eutectic solvents are biodegradable, biocompatible, cost - effective and are an extensively studied solution in diverse fields (Scelsi and Angelini 2021). The DESs are gaining prominence in a wide range of applications due to their environmentally friendly nature and unique physicochemical properties. They are utilized not only as solvent systems, but also as catalysts, adsorbents, electrolytes, nanocarriers for encapsulating anticancer drugs, and in many other diverse fields. The main applications of the DES are aligned to the 2030 Agenda for Sustainable Development plan (ASD) published in 2015 by the United Nations (UN) proposing an official sustainability-focused development plan to end poverty, protect the planet and improve the lives of everyone everywhere, (González-Campos *et al*. 2024), it relates to energy efficiency improvement, sustainable production patterns and action to combat climate change. The DESs are used to achieve cost effective, less labour-intensive, ecofriendly, safe, and highly effective approaches to achieve some of the Sustainable Development Goals (SDGs).

Traditional fuels, namely fossil fuels (coal, oil, and natural gas), continue to be dominant energy sources worldwide because of their accessibility, cost-effectiveness, and established infrastructure. For decades, these fuels have been the main energy sources for various sectors, including transportation, electricity generation, and industrial processes. However, there are substantial challenges associates with the ongoing use of conventional fuels, especially regarding their environmental impact. There is a pressing need for eco-friendly solvents to replace the hazardous and highly volatile traditional organic solvents namely: toluene, xylene, and benzene, (Paiva *et al.* 2014, Celebi, Vlugt and Moulos, 2019). The deep eutectic solvents have emerged as promising alternative to overcome these limitations, offering physicochemical properties like ionic liquids (IL). The DESs have garnered significant attention due to their exceptional attributes, such as tuneability, environmental compatibility, non-toxicity, inertness, low vapour pressure, wide liquid range, and excellent thermal stability (Abbort *et al.* 2004, Banab *et al.* 2021b, Liu *et al.* 2018). The DESs

customizable physical properties can be specifically tailored to suite various application needs based on the selected hydrogen bond acceptor (HBA) and hydrogen bond donor (HBD), (Liu *et al.* 2020, Makoś and Boczka. 2019). Assessing the structural physicochemical properties of the DESs is crucial to ascertain their appropriateness for different industrial applications. By customizing these properties, the DESs can be engineered to serve as sustainable and efficient alternatives to conventional solvents.

The knowledge of thermophysical and thermodynamic parameters comprising of deep eutectic solvents with organic volatile solvents (VOCs) is important, as this gives information about molecular interactions between the binary mixtures. This information is valuable as it can be utilized in improving the separation point. Some of the currently used solvents in separation processes are the source of toxic by-products, which are volatile and lead to adverse environmental effects.

1.2 Problem statement

Conventional organic solvents used in liquid-liquid extraction for azeotropic mixtures in distillation have many drawbacks. These conventional organic solvents are not environmentally friendly and are toxic to human beings, flammable, and are not easily recyclable due to their high volatility and can form azeotropes with compounds to be separated.

A search for alternative environmentally friendly solvents that are cost-effective and have high efficiency in extraction processes is ongoing (Verma *et al*. 2019, Reeves *et al*. 2021). Ionic liquids have received significant attention as alternative solvents to conventional organic solvents in different chemical industries due to their low volatility and high thermal stability. However, the synthesis and purification of ionic liquids is costly, and it is difficult to attain high purity of recycled ILs, hence this limits their application for industrial processes.

Deep eutectic solvents are considered as potential alternatives to ionic liquids as they are known to be environmentally friendly when compared to conventional organic. DESs are biodegradable, easy to prepare, relatively low production cost, less

hazardous, favour the green approach for chemical processing as they are mostly derived from bio-based materials.

In this study, four different types of deep eutectic solvents were prepared from type (III) quaternary salts, hydrogen bond acceptors with organic solvents, hydrogen bond donors at a specific mole ratio of 1:3. Two of the deep eutectic solvents were prepared using imidazolium ionic salts namely: 1-butyl-3-methyl imidazolium chloride + ethylene glycol ([BMIM]Cl: EG), and 1-butyl-2,3-dimethylimdazolium chloride + ethylene glycol ([BDMIM]Cl: EG) .The DESs were used to prepare the binary mixtures with selected alcohols and carboxylic acids at a mole fraction range of (0 – 1). The binary mixtures are as follows: ([BMIM]Cl: EG + methanol or ethanol) and ([BDMIM]Cl: EG + acetic acid or propanoic acid). Thermophysical properties such as densities, sound velocity and refractive indices were measured at different temperatures, T = (293.15, 298.15, 303.15, 308.15, and 313.15) K and at atmospheric pressure. The intermolecular interactions between the binary mixtures were further interpreted by computing thermodynamic properties such as excess molar volumes, intermolecular free length, isentropic compressibilities, deviation in isentropic compressibilities and deviation in refractive indices.

Furthermore, two deep eutectic solvents were prepared from an ammonium ionic salt with ethylene glycol or diethylene glycol at a 1:3 molar ratio namely: tetrabutylammonium acetate + ethylene glycol ([TBN AcO: EG) and tetrabutylammonium acetate + diethylene glycol ([TBN AcO: DEG). The selected DESs were tested in separating the molecular solutes by calculating activity coefficient at infinite dilution, ($\gamma_{13)}^{\infty}$). The molecular solutes include (alkanes, alkenes, alkynes, alcohols, ketones, aromatic hydrocarbons, tetrahydrofuran, thiophene and acetonitrile), and these were determined at T= (313.15 to 353.15) K at atmospheric pressure of 101 kPa using gas liquid chromatography. The column loading was composed of (29.8 – 33.4) mass percentage and 70 mass percentage of solvent and solid support material, respectively. Thermodynamic functions at excess infinite dilution namely entropy, Gibbs free energy and partial molar enthalpies were computed to gain a better understanding of the types of molecular interaction between the solutes. Selectivity and capacity values were evaluated to determine separation

feasibility and the effectiveness of the deep eutectic solvents for possible extraction of solvents in industrial different mixtures.

1.3 Aim and objectives

Aim

The aim of this work was to evaluate the impact of temperature on the intermolecular interactions occurring between imidazolium and or ammonium deep eutectic solvents and its binary mixtures with volatile organic solvents.

Objectives

- To prepare imidazolium and ammonium deep eutectic solvent (DESs).
- To determine the thermal stability of the prepared deep eutectic solvents using thermogravimetric analysis (TGA), and FTIR, and NMR to characterize the deep eutectic solvent.
- To measure the physical properties such as densities, sound velocity and refractive indices of imidazolium based DESs, mixtures with alcohols and or carboxylic acids at different temperatures.
- To evaluate the molecular interactions occurring between the mixtures by computing thermodynamic properties such as excess molar volumes (V_m^{E}), intermolecular free length (L_f), isentropic compressibilities (k_s), deviation of isentropic compressibilities (Δk_s) and deviation in refractive indices Δn_D.
- To correlate excess molar volumes and predict thermophysical properties (densities and refractive indices) data using the Lorenz-Lorentz equation.
- To calculate the activity coefficients at infinite dilution for different solutes in ammonium based DESs at different temperatures using retention data acquired by gas liquid chromatography (GLC).
- To ascertain the extraction performance of the ammonium based DESs by calculating selectivities and capacities.

1.4 Thesis Outline

Investigating thermophysical and thermodynamic properties at a molecular level plays a pivotal role in advancing the understanding of chemical systems, particularly when evaluating solvent behaviour in complex mixtures and designing materials for specialized industrial applications. Imidazolium and ammonium based DESs are especially noteworthy for their ability to establish extensive hydrogen bond networks and their compatibility with various organic compounds. Understanding how temperature affects molecular interactions within binary systems, particularly with volatile organic solvents, is crucial for optimizing their performance in separation technologies and improving the accuracy of property prediction models.

The thesis outline includes:

Chapter 1: Introduction entails background, aims and objectives.

Chapter 2: Literature review details the literature relevant to this study

(showing relevant studies done by researchers investigating thermophysical properties, thermodynamic properties and activity coefficients at infinite dilution related to this study).

Chapter 3: Theoretical framework details thermophysical and thermodynamic properties

Chapter 4: Experimental work details experimental procedures related to this work.

Chapter 5: Results and discussion of thermophysical properties of the investigated binary systems.

Chapter 6: Results and discussions of activity coefficient at infinite dilution of the investigated binary systems.

Chapter 7: Conclusion

References

CHAPTER 2

LITERATURE REVIEW

2.1 Introduction

The discovery of deep eutectic solvents opened new avenues in green chemistry due to the unique properties and potential applications of the solvents. Deep eutectic solvents were first introduced by Abbott *et al*. in 2003 for a mixture of ChCl (HBA) and urea (HBD), formed a clear, deep eutectic liquid with significantly lower melting point than the individual components (Abbott *et al.* 2003). Ongoing research continues to expand the understanding and capabilities of DESs, leading to the development of new formulations and applications that capitalize on their tunable nature and sustainability.

The chemical industry is a diverse industry with chemical products that are supplied into various industries, including the food, manufacturing, pharmaceutical, and petroleum industries (Martin *et al.* 2017, Cseri *et al.* 2018; Grundtvig *et al.* 2018; Murador *et al.* 2019). The chemical industry is under scrutiny because of its negative role in climate change (Pena-Pereira *et al.* 2015; Tobiszewski and Namiesnik, 2017; Joshi and Adhikari, 2019). This has initiated an interest in the search for alternate and innovative solvents for facilitating the production of chemical products in an environmentally friendly manner (Armenta *et al.*, 2019; Choi and Verpoorte, 2019; Pacheco-Fernández and Pino, 2019).

2.1.1 Classification of Deep eutectic solvents

Deep eutectic solvents can be classified into four main categories based on their composition and the nature of their components (Abbott 2007). Type (I), is made of quaternary ammonium salt with metal chloride which can be a mixture of choline chloride and zinc chloride, and these are often used in metal processing and electroplating. Type (II), is made of quaternary ammonium salt combined with metal chloride hydrated which can be a mixture of choline chloride combined with hydrated zinc chloride, Type (II) applications are like Type (I) but with different hydration states affecting their properties. Type (III) is made of quaternary ammonium salt with

hydrogen bond donor (HBD) which can be a mixture of choline chloride with urea, ethylene glycol, or glycerol, it is widely used in catalysis, separation processes, and as a solvent in various chemical reactions. Type (IV) is made of metal hydrate with hydrogen bond donor (HBD) which can be prepared by a mixture of hydrated zinc chloride with urea and is used in electrodeposition and electrochemical applications (Smith et al. 2014). Table 2.1 is the general formulae for the classification of deep eutectic solvents.

Table 2-1: General formulae for the classification of deep eutectic solvents

Group classification	**General formulae**	**Terms**
Type (I)	$\mathrm{Cat^+X^-zMCl_x}$	M = Zn, Sn, Fe, Ga, In, Al
Type (II)	$\mathrm{Cat^+X^-zMCl_x.yH_2O}$	M = Cr, Co, Cu, Fe, Ni
Type (III)	$\mathrm{Cat^+X^-zRZ}$	Z = OH, COOH, $CONH_2$
Type (IV)	$\mathrm{MCl_x}$ + RZ = $\mathrm{MCl_{x-1}}^{+}\cdot$RZ + $\mathrm{MCl_{x+1}}-$	Z = OH, $CONH_2$ and M = Al, Zn

2.1.2 Structures of hydrogen bond acceptors and hydrogen bond donors

Commonly used hydrogen bond donors and hydrogen bond acceptors in Deep eutectic solvent preparation, (Ijarda *et al.* 2022). Figure 2.1 is the list of commonly used HBA in DESs preparation.

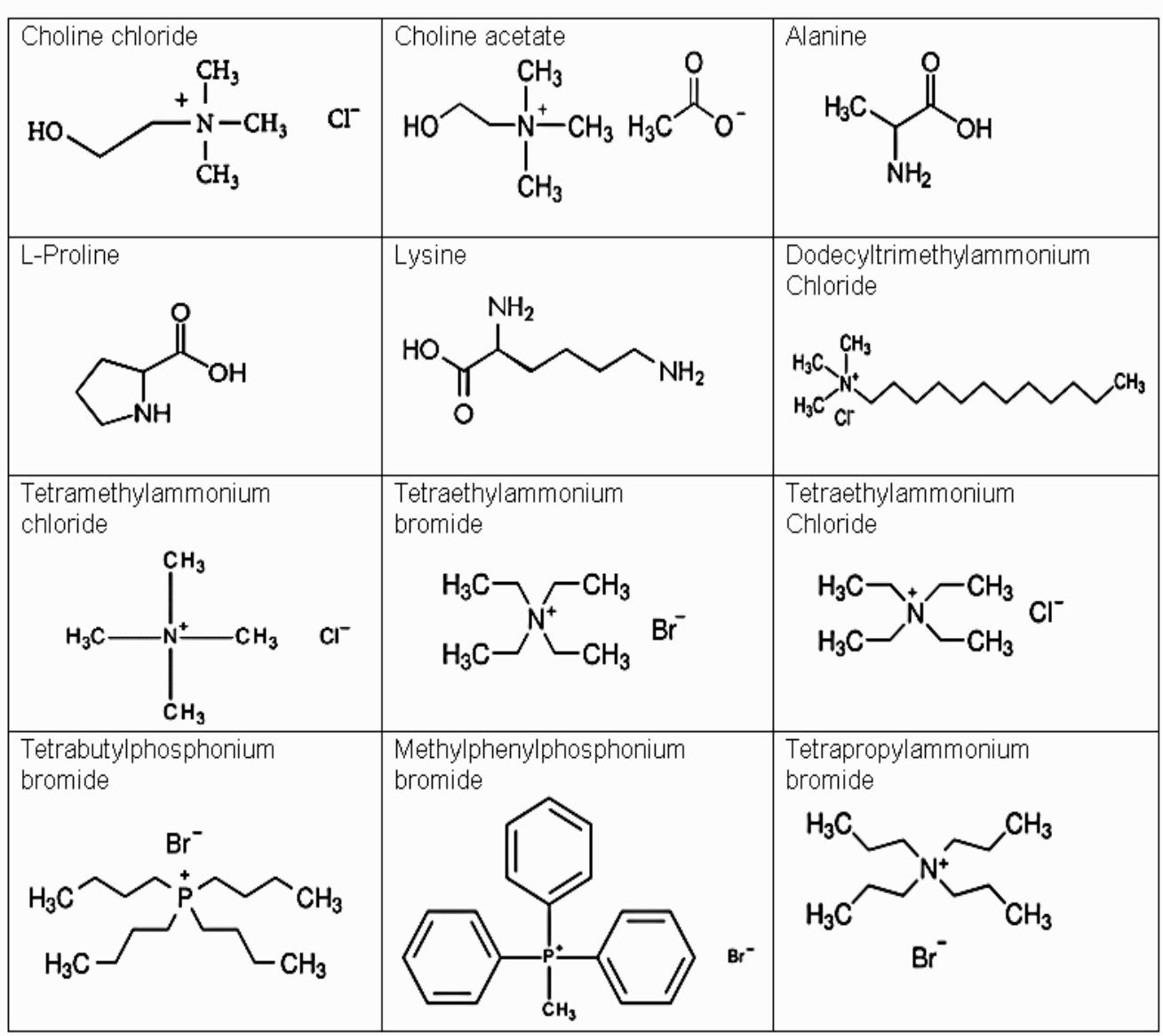

Figure 2.1: List of commonly used HBA in DESs preparation

Figure 2.2 is the list of commonly used HBD in DESs preparation.

Glutaric acid 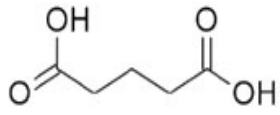	Citric acid 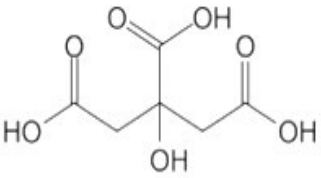	Succinic acid 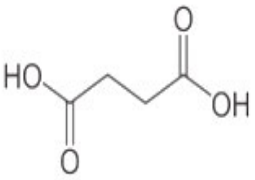	Salicylic acid 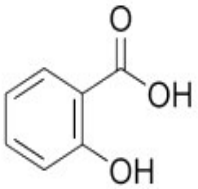
Octylic acid 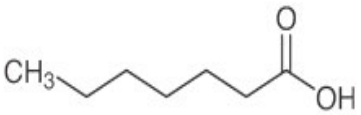	Acetamide 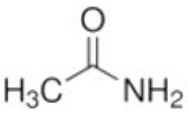	Benzamide 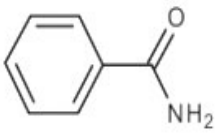	Urea 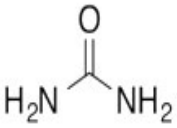
Methyl urea 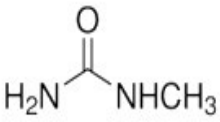	Ethanol 	Propanol 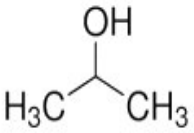	1,2-propandiol 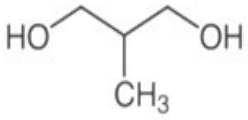
1,4-butanediol 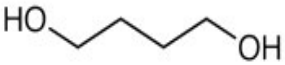	D-glucose 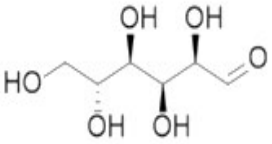	D-Sorbitol 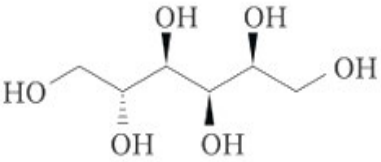	

Figure 2.2: List of commonly used HBD in DESs preparation.

2.1.3 Thermophysical and thermodynamic properties

Deep eutectic solvents have emerged as an alternative environmentally friendly solvent to both conventional organic solvents as well as ionic liquids for liquid-liquid extraction (LLE) and azeotropic distillation (Shishov *et al.* 2020; Shekaari *et al.* 2020; Smink *et al.* 2020; Zante *et al.* 2020). The effectiveness of the DES as a separating agent in the liquid-liquid extraction process is to evaluate the starting materials such as HBDs and HBAs with different molar ratios. The development of DESs with low viscosity is highly desirable. High viscosity of DES is often attributed to the presence of an extensive hydrogen bond network between each component in the binary mixture, that result in the lower mobility of free species within the DES. Other forces that contribute to high viscosity of the DES are electrostatic and van der Waals interactions. In general viscosities of the eutectic mixture are mainly affected by the chemical nature of the DES components, type of the ammonium salts and HBD, organic salts/HBD molar ratio, temperature and water content (Abbott and Capper 2006).

Densities and speed of sound data of the ionic liquid, 1-ethyl-3-methylimidazolium ethyl sulfate [EMIM][ES] in the deep eutectic solvents: choline chloride/glycerol; choline chloride/ethylene glycol; choline chloride/urea; and choline chloride/oxalic acid, in a dilute concentration of the ionic liquid at different temperatures 298.15 K - 318.15 K study was reported by Shekaar *et al.* (2020). Based on the obtained densities and speed of sounds data, the apparent molar isentropic compressibilities and apparent molar volumes were computed. The solute-solvent interactions between the ionic liquid and the deep eutectic solvents are stronger for choline chloride/urea systems than for the other deep eutectic solvents investigated. The Fitzer model was also used to correlate the values of the apparent molar volumes and molar isentropic compressibilities and a good correlation with the experimental data was obtained.

The study of experimental and theoretical excess molar properties of aqueous choline chloride-based deep eutectic solvents was conducted with (I) choline chloride/ethylene glycol, (II) choline chloride/glycerol, and (III) choline chloride/1.4-butenediol, all prepared at a mole ratio of 1:2, respectively. The density values of the systems were measured at temperatures between (293.15 - 323.15) K and at atmospheric pressure. Intermolecular interactions resulted in negative excess molar

volumes for all the studied systems. By comparing the values of excess molar volumes with the Prigogine-Flory-Patterson (PFP) theory and the extended real associated solution model (ERAS), the non-ideal behaviour of the investigated systems was determined (Patyar *et al.* 2021).

Another study focusing on thermophysical properties of deep eutectic solvents in the presence of water and without water was reported. Viscosities were measured and reverted the influence of cation and anion including temperature. In general, the results showed that with increasing temperature, the viscosity values of DESs decreases. Reline showed the highest viscosity than other DESs in this study, however; ethaline exhibits the lowest viscosity. Interestingly, this correlation is related to the change in the number of hydrogen bonding between the liquids under investigation. These findings are similar to that of Stefanovic *et al.* (2022) which showed that the density of hydrogen bond in reline was (13.8 bonds nm^{-3}), glycerine (10.8 bonds nm^{-3}) and ethaline (9.4 bonds nm^{-3}). This behaviour is due to the urea in reline, which can form four hydrogen bonds compared with glycerol, which can form three hydrogen bonds, and ethylene glycol, which can form two hydrogen bonds. The refractive indices data showed that low water content has high refractive index values due to an increase in ion arrangement and the efficient packing of the ions (Al-Murshedi *et al.* 2019).

Thermophysical properties of deep eutectic solvents (choline/urea) + water molecules at different temperatures (293.15 K - 323.15) K and at atmospheric pressure was presented by Shekaari *et al.* (2020). The results revealed strong intermolecular interactions between water molecules and the deep eutectic solvent.

The structural and physicochemical properties of ethaline deep eutectic solvents were reported by Rozas *et al.* (2021). This was based on the experimental and theoretical studies which revealed that water molecules change the ethaline properties through the development of hydrogen bonding. Nevertheless, the properties and structuring does not follow a linear behaviour with water content, three different regions were inferred: 1) up to 10 wt% (characterized by minimal perturbations of the ethaline properties and structuring), 2) 10 to 30 wt% (characterized by increasing water self-aggregation but maintaining the main features of the eutectic although decreasing the size of ethaline aggregates), and 3) water content greater than 30 wt%, in which water self-aggregation prevails and ethaline small clusters are dispersed into a water solvent

and thus forms hydrogen bonding between the ethaline components. The controlled exposure of hydrophilic deep eutectics such as ethaline may be used to obtain a reasonable degree of hydration, which may be used to control, fine-tune, and optimize relevant physicochemical properties such as viscosities, but to maintain the most relevant structural properties of the studied liquid mixtures.

A study by Mgxadeni *et al*. (2023) reported thermodynamic properties, and activity coefficients at infinite dilution and Cosmo- SAC modelling of the deep eutectic solvents at different temperatures. The deep understanding of the solute-deep eutectic solvent interactions required for the appropriate selection of DESs as absorption media in the extraction of binary mixtures can be explained by the measurements of activity coefficient at infinite dilution. The study was done to evaluate the values of the activity coefficient at infinite dilution γ_{13}^{∞}, and allowing us to define and understand the nature of the intermolecular interactions comprising the DES and mixtures with volatile organic solvents at different temperatures using gas liquid chromatography technique. The selectivity coefficient at infinite dilution values were determined in 34 solutes in the DESs [zinc chloride + acetic or phosphoric acid] prepared at 1:2 mole ratio at a temperature range (313.15 - 353.15) K. The thermal stability of the prepared deep eutectic solvents was determined by a thermogravimetric analyser. Excess thermodynamic parameters (excess molar enthalpies at infinite dilution, $\Delta H_1^{\mathrm{E},\infty}$, excess molar entropies at infinite dilution $\Delta S_i^{\mathrm{E},\infty}$, and excess molar excess Gibbs free energies at infinite dilution Gibbs energies, $\Delta G_i^{\mathrm{E},\infty}$ were derived from the γ_{13}^{∞} data. The selectivity and capacity values were calculated and compared with the literature values of other DESs. The selectivity and capacity values are high, [zinc chloride + acetic acid or phosphoric acid] and can be used as a potential solvent to replace the currently used conventional solvents in the separation of the selected azeotropes. Cosmo-SAC predictions were qualitatively in very good agreement with the experimental data.

Chemical substances utilized in industrial separation processes consume a significant amount of energy, are expensive, and toxic by-products are also formed (Lee *et al.* 2012). A major contributor to the constraints of currently used solvents is the volatile nature when solvents used in most chemical separation processes (Jakobsen *et al.* 2005; Cvetanovic *et al.* 2019; Thompson *et al.* 2019; Albuquerque *et al.* 2021). The

most used volatile organic compounds are: N-methyl-2-pyrrolidone (NMP); N-methyl formamide (NMF); glycerol (G); diethylene glycol (DEG); and triethylene glycol (TEG). These solvents have various shortcomings for the separation of close boiling mixtures, such as: highly volatility, non-recyclability and low yield of extract (Vanda *et al.* 2018; Gullón *et al.* 2020; Jalili *et al.* 2020; Makos *et al.* 2020). Ionic liquids (ILs) are a class of environmentally friendly organic solvents that could replace the volatile organic solvents as extractants. However, the disadvantages include their production which is energy intensive, highly toxic, high viscosity, and high cost (Singh and Savoy, 2020; Uddin *et al.* 2020; Paucar *et al.* 2021).

Density (ρ), viscosity (η), and speed of sound (u) have been determined at T = (288.15 – 303.15K) and P = 93.2 kPa for the binary mixture of (2- methyltetrahydrofuran + ethanol, or 1-propanol, or 1-butanol, or 1-pentanol) over the entire composition range was reported by Castro *et al.* (2024). The results were used to calculate the excess molar volumes (V_m^{E}), deviation in isentropic compressibilities (Δk_s), deviation in viscosity ($\Delta\eta$), and excess Gibbs activation energies ($\Delta G^{*\mathrm{E}}$), which were correlated by the Redlich-Kister polynomial. The values of the deviation properties were negative, which indicated a predominance of structural and chemical effects over physical effects. Five viscosity models were employed to fit the viscosity data. The V_m^{E} data were also correlated by the Prigogine-Flory-Patterson Theory (PFP Theory) and Peng-Robinson-Stryjek-Vera equation of State (PRSV EOS). Furthermore, a Fourier transform infrared (FT-IR) spectroscopy study was performed to explain the hydrogen bonding interactions. Lastly, theoretical calculations using Density Functional Theory (DFT) at B3LYP-GD3(BJ)/6-311++G(3df,2p) level of theory were performed to understand the inter-actions between compounds present in the mixture. The FT-IR and computational results were in good agreement with the experimental data.

2.1.4 Thermodynamic properties and activity coefficient at infinite dilution

Thermodynamic parameters and infinite dilution activity coefficients for 32 different organic solutes in a deep eutectic solvent: choline chloride + 1,5-pentanediol was investigated. Alkanes, alkenes, cycloalkane, cycloalkenes, alcohols, aromatics, ketones, ethers, esters, monocyclic, heterocyclic, alkyl halide, and water, were among the functional groups investigated by Li *et al.* (2022). Inverse-gas chromatography was used for the prediction of infinite dilution activity coefficient data at different temperatures (303.15 K - 343.15 K). The obtained infinite dilution activity coefficient data revealed higher values for all the solutes, indicating low solubility and weak intermolecular interactions of the studied deep eutectic solvent. The partial molar properties, namely: Gibbs free energies, entropies, and enthalpies, were computed from the obtained infinite dilution activity coefficient data. Partial molar excess enthalpies were positive, suggesting disruption of solute-solute and/or solvent-solvent interactions. Positive entropy values demonstrate that the dissolution of solutes in the deep eutectic solvent is an entropy-increasing process. The Gibbs free energy (+/-) considers the changes in enthalpy and entropy that occurs during the dissolution process, as well as solute and deep eutectic solvent.

The study of thermodynamic properties and activity coefficient at infinite dilution of solutes in a deep eutectic solvent 1-butyl-3-methylimidazolium chloride: glycerol revealed that the DESs selection in extraction processes can be affected by various factors, where the reduced extraction efficiency of the DES is affected by an increase in mole ratio of hydrogen bond acceptor to hydrogen bond donator. An increase of carbon atom chains that resulted from an increased HBD which in turn reduced the effect of HBD interactions resulting from steric impact. The packing impact of solutes in the DES was affected by an increase of HBD, because the HBD wraps around the anion and give a higher active hydrogen which resulted in higher separation. Furthermore, an increased number of carbon chains resulted to higher immiscibility which resulted to reduced interactions between DES and solutes reported by Kabane *et al.* (2020). An increase in temperature affects the yield of a particular extraction. This effect is associated to a decrease in viscosity and hence mass transfer due to an increase in solubility at high temperatures. The poor performance of the DES as a

separation parameter, as the capacity was not satisfactory, it was less than 1, (<1), but the high selectivity values were useful.

The influence of hydrogen bond donor on zinc chloride in the separation of binary mixtures based on the activity coefficients at infinite dilution was reported by Mgxadeni *et al.* (2022). Results obtained showed that the selectivity is high in zinc chloride: acetic acid prepared at 1:4 molar ratio indicating that this DES can be utilized in separating benzene/ethanol, cyclohexane/ethanol, ethylbenzene/butan-1-ol, and n-heptane/butan-1-ol with a capacity greater than 1. The selectivity for n-octane/acetonitrile is higher, however, the capacity (0.65) is very low indicating low solubility and therefore a low throughput of the separated component.

Limiting activity coefficient was estimated for 32 various volatile organic solutes (aliphatic and aromatic hydrocarbons, alcohols, THF, thiophene, acetonitrile, ketones) and water in [trihexyltetradecylphosphonium decanoate: ethylene glycol] prepared at 1:4 molar ratio, respectively. Measurements were conducted at different temperatures, T = (313.15 – 343.15) K and at atmospheric pressure. Gas liquid chromatography coupled with thermal conductivity detector was employed to obtain the experimental retention data of solutes in the deep eutectic solvent. The partial molar excess properties, enthalpies, entropies, and Gibbs energies were determined at infinite dilution from the calculated limiting activity coefficient. The selectivity and capacity values for the separation problems such as (acetone/ethanol, cyclohexane /benzene, benzene/toluene, and butanol/MEK) were determined from the limiting activity coefficients. The findings proved that triexyltetradecylphosphonium decanoate: ethylene glycol deep eutectic solvent could be used in separation of azeotropes. The results were based on the intermolecular interactions occurring in the deep eutectic solvent mixtures. The influence of hydrogen bond donor on deep eutectic solvent was discussed (Manyoni *et al.* 2022).

Measurements of activity coefficients at infinite dilution for organic solutes in tetramethylammonium chloride: ethylene glycol deep eutectic solvent using gas-liquid chromatography study conducted by Nkosi *et al.* (2018). The results showed that the values of limiting activity coefficient decreased with temperature for all investigative solutes, except esters, i.e. methylacetate and ethylacetate. The non-polar compounds such as alk-1-anes, alk-1-enes and cycloalkanes exhibited very high values of activity

coefficients. This behaviour indicated that these solutes had a very low solubility in the DES and the solutes-DES intermolecular interactions were relatively weak. The polar compounds such as alkanols, ketones, heterocyclics and esters had higher solubility than those of the non-polar solutes. This is an indication that the polar compounds interacted more strongly with DES than non-polar solutes. This could be attributed to strong dipole-dipole interactions between the components of DES and polar solutes.

A study conducted by Redhi *et al.* (2023) reported infinite dilution activity coefficient for 32 different solutes in (1-ethyl-1-methylpyrrolidinium chloride: 1,5-pentadiol), [[EMPYR]-Br: 1,5-PDO] DES using gas liquid chromatography method with pre-saturation of helium gas. The list of selected solutes included alkanes, alkenes, alkynes, cycloalkanes, cycloalkenes, aromatics, ketones, alcohols, and water. Pre-saturation was deemed necessary because of volatility of solvents at temperatures used for measurements. The measurements were taken at temperatures T = (313.15 – 343.15) K and at atmospheric pressure. Values of partial properties, i.e., enthalpies, entropies, and Gibbs free energies, were computed at a reference temperature of T_{ref} = 333.15 K. Moreover, the values of selectivity and capacity relating to ([EMPYR]-BR: 1,5-PDO) DES for different sets of binary systems that are normally problematic in the separation through solvent extraction or distillation were also computed. These include cyclohexene/benzene, acetone/methanol, and hexane/benzene. The obtained data was then compared to the literature data, at similar temperatures. The infinite dilution activity coefficient and partial molar properties revealed solvent-solute characteristics with the selected solutes, especially the nonpolar, i.e., alkanes, alkenes, aromatics, cycloalkanes, and cycloalkenes. Nevertheless, the obtained selectivity and capacity values for the studied problems revealed satisfactory values for some problems (e.g., Hexane/toluene) and unsatisfactory values for some separation problems (ethanol/cyclohexane).

Thermophysical properties and intermolecular interaction of tetrapropylammonium chloride: ethylene glycol DES at a 1:2 molar ratio was investigated by Hu *et al.* (2024) using inverse gas chromatography (IGC) techniques to study the DES thermodynamics in the temperature range of (303.15 – 333.15) K. Additionally, molecular dynamics (MD) simulations and density functional theory (DFT) were used to explore intermolecular interactions in DES at both molecular and atomic levels. The

finding of the study yielded crucial insights, including the successful determination of activity coefficients, Flory-Huggin's interaction parameter, solubility parameters, and the Abraham solvation parameters through IGC technique. A careful study of the temperature-dependent trends in these parameters were provided. Analysis of structural properties, including radial distribution functions, hydrogen bond counts, and thermal fluctuation indices, revealed that, at experimental temperatures, the amount and nature of intermolecular hydrogen bonds in the binary mixtures are the main factors influencing the thermodynamics properties of the DES. Based on the DFT calculations, a quantitative assessment of the molecular interaction mechanisms of the DES at atomic level confirmed the predominant role of hydrogen bonding in DES formation, with multicentre hydrogen bonds characterized by stronger bond strengths emerging as the primary type.

Azadeh *et al.* (2025) reported the characterization of deep eutectic solvents, tetrabutylammonium bromide (HBA): oleic acid (HBD) at 2:1 mole ratio was synthesized as the stationary phase of gas liquid chromatography. The measured thermodynamic parameters indicated the potential ability of the constructed stationary phase. The sum of McReynolds constants equal to 1420 indicated the stationary phase with moderate polarity. The performance of BTEX separation according to the short column length and the physical characteristics of the prepared column. The stationary phase DES had strong interactions with aromatic and alcohols, this can be related to the formation of hydrogen bonds. The prepared column separated the isopropanol and ethanol with a suitable retention time. It also improved the performance for the separation of isopropanol and ethanol compared to the carbowax column. The selectivity values for the different mixtures had shown that stationary phase DES had good applicability for separating a wide range of analytes.

The literature underscores the multifaceted nature of DESs highlighting their promising role in replacing conventional extractants through structurally driven selectivity, hydrogen bond mediated interactions, and enhanced extraction capacity. Across a spectrum of formulations, DESs exhibit strong intermolecular forces, particularly hydrogen bonding, which dictate their thermophysical properties such as viscosity, density, and compressibility. These molecular dynamics directly influence solute-solvent interactions and explain their preferential behaviour in liquid-liquid extraction

and azeotropic separations. Systems incorporating choline chloride and urea demonstrate superior selectivity and compressibility, with computational models and experimental data aligning to reveal non-ideal mixing patterns and strong association phenomena. Furthermore, activity coefficients at infinite dilution and excess thermodynamics parameters provide valuable insight into DESs, potential to outperform the traditional solvents in separation processes. As evidence by high selectivity and capacity values, especially in zinc chloride-based DESs, the ability to fine-tunes DESs compositions makes them potent candidates for energy efficient and environmentally benign separation technologies. Temperature effects further highlight the balance between viscosity, mass transfer, and hydrogen bond stability. Advance techniques such as inverse gas chromatography, DFT modelling, and MD simulations confirm that the strength and multiplicity of hydrogen bonds dictate the non-ideal behaviour, partial molar properties, and solvation dynamics of DESs. As a result, DESs exhibit significant promise as customizable, energy-efficient media for selective separation processes, though ongoing refinement is essential to optimize capacity without compromising sustainability.

CHAPTER 3

THEORETICAL FRAMEWORK

3.1 Thermophysical properties

3.1.1 Density

Density (ρ) can be expressed as mass per unit volume and it can be calculated by ratio of the mass to its volume (Equation 3,1).

$$\rho = \frac{m}{v} \tag{3.1}$$

Where m and v represent mass and volume of the compound, respectively. Density significantly influences the efficiency and application of deep eutectic solvents. The density of a DES impacts its efficiency as a solvent, where a higher density increases its ability to dissolve a wider range of compounds making it more effective for specific applications. Density influences thermophysical properties like viscosity, ion conductivity and surface tension, (Halder *et al.* 2021).

3.1.2 Speed of sound

Speed of sound (u) is determined by the property of the medium in which a solvent travels (Equation 3.2).

$$u = \frac{l \text{ x } \left(\frac{1}{1 \text{ x } 10^{-5} \text{ x } \Delta T}\right)}{\left(\frac{P_S}{512}\right) - A \text{ x } f_3} \tag{3.2}$$

ι represent the path length travelled by sound waves, ΔT is the deviation in temperature, P_s, represents the oscillation interval of the sound wave received,

A denotes constant speed of sound of medium property, and f_3 is the correction term for temperature. Both density and speed of sound are temperature dependent.

3.1.3 Refractive index

Refractive index (n) is the ratio of the velocity of light in a vacuum to the velocity of light in the specific medium. It is used to determine the concentration of solutes in solutions which is essential for various analytical and industrial applications. Refractive index is defined by (Equation 3.3).

$$n = \frac{c}{v} \tag{3.3}$$

Where $n,\ c,$ and v represent the refractive index, speed of light in a vacuum and speed of light in a medium, respectively.

3.1.4 Excess molar volume

Excess molar volume, V_m^{E}, is a fundamental property in the thermodynamic properties of liquid mixtures. The excess molar volume is defined from the molar volume equation given by Walas (1985) McGlashan (1979), and Letcher (1975) (Equation 3.4).

$$V_m^{\mathrm{E}} = \left(\frac{x_1 M_1 - x_2 M_2}{\rho_{mixture}}\right) - \left(\frac{x_1 M_1}{\rho_1} + \frac{x_2 M_2}{\rho_2}\right) \tag{3.4}$$

Where x_1, M_1 represents the molar fraction and molar mass of component 1, and x_2, M_2 represents the molar fraction and molar mass of component 2, $\rho,\ \rho_1$ and ρ_2 represents the density of the binary mixture, pure component 1, and pure component 2, respectively. Excess molar volumes of binary liquid mixtures is computed from the experimental densities of the mixtures. This parameter provides insight into the nature

of the molecular interactions, such as hydrogen bonding, dipole-dipole interactions and Van der Waal forces.

3.1.5 Isentropic compressibility

Isentropic compressibility is calculated from the density and speed of sound data by applying the Newton-Laplace (Equation 3.5).

$$k_s = \frac{1}{\rho u^2} \tag{3.5}$$

Where ρ, and u, represents the density and speed of sound of the binary mixture, respectively.

3.1.6 Deviation in isentropic compressibility

The deviation in isentropic compressibilities, Δk_s , indicate the nature of intermolecular interactions within the binary mixtures compared to the ideal components. This is calculated using (Equation 3.6) below.

$$\Delta k_s = \quad k_s^{id} - x_1 k_{s1} - x_2 k_{s1} \tag{3.6}$$

Where Δk_s, k_s, x_1 , x_2 and k_s^{id} are deviation in isentropic compressibilities, isentropic compressibilities, mole fraction of component 1 and 2 and isentropic compressibilities of the ideal mixtures, respectively. The term k_s^{id} is calculated from (Equation 3.7).

$$k_s^{id} = \sum_{i=1}^{n} \varphi_i k_{si} \tag{3.7}$$

Where φ_i and k_{si} are volume fractions and isentropic compressibility of pure component *i*, respectively.

3.1.7 Intermolecular free length

Jacobson (1951) presented the free length theory (FLT) in order to describe the speed of sound in pure liquids and their mixtures. The key importance of free length (L_f) is the distance between the two molecules. Jacobson gave an equation expressed in (Equation 3.8).

$$u_{liq} = \frac{K}{L_f \rho^{\frac{1}{2}}} \tag{3.8}$$

Where K is a temperature dependence constant, ρ is the density and L_f is the free length in the liquid. The free length theory of Jacobson was used to evaluate the sound velocities in the mixtures. Free length (L_f) of pure liquids is calculated using the (Equation 3.9.)

$$L_f = k_j (k_s)^{\frac{1}{2}} \tag{3.9}$$

Where k_j represent the Jacobson's constant dependent on temperature (93.875 + 0.375 T) x 10^{-8} and k_s denotes isentropic compressibility.

3.1.8 Molar refraction

3.1.8.1 Lorentz-Lorenz equation

The Lorentz-Lorenz equation was derived from work done by Lorentz on the theory of electrons and its application to behaviour of light and radiant heat (Lorentz *et al.*1953).

The Lorentz-Lorenz equation relates the refractive index at zero frequency and the mean molecular polarizability, *α*, of a nonpolar, nonmagnetic material results in the following equations (Equation 3.10) and (Equation 3.11) (Brocos *et al.* 2003).

$$R = V_m\left(\frac{n^2-1}{n^2+2}\right) \tag{3.10}$$

Where V_m, is the molar volume and n^2 is refractive index of the mixture.

The molar refraction, R is given by (Equation 3.11).

$$R = \frac{N_A\alpha}{3\varepsilon_0} \tag{3.11}$$

Where N_A is the Avogadro constant and ε_0 is the permittivity of free space.

3.2 Correlation

3.2.1 Correlation of excess molar volumes by Lorentz-Lorenz approximation

Lorentz-Lorenz approximation can be utilised for the correlation of excess molar volume of liquid mixtures using refractive indices obtained experimentally for the binary mixtures. Within the framework of Lorentz-Lorenz approximation, excess molar volumes (V_m^{E}) can be correlated via the change in reduced free volume (Equation 3.12)

$$\Delta\left(\frac{V_{m,f}}{R}\right) = \frac{V_{m,f}}{R} - \left(\frac{V_{m,f}}{R}\right)^{id} \quad (3.12)$$

Where $V_{m,f}$ represents molar free volume.

Application of the Lorentz-Lorenz equation allows this expression to be reduced to (Equation 3.13).

$$\Delta\left(\frac{V_{m,f}}{R}\right) = \frac{3}{n^2-1} - \frac{3}{\left(n^{id}\right)^2-1} \quad (3.13)$$

The assumption $R = R^{id},$ is most often a highly accurate approximation. The following can be obtained from (Equation 3.14), (Equation 3.15) and (Equation 3.16).

$$\Delta\left(\frac{V_{m,f}}{R}\right) = \frac{V_m^{\mathrm{E}}}{R} \quad (3.14)$$

Where $$V_m^f - V_{m,f}^{id} = V_{m,f} = V_m^{\mathrm{E}} \quad (3.15)$$

Therefore,

$$V_m^{\mathrm{E}} = (-\Delta n)\frac{3R\left(n^{id}+n\right)}{(n^2-1)\left[\left(n^{id}\right)^2-1\right]} \quad (3.16)$$

Where V_m^{E} represents excess molar volume, n, Δn, n^{id}, n^2 is the refractive index, deviation refractive index, an ideal refractive index,

3.2.2 Prediction of densities by Lorentz-Lorenz approximation

Equation (3.17) was used to predict the densities *(ρ)* of the binary system that is linked with refractive indices (n_D).

$$\rho = \frac{\left(\frac{n^2-1}{n^2+2}\right)(x_1M_1 + x_2M_2)}{\left(\frac{n_1^2-1}{n_1^2+2}\right)x_1\frac{M_1}{\rho_1} + \left(\frac{n_2^2-1}{n_2^2+2}\right)x_2\frac{M_2}{\rho_2}} \tag{3.17}$$

Where n, n_1, n_2 represent the refractive index for the mixture and refractive index of component 1 and component 2, x_1, x_2 molar ratio of component 1 and component 2, M_1, M_2 molar mass of component 1 and component 2, ρ, ρ_1, ρ_2 and density of mixture and density of component 1 and component 2, respectively.

3.2.3 Prediction of refractive indices by Lorentz-Lorenz approximation

Equation (3.18) is used to predict the refractive indices of the binary mixtures.

$$n = \left(\frac{2\left(\frac{n_1^2-1}{n_2^2+2}\right)x_1\rho\frac{M_1}{M_1} + \left(\frac{n_1^2-1}{n_2^2+2}\right)x_2\rho\frac{M_2}{M_2} + (x_1M_1 + x_2M_2)}{(x_1M_1 + x_2M_2) + \left(\frac{n_1^2-1}{n_2^2+2}\right)x_1\rho\frac{M_1}{\rho_1} + \left(\frac{n_1^2-1}{n_2^2+2}\right)x_2\,\rho\frac{M_1}{\rho_2}}\right)^{\frac{1}{2}} \tag{3.18}$$

Where n, n_1^2, n_2^2 and represents the refractive index of the mixture, component 1 and component 2, x_1, x_2 molar ratio of component 1 and component 2, M_1, M_2, the molar mass of component 1 and component 2 and ρ, ρ_1, ρ_2 are the density of the mixture and density of component 1 and component 2, respectively.

3.3 Root mean square deviation

The root mean square deviation of excess molar volumes, densities and refractive indices obtained by using the Lorentz-Lorenz equations are calculated using (Equation 3.19).

$$\sigma = \sqrt{\sum_{i=1}^{n}(x_i - \bar{x}_i)^2} \quad (3.19)$$

Where x_i is the set if n random variables, and $\bar{x}_i$ the corresponding set of accepted values.

3.4 Simulation of deep eutectic solvents

3.4.1 Density functional theory

Quantum chemical calculations are employed to investigate the electronic structure of the DES components and the strength of specific intermolecular interactions such as hydrogen bonding, van der Waals forces and electrostatic interactions. Density functional theory (DFT) computes the electronic properties of the molecules based on their wavefunctions and electronic densities, these methods are able to predict bond lengths, angles, interaction energies and provide data on binding energies, charge distribution, and nature of specific interactions (e.g., hydrogen bonds or donor-acceptor interactions).

Electronic energies of frontier molecular orbital, dipole moment and optimization energy are determined using DFT calculation. Gauss-view 6 and Gaussian 16 software are utilized for the calculations, employing B3LYP/6-311G parameters (Yadav and Sewariya, 2023). B3LYP/6-311G examines circular dichroism and vibrational absorption and organic compounds in the gas phase. Riley *et al.* (2007), evaluated the efficacy of various techniques and parameters in DFT computations, consistently finding improved outcomes with the B3LYP method across diverse basis sets. The basis set selection is tailored to the specific molecule studied and it comprises of mathematical functions (Aslam and Deshwal, 2024., Aslam and Singh 2023). The 6-1311G basis set represents the electronic wave functions, especially for atoms in the

first two rows of the periodic table. It offers computational efficiency while maintaining accuracy in modelling molecular systems, making it widely used in quantum chemistry calculations.

DFT calculations based on the following equations was used to ascertain physicochemical descriptors such as chemical potential, electronegativity, hardness, the global electrophilicity index and softness. The descriptors were calculated using Equations (3.20 to 3.27).

3.4.2 Chemical potential

The chemical potential, μ, is calculated from (Equation 3.20).

$$\mu = (E_{HOMO} + E_{LUMO}) / 2 \quad (3.20)$$

E_{HOMO} is the energy of highest molecular orbital that contains electrons and E_{LUMO} energy of lowest unoccupied molecular orbital, respectively.

3.4.3 Electronegativity

The electronegativity, χ, is calculated from (Equation 3.21).

$$\chi = -(E_{HOMO} + E_{LUMO}) / 2 \quad (3.21)$$

Electronegativity is an indicative of a molecule's ability to attract electron density, it aids in predicting its chemical reactivity (Raman and Singh. 2023., Singh and Jain. 2022).

3.4.4 Hardness

The hardness, η, is computed from (Equation 3.22).

$$\eta = (E_{LUMO} - E_{HOMO}) / 2 \quad (3.22)$$

3.4.5 Softness

The softness, S, is computed from (Equation 3.23).

$$S = 1 / 2\,\eta \quad (3.23)$$

Chemical hardness and softness reflect the molecule's polarizability, with higher hardness associated with smaller size and less dispersed electron cloud, while higher softness suggests greater ease of electron donation (Kaya and Puta. 2022., Miranda-Quintana and Heidar-Zadeh. 2022).

3.4.6 The global electrophilicity index

The global electrophilicity index, ω, Equation 3.24) predicts how a chemical species will interact with another chemical species by measuring its tendency to accept electrons. This is essential in designing chemical reactions, particularly when choosing DES that will effectively promote desired transformations.

$$\omega = \mu^2 / 2\,\eta \quad (3.24)$$

Global electrophilicity measures the molecules overall electron deficiency or Lewis acidity nature, with higher values indicating increased acidity and electron shortage (Ríos-Gutiérrez and Sousa. 2023).

3.4.7 Uncorrected interaction energy estimation

The uncorrected interaction energy, E_{inter} estimation was calculated using (Equation 3.25).

$$E_{inter} = E_{complex} - E_{solute} - E_{co-solvent} \quad (3.25)$$

Where $E_{complex}$ is the total phase energy of the binary DES as a complex, E_{solute} is the energy of the solute without the co-solvent, and $E_{co-solvent}$ is the energy of the co-solvent molecules computed in the presence of implicit solvent or in vacuo.

3.4.8 Basic set superposition error estimation

Equation (3.26) was used to calculate the estimation of basic set superposition error (BSSE).

$$BSSE \approx \Delta E_{complex}^{cp-corr} = E_{complex}^{uncorr} - E_{complex}^{cp-corr} \quad (3.26)$$

The BSSE was estimated as an approximation of $E_{complex}^{cp-corr}$, where $E_{complex}^{uncorr}$ is the gas phase energy of the optimized complex conformation, and an approximation of $E_{complex}^{cp-corr}$ is the counter poise corrected gas phase energy of the optimized conformation of the complex.

3.4.9 Counter poise corrected interaction energy

The counter poise corrected interaction energy, E_{inter}^{corr}, was obtained from (Equation 3.27) by taking the BSSE into consideration.

$$E_{inter}^{corr} = E_{inter} - BSSE \quad (3.27)$$

Where E_{inter} is the uncorrected interaction energy.

3.5 Activity coefficients at infinite dilution by gas liquid chromatography

Retention data measured using gas liquid chromatography was used to calculate the activity coefficient at infinite dilution, γ_{13}^{∞}, of the investigated deep eutectic solvents. Cruickshank et *al.*, (1969) and Everett (1965) presented (Equation 3.28) that was used to compute γ_{13}^{∞} of solutes in solvents.

$$\ln \gamma_{13}^{\infty} = \ln\left(\frac{n_3 RT}{V_N P_1^*}\right) - \frac{P_1^*(B_{11} - V_1^*)}{RT} + \frac{P_o J_2^3 (2B_{12} - V_1^{\infty})}{RT} \quad (3.28)$$

Where n_3 is the number of moles of solvent in the stationary column, R represents molar gas constant, T is column temperature in the gas chromatography oven, V_N is the net retention volume of the solute, P_o is the outlet pressure, P_1^* signifies the saturated vapour pressure of the solute at temperature T, B_{11} is the second virial coefficient of pure solutes, V_1^* represents the molar volume of the solute, B_{12} denotes the cross virial coefficient of solute (1) and carrier gas (2), and $P_o J_2^3$ is the mean column pressure.

Net retention volume of the solute was determined by (Equation 3.29).

$$V_N = J_2^3 (t_R - t_G) q_{ov} \quad (3.29)$$

Where t_R represents the retention time of a specific solute, q_{ov} denotes the corrected carrier gas flow rate at the outlet, t_G, is the unretained gas retention time.

The corrected gas flow rate taking into account the water vapour pressure was calculated using (Equation 3.30).

$$q_{ov} = q_o \left(\frac{T}{T_f}\right)\left[1 - \frac{P_w^*}{P_o}\right] \tag{3.30}$$

Where q_o is the measure of flow rate, T_f is the flow meter temperature and P_w^* is the saturated vapour pressure of water at T_f.

The pressure correction term J_2^3 is given in (Equation 3.31) which was detailed by Everett *et al*. (1965).

$$J_2^3 = \frac{2}{3}\frac{\left(\frac{P_i}{P_o}\right)^3 - 1}{\left(\frac{P_i}{P_o}\right) - 1} \tag{3.31}$$

P_i is the inlet flowmeter pressure.

The saturated vapour pressures were calculated using the Antione equations (Poling, Prausnitz and O'connel 2001). Literature by Poling, Praunsitz and O'connel, (2001) and Lide *et al.* (2004), presented correlation of constant vapour pressure. Critical data of solutes obtained from literature were used to calculate B_{11} and B_{12} and ionization energies utilized in the calculation of T_{12}^c, (Klincewicz and Reid,1984).

The second virial coefficients of pure solutes, B_{11}, were calculated using (Equations 3.32 to 3.37), (Mcglashan and Potter, 1962).

$$\frac{B_{11}}{V_c} = 0.430 - 0.886\left(\frac{T_c}{T}\right) - 0.694\left(\frac{T_c}{T}\right)^2 - 0.0375\,(n-1)\left(\frac{T_c}{T}\right)^{4.5} \tag{3.32}$$

$$\frac{BP_c}{RT_c} = \frac{B}{V^*} = f^{(0)} + \omega f^{(1)} + af^{(2)} + bf^{(3)} \tag{3.33}$$

$$f^{(0)} = 0.1445 - \frac{0.330}{T_r} - \frac{0.1385}{T_r^2} - \frac{0.0121}{T_r^3} - \frac{0.000607}{T_r^8}\pi r^2 \tag{3.34}$$

$$f^{(1)} = 0.0637 + \frac{0.331}{T_r^2} - \frac{0.423}{T_r^2} - \frac{0.008}{T_r^8} \tag{3.35}$$

$$f^{(2)} = \frac{1}{T_r^6} \tag{3.36}$$

$$f^{(3)} = -\frac{1}{T_r^8} \tag{3.37}$$

Where $f^{(0)}$, $f^{(1)}$, $f^{(2)}$, and $f^{(3)}$ denotes the correlation term explained by Tsonopolus, (1974), B_{11}, is the second virial coefficient, P_c, the critical pressure, T_c, the critical temperature, V^*, the characteristic volume, ω, the acentric factor, and T_r the reduced temperature. The *a* and *b* values, correlations were used from the study of Tsonopoulos and Heidman, (1990) and Tsonopoulos and Dymond, (1997).

The cross virial coefficient, B_{12}, was calculated by using (Equation 3.33) with mixing rules of Tsonopoulos, (1974).

The mixed critical parameters were calculated from (Equation 3.38 to 3.41).

$$T_{cij} = \left(T_{cii}T_{cjj}\right)^{\frac{1}{2}}\left(1 - k_{ij}\right) \tag{3.38}$$

$$V_{ij}^{*} = \frac{\left(V_{cii}^{\frac{1}{3}} + V_{cij}^{\frac{1}{3}}\right)^{3}}{4\left(Z_{cii} + Z_{cjj}\right)} \tag{3.39}$$

$$\omega_{ij} = \frac{\omega_{ii} + \omega_{jj}}{2} \tag{3.40}$$

$$a_{ij} = \frac{a_{ii} + a_{jj}}{2} \tag{3.41}$$

$$b_{ij} = \frac{b_{ii} + b_{jj}}{2} \tag{3.42}$$

Where the binary intermolecular parameter is specifically k_{ij} and V_c the critical volume.

3.5.1 Excess thermodynamic functions at infinite dilution

To calculate the values of entropies and enthalpies at infinite dilution, Vant Hoff's relation (Equation 3.43) was used (Bahadur and Govender, 2014). The excess thermodynamic parameters ($\Delta H_1^{\mathrm{E},\infty}$, $\Delta S_1^{E,\infty}$ and $\Delta G_1^{\mathrm{E},\infty}$) were used to further explain the interactions between DESs and solutes.

$$\ln(\gamma_{13}^{\infty}) = \frac{\Delta H_1^{\mathrm{E},\infty}}{RT} - \frac{\Delta S_1^{\mathrm{E},\infty}}{R} \tag{3.43}$$

The natural logarithm of experimental activity coefficients at infinite dilution versus 1/T data was fitted to a straight line and using (Equation 3.44) thermodynamics excess properties were determined.

$$\ln\gamma_{13}^{\infty} = \frac{a}{T} + b \tag{3.44}$$

Where b, denotes the intercept, a, the slope; $\Delta H_1^{\mathrm{E},\infty} = aR$ and $\Delta S_1^{\mathrm{E},\infty} = -bR$. The Gibbs energies were obtained by using (Equation 3.45).

$$\Delta G_i^{\mathrm{E},\infty} = RTln\left(\gamma_i^{\mathrm{E},\infty}\right) = \Delta H_i^{\mathrm{E},\infty} - T\Delta S_i^{\mathrm{E},\infty} \tag{3.45}$$

3.5.2 Selectivity and capacity

The selectivity and capacity values were calculated using (Equations 3.46 and 3.47).

$$S_{ij}^{\infty} = \frac{\gamma_i^{\infty}}{\gamma_j^{\infty}} \tag{3.46}$$

$$K_j^{\infty} = \frac{1}{\gamma_j^{\infty}} \tag{3.47}$$

S_{ij}^{∞} and K_j^{∞} denote the limiting values of selectivity and capacity at infinite dilution for a solvent mixture containing solutes i and j, respectively (Seader *et al.* 1998b).

3.5.3 Calculation of uncertainty

The propagation law of uncertainties principle was applied to determine the error values for thermodynamic data obtained. Accuracy, repeatability, uncertainties in conducting the experimental work were considered when calculating the error values. Error values were calculated using (Equation 3.48).

$$u(\theta) = \sqrt{\sum_{i=1}^{y} \left[\frac{\partial \theta}{\partial \theta}\, u(x_i)\right]^2} \qquad (3.48)$$

Where θ is the computed variable (γ_{13}^{∞}) activity coefficient at infinite dilution in this study, $u(\theta)$ is the error in (γ_{13}^{∞}), the number of independent variables and the independent variable in calculating θ is represented by x_1. Considering repeatability of type A, distributions of q repetitions. The error (u_r) is given by the standard deviation (Equation 3.49).

$$u_r(\theta) = \sigma = \sqrt{\frac{1}{n-1}\sum_{j=1}^{q}\left(\theta_j - \theta^{-}\right)^2} \qquad (3.49)$$

Where θ^{-} is the mean value of θ and θ_j is the j^{th} repetition.

CHAPTER 4

EXPERIMENTAL

4.1 Instrumentation

4.1.1 Densitometer and sound velocity analyser

Thermophysical properties including density and speed of sound were measured using a densitometer and sound velocity analyser, Anton Paar DSA 5000M (Graz, Austria) with microviscometer LOVIS 2000 ME AND Xs sampler 452 and refractive index using the Anton Paar refractometer, Abbemat 3200. Figure 4.1 is the photograph of the Anton Paar DSA 5000M coupled with microviscometer Lovis 2000ME and X sampler 452.

Figure 4.1: Photograph of the Anton Paar DSA 5000M coupled with microviscometer Lovis 2000ME and X sampler 452.

Table 4.1 is the density and sound velocity analyser DSA 5000 M instrument specifications.

Table 4-1: Density and sound velocity analyser DSA 5000 M instrument specifications.

Property	Range
Measurement range for density	(0 to 3) $g \cdot cm^{-3}$
Measurement rang for speed of sound	(1000 to 2000) $m \cdot s^{-1}$
Temperature measurement range	(298.15 to 343.15) K
Pressure range	(0 to 3) MPa
Repeatability density	0.000001 $g \cdot cm^{-3}$
Repeatability speed of sound	0.1 $m \cdot s^{-1}$
Repeatability temperature	298.15 K
Sample volume	Approximately 3 cm^3
Ambient air pressure sensor	Yes
Automatic bubble detection	Yes
Reference oscillator	Yes
Visual check of the density measuring cell	Camera

Figure 4.2 is the photograph of the Anton Paar Refractometer, Abbemat 3200.

Figure 4.2 is the photograph of the Anton Paar Refractometer, Abbemat 3200.

Table 4.2 is the refractive index analyser Anton Paar Refractometer, Abbemat 3200 instrument specifications.

Table 4-2: is the refractive index analyser Anton Paar Refractometer, Abbemat 3200 instrument specifications.

Property	Range
Measurement rang for refractive index	(1.30 to 1.72)
Temperature measurement range	(288.15 to 333.15) K

Table 4.2 is the ionic salts (HBA) and organic solvent (HBD) used for the preparation of deep eutectic solvent for thermophysical measurements together with the supplier, purity and CAS No.

Table 4-3: Ionic salts (HBA) and organic solvent (HBD) used for the preparation of deep eutectic solvent for thermophysical measurements together with the supplier, purity and CAS No.

Solvents	**Supplier**	**Purity**	**CAS No.**
1-butyl-3-methylimidazolium chloride	Sigma Aldrich	≥ 99%	79917-90-1
1-butyl-2,3-dimethylimidazoliun chloride	Sigma Aldrich	≥ 99%	98892-75-2
Ethylene glycol	Merck	≥ 99%	107-21-1

The list of alcohols and carboxylic acids used in the preparation of the binary mixtures together with the supplier, purity and CAS number is given in Table 4.3.

Table 4-4: Alcohols and carboxylic acids used in the preparation of the binary mixtures together with the supplier, purity and CAS No.

Solvents	**Supplier**	**Purity**	**CAS No.**
Methanol	Sigma Aldrich	≥ 99%	67-56-1
Ethanol	Sigma Aldrich	≥ 99%	64-17-5
Acetic acid	Sigma Aldrich	≥ 99%	64-19-7
Propanoic acid	Sigma Aldrich	≥ 99%	79-09-4

4.2 Procedure

4.2.1 Preparation of deep eutectic solvents

The method described by Smith and Abbott (2024) and Liu *et al.* (2021) was used for the preparation of the deep eutectic solvents. Deep eutectic solvents investigated were prepared at a mole ratio of 1:3 using ionic salts (1-butyl-3-methylimidazolium chloride, [BMIM]Cl and 1-butyl-2,3-dimethylimidazolium chloride, [BDMIM]Cl, and tetrabutylammonium acetate, [TBN AcO] as hydrogen bond acceptors, and ethylene glycol [EG] and diethylene glycol [DEG] was used as the hydrogen donors. The structure of these compounds are represented in Figure 4.3. and Figure 4.4, respectively. Before preparation of the DES, the individual components were purified using a Heidolph rotary evaporator (Schwabach, Germany) to ensure that no impurities or volatiles were present in the compounds. A known mass of 1-butyl-3-methylimidazolium chloride or 1-butyl-2,3-dimethylimidazolium chloride or tetrabutylammonium acetate pr ethylene glycol were measured using an analytical balance (AS 220.R2 PLUS), (Radwag, Poland) with a precision of 0.0001 g. Thermostatic water bath was used to mix the components for 2 – 3 hours with stirring at a specific temperature, T = 333.15 K until the clear and homogeneous solvents were obtained. The deep eutectic solvent was then further purified using a rotary evaporator for a period of 4-5 hours. Determination of water content was done prior to the DESs analysis using a Karl-Fischer auto titrator 870 KF Titrino plus (Herisau, Switzerland) and was found to have 0.0004% water content. The prepared DESs was cooled and stored in an airtight vial and placed in a desiccator. The structure of (a) [BMIM]Cl, (b) [BDMIM]Cl obtained from ChemDraw is given in Figure 4.3.

The structure of (a) [BMIM]Cl, (b) [BDMIM]Cl obtained from ChemDraw is given in Figure 4.3.

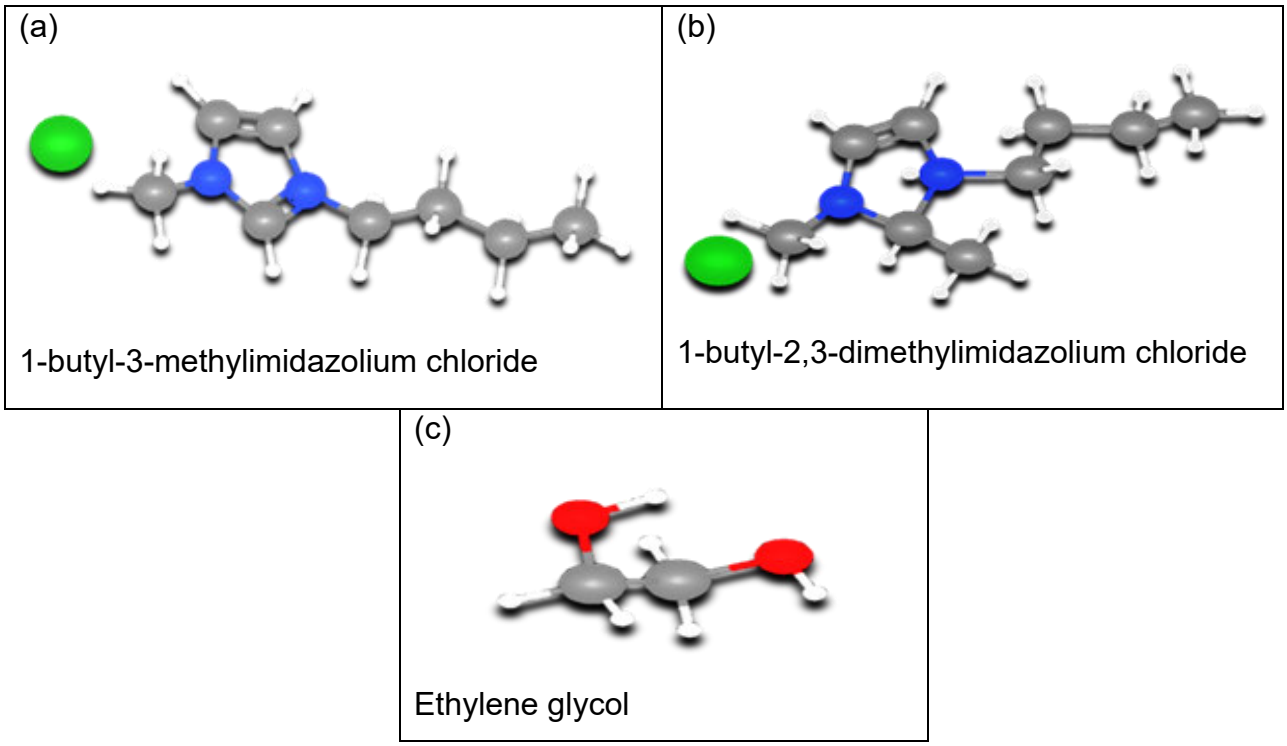

Figure 4.3: Structure of (a) [BMIM]Cl, (b) [BDMIM]Cl obtained from ChemDraw.

Figure 4.4 is the structure of (a) [TBN AcO], (b) [DEG], obtained from ChemDraw.

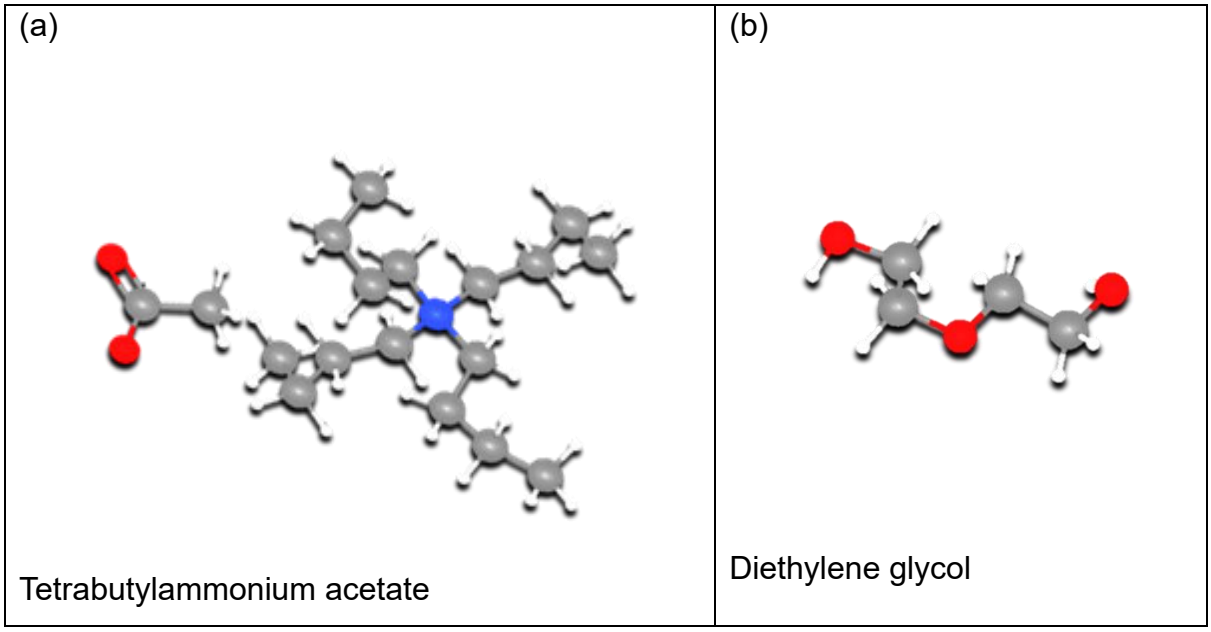

Figure 4.4: Structure of (a) [TBN AcO], (b) [DEG], obtained from ChemDraw.

The molar ratio used in this work was chosen because it offered a greater difference in the availability of HBA than HBD when compared to 1:2 molar ratio (Shekaari *et al*. 2020b). Additionally, the 1:3 molar ratio of HBA to HBD results in a lower melting point compared to the 1:2 molar ratio, making it more appropriate for low temperature applications. The following DESs were prepared according to the method above.

- DES1 - 1-butyl-3-methylimidazolium chloride + ethylene glycol, ([BMIM]Cl: EG).
- DES2 - 1-butyl-2,3-dimethylimidazolium chloride + ethylene glycol, ([BDMIM]Cl: EG).
- DES3 - Tetrabutylammonium acetate + ethylene glycol, ([TBN AcO]: EG)
- DES4 - Tetrabutylammonium acetate + diethylene glycol, ([TBN AcO]: DEG)

The physicochemical properties of the DES can be modified by the selection of the appropriate HBA and HBD and adjusting the mole ratio between the HBA and HBD.

The Heidolph rotary evaporator used in this work is shown in Figure 4.5.

Figure 4.5: Photograph of the Heidolph rotary evaporator.

Table 4.5 is the Heidolph rotary evaporator instrument specifications.

Table 4-5: is the Heidolph rotary evaporator instrument specifications.

Property	Range
Vacuum	(1 and 200) mbar; default value; 1000mbar
Rotation	(10 and 290) rm in 1 rm increment; default value; 100rm
Heating bath	313.15 K and max. temperature of the heating bath (to be assign in setup), however, no more than 503.15 K.

4.2.2 Preparation of binary mixturesp

The binary mixtures of the deep eutectic solvents DES1 and DES2 with alcohols namely: methanol or ethanol, and with carboxylic acids namely: acetic acid or propanoic acid, were prepared by mixing the two compounds over the whole mole fraction range (0 -1). The binary mixtures were prepared into a small airtight vial with known composition of the DES and alcohols and carboxylic acids. The binary mixtures were vigorously mixed to ensure homogeneity of the mixture. Each solvent was transferred to a glass vial using a dropper and accurately weighed using an AD 220.R2 PLUS analytical balance with an accuracy of 0.0001 g.

4.2.3 Thermophysical properties

4.2.3.1 Density and sound velocity measurements

Ethanol was used to rinse the measuring cell of the DSA 500M as it dissolves any sample residues in the U-tube cell. Acetone is volatile and is soluble in ethanol, it was used for the second rinsing to remove ethanol and accelerate the drying of the cell under a stream of dry air. After rinsing and cleaning, the instrument was calibrated by ultra-pure water and ambient air. The purpose of calibration was to ensure the precision of density measurements. Density and sound velocity of the

binary mixtures and of the pure components were measured using an Anton Paar DSA 5000M with microviscometer LOVIS 2000 ME and Xs sampler 452 fitted with the digital vibrating tube density and sound velocity analyser illustrated in Figure 4.1. The instrument has an accuracy of ±0.1 $m{\cdot}s^{-1}$ in sound velocity, ±7x10^{-6} $g{\cdot}cm^{-3}$ in density and ±0.01 K in temperature. After each run, ethanol was used to flush the U-tube and acetone to dry the cell. It was important to carry out the cleaning routine after each measurement to eliminate cross contamination. The instrument has peltier element to control and maintain the temperature at ±0.01 K during the measurements of density and sound velocity.

The instrument uses an oscillating U-tube to measure density simultaneously with sound velocity ranging between (1000 – 2000) $m{\cdot}s^{-1}$ and the density between (0-3 x10^{3}) $kg{\cdot}m^{-3}$ at temperature T = (273.15-343.15) K, pressure (0-0.2) MPa, and at a frequency of 3 MHz. Density and sound velocity uncertainties were ±0.002 $g{\cdot}cm^{-3}$ and 0.8$m{\cdot}s^{-1}$, respectively. Excess molar volume, isentropic compressibilities, variation isentropic compressibilities, and intermolecular free length were computed from the measured densities and speed of sound.

4.2.3.2 Refractive index measurements

The refractive index (n_D) was determined using an Anton Paar Refractometer Abbetmat 3200 with an accuracy of ±0.0001. De-ionized water was used to calibrate the refractometer, and calibration verification was done periodically after each measurement. The measurements were carried out at T = (293.15, 298.15, 303.15, 308.15 and 313.15) K and at ambient pressure.

4.2.4 Computational Analysis

4.2.4.1 Optimization of Binary Structures

Chemical structures of {1-butyl-2,3-dimethylimidazolium chloride [BDMIM]Cl: ethane-1,2-diol (ethylene glycol), or acetic acid or propanoic acid}. The structures were optimized with the help of ChemDraw Professional tool (Cousins *et al.* 2005). The structures were optimized using molecular mechanics force field or MM2 prior to DFT calculations. The structure of 1:3 [BDMIM]Cl: EG + acetic acid or propanoic acid and

1:3 [BMIM]Cl: EG, methanol or ethanol were designed in Gaussian using optimized structures obtained from ChemDraw.

The chemical structures of [BDMIM]Cl: EG + acetic acid or propanoic acid were designed with the help of ChemDraw Professional tool (Cousins *et al.* 2005). The structures were optimized using molecular mechanics forcefield or MM2 prior to DFT calculations. The structure of 1:3 DES [BDMIM]Cl: EG + acetic acid or propanoic acid were designed in Gaussian using optimized structures obtained from ChemDraw.

The binary systems {([BMIM]: EG) + methanol or ethanol} were generated using the following workflow that isolated the optimal configuration position of ethylene glycol before optimisation of the binary complex. The [BMIM]Cl complex and the ethylene glycol molecule were drawn and optimized separately using conjugate gradient minimization algorithm, Polak-Ribiere conjugate gradient (prcg) of Macromodel to acquire a low energy confirmation using the OPLS4 molecular mechanics forcefield for the computation of energy parameter, (Lu *et al.* 2022), (Mohamadi et al. 1990). The Jaguar Quantum Mechanics package with computations occurring at the 6-31G++** basis set of the dispersion corrected B3LYP-D3 functional in vacuo was used to optimize the [BMIM]Cl complex and late the EG molecule separately, (Banks *et al.* 2005), (Parr *et al.* 1984). The optimized [BMIM]Cl complex was merged with the optimized EG molecule isolating 6 distinct systems of the possible positions of the EG relative to Cl ion. Each of these 6 possible systems were optimized using the MacroModel geometry optimization algorithm with the [BMIM]Cl atoms restrained and the EG atoms allowed to move freely. The systems were further optimized at the 6-31G++** level using the M06-2X-D3 functional, (Long *et al.* 2020), (Kumar *et al.* 2022). Single Point Energy (SPE) calculations for each of the optimized configurations were calculated at the 6-31G++** level using the M06-2X-D3 density functional theory in vacuo. The lowest energy configuration was selected as the optional configuration for the purposes of our studies. This optimal configuration was optimized in the presence of either implicit methanol (dielectric constant, ε = 32.63), ethanol (dielectric constant, ε = 32.63) solvent models acquired from the Poisson Boltzmann Finite (PBF) element method, (Banks *et al.* 2005) prior to analysis of the interactions. The counterpoise correction method was applied to the solvent optimized systems to acquire a counterpoise corrected interaction energy of the complex obtained after optimization

in the presence of solvent, (Lu *et al.* 2021). Analyses of the optimized system in the presence of implicit solvent included determination of the electrostatic characteristics, measurement of interatomic distance, estimation of the interaction energies and calculations of the HOMO-LUMO gap. SPE calculations of the interacting partners were performed using the M06-2X-D3 functional at the 6-31G++** level and calculations of the HOMO/LUMO molecular orbitals, the partial charge and the electrostatic potential surfaces were computed at this level, (Mulliken *et al.* 1955), (Hevia *et al.* 2022). Where necessary the solvent phase calculations were performed using the PBF implicit solvation model prior to analysis of the interactions in the presence of either methanol (dielectric constant, ε = 32.63), or ethanol (dielectric constant, ε = 32.63) solvents, (Kiran Kumar *et al.* 2022). Jagua (version 12.0) was used for all DFT calculations conducted at a pressure of 1 atmospheric and temperature of 298.15 K with SCF convergence occurring within 200 interactions for all calculations, (Khirade, *et al.* 1999).

4.3 Characterization of deep eutectic solvents

4.3.1 Thermogravimetric analysis

Thermogravimetric instrument – TGA/SDTA851e/SF/110 (Greitfensee, Switzerland) was used to determine the stability of deep eutectic solvents under investigation. TGA technique is used to measure the change in weight of a sample as a function of temperature while it is subjected to controlled conditions. The TGA characterizes the materials that demonstrate weight loss or gain due to decomposition, oxidation or dehydration. The heat application ranges from 28℃ - 600℃.

4.3.2 FTIR analysis

To characterize and confirm the structural functional groups of the prepared DESs, ([TBN] AcO: EG) and ([TBN] AcO: DEG), FTIR PerkinElmer (originated from Waltham, Massachusetts, USA) was used to analyse the investigated DESs. The FTIR spectrum of DESs were analysed over a wavelength range of (4000 – 4000) cm^{-1}.

4.3.3 Nuclear Magnetic Resonance Spectrometer (NMR)

The Bruker's Fourier 80HD NMR (Rheinstetten, Germany) was used to identify the functional groups of the investigated DESs and the molecular structure based on the observed peaks positions in the spectrum.

4.4 Activity coefficients at dilution

4.4.1 Preparation of the stationary phase

The technique for column preparation was sourced from the literature, (Domańska *et al.* 2008), (Letcher *et al.* 1996), and (Moollan *et al.* 1993). The prepared solvents and chromosorb which served as the stationary phase were mixed with dichloromethane to enhance an even layer of DES on the chromosorb. This was further followed by the application of a rotary evaporator to remove dichloromethane. The mass of DES and chromosorb was weighed using an analytical balance AD 220.R2 Plus with a precision of 0.0001 g. A 1 m long and 4 mm in diameter of a stainless-steel column was used to pack the prepared loading material. The column was cleaned with a hot soapy water, rinsed with distilled water and was dried using acetone. The mass of the column was weighed before and after packing so as to calculate the mass of the stationary phase packed.

The ends of the column were stopped with glass wool. The column was coiled and inserted into the gas liquid chromatography oven and conditioned at a temperature of 358 K for a period of 6 hrs to remove any volatiles in the column. The packing of the column by mass percentage of deep eutectic ([TBN AcO]: EG) and ([TBN AcO]: DEG) as the entrainers was (26.3 – 31.4 %), high enough to reduce any adsorption on to the packed column. Two packed columns of each prepared entrainer ([TBN AcO]: EG) and ([TBN AcO]: DEG) were used for each set of experimental data and the average activity coefficients values were reported.

4.4.2 Gas liquid chromatography

Everett, (1965) and Cruckshank, Windsor and Young, (1996) developed a method for determining activity coefficient at infinite dilution (γ_{13}^{∞}) of volatile solutes in low volatility solvents using gas liquid chromatography. For this study gas liquid chromatography

was used to obtain the retention data for solutes in the DES. The retention data was utilized to compute activity coefficients at infinite dilution. The column temperature for analysis was set at T = (313.15, 323.15, 335.15, 343.15 and 535.15) K and the column temperature was kept constant at $\pm$ 0.02 K.

4.4.3 Gas liquid chromatography measurements

Measurements of the retention data for the volatile organic solvents in the deep eutectic solvents by gas-liquid chromatography (Shimadzu GC-2014), (Tokyo, Japan) integrated with a thermal conductivity detector (TCD). The gas liquid chromatography oven was operated at different temperature between temperature range of (313.15 – 353.15) K and at 10K interval. Helium was used as an inert carrier gas and set at a flow rate of 30 mL/min. A soap bubble flow meter located at the outlet of the gas chromatography detector was used to determine the flow rate of the carrier gas. To maintain the state of infinite dilution, the solute injection volume of (0.1 – 0.5) µL was manually injected into the gas liquid chromatography injector port that was set at T = 473 K. The flow rate was corrected for the water vapor in the flow meter. The solute injection was repeated at least two to three times for each experimental temperature to evaluate the stability and reproducibility of the experimental conditions. At each investigated temperature, the values of the dead time (t_G) were measured by utilizing air as non-retainable component with the assumption that the solubility impact of air in the stationary phase is trivial. This measurement was repeated at least two times to determine the repeatability. A pressure transducer application in the gas liquid chromatography was utilized to measure the pressure drop $(P_1 - P_o)$ and was within the range of (38 – 61) kPa depending on the temperature conditions and uncertainty. A digital barometer was used to measure the outlet pressure (P_o), which was the same as the atmospheric pressure.

Figure 4.6 is the schematic diagram of gas-liquid chromatography obtained from google GLC images.

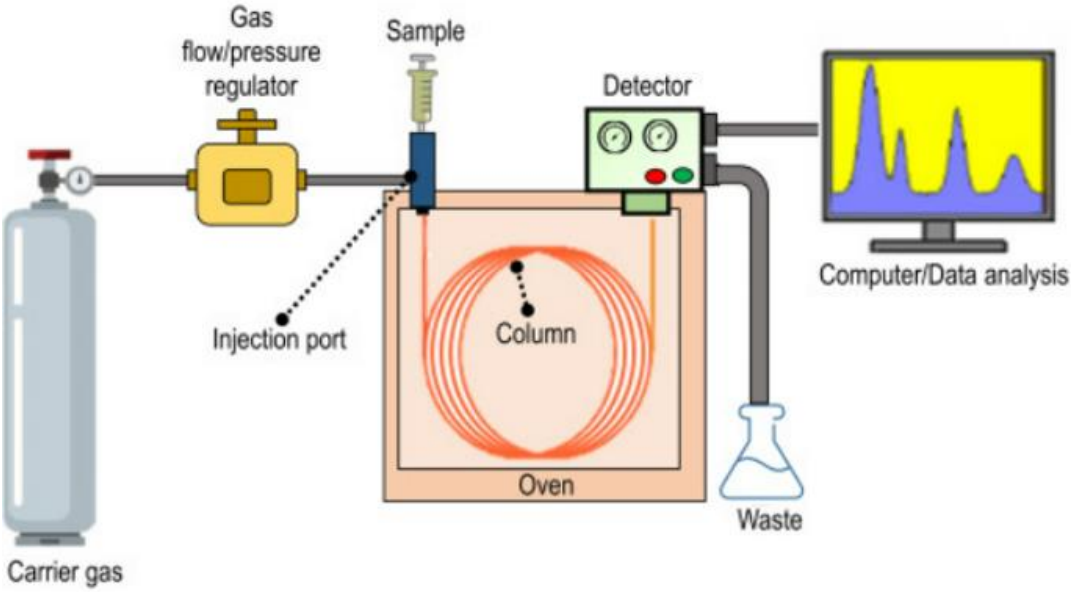

Figure 4.6: Schematic diagram of gas-liquid chromatography obtained from google GLC images.

Figure 4.7 is the schematic diagram of thermal conductivity obtained from google thermal conductivity images.

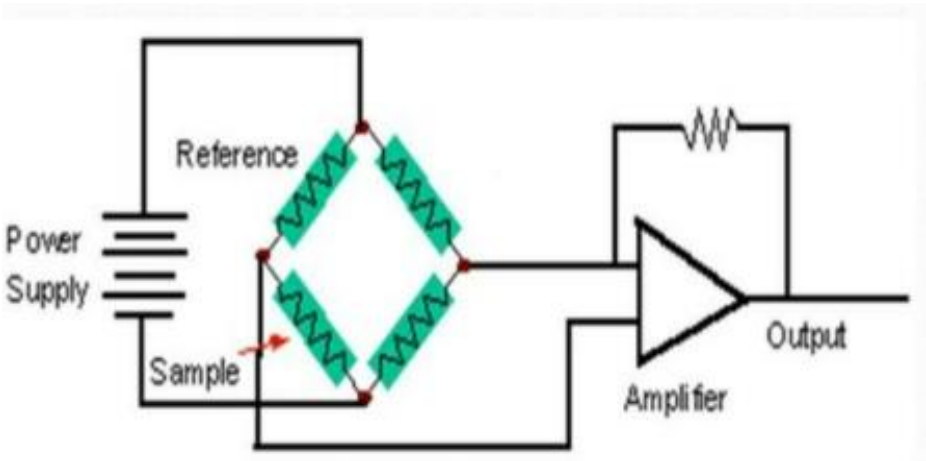

Figure 4.7: Schematic diagram of thermal conductivity obtained from google thermal conductivity images.

Thermal conductivity detector is a chemical specific and bulk property detector primarily used in gas chromatography. Since most compounds utilized have lower thermal conductivities compared to the inert gas used in gas chromatography, the effluent thermal conductivity decreases when an analyte elutes the column, resulting in a detectable signal. This type of detector consists of an electrically heated filament within a temperature-controlled cell. Although this detector is less sensitive compared to other detectors, it is non-specific and non-destructive, and it is particularly useful for initial examinations involving unknown samples. The chemical specification: supplier, mass fraction purity and CAS number of all studied organic solvents are given in Table 4.4.

Table 4-6: Chemical specification: supplier, mass fraction purity and CAS number of all studied organic solvents.

Solutes	Chemical formula	Supplier	Mass fraction purity	CAS No.
2.2-dimethylbutane	$(CH_3)_3CCH_2CH_3$	Sigma Aldrich	≥ 0.99	75-83-2
Pentane	C_5H_{12}	Sigma Aldrich	≥ 0.99	109-66-0
Hexane	C_6H_{14}	Sigma Aldrich	≥ 0.99	110-54-3
Heptane	C_7H_{16}	Sigma Aldrich	≥ 0.99	142-82-5
Octane	C_8H_{18}	Sigma Aldrich	≥ 0.99	111-65-9
n-Nonane	C_9H_{20}	Merck	≥ 0.99	111-84-2
n-Decane	$C_{10}H_{22}$	Merck	≥ 0.99	124-18-5
1-Pentene	C_2H_4	Sigma Aldrich	≥ 0.99	109-67-1
1-Hexene	C_6H_{12}	Sigma Aldrich	≥ 0.99	592-41-6
1-Heptene	C_7H_{14}	Sigma Aldrich	≥ 0.99	592-76-7
1-Nonene	C_9H_{18}	Fluka	≥ 0.99	124-11-8
1-Decene	$C_{10}H_{20}$	Fluka	≥ 0.99	872-05-9
Cyclohexene	C_6H_{10}	Merck	≥ 0.97	110-83-8
Cyclohexane	C_6H_{12}	Merck	≥ 0.98	110-82-7
Cyclooctane	C_8H_{16}	Merck	≥ 0.99	292-64-8
1-Pentyne	C_5H_8	Sigma Aldrich	≥ 0.99	627-19-0
1-Hexyne	C_6H_{10}	Sigma Aldrich	≥ 0.99	693-02-7
1-Heptyne	C_7H_{12}	Sigma Aldrich	≥ 0.99	628-71-7

Benzene	C_6H_6	Sigma Aldrich	≥ 0.99	71-43-2
Toluene	$C_6H_2CH_3$	Sigma Aldrich	≥ 0.99	108-88-3
Ethylbenzene	C_8H_{10}	Sigma Aldrich	≥ 0.99	100-41-4
m-Xylene	C_8H_{10}	Sigma Aldrich	≥ 0.99	108-38-3
p-Xylene	C_8H_{10}	Sigma Aldrich	≥ 0.99	106-42-3
o-Xylene	C_8H_{10}	Sigma Aldrich	≥ 0.99	95-47-6
Methanol	CH_3OH	Sigma Aldrich	≥ 0.99	67-56-1
Ethanol	C_2H_6O	Sigma Aldrich	≥ 0.99	64-17-5
1-Propanol	C_3H_8O	Sigma Aldrich	≥ 0.99	71-23-8
1-Butanol	$C_4H_{10}O$	Sigma Aldrich	≥ 0.99	71-36-3
THF	C_4H_8O	Sigma Aldrich	≥ 0.99	109-99-9
Acetonitrile	C_2H_3N	Sigma Aldrich	≥ 0.99	75-05-8
Thiophene	C_4H_4S	Sigma Aldrich	≥ 0.99	110-02-1
Acetone	C_3H_6O	Sigma Aldrich	≥ 0.99	67-64-1
2-Butanone	C_4H_8O	Sigma Aldrich	≥ 0.99	78-93-3
Tetrabutyl ammonium acetate	$C_{18}H_{39}NO_2$	Sigma Aldrich	≥ 0.99	10534-59-5
Ethylene glycol	$C_2H_6O_2$	Sigma Aldrich	≥ 0.95	107-21-1
Diethylene glycol	$C_4H_{10}O_3$	Sigma Aldrich	≥ 0.95	111-46-6

CHAPTER 5

RESULTS

5.1 Thermophysical properties of DES and its binary mixtures

5.1.1 1-Butyl-3-methylimidazolium chloride: ethylene glycol + methanol or ethanol

The results for the density, ρ , speed of sound,u , and refractive index, n_D is given in Table 5.1

Table 5-1: Density, $\boldsymbol{\rho}$, speed of sound, $\boldsymbol{u}$, and refractive index, $\boldsymbol{n_D}$ of {[BMIM]Cl: EG + methanol or ethanol} binary mixtures at different temperatures and at atmospheric pressure.

DES + methanol				DES + ethanol				% Deviation
x_1	ρ/(g·cm^{-}	u/(m·s^{-1})	n_D	x_1	ρ/(g·cm^{-3})	u/(m·s^{-1})	n_D	u
***T* = 293.15 K**								
0.0000	0.7924	1120.39	1.3298	0.0000	0.7954	1173.42	1.3599	-4,7332
0.0399	0.8861	1264.92	1.3731	0.0400	0.8589	1272.75	1.3842	-0,6190
0.0900	0.9450	1383.56	1.4010	0.0905	0.9119	1362.81	1.4040	1,4998
0.1050	0.9596	1457.28	1.4065	0.1050	0.9236	1384.11	1.4080	5,0210
0.2034	1.0110	1545.46	1.4318	0.2044	0.9804	1497.32	1.4313	3,1149
0.3050	1.0362	1617.22	1.4431	0.3049	1.0137	1571.84	1.4434	2,8060
0.4045	1.0517	1658.49	1.4510	0.4050	1.0353	1623.38	1.4492	2,1170
0.5047	1.0624	1686.97	1.4562	0.5045	1.0506	1660.80	1.4547	1,5513
0.6045	1.0705	1707.40	1.4597	0.6039	1.0621	1687.95	1.4588	1,1392
0.7047	1.0768	1722.99	1.4628	0.7040	1.0709	1710.63	1.4618	0,7174
0.7988	1.0816	1734.60	1.4647	0.8046	1.0783	1728.42	1.4643	0,3563
0.9045	1.0861	1745.34	1.4665	0.9019	1.0843	1742.02	1.4665	0,1902
1.0000	1.0893	1752.93	1.4681	1.0000	1.0893	1752.93	1.4681	0,0000
***T* = 298.15 K**								
0.0000	0.7872	1104.59	1.3279	0.0000	0.7910	1156.58	1.3579	-3.1786
0.0399	0.8820	1250.57	1.3713	0.0400	0.8549	1257.45	1.3825	-1.6933

0.0900	0.9411	1370.10	1.3997	0.0905	0.9081	1348.46	1.4023	2,6451
0.1050	0.9559	1443.99	1.4052	0.1050	0.9199	1369.70	1.4064	6,1482
0.2034	1.0074	1532.70	1.4304	0.2044	0.9768	1483.82	1.4309	4,0732
0.3050	1.0329	1604.90	1.4417	0.3049	1.0103	1559.06	1.4414	3,6681
0.4045	1.0483	1646.32	1.4497	0.4050	1.0320	1610.57	1.4478	2,9508
0.5047	1.0591	1674.93	1.4548	0.5045	1.0473	1648.29	1.4534	2,3231
0.6045	1.0673	1695.45	1.4584	0.6039	1.0588	1675.54	1.4575	1,9069
0.7047	1.0735	1711.05	1.4614	0.7040	1.0677	1698.39	1.4606	1,4418
0.7988	1.0785	1722.77	1.4634	0.8046	1.0751	1716.28	1.4630	1,0680
0.9045	1.0830	1733.54	1.4652	0.9019	1.0811	1729.93	1.4652	0,9028
1.0000	1.0862	1741.24	1.4668	1.0000	1.0862	1741.24	1.4668	0,6909
	T = 303.15 K							
0.0000	0.7843	1088.64	1.3261	0.0000	0.7867	1139.70	1.3559	-4,6866
0.0399	0.8799	1235.96	1.3700	0.0400	0.8509	1241.90	1.3807	-0,4275
0.0900	0.9384	1356.39	1.3984	0.0905	0.9043	1333.86	1.4008	1,7238
0.1050	0.9537	1430.16	1.4037	0.1050	0.9161	1355.21	1.4048	5,3536
0.2034	1.0050	1519.71	1.4290	0.2044	0.9733	1470.27	1.4292	3,2928
0.3050	1.0302	1592.10	1.4403	0.3049	1.0069	1546.03	1.4395	2,9557
0.4045	1.0456	1633.93	1.4483	0.4050	1.0286	1597.74	1.4464	2,2621
0.5047	1.0561	1662.73	1.4536	0.5045	1.0440	1636.02	1.4519	1,6499
0.6045	1.0643	1683.30	1.4569	0.6039	1.0555	1663.12	1.4560	1,2243
0.7047	1.0704	1698.87	1.4599	0.7040	1.0645	1686.38	1.4592	0,7607
0.7988	1.0754	1710.71	1.4620	0.8046	1.0719	1704.37	1.4616	0,3791
0.9045	1.0797	1721.51	1.4638	0.9019	1.0779	1717.89	1.4638	0,2176
1.0000	1.0830	1729.21	1.4655	1.0000	1.0830	1729.21	1.4655	0,0000
	T = 308.15 K							
0.0000	0.7820	1072.63	1.3259	0.0000	0.7823	1122.90	1.3539	-4,6866
0.0399	0.8782	1221.14	1.3683	0.0400	0.8468	1226.36	1.3797	-0,4275
0.0900	0.9364	1342.39	1.3967	0.0905	0.9004	1319.25	1.3992	1,7238
0.1050	0.9519	1416.61	1.4022	0.1050	0.9123	1340.77	1.4032	5,3536
0.2034	1.0028	1506.33	1.4277	0.2044	0.9697	1456.73	1.4275	3,2928
0.3050	1.0277	1579.34	1.4389	0.3049	1.0034	1532.66	1.4380	2,9557
0.4045	1.0430	1621.50	1.4469	0.4050	1.0252	1584.82	1.4450	2,2621

0.5047	1.0533	1650.43	1.4521	0.5045	1.0406	1623.20	1.4506	1,6499
0.6045	1.0614	1671.10	1.4555	0.6039	1.0523	1650.64	1.4546	1,2243
0.7047	1.0673	1686.63	1.4585	0.7040	1.0612	1673.80	1.4578	0,7607
0.7988	1.0722	1698.61	1.4607	0.8046	1.0686	1692.17	1.4603	0,3791
0.9045	1.0766	1709.46	1.4625	0.9019	1.0747	1705.74	1.4625	0,2176
1.0000	1.0798	1717.26	1.4641	1.0000	1.0798	1717.26	1.4641	0,0000
	T = 313.15 K							
0.0000	0.7794	1057.31	1.3249	0.0000	0.7779	1106.24	1.3518	-4,6278
0.0399	0.8762	1206.85	1.3663	0.0400	0.8427	1210.87	1.3771	-0,3331
0.0900	0.9345	1328.78	1.3952	0.0905	0.8966	1304.65	1.3976	1,8160
0.1050	0.9499	1403.14	1.4006	0.1050	0.9085	1326.34	1.4017	5,4734
0.2034	1.0003	1493.21	1.4262	0.2044	0.9662	1443.11	1.4260	3,3552
0.3050	1.0251	1566.45	1.4376	0.3049	1.0000	1519.52	1.4366	2,9959
0.4045	1.0402	1609.02	1.4456	0.4050	1.0218	1571.94	1.4435	2,3045
0.5047	1.0506	1638.10	1.4507	0.5045	1.0373	1610.54	1.4491	1,6824
0.6045	1.0583	1658.83	1.4541	0.6039	1.0489	1638.02	1.4532	1,2545
0.7047	1.0643	1674.34	1.4571	0.7040	1.0580	1661.34	1.4563	0,7764
0.7988	1.0690	1686.46	1.4594	0.8046	1.0653	1679.52	1.4588	0,4115
0.9045	1.0734	1697.37	1.4611	0.9019	1.0714	1693.46	1.4611	0,2304
1.0000	1.0766	1705.28	1.4627	1.0000	1.0766	1705.28	1.4627	0,0000

Figure 5.1 is the graph of {[BMIM]Cl: EG + methanol} binary mixtures density, $\boldsymbol{\rho}$, against mole fraction, $\boldsymbol{x_1}$, at different temperatures (293.15 – 313.15) K and at atmospheric pressure.

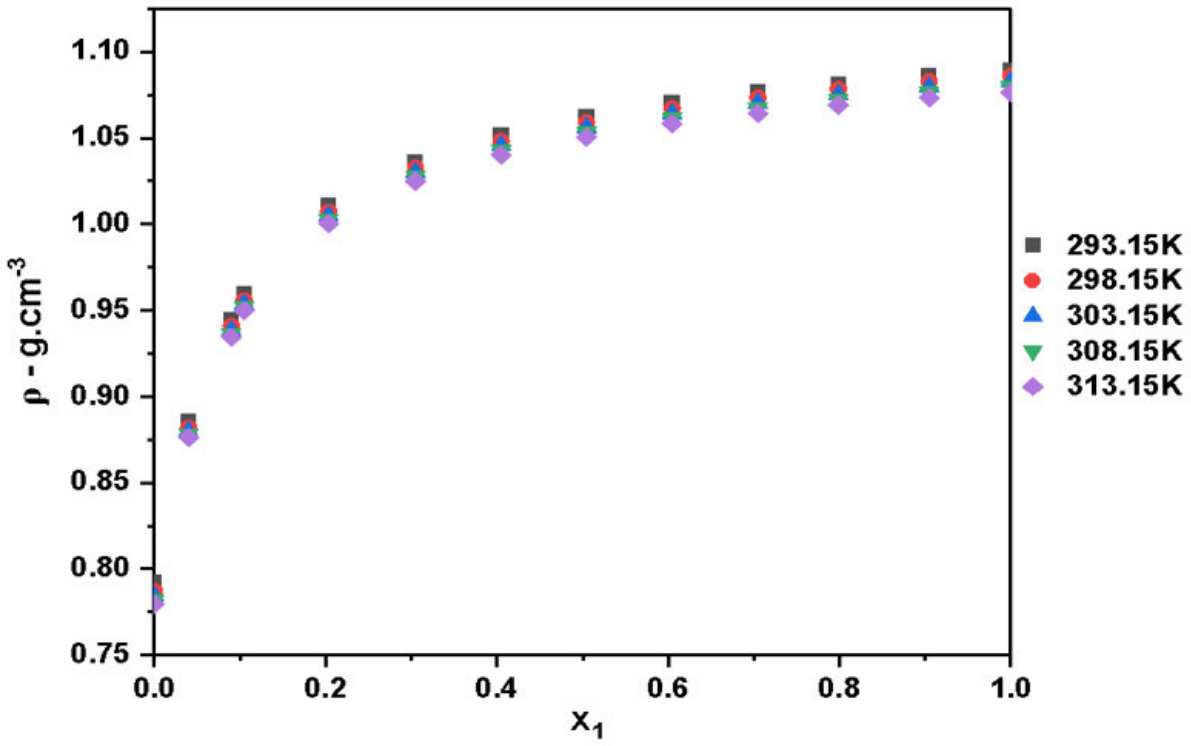

Figure 5.1: Graph of density, $\boldsymbol{\rho}$, of {[BMIM]Cl: EG + methanol} binary mixtures against mole fraction, $\boldsymbol{x_1}$, at different temperatures (293.15 – 313.15) K and at atmospheric pressure.

The graph of density, $\boldsymbol{\rho}$, of {[BMIM]Cl: EG + ethanol} binary mixtures against mole fraction, $\boldsymbol{x_1}$, at different temperatures (293.15 – 313.15) K and at atmospheric pressure is given in Figure 5.2.

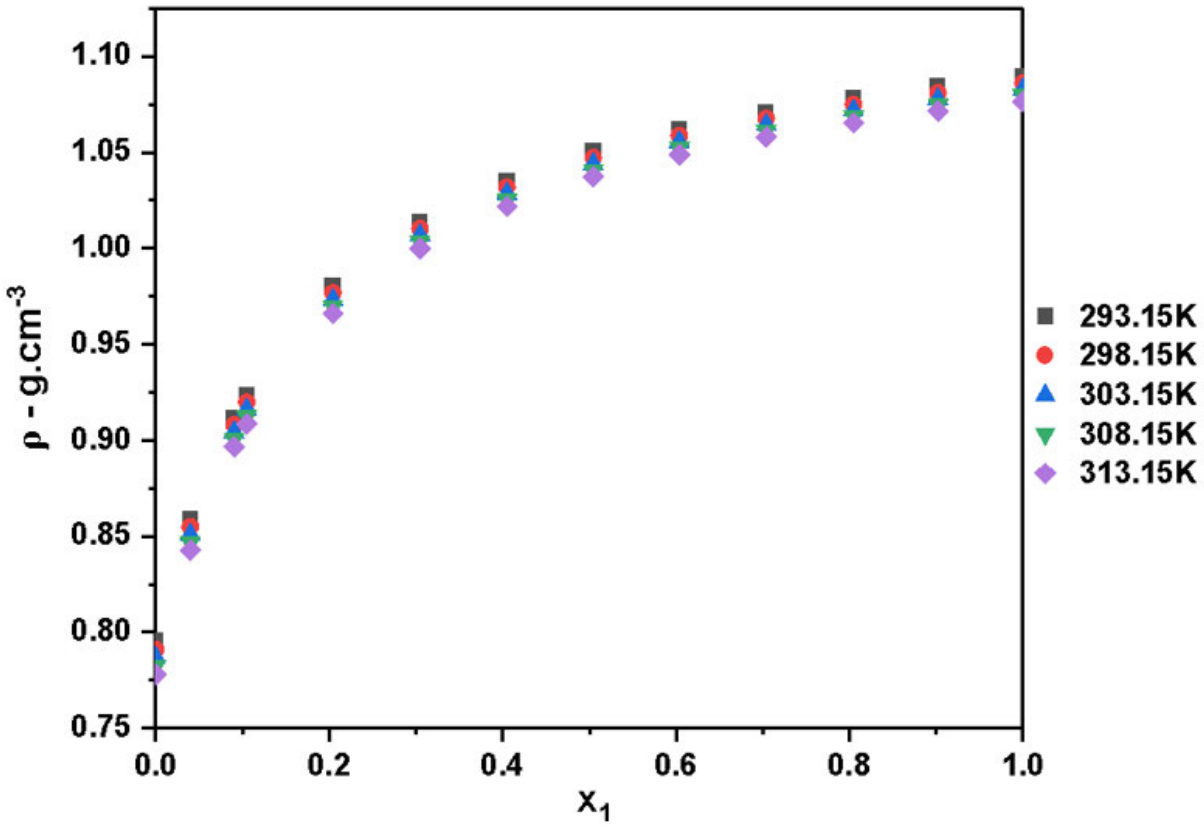

Figure 5.2: Graph of density, $\boldsymbol{\rho}$, of {[BMIM]Cl: EG + ethanol} binary mixtures against mole fraction, $\boldsymbol{x_1}$, at different temperatures (293.15 – 313.15) K and at atmospheric pressure.

Figure 5.3 is the graph of speed of sound, $\boldsymbol{u}$, of ({[BMIM]Cl: EG + methanol} binary mixtures against mole fraction, $\boldsymbol{x_1}$, at different temperatures (293.15 – 313.15) K and at atmospheric pressure.

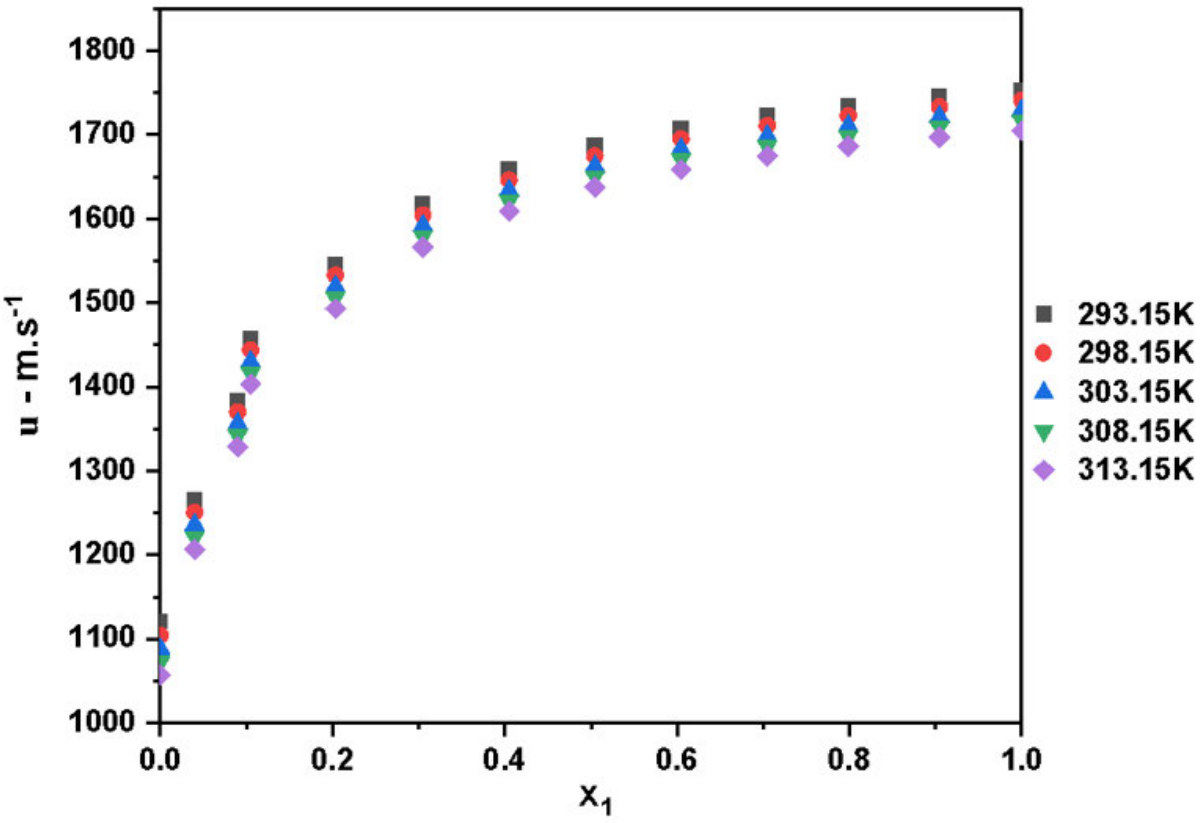

Figure 5.3: Graph of speed of sound, $\boldsymbol{u}$, of {[BMIM]Cl: EG + methanol} binary mixtures against mole fraction, $\boldsymbol{x_1}$, at different temperatures (293.15 – 313.15) K and at atmospheric pressure.

The graph of speed of sound, $\boldsymbol{u}$, of {[BMIM]Cl: EG + ethanol} binary mixtures against mole fraction, $\boldsymbol{x_1}$, at different temperatures (293.15 – 313.15) K and at atmospheric pressure are given in Figure 5.4.

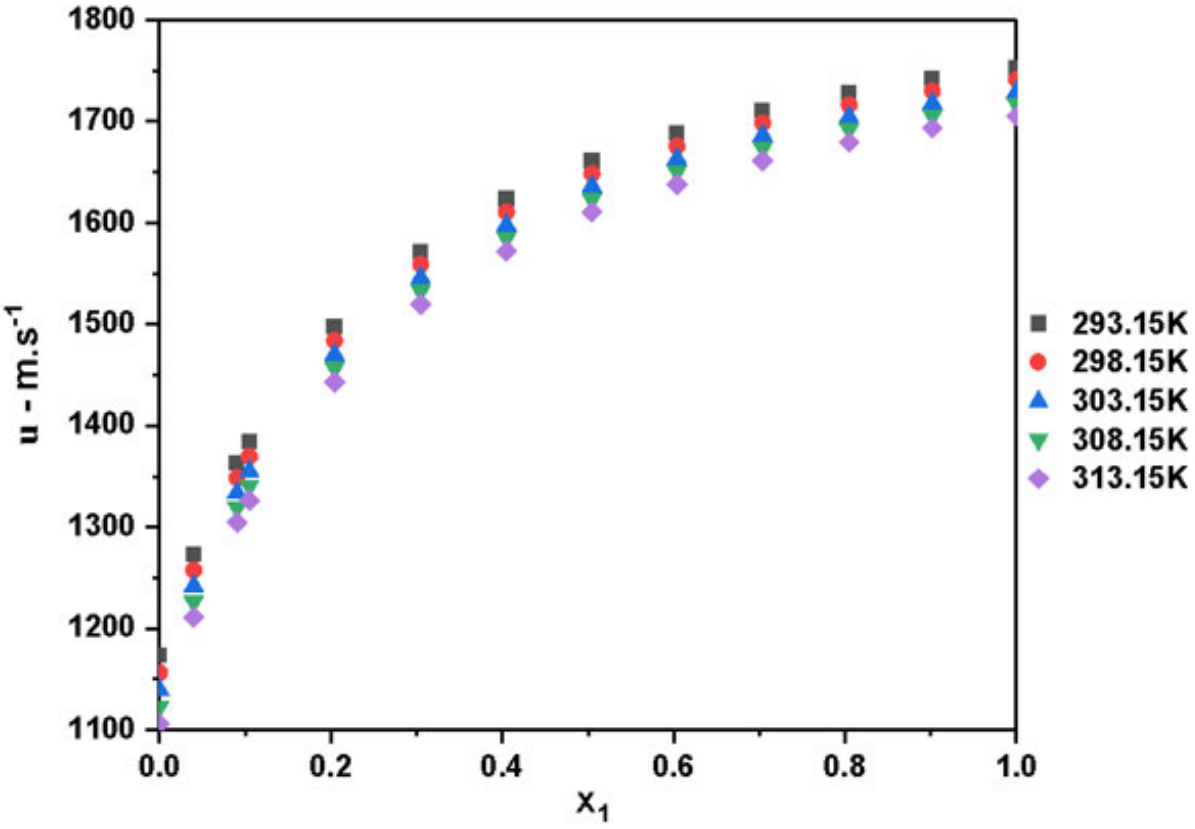

Figure 5.4: Graph of speed of sound, u, of {[BMIM]Cl: EG + ethanol} binary mixtures against mole fraction, x_1, at different temperatures (293.15 – 313.15) Kand at atmospheric pressure.

Figure 5.5 is the graph of refractive index, n_D, of {[BMIM]Cl: EG + methanol} binary mixtures against mole fraction, x_1, at different temperatures (293.15 – 313.15) K and at atmospheric pressure.

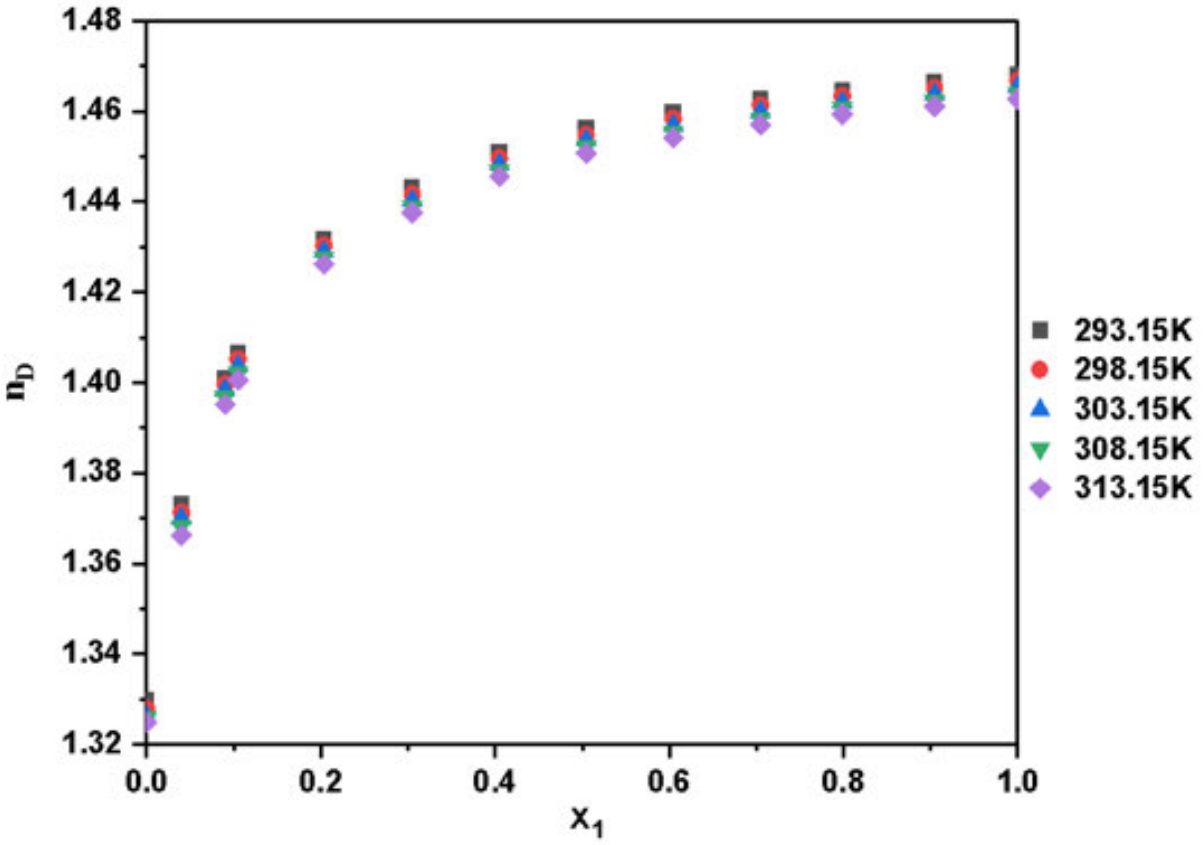

Figure 5.5: Graph of refractive index, n_D, of {[BMIM]Cl: EG + methanol} binary mixtures against mole fraction, x_1, at different temperatures (293.15 – 313.15) K and at atmospheric pressure.

The graph of refractive index, n_D, of {[BMIM]Cl: EG + ethanol} binary mixtures against mole fraction, x_1, at different temperatures (293.15 – 313.15) K and at atmospheric pressure is given in Figure 5.6.

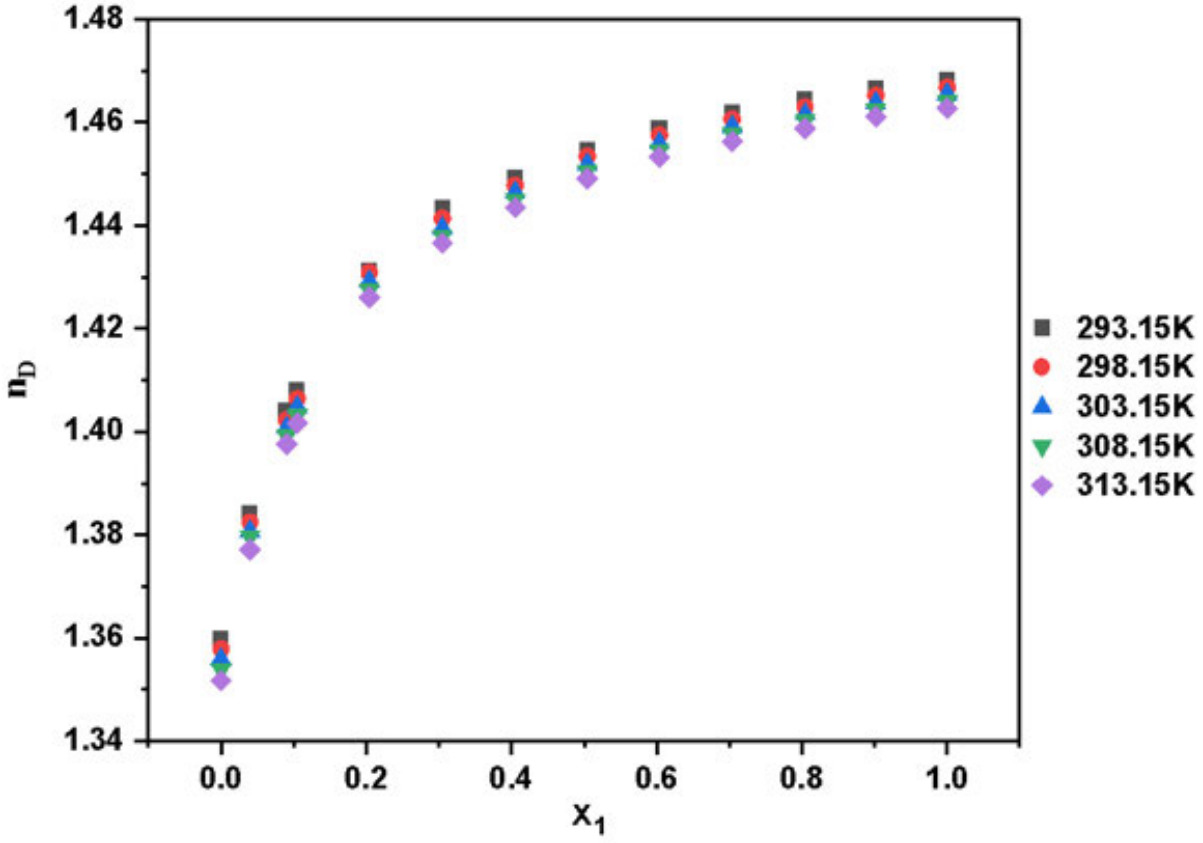

Figure 5.6: Graph of refractive index, n_D, of (BMIM]Cl: EG + ethanol} binary mixtures against mole fraction, x_1, at different temperatures (293.15 – 313.15) K and at atmospheric pressure.

The results for the excess molar volume, V_m^{E}, intermolecular free length, L_f, isentropic compressibilities, k_s, deviation in isentropic compressibilities, Δk_s, deviation refractive index, Δn_D, and molar refraction, R, of {[BMIM]Cl: EG + methanol or ethanol} binary mixtures at different temperatures and at atmospheric pressure is given in Table 5.2.

Table 5-2: Calculated excess molar volumes, $\boldsymbol{V_m^{\mathrm{E}}}$, intermolecular free length, $\boldsymbol{L_f}$, isentropic compressibilities, $\boldsymbol{k_s}$, deviation in isentropic compressibilities, $\Delta\boldsymbol{k_s}$, deviation in refractive indices, $\Delta\boldsymbol{n_D}$ and molar refraction, $\boldsymbol{R}$ of {[BMIM]Cl: EG + methanol or ethanol} binary mixtures at different temperatures and at atmospheric pressure.

[BMIM]Cl: EG + methanol						
x_1	V_m^{E}/(cm^3.mol^{-1})	L_f/10^{-11}(m)	k_s/10^{10}(Pa^{-1})	Δk_s/10^{10} (Pa^{-1})	Δn_D	R/(cm^{-3}.mol^{-1})
T = 293.15 K						
0.0000	0.0000	6.4622	10.0536	0.0000	0.0000	8.24
0.0399	-1.0686	5.4128	7.0536	-2.7178	0.0378	11.62
0.0900	-1.3900	4.7918	5.5278	-3.8897	0.0588	15.85
0.1050	-1.6066	4.5146	4.9070	-4.4049	0.0622	17.06
0.2034	-1.7423	4.1476	4.1414	-4.4752	0.0739	25.37
0.3050	-1.4305	3.9150	3.6900	-4.2085	0.0711	33.87
0.4045	-1.1279	3.7894	3.4570	-3.7356	0.0652	42.29
0.5047	-0.8540	3.7065	3.3075	-3.1801	0.0566	50.68
0.6045	-0.6305	3.6483	3.2044	-2.5778	0.0463	59.02
0.7047	-0.4440	3.6046	3.1282	-1.9460	0.0355	67.44
0.7988	-0.2814	3.5726	3.0728	-1.3362	0.0244	75.29
0.9045	-0.1578	3.5432	3.0225	-0.6400	0.0116	84.09
1.0000	0.0000	3.5227	2.9875	0.0000	0.0000	92.11
T = 298.15 K						
0.0000	0.0000	6.6365	10.0411	0.0000	0.0000	8.26
0.0399	-1.1246	5.5381	7.2499	-2.8669	0.0379	11.62
0.0900	-1.4412	4.8937	5.6609	-4.0866	0.0593	15.87
0.1050	-1.6734	4.6071	5.0173	-4.6199	0.0627	17.07
0.2034	-1.8074	4.2279	4.2254	-4.6862	0.0743	25.38
0.3050	-1.5012	3.9877	3.7588	-4.4032	0.0714	33.88

0.4045	-1.1802	3.8586	3.5194	-3.9060	0.0656	42.32
0.5047	-0.8970	3.7733	3.3659	-3.3240	0.0568	50.70
0.6045	-0.6657	3.7135	3.2596	-2.6938	0.0465	59.06
0.7047	-0.4467	3.6689	3.1818	-2.0326	0.0356	67.48
0.7988	-0.3217	3.6355	3.1242	-1.3961	0.0245	75.33
0.9045	-0.1724	3.6054	3.0727	-0.6684	0.0117	84.14
1.0000	0.0000	3.5842	3.0366	0.0000	0.0000	92.16
T = 303.15 K						
0.0000	0.0000	6.8079	10.7585	0.0000	0.0000	8.24
0.0399	-1.1872	5.6614	7.4401	-3.0120	0.0383	11.61
0.0900	-1.4862	4.9951	5.7919	-4.2761	0.0598	16.57
0.1050	-1.7550	4.6994	5.1264	-4.8270	0.0630	17.06
0.2034	-1.8906	4.3081	4.3083	-4.8903	0.0746	25.37
0.3050	-1.5692	4.0617	3.8295	-4.5895	0.0717	33.88
0.4045	-1.2548	3.9284	3.5823	-4.0705	0.0658	42.32
0.5047	-0.9361	3.8411	3.4248	-3.4626	0.0572	50.73
0.6045	-0.7164	3.7796	3.3160	-2.8058	0.0465	59.06
0.7047	-0.4608	3.7343	3.2370	-2.1161	0.0356	67.48
0.7988	-0.3386	3.6999	3.1776	-1.4536	0.0245	75.35
0.9045	-0.1427	3.6693	3.1253	-0.6955	0.0116	84.18
1.0000	0.0000	3.6474	3.0881	0.0000	0.0000	92.21
T = 308.15 K						
0.0000	0.0000	6.9198	11.1153	0.0000	0.0000	8.26
0.0399	-1.2488	5.7355	7.6360	-3.1608	0.0369	11.59
0.0900	-1.5447	5.0527	5.9262	-4.4713	0.0584	15.84
0.1050	-1.8313	4.7490	5.2352	-5.0430	0.0618	17.03
0.2034	-1.9669	4.3513	4.3951	-5.0985	0.0737	26.36
0.3050	-1.6436	4.0995	3.9011	-4.7819	0.0709	33.86
0.4045	-1.3264	3.9636	3.6467	-4.2397	0.0650	42.31
0.5047	-0.9966	3.8749	3.4853	-3.6053	0.0565	50.72
0.6045	-0.7750	3.8123	3.3737	-2.9209	0.0461	59.06
0.7047	-0.4751	3.7669	3.2937	-2.2017	0.0352	67.50
0.7988	-0.3518	3.7316	3.2324	-1.5124	0.0244	75.39

0.9045	-0.1777	3.7004	3.1786	-0.7237	0.0116	84.21
1.0000	0.0000	3.6782	3.1405	0.0000	0.0000	92.24
***T* = 313.15 K**						
0.0000	0.0000	7.0317	11.4776	0.0000	0.0000	8.27
0.0399	-1.2984	5.8102	7.8362	-3.3106	0.0359	11.56
0.0900	-1.6204	5.1098	6.0608	-4.6712	0.0579	15.82
0.1050	-1.9126	4.7995	5.3472	-5.2609	0.0612	17.01
0.2034	-2.0376	4.3949	4.4835	-5.3096	0.0733	25.35
0.3050	-1.7127	4.1385	3.9757	-4.9755	0.0707	33.86
0.4045	-1.3923	3.9996	3.7132	-4.4105	0.0649	42.31
0.5047	-1.0670	3.9092	3.5473	-3.7499	0.0563	50.72
0.6045	-0.7813	3.8462	3.4340	-3.0364	0.0459	59.08
0.7047	-0.5326	3.7998	3.3515	-2.2888	0.0351	67.51
0.7988	-0.3552	3.7641	3.2889	-1.5717	0.0244	75.43
0.9045	-0.1903	3.7323	3.2335	-0.7520	0.0116	84.24
1.0000	0.0000	3.7095	3.1942	0.0000	0.0000	92.28

[BMIM]Cl: EG + ethanol						
x_1	V_m^{E}/(cm^3.mol^{-1})	L_f/10^{-11}(m)	k_s/10^{10}(Pa^{-1})	Δk_s/10^{10} (Pa^{-1})	Δn_D	R/(cm^3.mol^{-1})
***T* = 293.15K**						
0.0000	0.0000	6.1586	9.1312	0.0000	0.0000	12.78
0.0400	-0.5583	5.4639	7.1873	-1.6981	0.0200	15.98
0.0905	-0.8961	4.9524	5.9048	-2.6705	0.0343	19.99
0.1050	-0.9576	4.8451	5.6515	-2.8346	0.0367	21.13
0.2044	-1.1696	4.3472	4.5496	-3.3255	0.0493	29.18
0.3049	-1.1383	4.0724	3.9927	-3.2653	0.0505	37.18
0.4050	-0.9860	3.9018	3.6687	-2.9745	0.0455	44.98
0.5045	-0.8018	3.7861	3.4510	-2.5806	0.0402	52.89
0.6039	-0.6244	3.7050	3.3016	-2.1196	0.0336	60.77
0.7040	-0.4049	3.6407	3.1910	-1.6152	0.0257	68.69
0.8046	-0.2352	3.5909	3.1041	-1.0840	0.0173	76.65
0.9019	-0.1154	3.5530	3.0390	-0.5512	0.0090	84.13
1.0000	0.0000	3.5227	2.9875	0.0000	0.0000	92.11

			***T* = 298.15 K**			
0.0000	0.0000	6.2653	9.4504	0.0000	0.0000	12.79
0.0400	-0.5802	5.5433	7.3979	-1.7959	0.0202	15.99
0.0905	-0.9297	5.0156	6.0563	-2.8137	0.0346	20.00
0.1050	-0.9929	4.9060	5.7946	-2.9823	0.0371	21.15
0.2044	-1.2102	4.3947	4.6496	-3.4895	0.0507	29.26
0.3049	-1.1784	4.1127	4.0722	-3.4227	0.0503	37.16
0.4050	-1.0255	3.9392	3.7393	-3.1136	0.0458	45.01
0.5045	-0.8346	3.8208	3.5146	-2.6999	0.0406	52.92
0.6039	-0.6499	3.7382	3.3610	-2.2163	0.0338	60.81
0.7040	-0.4260	3.6724	3.2469	-1.6883	0.0260	68.75
0.8046	-0.2470	3.6217	3.1575	-1.1324	0.0175	76.70
0.9019	-0.1212	3.5831	3.0907	-0.5751	0.0091	84.42
1.0000	0.0000	3.5515	3.0366	0.0000	0.0000	92.16
			***T* = 303.15 K**			
0.0000	0.0000	6.3757	9.7862	0.0000	0.0000	12.79
0.0400	-0.6029	5.6260	7.6203	-1.8980	0.0204	16.00
0.0905	-0.9651	5.0812	6.2157	-2.9645	0.0350	20.02
0.1050	-1.0298	4.9687	5.9435	-3.1394	0.0374	21.16
0.2044	-1.2541	4.4432	4.7530	-3.6638	0.0509	29.26
0.3049	-1.2204	4.1545	4.1553	-3.5888	0.0502	37.15
0.4050	-1.0629	3.9773	3.8121	-3.2616	0.0461	45.03
0.5045	-0.8674	3.8556	3.5788	-2.8280	0.0407	52.94
0.6039	-0.6751	3.7719	3.4220	-2.3194	0.0339	60.82
0.7040	-0.4445	3.7042	3.3034	-1.7675	0.0261	68.78
0.8046	-0.2625	3.6525	3.2114	-1.1855	0.0175	76.73
0.9019	-0.1265	3.6136	3.1435	-0.6016	0.0091	84.45
1.0000	0.0000	3.5815	3.0881	0.0000	0.0000	92.21
			***T* = 308.15 K**			
0.0000	0.0000	6.4892	10.1379	0.0000	0.0000	12.80
0.0400	-0.6273	5.7110	7.8521	-2.0058	0.0214	16.04
0.0905	-1.0027	5.1484	6.3812	-3.1236	0.0353	20.04
0.1050	-1.0693	5.0326	6.0975	-3.3057	0.0377	21.17

0.2044	-1.3014	4.4928	4.8595	-3.8478	0.0511	29.27
0.3049	-1.2665	4.1979	4.2426	-3.7619	0.0505	37.16
0.4050	-1.1037	4.0163	3.8872	-3.4169	0.0465	45.06
0.5045	-0.9029	3.8922	3.6472	-2.9604	0.0411	52.98
0.6039	-0.7055	3.8063	3.4847	-2.4276	0.0342	60.85
0.7040	-0.4665	3.7378	3.3635	-1.8484	0.0263	68.80
0.8046	-0.2759	3.6844	3.2678	-1.2401	0.0177	76.77
0.9019	-0.1349	3.6448	3.1979	-0.6289	0.0092	84.50
1.0000	0.0000	3.6117	3.1405	0.0000	0.0000	92.24
***T* = 313.15 K**						
0.0000	0.0000	6.6057	10.5052	0.00000	0.0000	12.80
0.0400	-0.6528	5.7981	8.0935	-2.1192	0.0209	16.02
0.0905	-1.0418	5.2172	6.5530	-3.2908	0.0358	20.05
0.1050	-1.1105	5.0980	6.2570	-3.4528	0.0383	21.19
0.2044	-1.3492	4.5436	4.9700	-4.0404	0.0515	29.29
0.3049	-1.3129	4.2415	4.3312	-3.9449	0.0510	37.19
0.4050	-1.1429	4.0559	3.9643	-3.5801	0.0468	45.07
0.5045	-0.9380	3.9291	3.7166	-3.1000	0.0414	52.99
0.6039	-0.7131	3.8419	3.5497	-2.5406	0.0344	60.88
0.7040	-0.4874	3.7716	3.4247	-1.9338	0.0264	68.82
0.8046	-0.2905	3.7178	3.3272	-1.2956	0.0178	76.79
0.9019	-0.1415	3.6767	3.2542	-0.6571	0.0093	84.53
1.0000	0.0000	3.6425	3.1942	0.0000	0.0000	92.28

The graph of excess molar volume, V_m^E, of {[BMIM]Cl: EG + methanol} binary mixtures against mole fraction, x_1, at different temperatures (293.15 – 313.15) K and at atmospheric pressure is given in Figure 5.7.

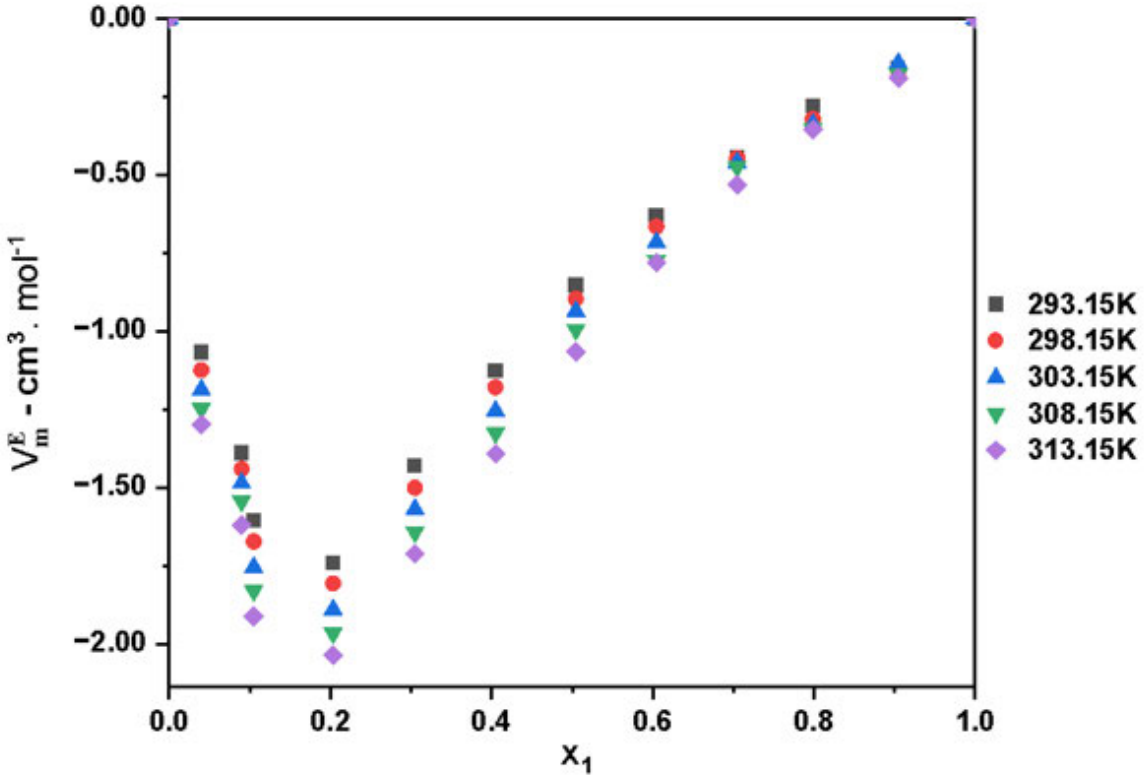

Figure 5.7: Graph of excess molar volume, V_m^E, of {[BMIM]Cl: EG + methanol} binary mixtures against mole fraction, x_1, at different temperatures (293.15 – 313.15) K and at atmospheric pressure.

Figure 5.8 is the graph of excess molar volume, $\boldsymbol{V_m^E}$, of {[BMIM]Cl: EG + ethanol} binary mixtures against mole fraction, $\boldsymbol{x_1}$, at different temperatures (293.15 – 313.15) K and at atmospheric pressure.

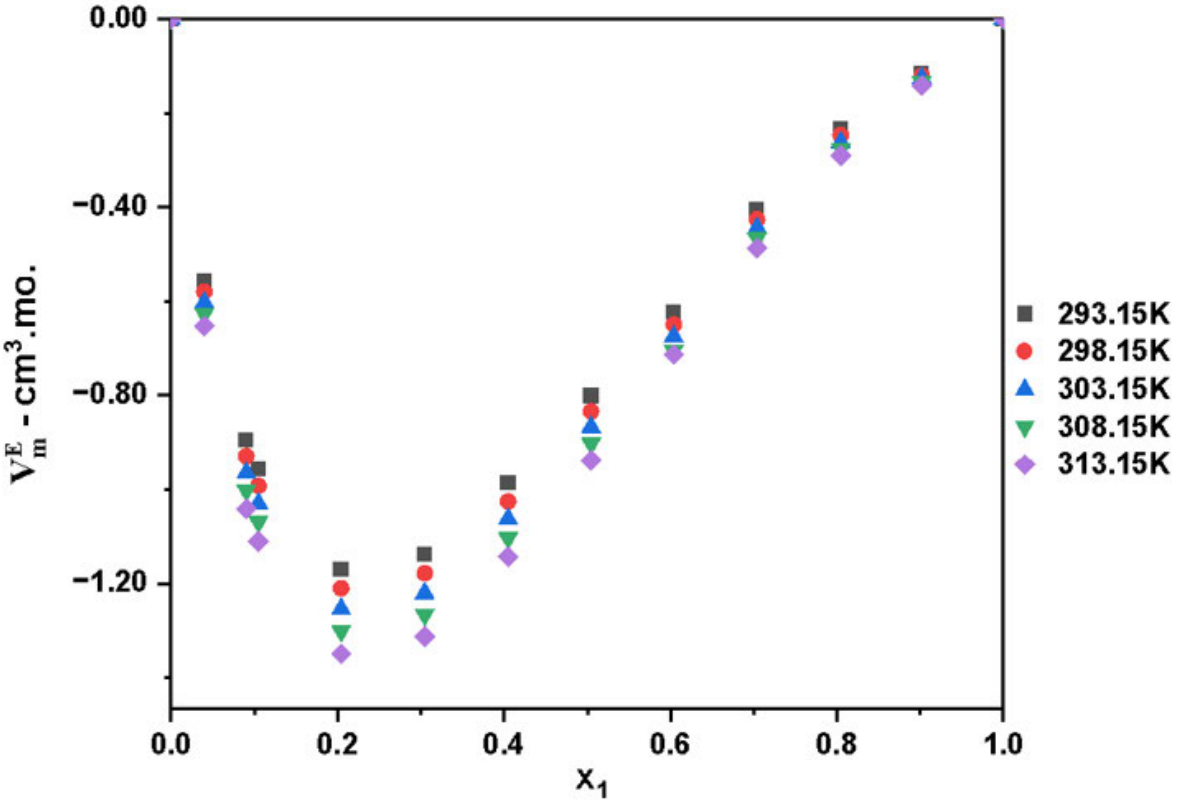

Figure 5.8: Graph of excess molar volume, V_m^E, of {[BMIM]Cl: EG + ethanol} binary mixtures against mole fraction, x_1, at different temperatures (293.15 – 313.15) K and at atmospheric pressure.

The graph of intermolecular free length, L_f, of {[BMIM]Cl: EG + methanol} binary mixtures against mole fraction, x_1, at different temperatures (293.15 – 313.15) K and at atmospheric pressure is given in Figure 5.9.

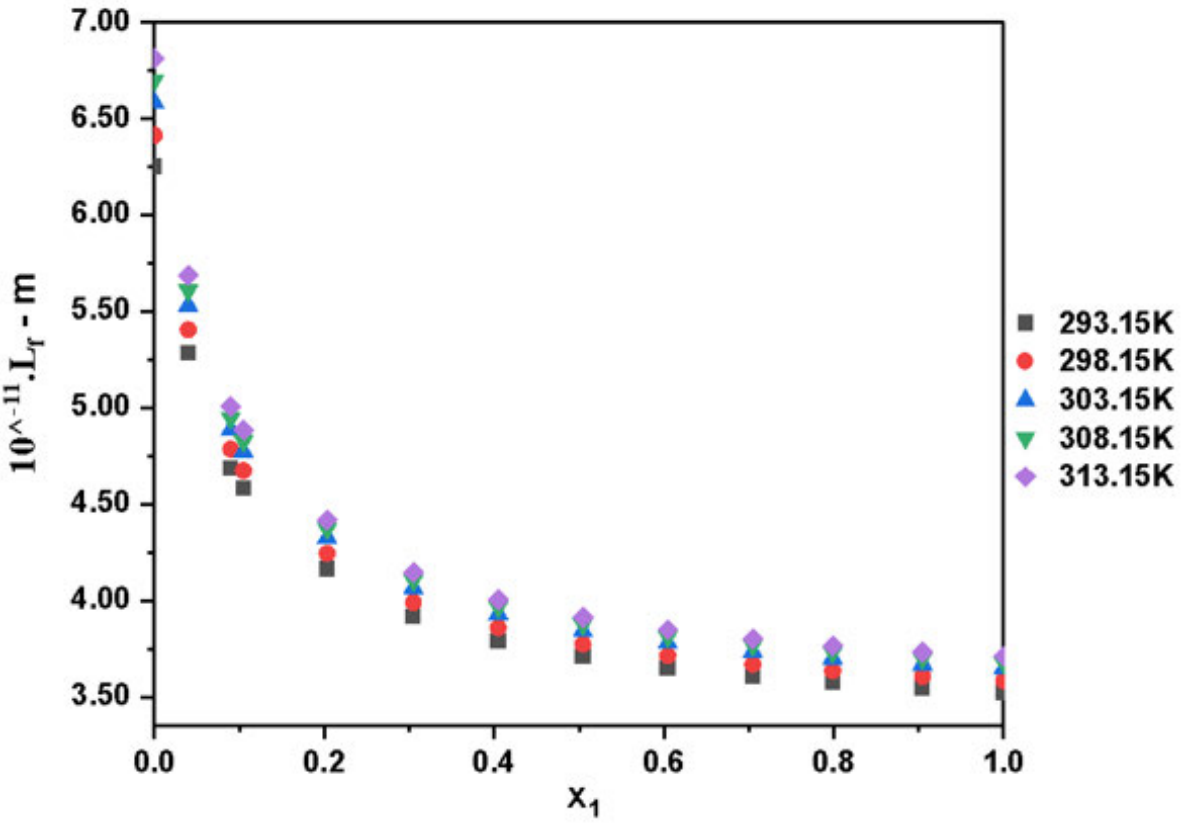

Figure 5.9: Graph of intermolecular free length, L_f, of {[BMIM]Cl: EG + methanol} binary mixtures against mole fraction, x_1, at different temperatures (293.15 – 313.15) K and at atmospheric pressure.

Figure 5.10 is the graph of intermolecular free length, L_f, of {[BMIM]Cl: EG + ethanol} binary mixtures against mole fraction, x_1, at different temperatures (293.15 – 313.15) K and at atmospheric pressure.

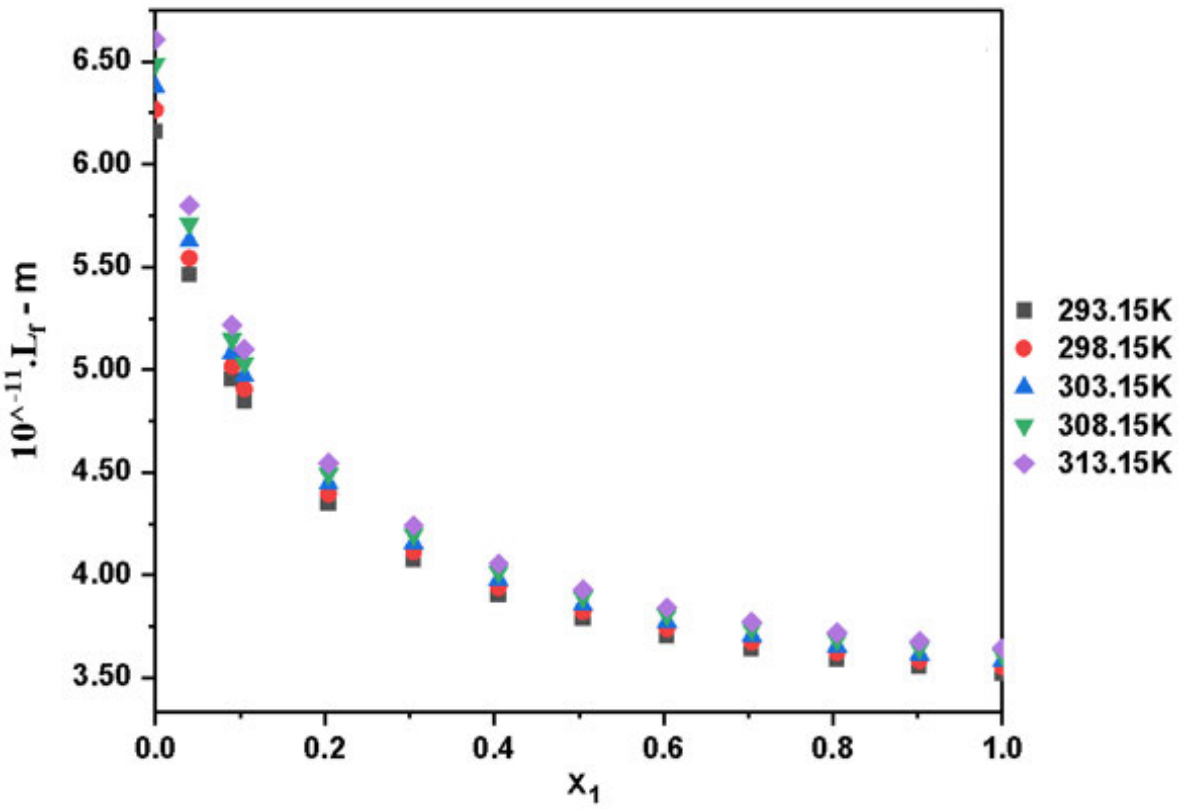

Figure 5.10: Graph of intermolecular free length, L_f, of {[BMIM]Cl: EG + ethanol} binary mixtures against mole fraction, x_1, at different temperatures (293.15 – 313.15) K and at atmospheric pressure.

The graph of isentropic compressibility, k_s of {[BMIM]Cl: EG + methanol} binary mixtures against mole fraction, x_1, at different temperatures (293.15 – 313.15) K and at atmospheric pressure is given in Figure 5.11.

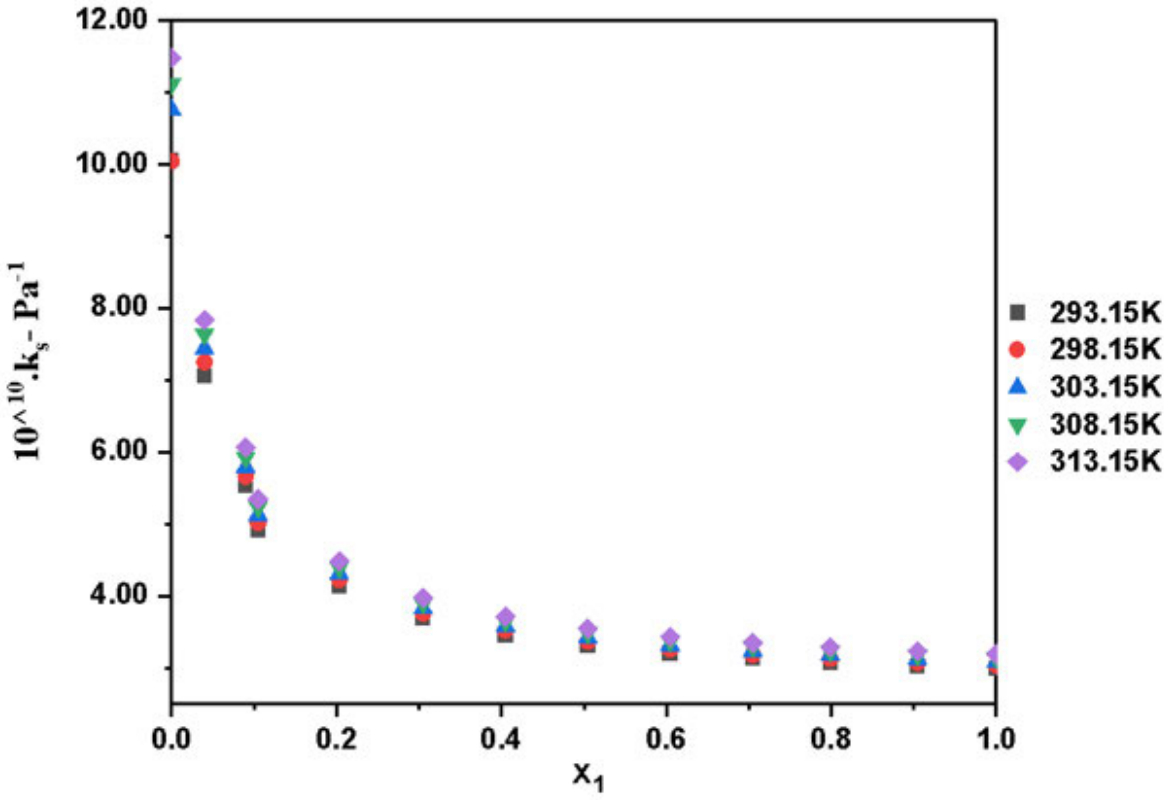

Figure 5.11: Graph of isentropic compressibility, k_s of {[BMIM]Cl: EG + methanol} binary mixtures against mole fraction, x_1, at different temperatures (293.15 – 313.15) K and at atmospheric pressure.

Figure 5.12 is the graph of isentropic compressibility, k_s, of {[BMIM]Cl: EG + ethanol} binary mixtures against mole fraction, x_1, at different temperatures (293.15 – 313.15) K and at atmospheric pressure.

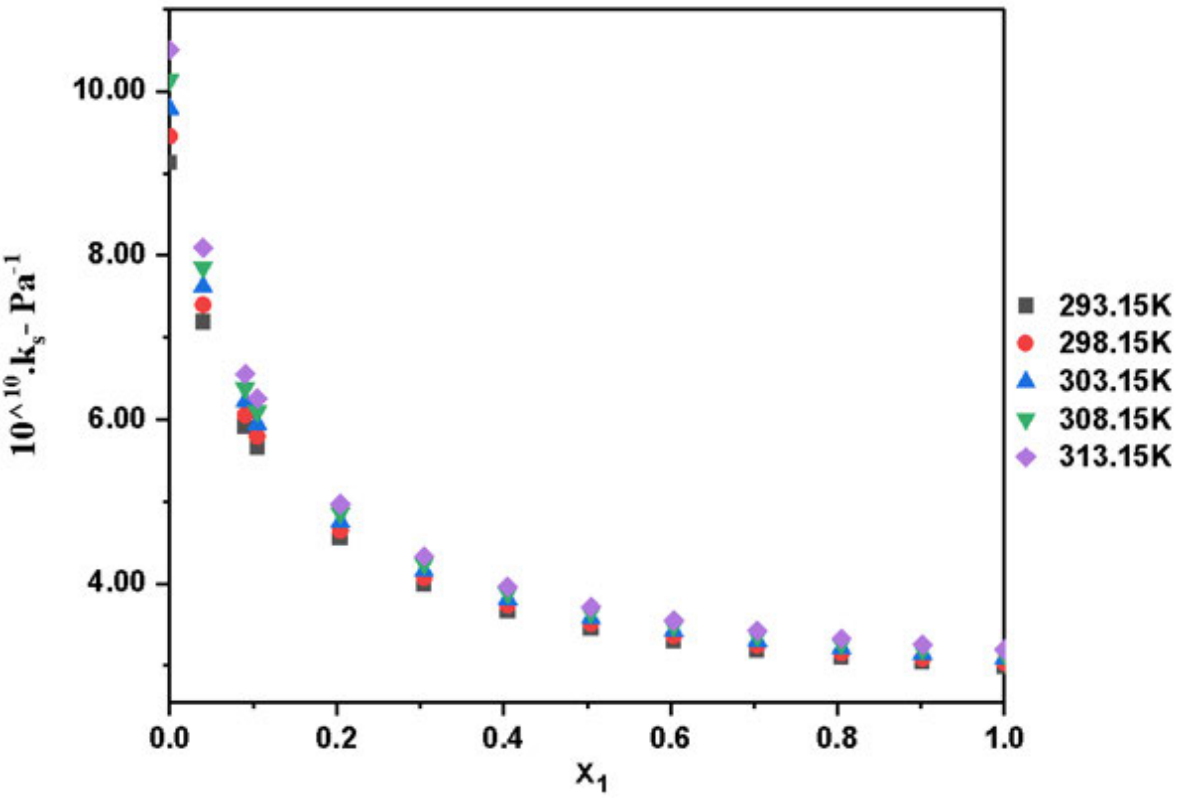

Figure 5.12: Graph of isentropic compressibility, k_s, of {[BMIM]Cl: EG + ethanol} binary mixtures against mole fraction, x_1, at different temperatures (293.15 – 313.15) K and at atmospheric pressure.

The graph of deviation of isentropic compressibility, Δk_s, of {[BMIM]Cl: EG + methanol} binary mixtures against mole fraction, x_1, at different temperatures (293.15 – 313.15) K and at atmospheric pressure is given in Figure 5.13.

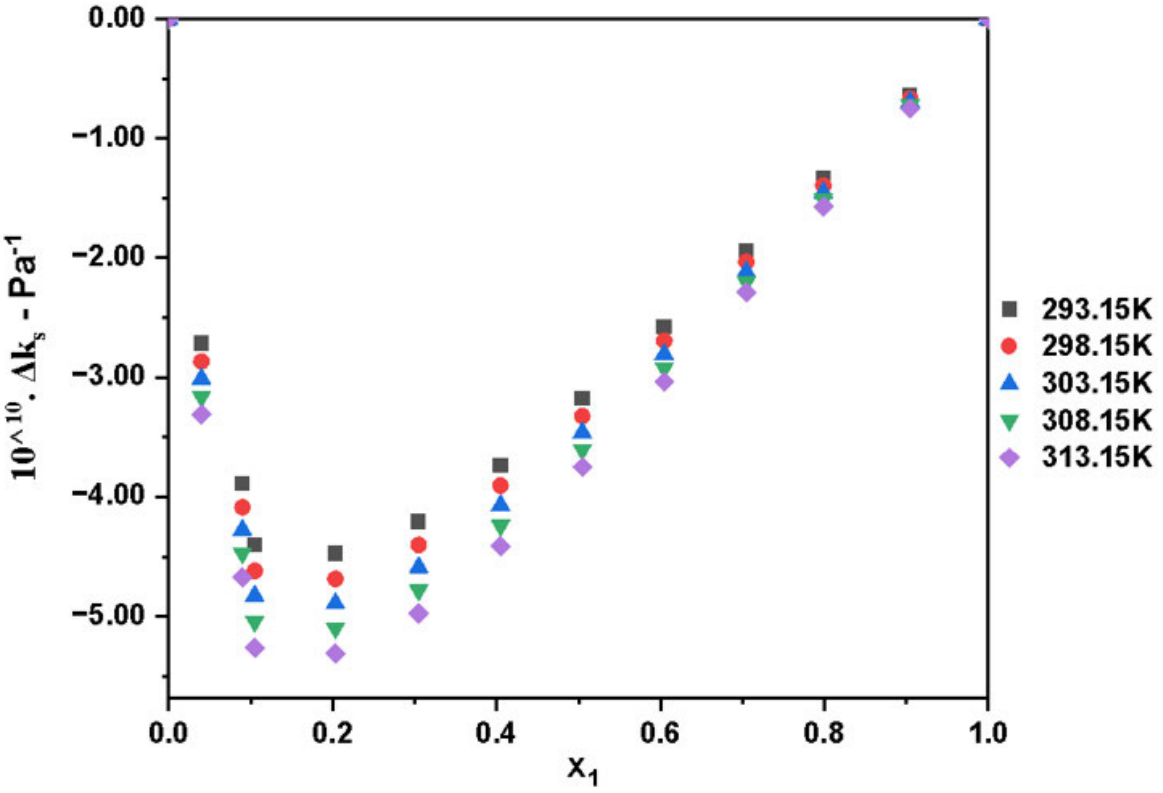

Figure 5.13: Graph of deviation of isentropic compressibility, Δk_s, of {[BMIM]Cl: EG + methanol} binary mixtures against mole fraction, x_1, at different temperatures (293.15 – 313.15) K and at atmospheric pressure.

Figure 5.14 is the graph of deviation of isentropic compressibility, Δk_s, of {[BMIM]Cl: EG + ethanol} binary mixtures against mole fraction, x_1, at different temperatures (293.15 – 313.15) K and at atmospheric pressure.

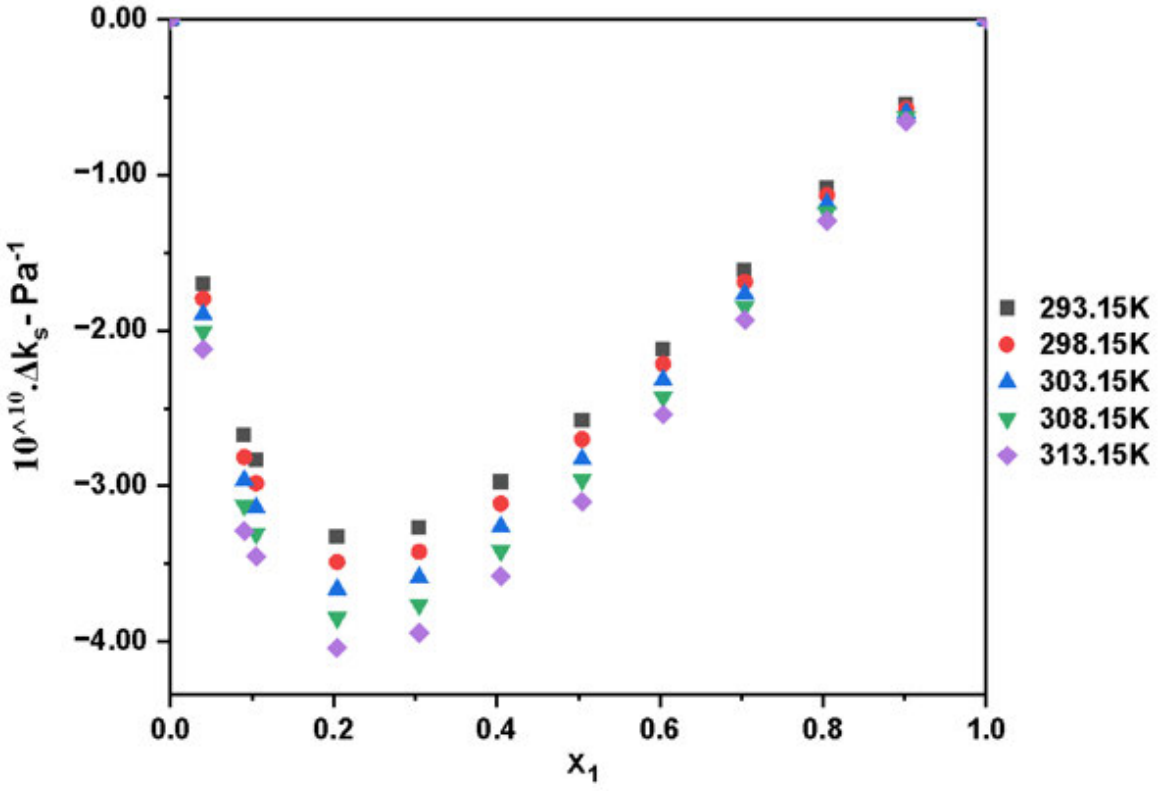

Figure 5.14: Graph of deviation of isentropic compressibility, Δk_s, of {[BMIM]Cl: EG + ethanol} binary mixtures against mole fraction, x_1, at different temperatures (293.15 – 313.15) K and at atmospheric pressure.

The graph of deviation of refractive index, Δn_D, of {[BMIM]Cl: EG + methanol} binary mixtures against mole fraction, x_1, at different temperatures (293.15 – 313.15) K and at atmospheric pressure is given in Figure 5.15.

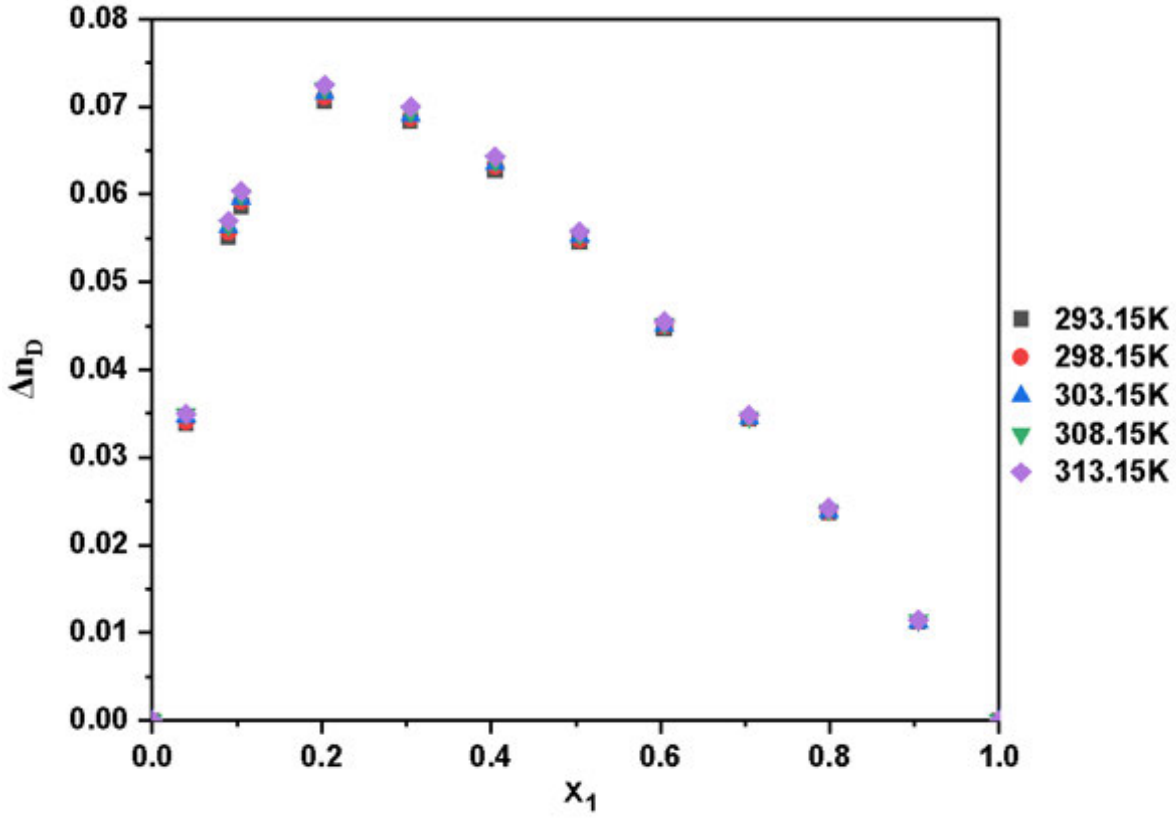

Figure 5.15: Graph of deviation of refractive index, Δn_D, of {[BMIM]Cl: EG + methanol} binary mixtures against mole fraction, x_1, at different temperatures (293.15 – 313.15) K and at atmospheric pressure.

Figure 5.16 is the plot of deviation of refractive index, Δn_D, of {[BMIM]Cl: EG + ethanol} binary mixtures against mole fraction, x_1, at different temperatures (293.15 – 313.15) K and at atmospheric pressure.

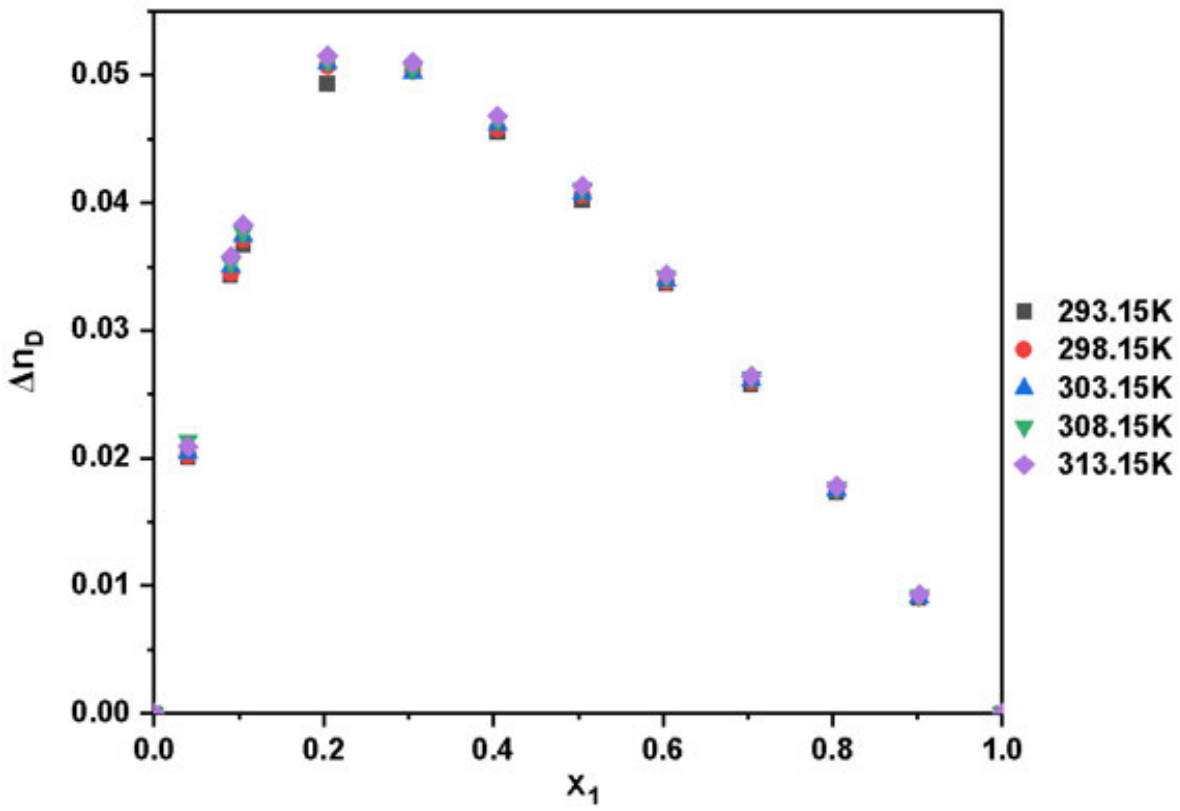

Figure 5.16: Graph of deviation of refractive index, Δn_D, of {[BMIM]Cl: EG + ethanol} binary mixtures against mole fraction, x_1, at different temperatures (293.15 – 313.15) K and at atmospheric pressure.

The results of the Lorentz-Lorenz correlation of excess molar volume, V_m^E, of {[BMIM]Cl: EG + methanol or ethanol} binary mixtures at different temperatures at atmospheric pressure is given in Table 5.3.

Table 5-3: Correlation values for excess molar volume, $\boldsymbol{V_m^E}$, of {[BMIM]Cl: EG + methanol or ethanol} binary mixtures at different temperatures and at atmospheric pressure along with the measured values.

DES + methanol			DES + ethanol		
L-L, V_m^E/(cm^{-3}.mol)			L-L, V_m^E/(cm^{-3}.mol)		
x_1	Exp. V_m^E	Calc. V_m^E	x_1	Exp. V_m^E	Calc. V_m^E
***T* = 293.15 K**					
0.0000	0.0000	0.0000	0.0000	0.0000	0.0000
0.0399	-1.0686	-1.3745	0.4001	-0.5583	-1.3854
0.0900	-1.3900	-1.4020	0.0905	-0.8961	-1.4050
0.1050	-1.6066	-1.4074	0.1050	-0.9576	-1.4089
0.2034	-1.7423	-1.4325	0.2044	-1.1696	-1.4321
0.3050	-1.4305	-1.4438	0.3049	-1.1383	-1.4441
0.4045	-1.1279	-1.4516	0.4050	-0.9860	-1.4498
0.5047	-0.8540	-1.4568	0.5045	-0.8018	-1.4553
0.6045	-0.6305	-1.4603	0.6039	-0.6244	-1.4594
0.7047	-0.4440	-1.4633	0.7040	-0.4049	-1.4624
0.7988	-0.2814	-1.4652	0.8045	-0.2352	-1.4648
0.9045	-0.1578	-1.4670	0.9019	-0.1154	-1.4670
1.0000	0.0000	0.0000	1.0000	0.00000	0.0000
***T* = 298.15 K**					
0.0000	0.0000	0.0000	0.0000	0.0000	0.0000
0.0399	-1.1246	-1.3727	0.4001	-0.5802	-1.3838
0.0900	-1.4412	-1.4007	0.0905	-0.9297	-1.4033
0.1050	-1.6734	-1.4061	0.1050	-0.9929	-1.4074
0.2034	-1.8074	-1.4311	0.2044	-1.2102	-1.4317
0.3050	-1.5012	-1.4424	0.3049	-1.1784	-1.4421
0.4045	-1.1802	-1.4503	0.4050	-1.0255	-1.4484

0.5047	-0.8970	-1.4554	0.5045	-0.8346	-1.4540
0.6045	-0.6657	-1.4590	0.6039	-0.6499	-1.4581
0.7047	-0.4467	-1.4620	0.7040	-0.4260	-1.4612
0.7988	-0.3217	-1.4639	0.8045	-0.2467	-1.4635
0.9045	-0.1724	-1.4657	0.9019	-0.1212	-1.4657
1.0000	0.0000	0.0000	1.0000	0.0000	0.0000
T = 303.15 K					
0.0000	0.0000	0.0000	0.0000	0.0000	0.0000
0.0399	-1.1872	-1.3714	0.4001	-0.6029	-1.3820
0.0900	-1.4862	-1.3994	0.0905	-0.9651	-1.4018
0.1050	-1.7550	-1.4047	0.1050	-1.0298	-1.4058
0.2034	-1.8906	-1.4297	0.2044	-1.2541	-1.4300
0.3050	-1.5692	-1.4410	0.3049	-1.2204	-1.4402
0.4045	-1.2548	-1.4489	0.4050	-1.0629	-1.4470
0.5047	-0.9361	-1.4542	0.5045	-0.8674	-1.4525
0.6045	-0.7164	-1.4575	0.6039	-0.6751	-1.4566
0.7047	-0.4608	-1.4605	0.7040	-0.4445	-1.4598
0.7988	-0.3386	-1.4625	0.8045	-0.2645	-1.4622
0.9045	-0.1427	-1.4643	0.9019	-0.1265	-1.4643
1.0000	0.0000	0.0000	1.0000	0.0000	0.0000
T = 308.15 K					
0.0000	0.0000	0.0000	0.0000	0.0000	
0.0399	-1.2488	-1.3697	0.4001	-0.6273	-1.3809
0.0900	-1.5447	-1.3977	0.0905	-1.0027	-1.4002
0.1050	-1.8313	-1.4032	0.1050	-1.0693	-1.4042
0.2034	-1.9669	-1.4284	0.2044	-1.3015	-1.4283
0.3050	-1.6436	-1.4396	0.3049	-1.2665	-1.4387
0.4045	-1.3264	-1.4475	0.4050	-1.1037	-1.4456
0.5047	-0.9966	-1.4527	0.5045	-0.9029	-1.4512
0.6045	-0.7750	-1.4561	0.6039	-0.7055	-1.4552
0.7047	-0.4751	-1.4591	0.7040	-0.4665	-1.4584
0.7988	-0.3518	-1.4612	0.8045	-0.2759	-1.4609
0.9045	-0.1777	-1.4630	0.9019	-0.1349	-1.4630

1.0000	0.0000	0.0000	1.0000	0.0000	0.0000
***T* = 313.15 K**					
0.0000	0.0000	0.0000	0.0000	0.0000	0.0000
0.0399	-1.2984	-1.3678	0.4001	-0.6528	-1.3784
0.0900	-1.6204	-1.3962	0.0905	-1.0418	-1.3986
0.1050	-1.9126	-1.4016	0.1050	-1.1105	-1.4027
0.2034	-2.0376	-1.4270	0.2044	-1.3493	-1.4268
0.3050	-1.7127	-1.4383	0.3049	-1.3129	-1.4373
0.4045	-1.3923	-1.4462	0.4050	-1.1429	-1.4442
0.5047	-1.0670	-1.4513	0.5045	-0.9380	-1.4497
0.6045	-0.7813	-1.4547	0.6039	-0.7131	-1.4538
0.7047	-0.5326	-1.4577	0.7040	-0.4874	-1.4569
0.7988	-0.3552	-1.4599	0.8045	-0.2905	-1.4594
0.9045	-0.1903	-1.4616	0.9019	-0.1416	-1.4616
1.0000	0.0000	0.0000	1.0000	0.0000	0.0000

The results for the predicted values for densities, ρ, and the refractive index, n_D, of {[BMIM]Cl: EG + methanol or ethanol} binary mixtures at different temperatures and at atmospheric pressure is given in Table 5.4.

Table 5-4: is the predicted values for densities, $\boldsymbol{\rho}$, and refractive indices, $\boldsymbol{n_D}$, of {[BMIM]Cl: EG + methanol or ethanol} binary mixtures at different temperatures and at atmospheric pressure along with the measured values.

DES + methanol					DES + ethanol				
	L-L, ρ/(g·cm^{-3})		L-L - n_D			L-L, ρ/(g·cm^{-3})		L-L - n_D	
x_1	Exp. ρ	Calc. ρ	Exp. n	Calc. n	x_1	Exp. ρ	Calc. ρ	Exp. n	Calc. n
***T* = 293.15K**									
0.0000	0.7924	0.7924	1.3298	1.3298	0.0000	0.7954	0.7954	1.3599	1.2193
0.0399	0.8861	0.8879	1.3731	1.3722	0.0400	0.8589	0.8601	1.3842	1.2838
0.0900	0.9450	0.9482	1.4010	1.3995	0.0905	0.9119	0.9136	1.4040	1.3423
0.1050	0.9596	0.9600	1.4065	1.4063	0.1050	0.9236	0.9247	1.4080	1.3559
0.2034	1.0110	1.0137	1.4318	1.4305	0.2044	0.9804	0.9863	1.4313	1.4246
0.3050	1.0362	1.0375	1.4431	1.4425	0.3049	1.0137	1.0195	1.4434	1.4679
0.4045	1.0517	1.0539	1.4510	1.4499	0.4050	1.0353	1.0371	1.4492	1.4972
0.5047	1.0624	1.0647	1.4562	1.4550	0.5045	1.0506	1.0522	1.4547	1.5185
0.6045	1.0705	1.0720	1.4597	1.4589	0.6039	1.0621	1.0635	1.4588	1.5348
0.7047	1.0768	1.0784	1.4628	1.4620	0.7040	1.0709	1.0720	1.4618	1.5476
0.7988	1.0816	1.0823	1.4647	1.4643	0.8046	1.0783	1.0789	1.4643	1.5581
0.9045	1.0861	1.0860	1.4665	1.4665	0.9019	1.0843	1.0848	1.4665	1.5666
1.0000	1.0893	1.0893	1.4681	1.4681	1.0000	1.0893	1.0893	1.4681	1.5739
***T* = 298.15K**									
0.0000	0.7872	0.7872	1.3318	1.3279	0.0000	0.7910	0.7910	1.3579	1.2156
0.0399	0.8820	0.8831	1.3713	1.3708	0.0400	0.8549	0.8563	1.3825	1.2797
0.0900	0.9411	0.9447	1.3997	1.3980	0.0905	0.9081	0.9098	1.4023	1.3379
0.1050	0.9559	0.9565	1.4052	1.4049	0.1050	0.9199	0.9211	1.4064	1.3514
0.2034	1.0074	1.0101	1.4304	1.4291	0.2044	0.9768	0.9851	1.4309	1.4197
0.3050	1.0329	1.0340	1.4417	1.4412	0.3049	1.0103	1.0150	1.4414	1.4628
0.4045	1.0483	1.0507	1.4497	1.4486	0.4050	1.0320	1.0337	1.4478	1.4920

0.5047	1.0591	1.0613	1.4548	1.4537	0.5045	1.0473	1.0491	1.4534	1.5131
0.6045	1.0673	1.0688	1.4584	1.4576	0.6039	1.0588	1.0604	1.4575	1.5293
0.7047	1.0735	1.0750	1.4614	1.4607	0.7040	1.0677	1.0690	1.4606	1.5420
0.7988	1.0785	1.0791	1.4634	1.4631	0.8046	1.0751	1.0757	1.4630	1.5525
0.9045	1.0830	1.0829	1.4652	1.4652	0.9019	1.0811	1.0817	1.4652	1.5609
1.0000	1.0862	1.0862	1.4668	1.4668	1.0000	1.0862	1.0862	1.4668	1.5682
T = 303.15K									
0.0000	0.7843	0.7843	1.3261	1.3261	0,0000	0.7867	0.7867	1.3559	1.2120
0.0399	0.8799	0.8810	1.3700	1.3695	0,0400	0.8509	0.8523	1.3807	1.2757
0.0900	0.9384	0.9423	1.3984	1.3966	0,0905	0.9042	0.9063	1.4008	1.3336
0.1050	0.9537	0.9536	1.4037	1.4037	0,1050	0.9161	0.9174	1.4048	1.3470
0.2034	1.0050	1.0071	1.4290	1.4280	0,2044	0.9733	0.9812	1.4292	1.4149
0.3050	1.0302	1.0309	1.4403	1.4400	0,3049	1.0069	1.0107	1.4395	1.4577
0.4045	1.0456	1.0475	1.4483	1.4474	0,4050	1.0286	1.0304	1.4464	1.4867
0.5047	1.0561	1.0585	1.4536	1.4525	0,5045	1.0440	1.0455	1.4519	1.5078
0.6045	1.0643	1.0653	1.4569	1.4564	0,6039	1.0555	1.0568	1.4560	1.5238
0.7047	1.0704	1.0715	1.4599	1.4594	0,7040	1.0645	1.0656	1.4592	1.5365
0.7988	1.0754	1.0758	1.4620	1.4618	0,8046	1.0719	1.0724	1.4616	1.5469
0.9045	1.0797	1.0795	1.4638	1.4639	0,9019	1.0779	1.0783	1.4638	1.5553
1.0000	1.0830	1.0830	1.4655	1.4655	1,0000	1.0830	1.0830	1.4655	1.5625
T = 308.15K									
0.0000	0.7820	0.7820	1.3259	1.3259	0,0000	0.7823	0.7823	1.3539	1.2084
0.0399	0.8782	0.8758	1.3683	1.3694	0,0400	0.8468	0.8499	1.3797	1.2717
0.0900	0.9364	0.9375	1.3967	1.3962	0,0905	0.9004	0.9027	1.3992	1.3292
0.1050	0.9519	0.9493	1.4022	1.4034	0,1050	0.9123	0.9138	1.4032	1.3425
0.2034	1.0028	1.0036	1.4277	1.4273	0,2044	0.9697	0.9773	1.4275	1.4101
0.3050	1.0277	1.0273	1.4389	1.4391	0,3049	1.0034	1.0073	1.4380	1.4526
0.4045	1.0430	1.0440	1.4469	1.4464	0,4050	1.0252	1.0271	1.4450	1.4814
0.5047	1.0533	1.0549	1.4521	1.4513	0,5045	1.0406	1.0425	1.4506	1.5023
0.6045	1.0614	1.0620	1.4555	1.4552	0,6039	1.0523	1.0536	1.4546	1.5183
0.7047	1.0673	1.0682	1.4585	1.4580	0,7040	1.0612	1.0624	1.4578	1.5309
0.7988	1.0722	1.0727	1.4607	1.4604	0,8046	1.0686	1.0694	1.4603	1.5412

0.9045	1.0766	1.0765	1.4625	1.4626	0,9019	1.0747	1.0753	1.4625	1.5496
1.0000	1.0798	1.0798	1.4641	1.4641	1,0000	1.0798	1.0798	1.4641	1.5567
***T* = 313.15K**									
0.0000	0.7794	0.7794	1.3249	1.3249	0,0000	0.7779	0.7779	1.3518	1.2048
0.0399	0.8711	0.8762	1.3663	1.3687	0,0400	0.8427	0.8444	1.3771	1.2677
0.0900	0.9339	0.9345	1.3952	1.3955	0,0905	0.8966	0.8992	1.3976	1.3248
0.1050	0.9456	0.9499	1.4006	1.4027	0,1050	0.9085	0.9105	1.4017	1.3381
0.2034	1.0001	1.0003	1.4262	1.4263	0,2044	0.9662	0.9740	1.4260	1.4052
0.3050	1.0242	1.0251	1.4376	1.4380	0,3049	1.0000	1.0041	1.4366	1.4475
0.4045	1.0410	1.0402	1.4456	1.4452	0,4050	1.0218	1.0238	1.4435	1.4762
0.5047	1.0516	1.0506	1.4507	1.4502	0,5045	1.0373	1.0391	1.4491	1.4969
0.6045	1.0588	1.0583	1.4541	1.4539	0,6039	1.0489	1.0504	1.4532	1.5128
0.7047	1.0650	1.0643	1.4571	1.4568	0,7040	1.0580	1.0590	1.4563	1.5253
0.7988	1.0697	1.0690	1.4594	1.4591	0,8046	1.0654	1.0660	1.4588	1.5356
0.9045	1.0733	1.0734	1.4611	1.4612	0,9019	1.0714	1.0721	1.4611	1.5439
1.0000	1.0766	1.0766	1.4627	1.4627	1,0000	1.0766	1.0766	1.4627	1.5510

Figure 5.17 is the graph of L-L density approximation of {[BMIM]Cl: EG + methanol} binary mixtures against mole fraction, x_1, at different temperatures (293.15 – 313.15) K and at atmospheric pressure.

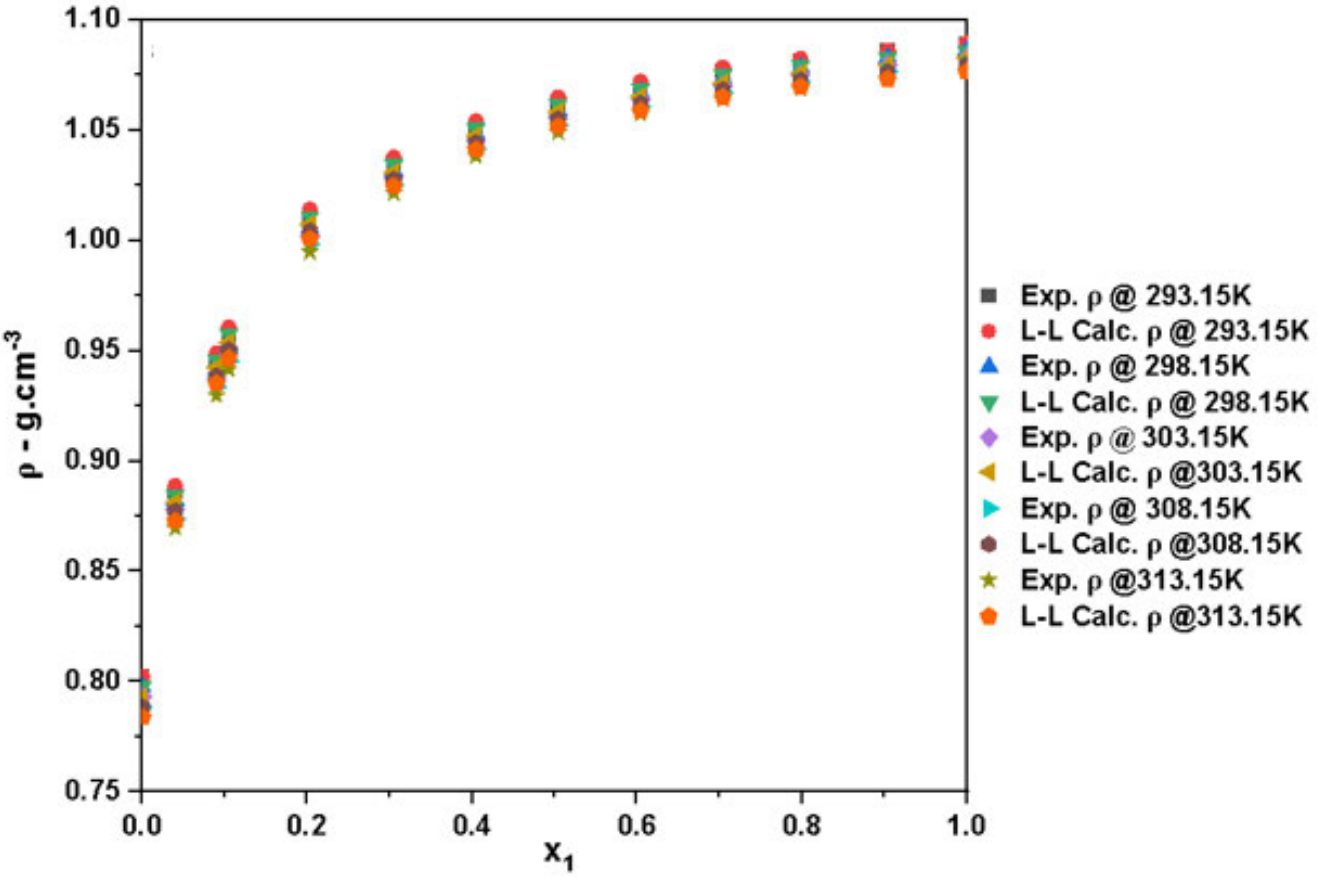

Figure 5.17: Graph of L-L density approximation of {[BMIM]Cl: EG + methanol} binary mixtures against mole fraction, x_1, at different temperatures (293.15 – 313.15) K and at atmospheric pressure.

The graph of L-L density approximation of {[BMIM]Cl: EG + ethanol} binary mixtures against mole fraction, x_1, at different temperatures (293.15 – 313.15) K and at atmospheric pressure is given in Figure 5.18.

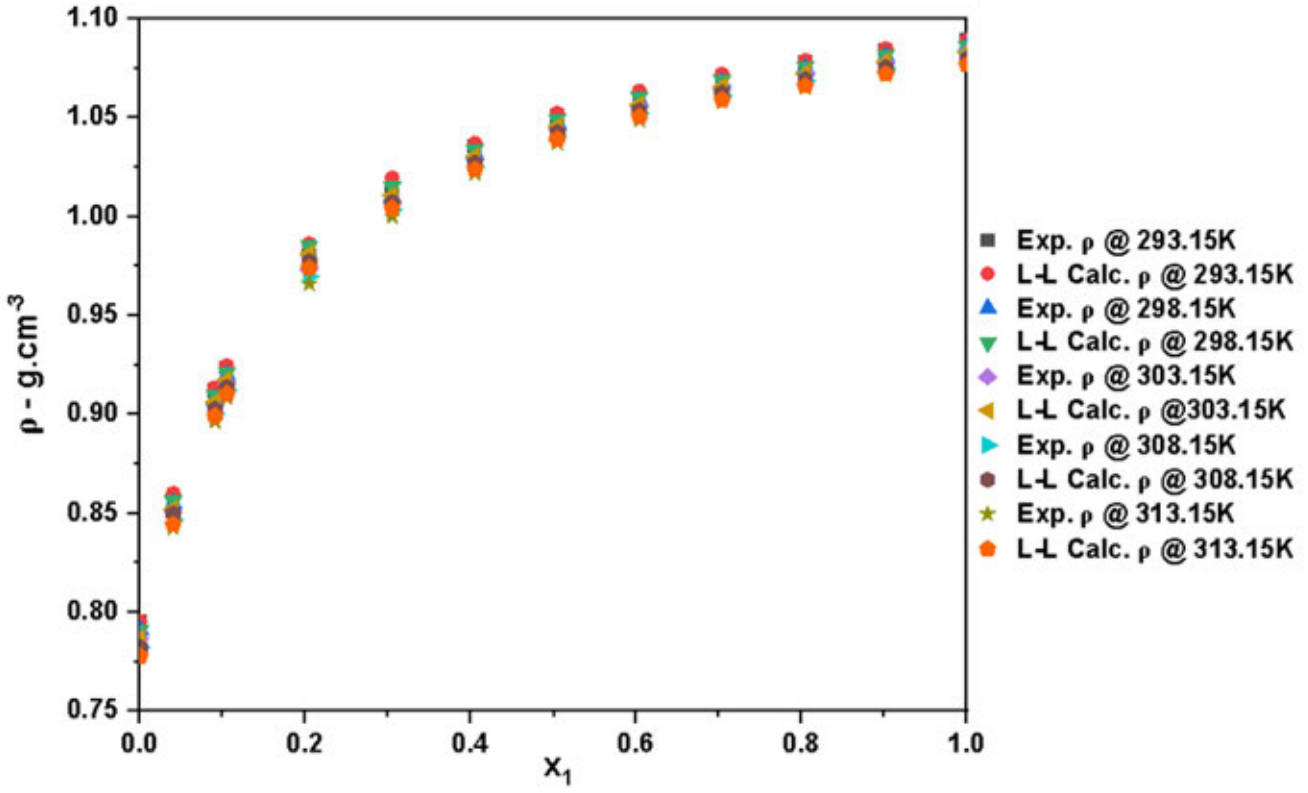

Figure 5.18: Graph of L-L refractive indices approximation of {[BMIM]Cl: EG + ethanol} binary mixtures against mole fraction, x_1, at different temperatures (293.15 – 313.15) K and at atmospheric pressure.

Figure 5.19 is the graph of L-L refractive indices approximation of {[BMIM]Cl: EG + methanol} binary mixtures against mole fraction, x_1, at different temperatures (293.15 – 313.15) K and at atmospheric pressure.

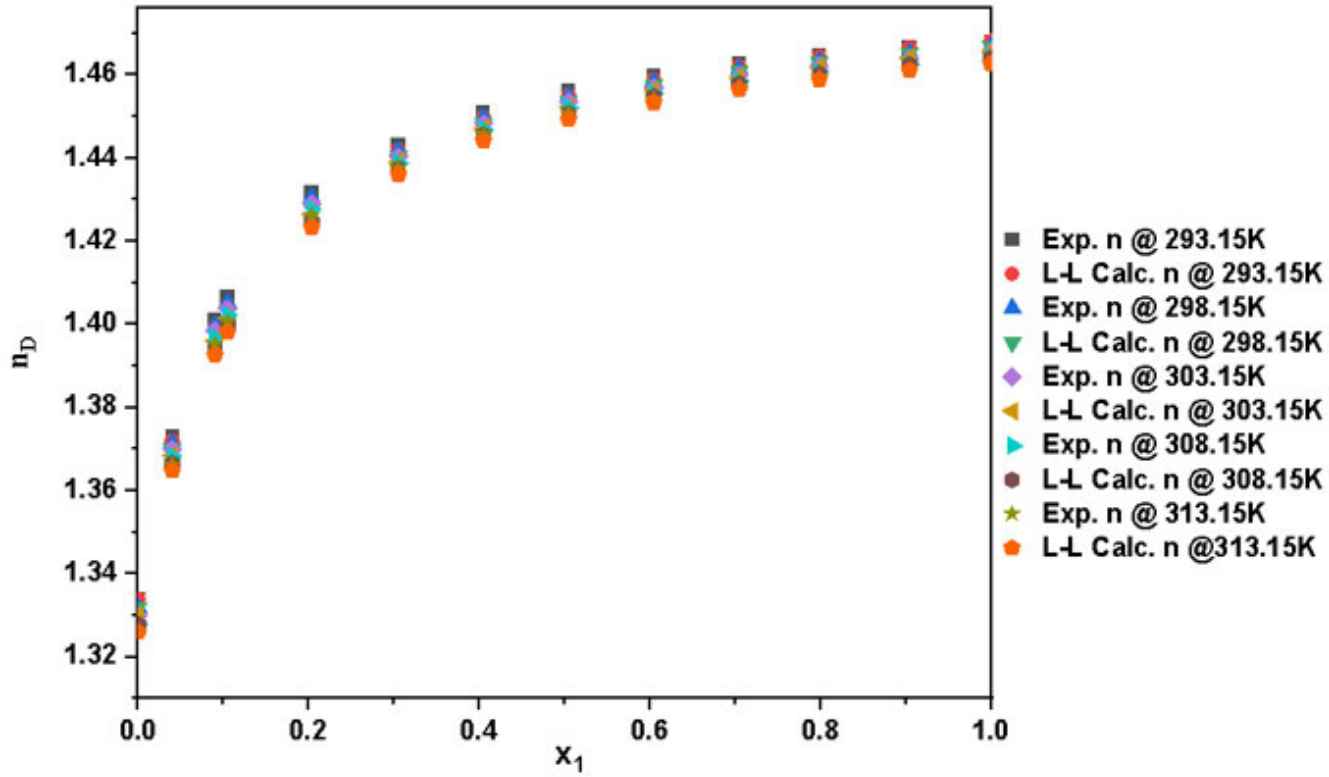

Figure 5.19: Graph of L-L refractive indices approximation of {[BMIM]Cl: EG + methanol} binary mixtures against mole fraction, x_1, at different temperatures (293.15 – 313.15) K and at atmospheric pressure.

The graph of L-L refractive indices approximation of {[BMIM]Cl: EG + ethanol} binary mixtures against mole fraction, x_1, at different temperatures (293.15 – 313.15) K and at atmospheric pressure is given in Figure 5.20.

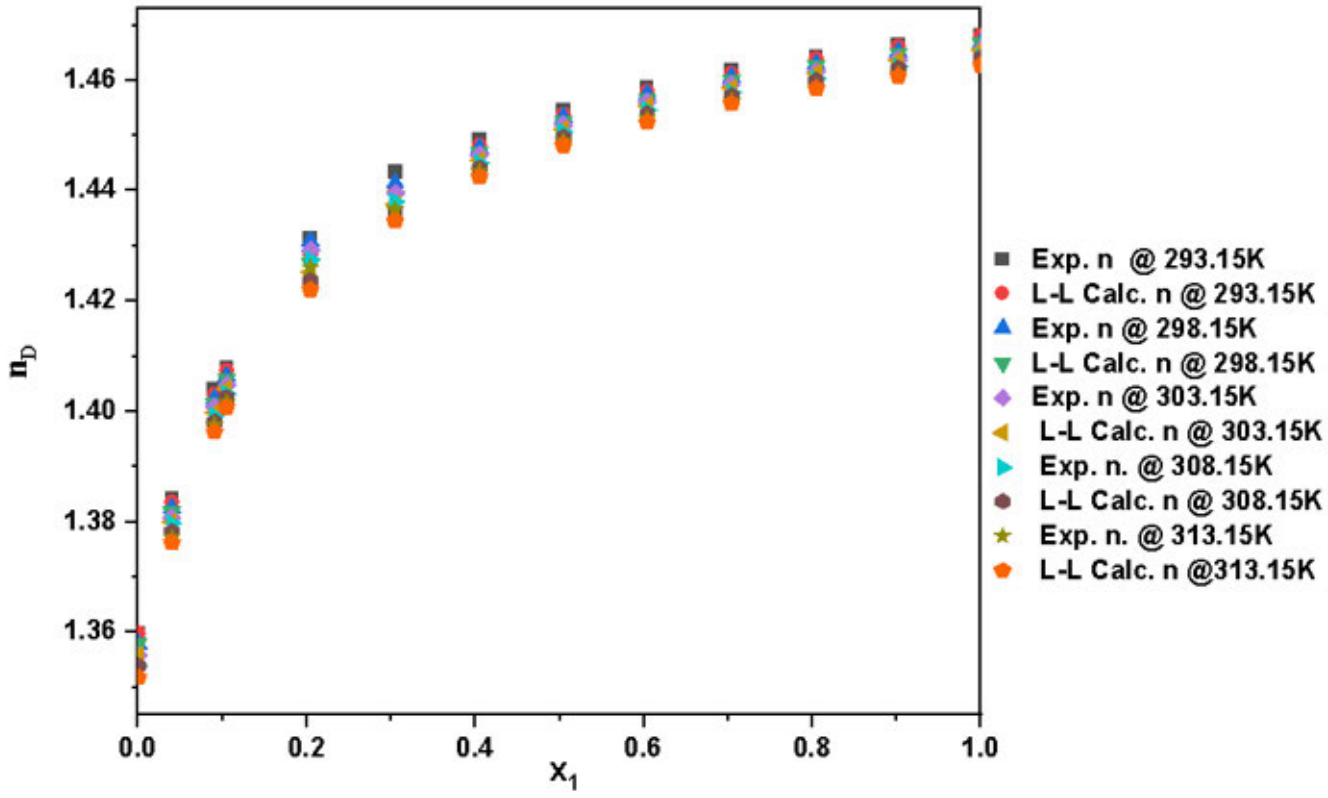

Figure 5.20: Graph of L-L refractive indices approximation of {[BMIM]Cl: EG + methanol} binary mixtures against mole fraction, x_1, at different temperatures (293.15 – 313.15) K and at atmospheric pressure.

The results for the root mean square, σ, obtained from the Lorentz-Lorenz correlation for V_m^{E}, ρ, and Δn_D for {[BMIM]Cl: EG + methanol, or ethanol} binary mixtures at T = (293.15, 298.15, 303.15, 308.15 and 313.15) K is given in Table 5.5.

Table 5-5: is the root mean square deviation, $\boldsymbol{\sigma}$, obtained from the Lorentz-Lorenz correlation for $\boldsymbol{V_m^{\mathrm{E}}}$, $\boldsymbol{\rho}$, and $\Delta \boldsymbol{n_D}$, for binary mixture and at $\boldsymbol{T}$ = (293.15, 298.15, 303.15, 308.15, and 313.15) K.

σ					
Properties	[BMIM]Cl: EG + methanol				
	T/ K				
	293.15	298.15	303.15	308.15	313.15
V_m^{E}/ cm^3.mol^{-1}	0.680	0.665	0.662	0.651	0.649
ρ/ g·cm^{-3}	0.00179	0.00178	0.00164	0.00126	0.000201
n_D	0.00087	0.00087	0.00080	0.00061	0.00095
[BMIM]Cl: EG + ethanol					
V_m^{E}/ cm^3.mol^{-1}	0.770	0.749	0.729	0.708	0.690
ρ/ g·cm^{-3}	0.00266	0.00300	0.00279	0.00291	0.00201
n_D	0.00133	0.00150	0.00140	0.00145	0.00147

5.1.2 1-butyl-2,3-dimethylimidazolium chloride ethylene glycol + acetic acid or propanoic acid binary systems

The results for the density, ρ, speed of sound, u , and refractive index, n_D, is given in Table 5.6.

Table 5-6: is the density, $\boldsymbol{\rho}$, speed of sound, $\boldsymbol{u}$, and refractive index, $\boldsymbol{n_D}$, of {[BDMIM]Cl: EG + acetic acid or propanoic acid} binary mixtures at different temperatures and at atmospheric pressure.

DES + acetic acid				DES + propanoic acid			
x_1	ρ. (g·cm^{-3})	u. (m·s^{-1})	n_D	x_1	ρ. (g·cm^{-3})	u. (m·s^{-1})	n_D
***T* = 293.15K**							
0.0000	1.0495	1151.16	1.3722	0.0000	0.9935	1151.16	1.3881
0.0400	1.0712	1312.62	1.3981	0.0400	1.0211	1298.03	1.4074
0.0899	1.0797	1435.78	1.4177	0.0899	1.0385	1408.29	1.4216
0.1049	1.0812	1459.36	1.4215	0.1050	1.0444	1439.53	1.4260
0.2045	1.0850	1561.90	1.4385	0.2047	1.0592	1538.51	1.4405
0.3049	1.0861	1624.23	1.4486	0.3047	1.0670	1599.68	1.4495
0.4049	1.0866	1668.22	1.4553	0.4046	1.0724	1646.17	1.4553
0.4614	1.0869	1687.17	1.4584	0.5044	1.0767	1682.70	1.4603
0.6035	1.0875	1726.64	1.4640	0.6052	1.0801	1713.19	1.4633
0.7048	1.0877	1747.00	1.4670	0.7051	1.0825	1737.51	1.4666
0.7744	1.0879	1758.99	1.4686	0.8039	1.0846	1758.14	1.4692
0.9041	1.0882	1777.01	1.4712	0.9049	1.0867	1776.03	1.4711
1.0000	1.0884	1788.42	1.4727	1.0000	1.0884	1788.42	1.4713
298.15K							
0.0000	1.0438	1134.33	1.3707	0.0000	0.9881	1134.33	1.3866
0.0400	1.0663	1297.05	1.3968	0.0400	1.0164	1282.21	1.4060
0.0899	1.0753	1421.25	1.4165	0.0899	1.0344	1387.79	1.4202
0.1049	1.0769	1445.01	1.4203	0.1050	1.0401	1424.20	1.4247
0.2045	1.0811	1548.38	1.4375	0.2047	1.0553	1524.17	1.4393
0.3049	1.0824	1611.03	1.4476	0.3047	1.0634	1585.98	1.4484
0.4049	1.0832	1655.24	1.4543	0.4046	1.0689	1632.90	1.4542

0.4614	1.0834	1674.33	1.4574	0.5044	1.0733	1669.70	1.4593
0.6035	1.0843	1714.01	1.4631	0.6052	1.0767	1700.38	1.4623
0.7048	1.0845	1734.42	1.4661	0.7051	1.0792	1724.83	1.4657
0.7744	1.0847	1746.46	1.4677	0.8039	1.0815	1745.59	1.4683
0.9041	1.0851	1764.57	1.4704	0.9049	1.0835	1763.55	1.4702
1.0000	1.0853	1776.04	1.4719	1.0000	1.0853	1776.04	1.4703
***T* = 303.15K**							
0.0000	1.0382	1117.20	1.3694	0.0000	0.9826	1117.20	1.3851
0.0400	1.0614	1281.25	1.3955	0.0400	1.0117	1266.19	1.4046
0.0899	1.0710	1406.46	1.4153	0.0899	1.0299	1367.77	1.4189
0.1049	1.0727	1430.45	1.4192	0.1050	1.0358	1408.60	1.4234
0.2045	1.0774	1534.61	1.4365	0.2047	1.0514	1509.62	1.4383
0.3049	1.0786	1597.64	1.4467	0.3047	1.0597	1572.05	1.4474
0.4049	1.0797	1642.07	1.4534	0.4046	1.0653	1619.39	1.4533
0.4614	1.0799	1661.29	1.4565	0.5044	1.0699	1656.46	1.4584
0.6035	1.0811	1701.19	1.4622	0.6052	1.0734	1687.34	1.4614
0.7048	1.0812	1721.66	1.4652	0.7051	1.0759	1711.94	1.4648
0.7744	1.0814	1733.69	1.4669	0.8039	1.0780	1732.82	1.4675
0.9041	1.0819	1751.93	1.4695	0.9049	1.0802	1750.84	1.4693
1.0000	1.0821	1763.45	1.4710	1.0000	1.0821	1763.45	1.4696
***T* = 308.15K**							
0.0000	1.0325	1100.06	1.3681	0.0000	0.9772	1100.06	1.3836
0.0400	1.0565	1265.48	1.3943	0.0400	1.0070	1249.87	1.4033
0.0899	1.0666	1391.70	1.4142	0.0899	1.0257	1353.98	1.4179
0.1049	1.0684	1415.91	1.4181	0.1050	1.0315	1393.03	1.4223
0.2045	1.0735	1520.85	1.4355	0.2047	1.0475	1495.08	1.4372
0.3049	1.0752	1584.21	1.4457	0.3047	1.0560	1558.12	1.4464
0.4049	1.0759	1628.87	1.4526	0.4046	1.0618	1605.87	1.4524
0.4614	1.0766	1648.20	1.4556	0.5044	1.0665	1643.22	1.4574
0.6035	1.0778	1688.31	1.4614	0.6052	1.0700	1674.29	1.4606
0.7048	1.0781	1708.87	1.4644	0.7051	1.0726	1698.99	1.4640
0.7744	1.0782	1720.93	1.4660	0.8039	1.0749	1719.99	1.4667
0.9041	1.0787	1739.23	1.4687	0.9049	1.0770	1738.10	1.4686
1.0000	1.0789	1750.84	1.4702	1.0000	1.0789	1750.84	1.4688

T = 313.15K							
0.0000	1.0269	1082.86	1.3668	0.0000	0.9718	1082.86	1.3823
0.0400	1.0517	1249.77	1.3932	0.0400	1.0023	1233.44	1.4022
0.0899	1.0622	1377.00	1.4132	0.0899	1.02150	1340.02	1.4168
0.1049	1.0641	1401.40	1.4171	0.1050	1.0272	1377.47	1.4213
0.2045	1.0697	1507.14	1.4346	0.2047	1.0435	1480.59	1.4363
0.3049	1.0715	1570.82	1.4449	0.3047	1.0523	1544.23	1.4456
0.4049	1.0725	1615.67	1.4518	0.4046	1.0582	1592.38	1.4517
0.4614	1.0732	1635.13	1.4549	0.5044	1.0630	1630.02	1.4567
0.6035	1.0744	1675.45	1.4606	0.6052	1.0666	1661.26	1.4599
0.7048	1.0749	1696.07	1.4637	0.7051	1.0693	1686.07	1.4633
0.7744	1.0750	1708.15	1.4654	0.8039	1.0717	1707.18	1.4660
0.9041	1.0755	1726.54	1.4680	0.9049	1.0738	1725.39	1.4679
1.0000	1.0757	1738.19	1.4695	1.0000	1.0757	1738.19	1.4680

Figure 5.22 is the graph of density, $\boldsymbol{\rho}$, of {[BDMIM]Cl: EG + acetic acid} binary mixtures against mole fraction, $\boldsymbol{x_1}$, at different temperatures (293.15 – 313.15) K and at atmospheric pressure.

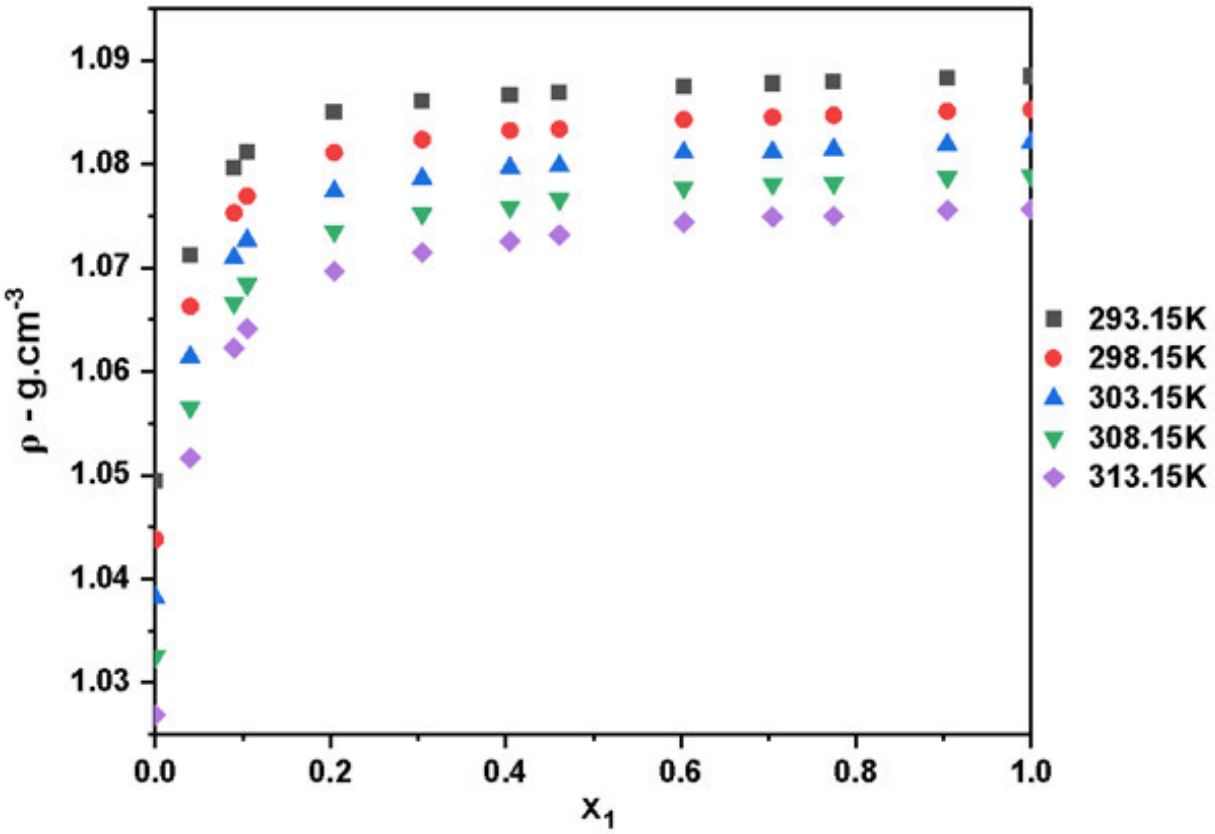

Figure 5.21: Graph of density, $\boldsymbol{\rho}$, of {[BDMIM]Cl: EG + acetic acid} binary mixtures against mole fraction, $\boldsymbol{x_1}$, at different temperatures (293.15 – 313.15) K and at atmospheric pressure.

The graph of density, $\boldsymbol{\rho}$, of {[BDMIM]Cl: EG + propanoic acid} binary mixtures against mole fraction, $\boldsymbol{x_1}$, at different temperatures (293.15 – 313.15) K and at atmospheric pressure is given in Figure 5.22.

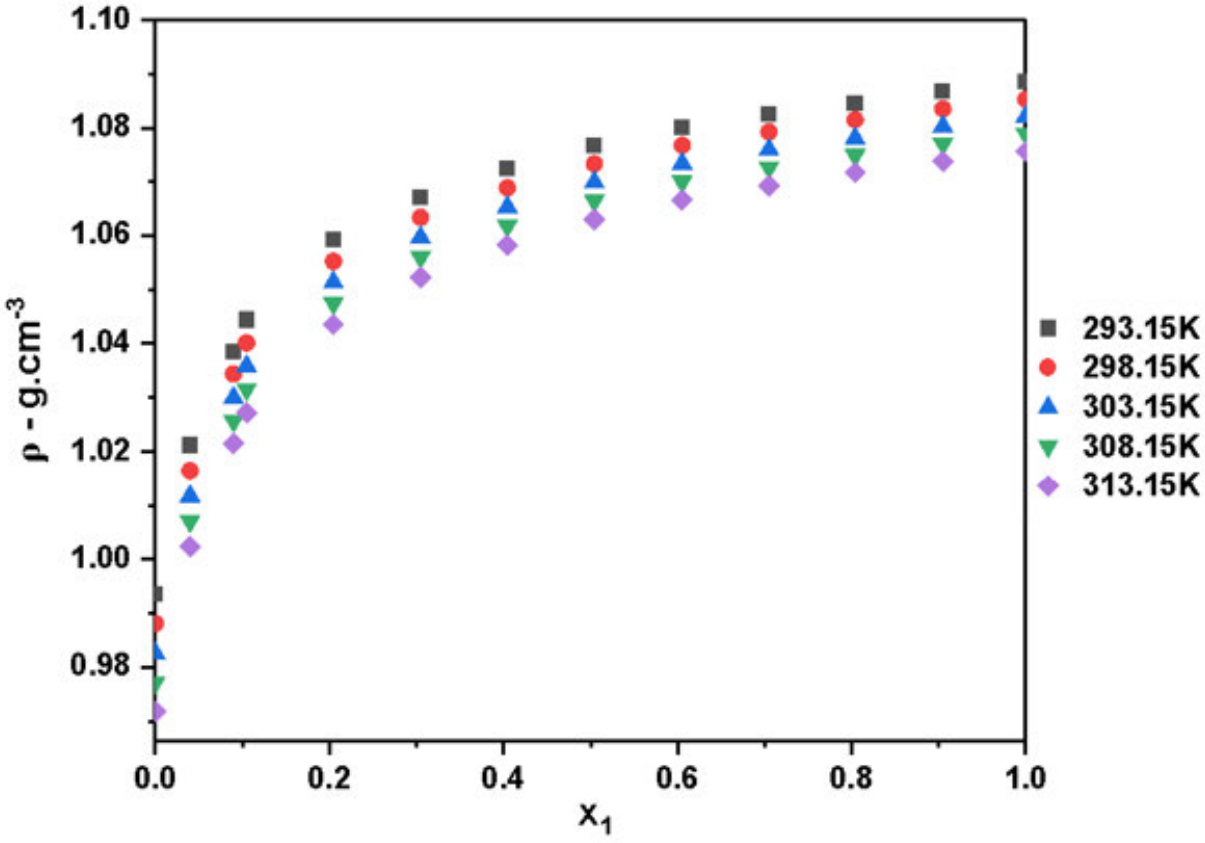

Figure 5.22: Graph density, $\boldsymbol{\rho}$, of {[BDMIM]Cl: EG + propanoic acid} binary mixtures against mole fraction, $\boldsymbol{x_1}$, at different temperatures (293.15 – 313.15) K and at atmospheric pressure

Figure 5.23 is the graph of speed of sound, $\boldsymbol{u}$, of (b), {[BDMIM]Cl: EG + acetic acid} binary mixtures against mole fraction, $\boldsymbol{x_1}$, at different temperatures (293.15 – 313.15) K and at atmospheric pressure.

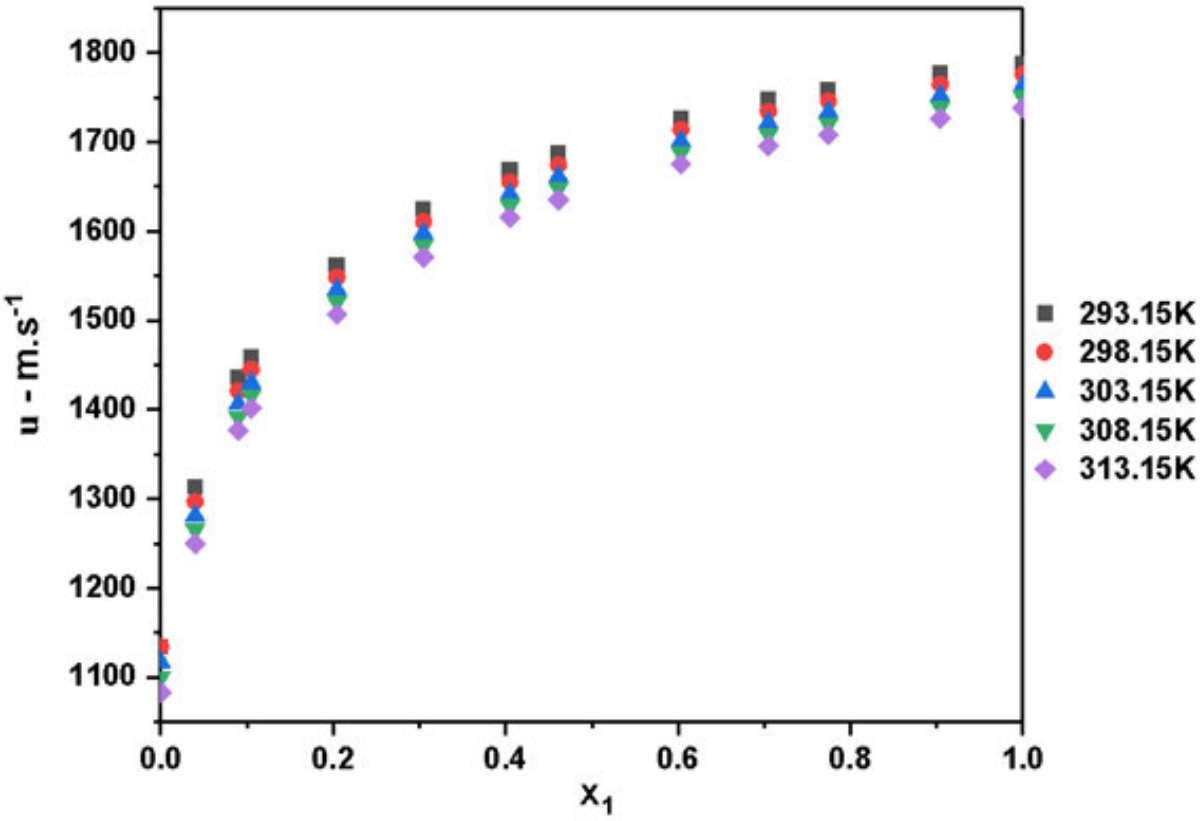

Figure 5.23: Graph of speed of sound, $\boldsymbol{u}$, of {[BDMIM]Cl: EG + acetic acid} binary mixtures against mole fraction, $\boldsymbol{x_1}$, at different temperatures (293.15 – 313.15) K and at atmospheric pressure.

The graph of speed of sound, $\boldsymbol{u}$, of {[BDMIM]Cl: EG + propanoic acid} binary mixtures against mole fraction, $\boldsymbol{x_1}$, at different temperatures (293.15 – 313.15) K and at atmospheric pressure is given by Figure 5.24.

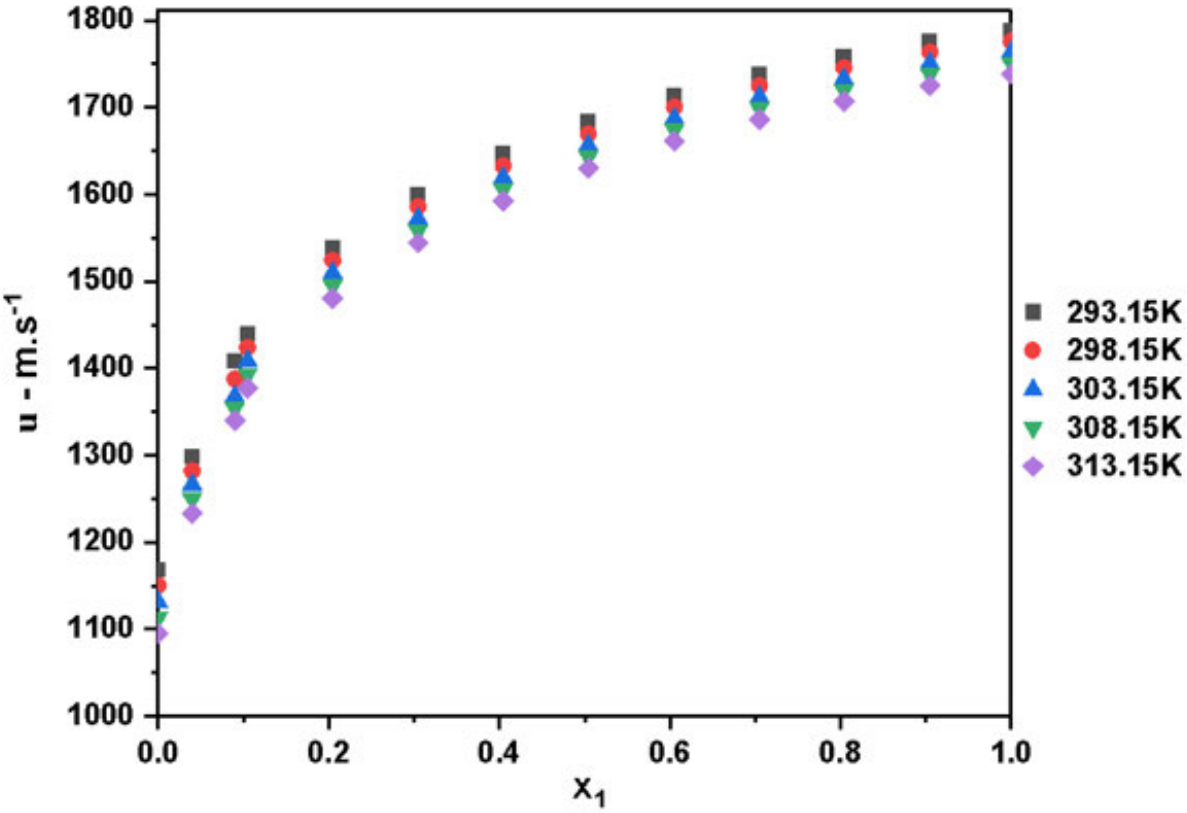

Figure 5.24: Graph of speed of sound, $\boldsymbol{u}$, of {[BDMIM]Cl: EG + propanoic acid} binary mixtures against mole fraction, $\boldsymbol{x_1}$, at different temperatures (293.15 – 313.15) K and at atmospheric pressure.

Figure 5.24 is the graph of refractive index, n_D, of {[BDMIM]Cl: EG + acetic acid} binary mixtures against mole fraction, x_1, at different temperatures (293.15 – 313.15) K and at atmospheric pressure.

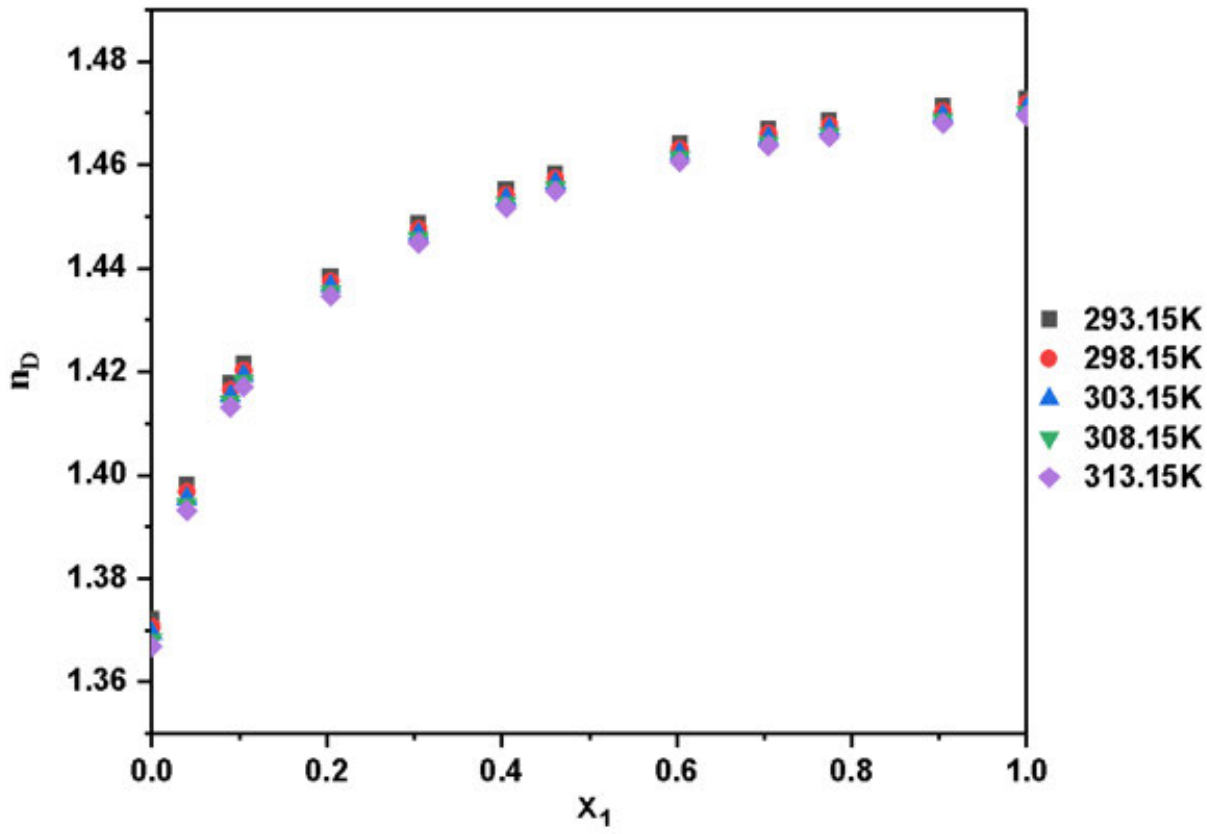

Figure 5.25: Graph of refractive index, n_D, of {[BDMIM]Cl: EG + acetic acid} binary mixtures against mole fraction, x_1, at different temperatures (293.15 – 313.15) K and at atmospheric pressure.

The graph of refractive index, n_D, of {[BDMIM]Cl: EG + propanoic acid} binary mixtures against mole fraction, x_1, at different temperatures (293.15 – 313.15) K and at atmospheric pressure.

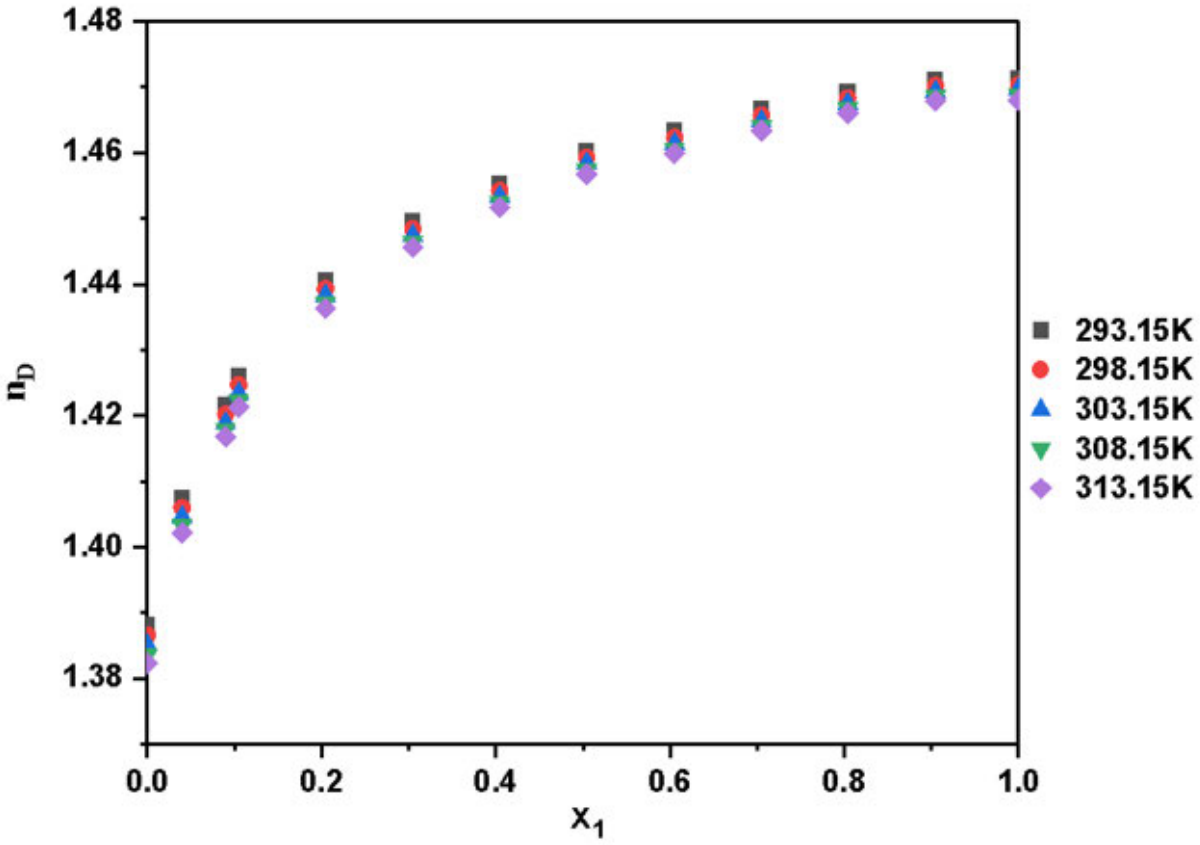

Figure 5.26: Graph of refractive index, n_D, of {[BDMIM]Cl: EG + propanoic acid} binary mixtures against mole fraction, x_1, at different temperatures (293.15 – 313.15) K and at atmospheric pressure.

The results for the excess molar volume, V_m^{E}, intermolecular free length, L_f, isentropic compressibilities, k_s, deviation in isentropic compressibilities, Δk_s, deviation refractive index, Δn_D, and molar refraction, R, of {[BDMIM]Cl: EG + acetic acid or propanoic acid} binary mixtures at different temperatures and at atmospheric pressure is given in Table 5.7.

Table 5-7: is the calculated excess molar volumes, $\boldsymbol{V_m^{\mathrm{E}}}$, intermolecular free length, $\boldsymbol{L_f}$, isentropic compressibility, $\boldsymbol{k_s}$, deviation in isentropic compressibility, $\Delta\boldsymbol{k_s}$, deviation in refractive indices, $\Delta\boldsymbol{n_D}$, and molar refraction, $\boldsymbol{R}$, of {[BDMIM]Cl: EG + acetic acid or propanoic acid} binary mixtures at different temperatures and at atmospheric pressure.

DES with acetic acid						
x_1	V_m^{E}/(cm^{-3}.mol^{-1})	L_f/10^-11(m)	k_s/10^10(Pa^{-1})	Δk_s/10^10 (Pa^{-1})	Δn_D	R/(cm^3.mol^{-1})
***T* = 293.15K**						
0.0000	0.0000	5.4651	7.1905	0.0000	0.0000	13.01
0.0400	-0.8898	4.7441	5.4184	-1.5991	0.0219	16.38
0.0899	-1.2037	4.3200	4.4930	-2.3089	0.0365	20.62
0.1049	-1.2574	4.2473	4.3430	-2.3942	0.0388	21.86
0.2045	-1.2714	3.9613	3.7779	-2.5297	0.0458	30.13
0.3049	-1.1131	3.8075	3.4901	-2.3839	0.0458	38.51
0.4049	-0.9335	3.7061	3.3068	-2.1355	0.0424	46.85
0.4614	-0.8398	3.6640	3.2318	-1.9663	0.0398	51.58
0.6035	-0.6152	3.5793	3.0844	-1.5004	0.0312	63.45
0.7048	-0.4388	3.5372	3.0128	-1.1348	0.0240	71.93
0.7744	-0.3266	3.5128	2.9710	-0.8760	0.0186	77.73
0.9041	-0.1392	3.4767	2.9104	-0.3766	0.0081	88.57
1.0000	0.0000	3.4542	2.8725	0.0000	0.0000	96.57
***T* = 298.15K**						
0.0000	0.0000	5.6123	7.4455	0.0000	0.0000	13.03
0.0400	-0.9168	4.8563	5.5746	-1.6896	0.0220	16.40
0.0899	-1.2439	4.4133	4.6040	-2.4343	0.0367	20.65
0.1049	-1.3002	4.3375	4.4471	-2.5233	0.0390	21.89
0.2045	-1.3065	4.0400	3.8581	-2.6622	0.0461	30.18

0.3049	-1.1409	3.8807	3.5598	-2.5063	0.0461	38.57
0.4049	-0.9842	3.7755	3.3694	-2.2443	0.0426	46.91
0.4614	-0.8544	3.7322	3.2920	-2.0656	0.0400	51.65
0.6035	-0.6632	3.6443	3.1397	-1.5760	0.0313	63.53
0.7048	-0.4706	3.6010	3.0657	-1.1915	0.0241	72.02
0.7744	-0.3533	3.5759	3.0226	-0.9195	0.0186	77.83
0.9041	-0.1597	3.5385	2.9603	-0.3953	0.0082	88.70
1.0000	0.0000	3.5154	2.9209	0.0000	0.0000	96.72
T = 303.15K						
0.0000	0.0000	5.7659	7.7173	0.0000	0.0000	13.06
0.0400	-0.9455	4.9723	5.7391	-1.7880	0.0220	16.43
0.0899	-1.2876	4.5094	4.7204	-2.5700	0.0368	20.68
0.1049	-1.3447	4.4303	4.5561	-2.6630	0.0391	21.93
0.2045	-1.3660	4.1205	3.9413	-2.8057	0.0463	30.23
0.3049	-1.1730	3.9557	3.6322	-2.6383	0.0463	38.63
0.4049	-1.0093	3.8468	3.4351	-2.3609	0.0429	46.98
0.4614	-0.8746	3.8020	3.3554	-2.1725	0.0402	51.73
0.6035	-0.7241	3.7107	3.1965	-1.6574	0.0315	63.61
0.7048	-0.4783	3.6664	3.1207	-1.2522	0.02420	72.13
0.7744	-0.3675	3.6405	3.0772	-0.9661	0.0188	77.95
0.9041	-0.1758	3.6019	3.0123	-0.4154	0.0082	88.81
1.0000	0.0000	3.5787	2.9716	0.0000	0.0000	96.84
T = 308.15K						
0.0000	0.0000	5.9248	8.0033	0.0000	0.0000	13.09
0.0400	-0.9747	5.0915	5.9102	-1.8935	0.0221	16.46
0.0899	-1.3311	4.6078	4.8407	-2.7144	0.0369	20.72
0.1049	-1.3907	4.5252	4.6687	-2.8118	0.0393	21.97
0.2045	-1.4142	4.2029	4.0273	-2.9578	0.0465	30.28
0.3049	-1.2444	4.0317	3.7058	-2.7792	0.0465	38.68
0.4049	-1.0008	3.9199	3.5033	-2.4839	0.0432	47.08
0.4614	-0.9459	3.8726	3.4192	-2.2867	0.0404	51.80
0.6035	-0.7509	3.7786	3.2556	-1.7431	0.0317	63.71
0.7048	-0.5460	3.7326	3.1770	-1.3171	0.0243	72.23

0.7744	-0.3792	3.7063	3.1324	-1.0155	0.0188	78.06
0.9041	-0.1966	3.6663	3.0654	-0.4366	0.0083	88.95
1.0000	0.0000	3.6418	3.0235	0.0000	0.0000	96.99
***T* = 313.15K**						
0.0000	0.0000	6.0895	8.3050	0.0000	0.0000	13.12
0.0400	-1.0046	5.2137	6.0879	-2.0077	0.0223	16.50
0.0899	-1.3757	4.7084	4.9649	-2.8696	0.0372	20.76
0.1049	-1.4377	4.6222	4.7849	-2.9712	0.0395	22.01
0.2045	-1.4643	4.2868	4.1157	-3.1204	0.0468	30.33
0.3049	-1.2772	4.1096	3.7824	-2.9287	0.0468	38.75
0.4049	-1.0725	3.9935	3.5718	-2.6166	0.0434	47.15
0.4614	-0.9837	3.9449	3.4853	-2.4078	0.0407	51.90
0.6035	-0.7770	3.8477	3.3161	-1.8344	0.0318	63.82
0.7048	-0.5925	3.8001	3.2347	-1.3861	0.0245	72.35
0.7744	-0.4220	3.7730	3.1889	-1.0685	0.0191	78.20
0.9041	-0.2138	3.7319	3.1200	-0.4593	0.0084	89.10
1.0000	0.0000	3.7066	3.0771	0.0000	0.0000	97.16

DES with Propanoic acid						
x_1	V_m^{E}/(cm^3.mol^{-1})	L_f/10^-11(m)	k_s/10^10(Pa^{-1})	Δk_s/10^10 (Pa^{-1})	Δn_D	R/(cm^3.mol^{-1})
***T* = 293.15K**						
0.0000	0.0000	5.5342	7.3735	0.0000	0.0000	17.60
0.0400	-1.0285	4.9136	5.8125	-1.5943	0.0160	20.78
0.0899	-1.4531	4.4908	4.8553	-2.3161	0.0260	24.72
0.1050	-1.7282	4.3810	4.6206	-2.4793	0.0292	25.93
0.2047	-1.7301	4.0704	3.9888	-2.6403	0.0354	33.79
0.3047	-1.4673	3.9003	3.6624	-2.4941	0.0360	41.71
0.4046	-1.1812	3.7807	3.4411	-2.2438	0.0335	49.56
0.5044	-0.9689	3.6911	3.2800	-1.9333	0.0302	57.48
0.6052	-0.7443	3.6198	3.1546	-1.5829	0.0249	65.35
0.7051	-0.4810	3.5651	3.0599	-1.2057	0.0198	73.30
0.8039	-0.2407	3.5199	2.9829	-0.8160	0.0142	81.15

0.9049	-0.0943	3.4812	2.9175	-0.4040	0.0077	89.10
1.0000	0.0000	3.4542	2.8725	0.0000	0.0000	96.33
***T* = 298.15K**						
0.0000	0.0000	5.6893	7.6510	0.0000	0.0000	17.63
0.0400	-1.0683	5.0315	5.9842	-1.6832	0.0161	20.81
0.0899	-1.5222	4.6083	5.0198	-2.4012	0.0261	24.75
0.1050	-1.7799	4.4780	4.7400	-2.6061	0.0293	25.96
0.2047	-1.7852	4.1541	4.0792	-2.7742	0.0356	33.83
0.3047	-1.5196	3.9770	3.7388	-2.6199	0.0363	41.76
0.4046	-1.2289	3.8528	3.5088	-2.3562	0.0337	49.62
0.5044	-1.0097	3.7601	3.3419	-2.0295	0.0305	57.55
0.6052	-0.7772	3.6864	3.2122	-1.6611	0.0251	65.43
0.7051	-0.5030	3.6299	3.1146	-1.2649	0.0201	73.40
0.8039	-0.2919	3.5830	3.0347	-0.8562	0.0144	81.25
0.9049	-0.1289	3.5431	2.9675	-0.4238	0.0079	89.21
1.0000	0.0000	3.5154	2.9212	0.0000	0.0000	96.44
***T* = 303.15K**						
0.0000	0.0000	5.8516	7.9483	0.0000	0.0000	17.67
0.0400	-1.1192	5.1535	6.1651	-1.7812	0.0161	20.85
0.0899	-1.5775	4.7284	5.1900	-2.4981	0.0262	24.79
0.1050	-1.8423	4.5783	4.8657	-2.7440	0.0294	26.00
0.2047	-1.8503	4.2403	4.1736	-2.9195	0.0359	33.89
0.3047	-1.5812	4.0559	3.8185	-2.7561	0.0366	41.83
0.4046	-1.2845	3.9268	3.5794	-2.4778	0.0340	49.70
0.5044	-1.0590	3.8308	3.4065	-2.1335	0.0307	57.64
0.6052	-0.8156	3.7546	3.2723	-1.7455	0.0252	65.53
0.7051	-0.5353	3.6962	3.1713	-1.3289	0.0201	73.51
0.8039	-0.2709	3.6481	3.0893	-0.8989	0.0145	81.39
0.9049	-0.1110	3.6069	3.0199	-0.4445	0.0077	89.33
1.0000	0.0000	3.5781	2.9718	0.0000	0.0000	90.60
***T* = 308.15K**						
0.0000	0.0000	6.0180	8.2569	0.0000	0.0000	17.71
0.0400	-1.1639	5.2802	6.3566	-1.8822	0.0163	20.88

0.0899	-1.6428	4.8297	5.3181	-2.6499	0.0266	24.84
0.1050	-1.8990	4.6810	4.9957	-2.8901	0.0298	26.05
0.2047	-1.9107	4.3282	4.2711	-3.0733	0.0362	33.94
0.3047	-1.6380	4.1363	3.9007	-2.9001	0.0368	41.89
0.4046	-1.3361	4.0023	3.6521	-2.6063	0.0343	49.78
0.5044	-1.1039	3.9028	3.4727	-2.2433	0.0308	57.71
0.6052	-0.8514	3.8240	3.3340	-1.8347	0.0254	65.64
0.7051	-0.5612	3.7638	3.2298	-1.3962	0.0203	73.62
0.8039	-0.3159	3.7140	3.1448	-0.9444	0.0146	81.51
0.9049	-0.1200	3.6717	3.0736	-0.4667	0.0079	89.49
1.0000	0.0000	3.6418	3.0237	0.0000	0.000	96.74
T = 313.15K						
0.0000	0.0000	6.1881	8.5762	0.0000	0.0000	17.75
0.0400	-1.2090	5.4111	6.5577	-1.9898	0.0165	20.93
0.0899	-1.7123	4.9339	5.4519	-2.8115	0.0268	24.88
0.1050	-1.9562	4.7863	5.1306	-3.0466	0.0300	26.10
0.2047	-1.9720	4.4180	4.3714	-3.2377	0.0365	34.01
0.3047	-1.6967	4.2183	3.9851	-3.0539	0.0372	41.97
0.4046	-1.3888	4.0792	3.7267	-2.7434	0.0347	49.88
0.5044	-1.1506	3.9761	3.5406	-2.3606	0.0312	57.82
0.6052	-0.8904	3.8947	3.3972	-1.9299	0.0254	65.76
0.7051	-0.5901	3.8326	3.2897	-1.4681	0.0206	73.76
0.8039	-0.3650	3.7809	3.2016	-0.9931	0.0148	81.64
0.9049	-0.1372	3.7374	3.1283	-0.4905	0.0081	89.64
1.0000	0.0000	3.7066	3.0771	0.0000	0.0000	96.89

Figure 5.27 is the graph of excess molar volume, $\boldsymbol{V_m^E}$, of {[BDMIM]Cl: EG + acetic acid} binary mixtures against mole fraction, $\boldsymbol{x_1}$, at different temperatures (293.15 – 313.15) K and at atmospheric pressure.

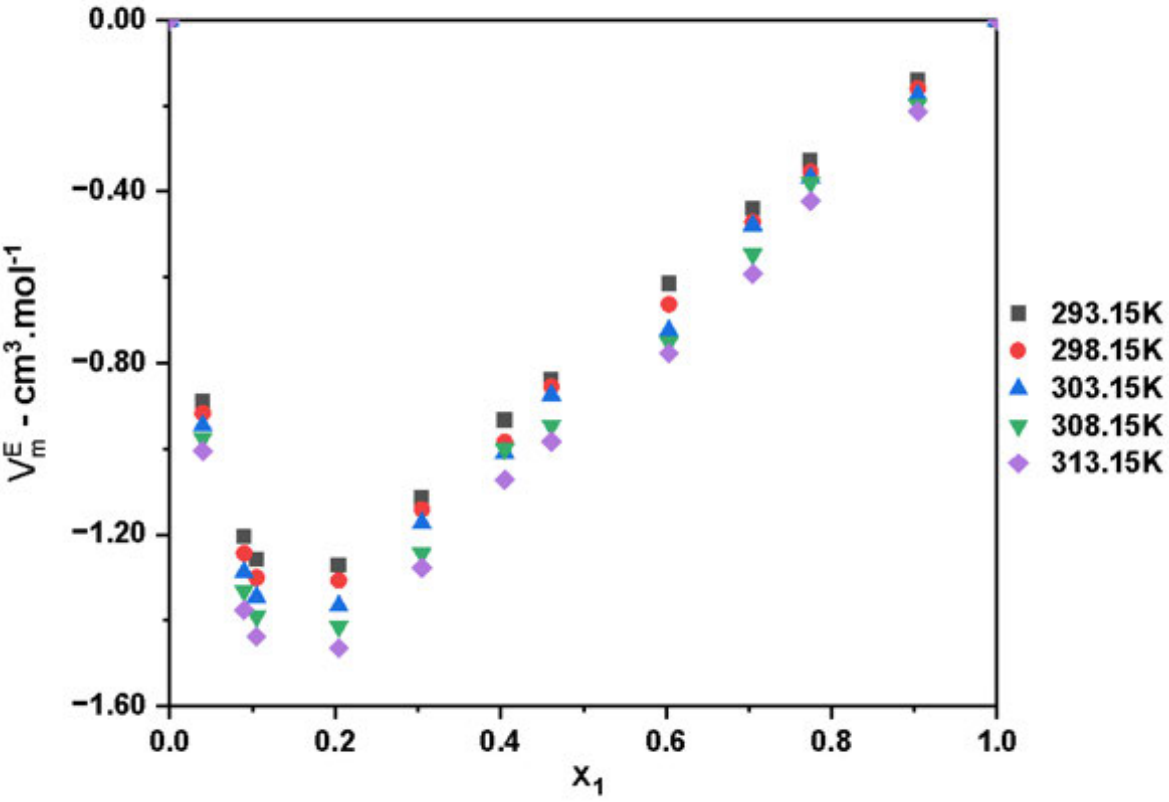

Figure 5.27: Graph of excess molar volume, $\boldsymbol{V_m^E}$, of {[BDMIM]Cl: EG + acetic acid} binary mixtures against mole fraction, $\boldsymbol{x_1}$, at different temperatures (293.15 – 313.15) K and at atmospheric pressure.

The graph of excess molar volume, V_m^E, of {[BDMIM]Cl: EG + propanoic acid} binary mixtures against mole fraction, x_1, at different temperatures (293.15 – 313.15) K and at atmospheric pressure is given in Figure 5.28.

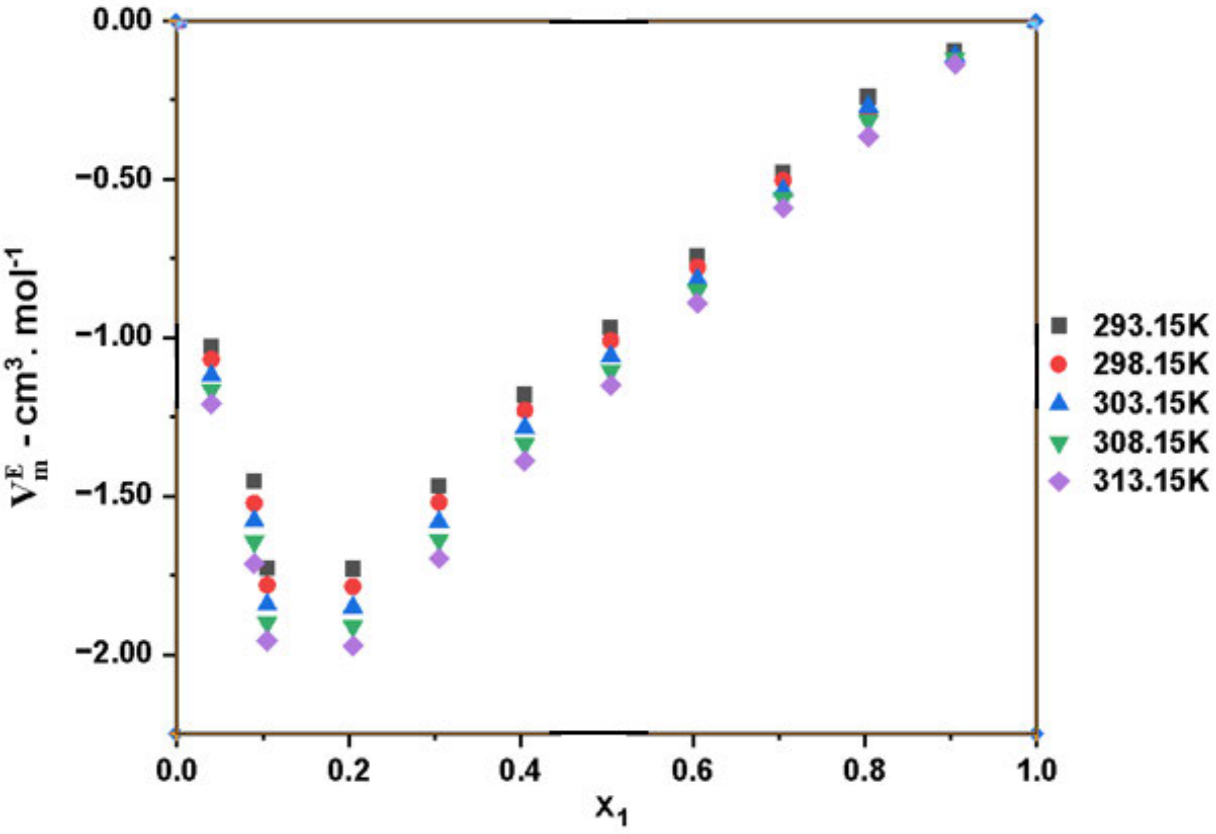

Figure 5.28: Graph of excess molar volume, V_m^E, of {[BDMIM]Cl: EG + propanoic acid} binary mixtures against mole fraction, x_1, at different temperatures (293.15 – 313.15) K and at atmospheric pressure.

Figure 5.29 is the graph of intermolecular free length, L_f, of {[BDMIM]Cl: EG + acetic acid} binary mixtures against mole fraction, x_1, at different temperatures (293.15 – 313.15) K and at atmospheric pressure.

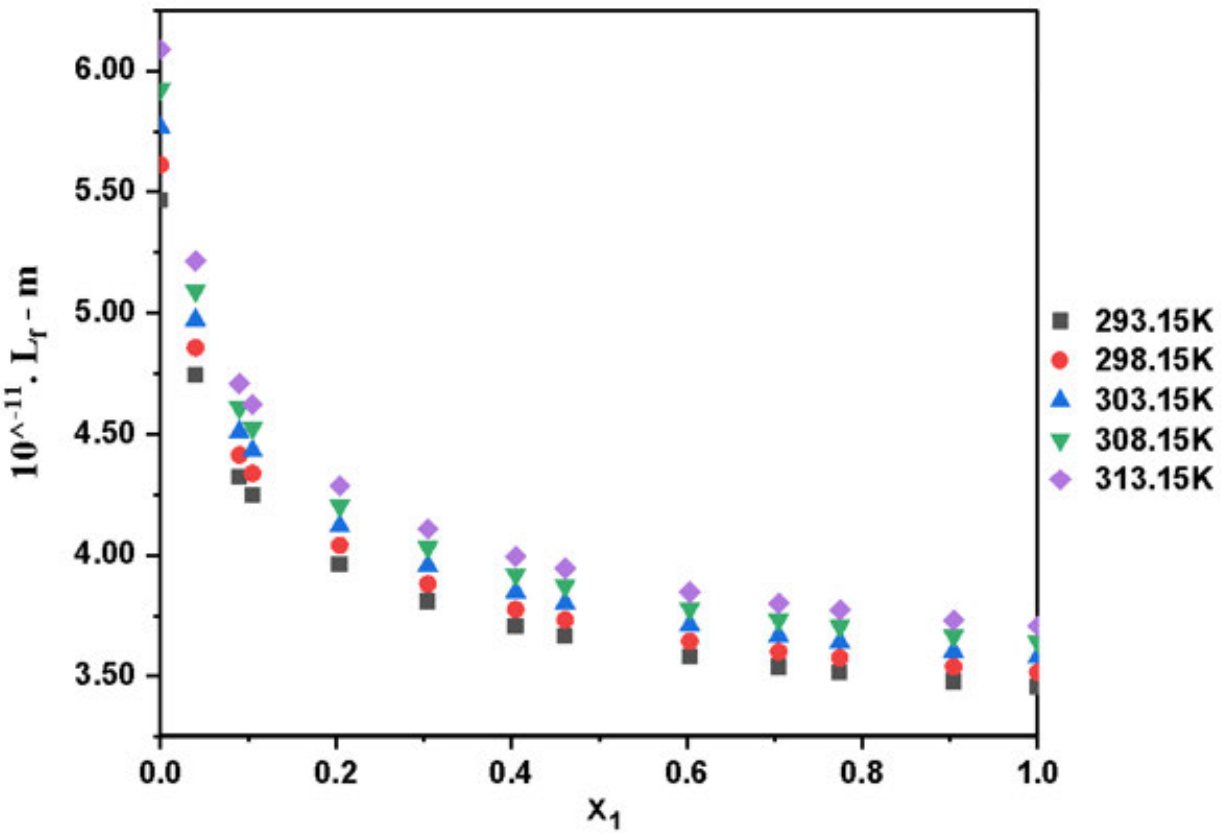

Figure 5.29: Graph of intermolecular free length, L_f, of {[BDMIM]Cl: EG + acetic acid} binary mixtures against mole fraction, x_1, at different temperatures (293.15 – 313.15) K and at atmospheric pressure.

The graph of intermolecular free length, L_f, of {[BDMIM]Cl: EG + propanoic acid} binary mixtures against mole fraction, x_1, at different temperatures (293.15 – 313.15) K and at atmospheric pressure is given in Figure 5.30.

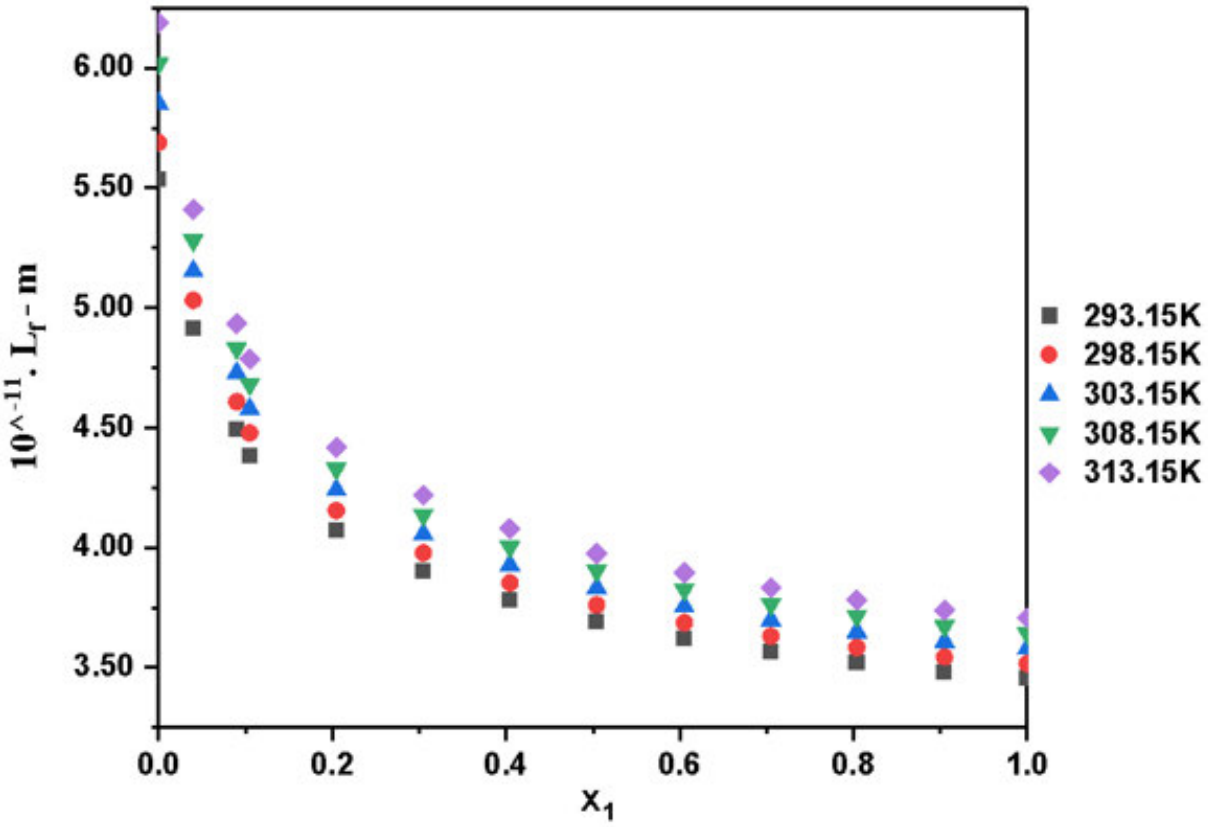

Figure 5.30: Graph of intermolecular free length, L_f, of {[BDMIM]Cl: EG-+ propanoic acid} binary mixtures against mole fraction, x_1, at different temperatures (293.15 – 313.15) K and at atmospheric pressure.

Figure 5.31 is the plot of isentropic compressibility, k_s, of {[BDMIM]Cl: EG + acetic acid} binary mixtures against mole fraction, x_1, at different temperatures (293.15 – 313.15) K and at atmospheric pressure.

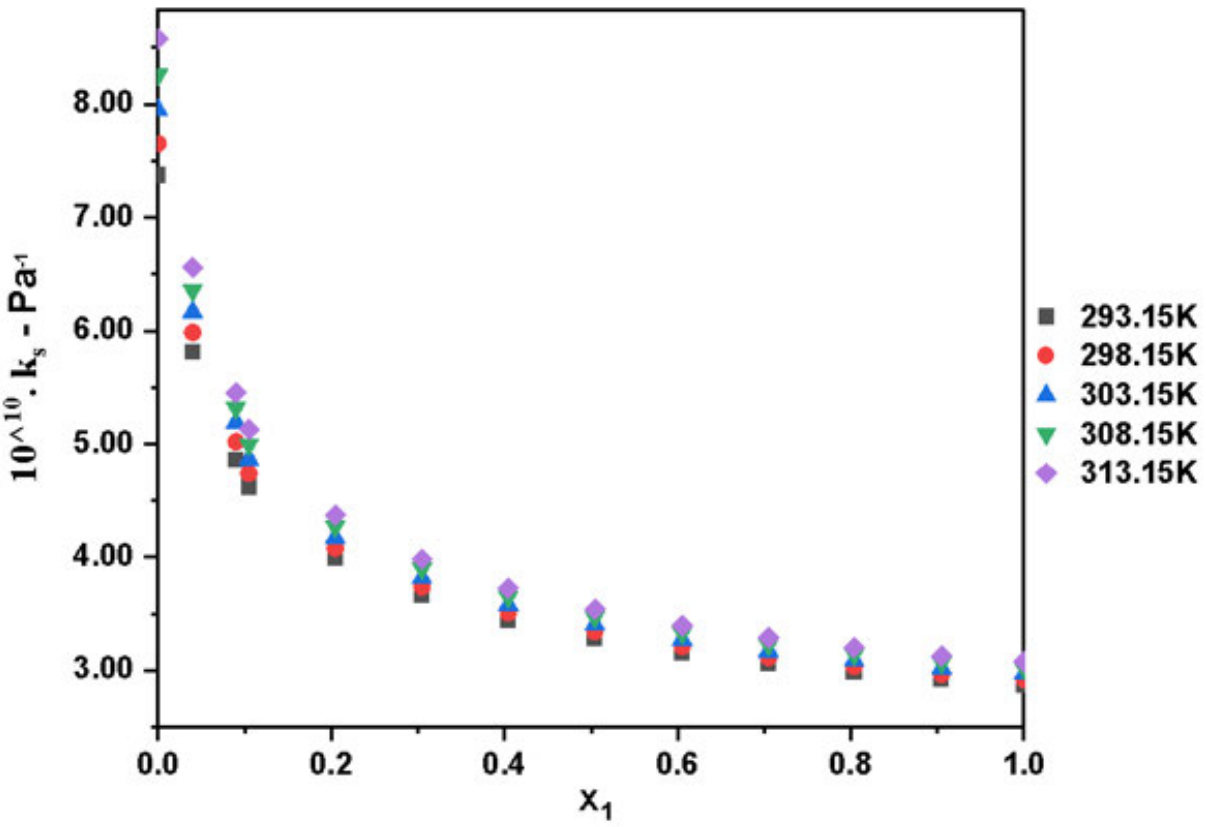

Figure 5.31: Graph of isentropic compressibility, k_s, of {[BDMIM]Cl: EG + acetic acid} binary mixtures against mole fraction, x_1, at different temperatures (293.15 – 313.15) K and at atmospheric pressure.

The graph of isentropic compressibility, k_s, of {[BDMIM]Cl: EG + propanoic acid} binary mixtures against mole fraction, x_1, at different temperatures (293.15 – 313.15) K and at atmospheric pressure is given in Figure 5.32.

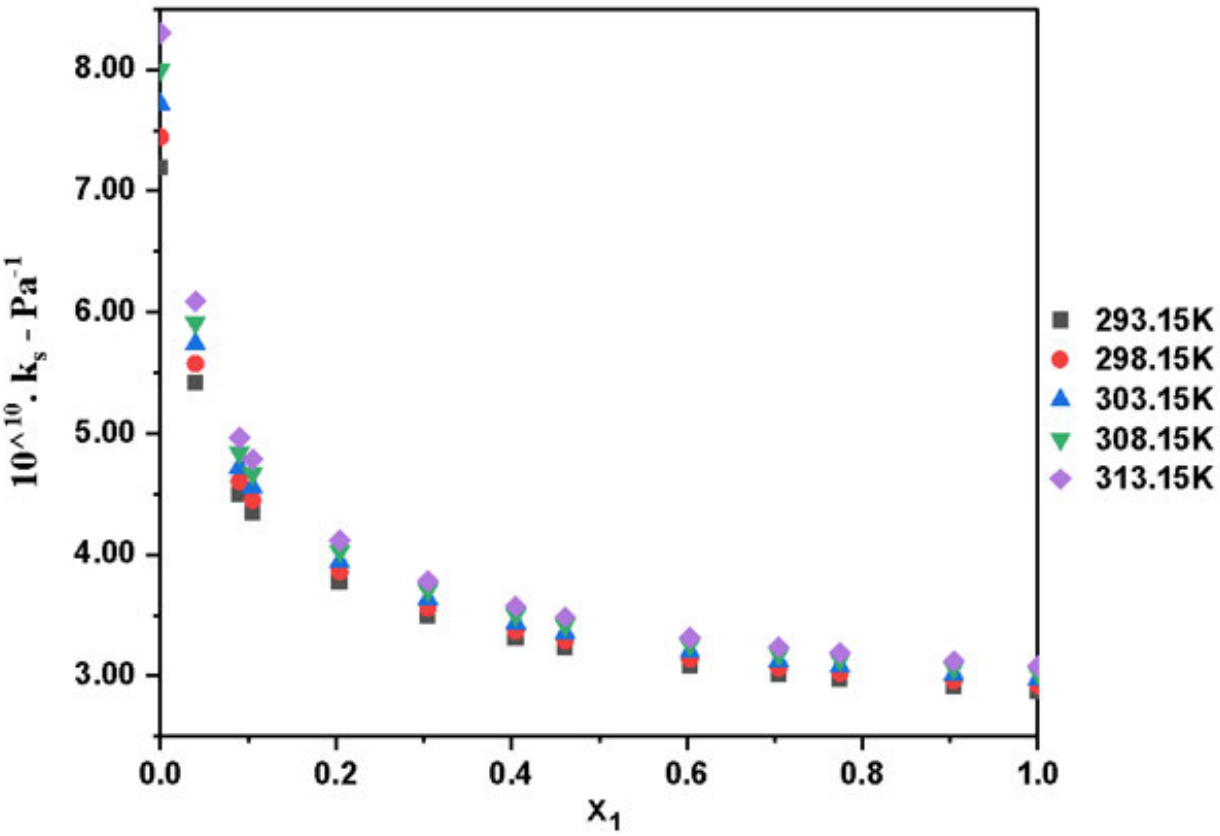

Figure 5.32: is the plot of isentropic compressibility, k_s, of {[BDMIM]Cl: EG + propanoic acid} binary mixtures against mole fraction, x_1, at different temperatures (293.15 – 313.15) K and at atmospheric pressure.

Figure 5.33 is the graph of deviation of isentropic compressibility, Δk_s, of {[BDMIM]Cl: EG + acetic acid} binary mixtures against mole fraction, x_1, at different temperatures (293.15 – 313.15) K and at atmospheric pressure.

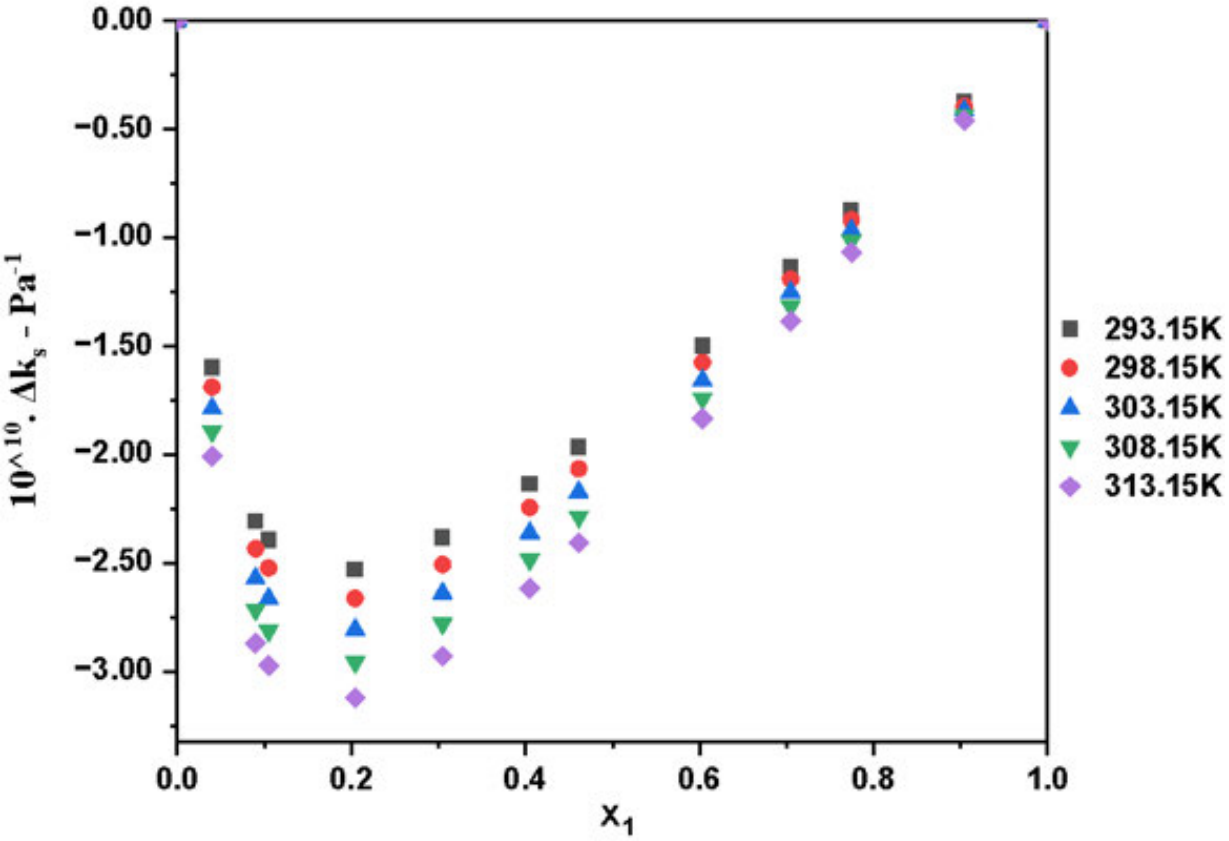

Figure 5.33: Graph of deviation of isentropic compressibility, Δk_s, of {[BDMIM]Cl: EG + acetic acid} binary mixtures against mole fraction, x_1, at different temperatures (293.15 – 313.15) K and at atmospheric pressure.

The graph of deviation of isentropic compressibility, Δk_s, of {[BDMIM]Cl: EG + propanoic acid} binary mixtures against mole fraction, x_1, at different temperatures (293.15 – 313.15) K and at atmospheric pressure is given in Figure 5.34.

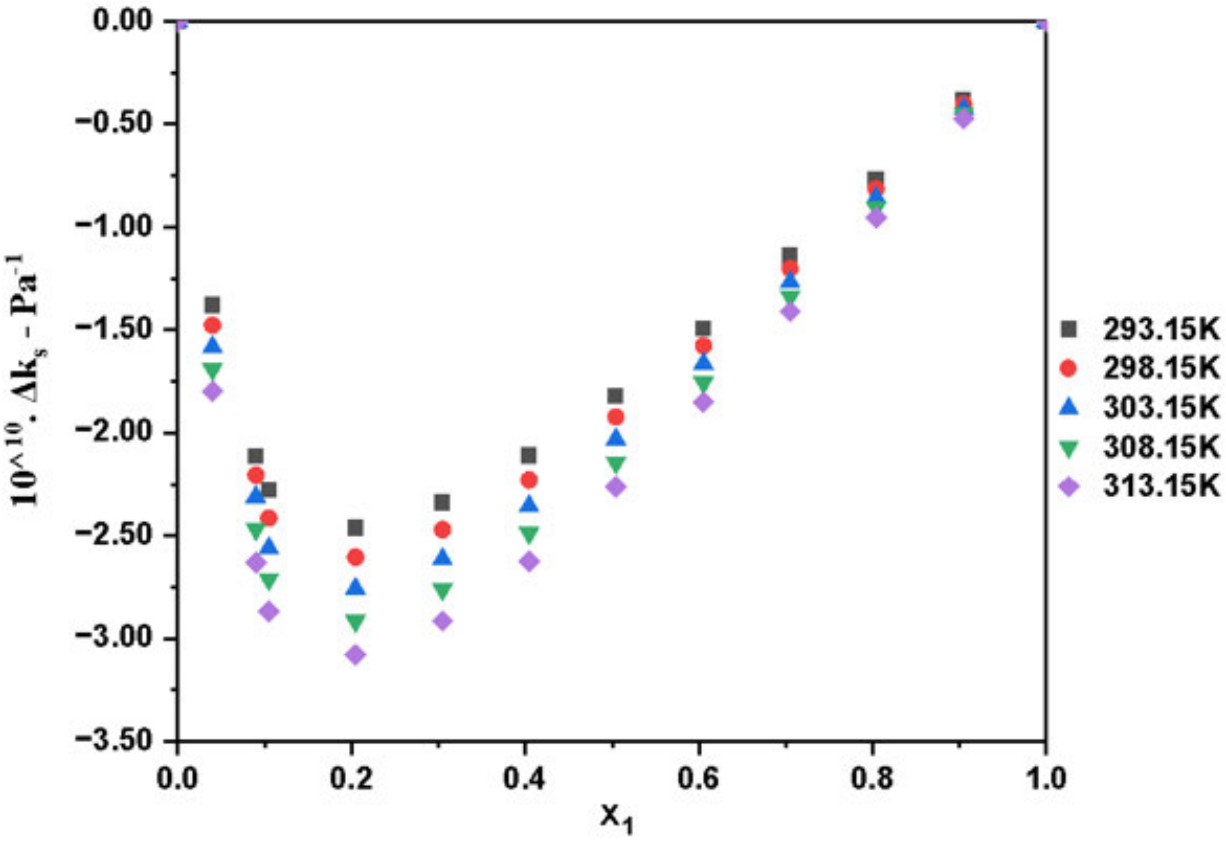

Figure 5.34 Graph of deviation of isentropic compressibility, Δk_s, of {[BDMIM]Cl: EG + propanoic acid} binary mixtures against mole fraction, x_1, at different temperatures (293.15 – 313.15) K and at atmospheric pressure.

Figure 5.35 is the graph of deviation of refractive index, Δn_D, of {[BDMIM]Cl: EG + acetic acid} binary mixtures against mole fraction, x_1, at different temperatures (293.15 – 313.15) K and at atmospheric pressure

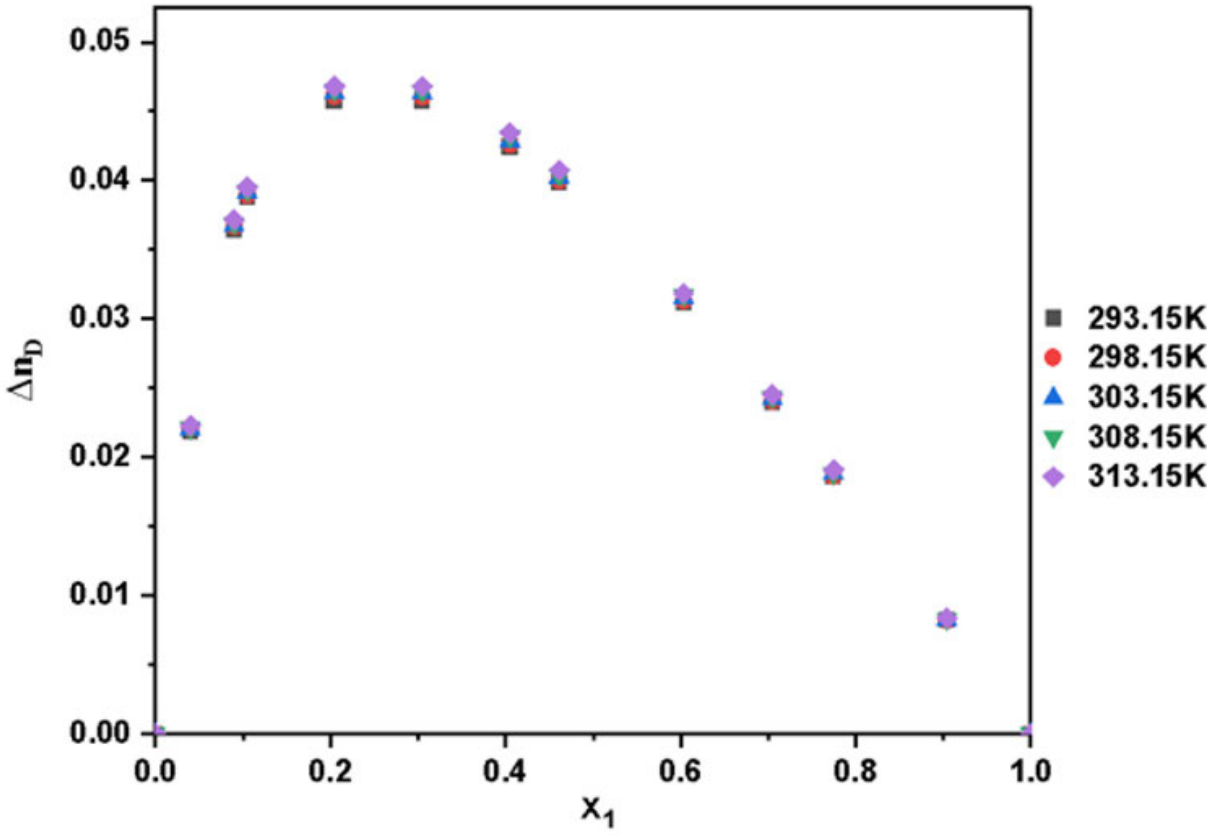

Figure 5.35: Graph of deviation of refractive index, Δn_D, of {[BDMIM]Cl: EG + acetic acid} binary mixtures against mole fraction, x_1, at different temperatures (293.15 – 313.15) K and at atmospheric pressure.

The graph of deviation of refractive index, Δn_D, of {[BDMIM]Cl: EG + propanoic acid} binary mixtures against mole fraction, x_1, at different temperatures (293.15 – 313.15) K and at atmospheric pressure is given by Figure 5.36.

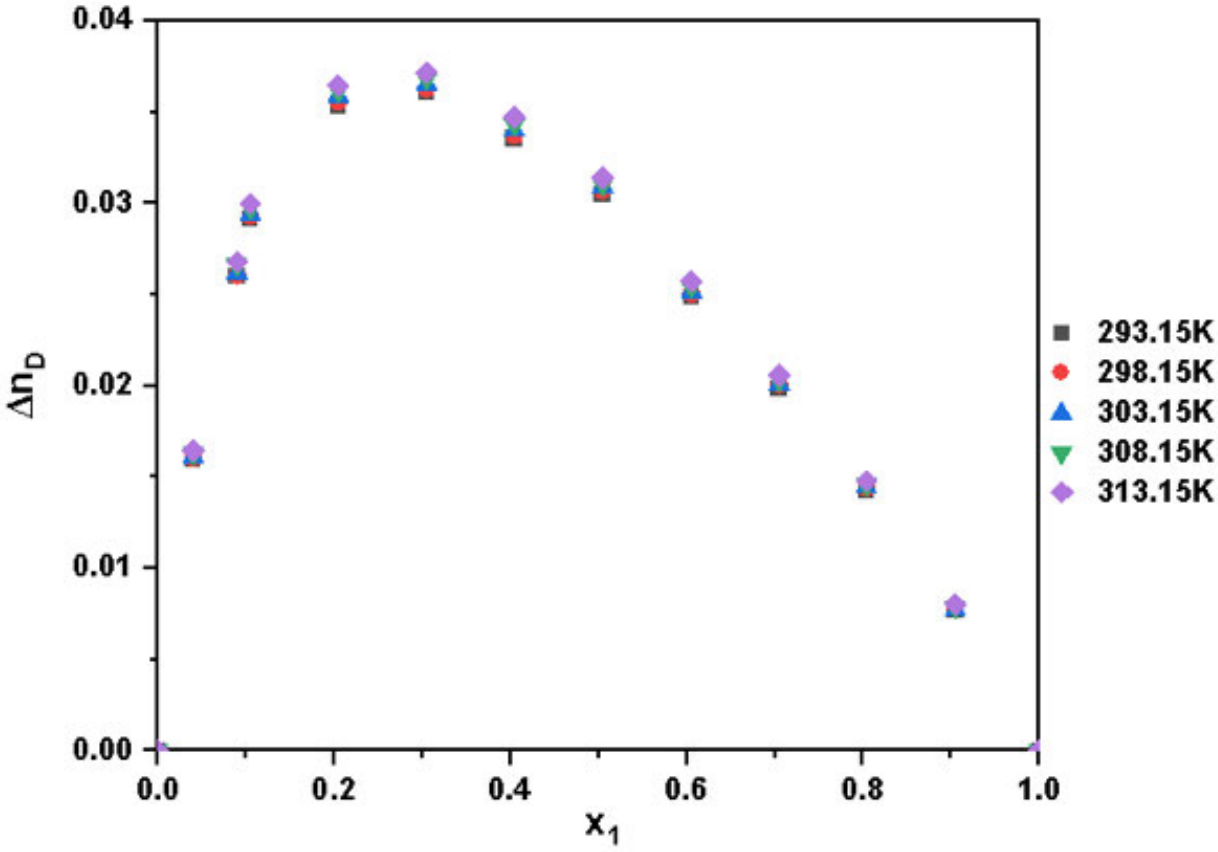

Figure 5.36: Graph of deviation of refractive index, Δn_D, of {[BDMIM]Cl: EG + propanoic acid} binary mixtures against mole fraction, x_1, at different temperatures (293.15 – 313.15) K and at atmospheric pressure.

The results of the Lorentz-Lorenz correlation of excess molar volume, V_m^E, of {[BDMIM]Cl: EG + acetic acid or propanoic acid} binary mixtures at different temperatures at atmospheric pressure is given in Table 5.8.

Table 5-8: is the correlation values for excess molar volume, $\boldsymbol{V_m^E}$, of {[BDMIM]Cl: EG + acetic acid or propanoic acid} binary mixtures at different temperatures and at atmospheric pressure along with the measured values.

DES + acetic acid			DES + propanoic acid		
	L-L, V_m^E/(cm^{-3}.mol)			L-L, V_m^E/(cm^{-3}.mol)	
x_1	Exp. V_m^E	Calc. V_m^E	x_1	Exp. V_m^E	Calc. V_m^E
T = 293.15K					
0.0000	0.0000	0.0000	0.0000	0.0000	0.0000
0.0400	-0.8898	-1.3984	0.0400	-1.0285	-1.4083
0.0899	-1.2037	-1.4179	0.0899	-1.4531	-1.4224
0.1049	-1.2574	-1.4216	0.1050	-1.7282	-1.4268
0.2045	-1.2714	-1.4386	0.2047	-1.7301	-1.4412
0.3049	-1.1131	-1.4457	0.3047	-1.4673	-1.4501
0.4049	-0.9335	-1.4554	0.4046	-1.1812	-1.4559
0.4614	-0.8398	-1.4585	0.5044	-0.9689	-1.4609
0.6035	-0.6152	-1.4640	0.6052	-0.7443	-1.4639
0.7048	-0.4388	-1.4670	0.7051	-0.4810	-1.4672
0.7744	-0.3266	-1.4686	0.8039	-0.2407	-1.4698
0.9041	-0.1392	-0.1392	0.9049	-0.0943	-1.4717
1.0000	0.0000	0.0000	1.0000	0.0000	0.0000
T = 298.15K					
0.0000	0.0000	0.0000	0.0000	0.00000	0.0000
0.0400	-0.9168	-1.4063	0.0400	-1.0683	-14069
0.0899	-1.2439	-1.4204	0.0899	-1.5222	-1.4210
0.1049	-1.3002	-1.4248	0.1050	-1.7799	-1.4255
0.2045	-1.3065	-1.4394	0.2047	-1.7852	-1.4401
0.3049	-1.1409	-1.4485	0.3047	-1.5196	-1.4492
0.4049	-0.9842	-1.4543	0.4046	-1.2289	-1.4550
0.4614	-0.8544	-1.4594	0.5044	-1.0097	-1.4601

0.6035	-0.6632	-1.4623	0.6052	-0.7772	-1.4631
0.7048	-0.4706	-1.4657	0.7051	-0.5030	-1.4664
0.7744	-0.3532	-1.4683	0.8039	-0.2919	-1.4690
0.9041	-0.1597	-1.4702	0.9049	-0.1289	-1.4709
1.0000	0.0000	0.0000	1.0000	0.0000	0.0000
***T* = 303.15K**					
0.0000	0.0000	0.0000	0.0000	0.0000	0.0000
0.0400	-0.9455	-1.3958	0.0400	-1.1192	-1.4055
0.0899	-1.2876	-1.4155	0.0899	-1.5775	-1.4197
0.1049	-1.3447	-1.4193	0.1050	-1.8423	-1.4242
0.2045	-1.3660	-1.4366	0.2047	-1.8503	-1.4391
0.3049	-1.1730	-1.4468	0.3047	-1.5812	-1.4482
0.4049	-1.0093	-1.4535	0.4046	-1.2845	-1.4541
0.4614	-0.8746	-1.4566	0.5044	-1.0590	-1.4592
0.6035	-0.7241	-1.4622	0.6052	-0.8156	-1.4622
0.7048	-0.4783	-1.4652	0.7051	-0.5353	-14655
0.7744	-0.3675	-1.4669	0.8039	-0.2710	-1.4682
0.9041	-0.1758	-1.4695	0.9049	-0.1110	-1.4700
1.0000	0.0000	0.0000	1.0000	0.0000	0.0000
***T* = 308.15K**					
0.0000	0.0000	0.0000	0.0000	0.0000	0.0000
0.0400	-0.9747	-1.3946	0.0400	-1.1639	-1.4042
0.0899	-1.3311	-1.4144	0.0899	-1.6428	-1.4187
0.1049	-1.3907	-1.4182	0.1050	-1.8990	-1.4231
0.2045	-1.4142	-1.4356	0.2047	-1.9107	-1.4380
0.3049	-1.2444	-1.4458	0.3047	-1.6380	-1.4472
0.4049	-1.0008	-1.4527	0.4046	-1.3361	-1.4532
0.4614	-0.9459	-1.4557	0.5044	-1.1039	-1.4582
0.6035	-0.7509	-1.4614	0.6052	-0.8514	-1.4614
0.7048	-0.5460	-1.4544	0.7051	-0.5612	-1.4647
0.7744	-0.3792	-1.4660	0.8039	-0.3159	-1.4674
0.9041	-0.1966	-1.4687	0.9049	-0.1200	-1.4693

1.0000	0.0000	0.0000	1.0000	0.0000	0.0000
***T* = 313.15K**					
0.0000	0.0000	0.0000	0.0000	0.0000	0.0000
0.0400	-1.0046	-1.3935	0.0400	-1.2090	-1.4031
0.0899	-1.3757	-1.4134	0.0899	-1.7123	-1.4176
0.1049	-1.4377	-1.4172	0.1050	-1.9562	-1.4221
0.2045	-1.4643	-1.4347	0.2047	-1.9720	-1.4371
0.3049	-1.2772	-1.4450	0.3047	-1.6967	-1.4464
0.4049	-1.0725	-1.4519	0.4046	-1.3888	-1.4525
0.4614	-0.9837	-1.4550	0.5044	-1.1506	-1.4575
0.6035	-0.7770	-1.4607	0.6052	-0.8904	-1.4607
0.7048	-0.5925	-1.4637	0.7051	-0.5901	-1.4640
0.7744	-0.4220	-1.4654	0.8039	-0.3650	-1.4667
0.9041	-0.2138	-1.4680	0.9049	-0.1372	-1.4686
1.0000	0.0000	0.0000	1.0000	0.0000	0.0000

The results for the predicted values for densities, ρ, and the refractive index, n_D, of {[BDMIM]Cl: EG + acetic acid or propanoic acid} binary mixtures at different temperatures and at atmospheric pressure is given in Table 5.9.

Table 5-9: Predicted values for densities, $\boldsymbol{\rho}$, and refractive indices, $\boldsymbol{n_D}$, of {[BDMIM]Cl: EG + acetic acid or propanoic acid} binary mixtures at different temperatures and at atmospheric pressure along with the measured values.

DES with acetic acid					DES with propanoic acid				
L-L, ρ/(g·cm^3)			L-L - n_D		L-L, ρ/(g·cm^3)			L-L - n_D	
x_1	Exp. ρ	Calc. ρ	Exp. n	Calc. n	x_1	Exp. ρ	Calc. ρ	Exp. n	Calc. n
T = 293.15K									
0.0000	1.0495	1.0495	1.3722	1.3722	0.0000	0.9935	0.9935	1.3881	1.3881
0.0400	1.0712	1.0723	1.3981	1.3976	0.0400	1.0211	1.0225	1.4074	1.4068
0.0899	1.0797	1.0842	1.4177	1.4157	0.0899	1.0385	1.0405	1.4216	1.4207
0.1049	1.0812	1.0850	1.4215	1.4198	0.1050	1.0444	1.0467	1.4260	1.4249
0.2045	1.0850	1.0864	1.4385	1.4379	0.2047	1.0592	1.0615	1.4405	1.4394
0.3049	1.0861	1.0866	1.4486	1.4483	0.3047	1.0670	1.0700	1.4495	1.4481
0.4049	1.0866	1.0868	1.4553	1.4552	0.4046	1.0724	1.0748	1.4553	1.4541
0.4614	1.0869	1.0873	1.4584	1.4582	0.5044	1.0767	1.0798	1.4603	1.4588
0.6035	1.0875	1.0877	1.4640	1.4639	0.6052	1.0801	1.0819	1.4633	1.4624
0.7048	1.0877	1.0880	1.4670	1.4669	0.7051	1.0825	1.0854	1.4666	1.4652
0.7744	1.0879	1.0880	1.4686	1.4685	0.8039	1.0846	1.0881	1.4692	1.4675
0.9041	1.0882	1.0886	1.4713	1.4711	0.9049	1.0867	1.0897	1.4711	1.4696
1.0000	1.0884	1.0884	1.4727	1.4727	1.0000	1.0884	1.0884	1.4713	1.4713
T = 298.15K									
0.0000	1.0438	1.0438	1.3707	1.3707	0.0000	0.9881	0.9881	1.3866	1.3866
0.0400	1.0663	1.0674	1.3968	1.3963	0.0400	1.0164	1.0176	1.4060	1.4055
0.0899	1.0753	1.0797	1.4165	1.4146	0.0899	1.0344	1.0357	1.4202	1.4196
0.1049	1.0769	1.0805	1.4203	1.4187	0.1050	1.0401	1.0422	1.4247	1.4237
0.2045	1.0811	1.0825	1.4375	1.4369	0.2047	1.0553	1.0574	1.4393	1.4383
0.3049	1.0824	1.0829	1.4476	1.4474	0.3047	1.0634	1.0663	1.4484	1.4470
0.4049	1.0832	1.0831	1.4543	1.4544	0.4046	1.0689	1.0712	1.4542	1.4531

0.4614	1.0834	1.0836	1.4574	1.4573	0.5044	1.0733	1.0764	1.4593	1.4578
0.6035	1.0843	1.0842	1.4631	1.4631	0.6052	1.0767	1.0786	1.4623	1.4614
0.7048	1.0845	1.0846	1.4661	1.4661	0.7051	1.0792	1.0823	1.4657	1.4642
0.7744	1.0847	1.0846	1.4677	1.4677	0.8039	1.0815	1.0850	1.4683	1.4665
0.9041	1.0851	1.0852	1.4704	1.4704	0.9049	1.0835	1.0867	1.4702	1.4686
1.0000	1.0853	1.0853	1.4719	1.4719	1.0000	1.0853	1.0853	1.4703	1.4703
***T* = 303.15K**									
0.0000	1.0382	1.0382	1.3694	1.3694	0.0000	0.9826	0.9826	1.3851	1.3851
0.0400	1.0614	1.0621	1.3955	1.3952	0.0400	1.0117	1.0124	1.4046	1.4043
0.0899	1.0710	1.0749	1.4153	1.4136	0.0899	1.0299	1.0309	1.4189	1.4185
0.1049	1.0727	1.0761	1.4192	1.4177	0.1050	1.0358	1.0374	1.4234	1.4227
0.2045	1.0774	1.0786	1.4365	1.4360	0.2047	1.0514	1.0534	1.4383	1.4373
0.3049	1.0786	1.0793	1.4467	1.4464	0.3047	1.0597	1.0623	1.4474	1.4461
0.4049	1.0797	1.0796	1.4534	1.4534	0.4046	1.0653	1.0675	1.4533	1.4523
0.4614	1.0799	1.0802	1.4565	1.4563	0.5044	1.0699	1.0728	1.4584	1.4570
0.6035	1.0811	1.0809	1.4622	1.4623	0.6052	1.0734	1.0749	1.4614	1.4606
0.7048	1.0812	1.0813	1.4652	1.4651	0.7051	1.0759	1.0787	1.4648	1.4634
0.7744	1.0814	1.0816	1.4669	1.4668	0.8039	1.0780	1.0816	1.4675	1.4657
0.9041	1.0819	1.0820	1.4695	1.4695	0.9049	1.0802	1.0831	1.4693	1.4678
1.0000	1.0821	1.0821	1.4710	1.4710	1.0000	1.0821	1.0821	1.4696	1.4696
***T* = 308.15K**									
0.0000	1.0325	1.0325	1.3681	1.3681	0.0000	0.9772	0.9772	1.3836	1.3836
0.0400	1.0565	1.0570	1.3943	1.3941	0.0400	1.0070	1.0076	1.4033	1.4031
0.0899	1.0666	1.0703	1.4142	1.4126	0.0899	1.0257	1.0268	1.4179	1.4174
0.1049	1.0684	1.0715	1.4181	1.4167	0.1050	1.0315	1.0331	1.4223	1.4215
0.2045	1.0735	1.0745	1.4355	1.4351	0.2047	1.0475	1.0493	1.4372	1.4363
0.3049	1.0752	1.0754	1.4457	1.4456	0.3047	1.0560	1.0585	1.4464	1.4452
0.4049	1.0759	1.0762	1.4526	1.4524	0.4046	1.0618	1.0639	1.4524	1.4514
0.4614	1.0766	1.0766	1.4556	1.4556	0.5044	1.0665	1.0690	1.4574	1.4561
0.6035	1.0778	1.0776	1.4614	1.4615	0.6052	1.0700	1.0716	1.4606	1.4598
0.7048	1.0781	1.0781	1.4644	1.4644	0.7051	1.0726	1.0754	1.4640	1.4626
0.7744	1.0782	1.0781	1.4660	1.4660	0.8039	1.0749	1.0784	1.4667	1.4649
0.9041	1.0787	1.0787	1.4687	1.4687	0.9049	1.0770	1.0801	1.4686	1.4670

1.0000	1.0789	1.0789	1.4702	1.4702	1.0000	1.0789	1.0789	1.469	1.4688
***T* = 313.15K**									
0.0000	1.0269	1.0269	1.3668	1.3668	0.0000	0.9718	0.9718	1.3823	1.3823
0.0400	1.0517	1.0521	1.3932	1.3930	0.0400	1.0023	1.0028	1.4022	1.4020
0.0899	1.0622	1.0658	1.4132	1.4116	0.0899	1.0215	1.0222	1.4168	1.4165
0.1049	1.0641	1.0675	1.4171	1.4158	0.1050	1.0272	1.0288	1.4213	1.4206
0.2045	1.0697	1.0705	1.4346	1.4342	0.2047	1.0435	1.0454	1.4363	1.4354
0.3049	1.0715	1.0717	1.4449	1.4448	0.3047	1.0523	1.0549	1.4456	1.4443
0.4049	1.0725	1.0726	1.4518	1.4518	0.4046	1.0582	1.0607	1.4517	1.4505
0.4614	1.0732	1.0733	1.4549	1.4548	0.5044	1.0630	1.0658	1.4567	1.4553
0.6035	1.0744	1.0741	1.4606	1.4607	0.6052	1.0666	1.0685	1.4599	1.4590
0.7048	1.0749	1.0748	1.4637	1.4637	0.7051	1.0693	1.0723	1.4633	1.4618
0.7744	1.0750	1.0751	1.4654	1.4653	0.8039	1.0717	1.0753	1.4660	1.4642
0.9041	1.0755	1.0755	1.4680	1.4680	0.9049	1.0738	1.0770	1.4679	1.4662
1.0000	1.0757	1.0757	1.4695	1.4695	1.0000	1.0757	1.0757	1.4680	1.4680

Figure 5.37 is the graph of L-L density approximation of {[BDMIM]Cl: EG + acetic acid} binary mixtures against mole fraction, x_1, at different temperatures (293.15 – 313.15) K and at atmospheric pressure.

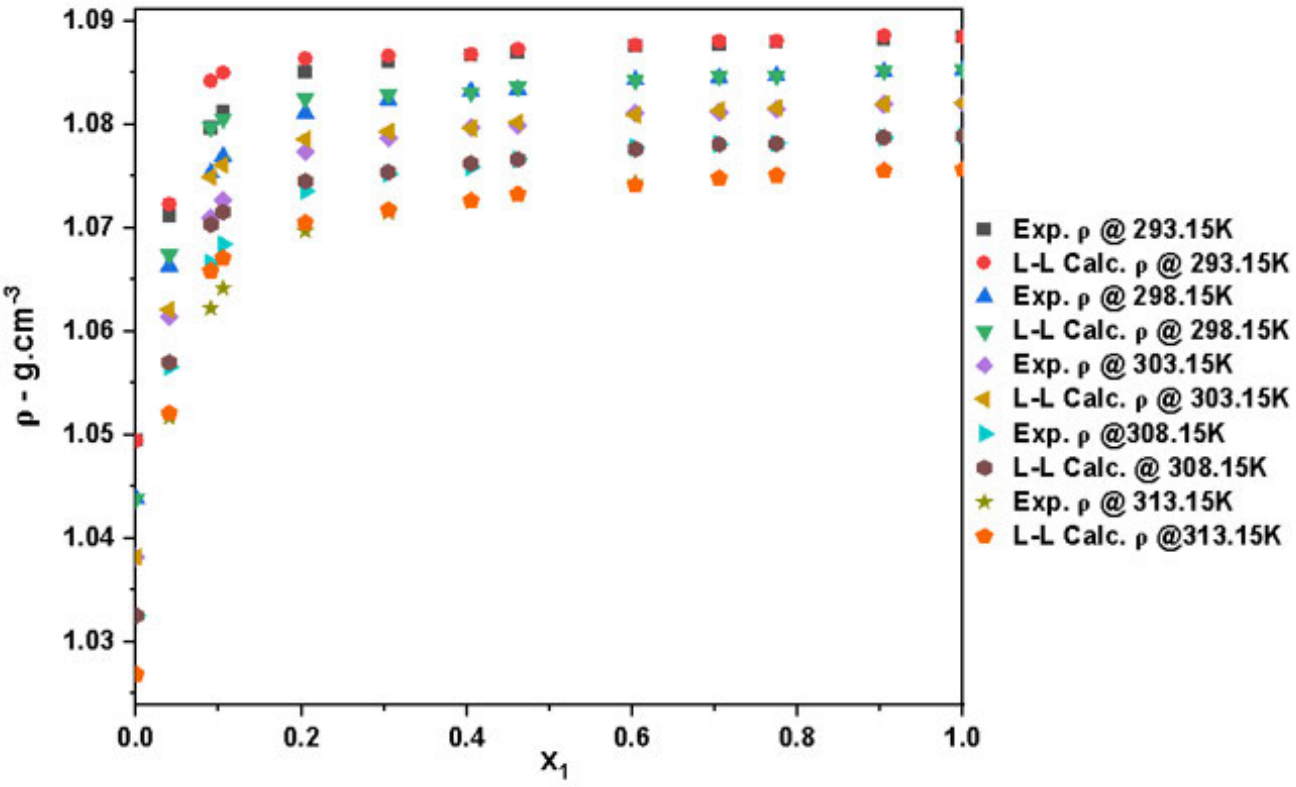

Figure 5.37: Graph of L-L density approximation of {[BDMIM]Cl: EG + acetic acid} binary mixtures against mole fraction, $\boldsymbol{x_1}$, at different temperatures (293.15 – 313.15) K and at atmospheric pressure.

The graph of L-L density approximation of {[BDMIM]Cl: EG + propanoic acid} binary mixtures against mole fraction, x_1, at different temperatures (293.15 – 313.15) K and at atmospheric pressure is given by Figure 5.38.

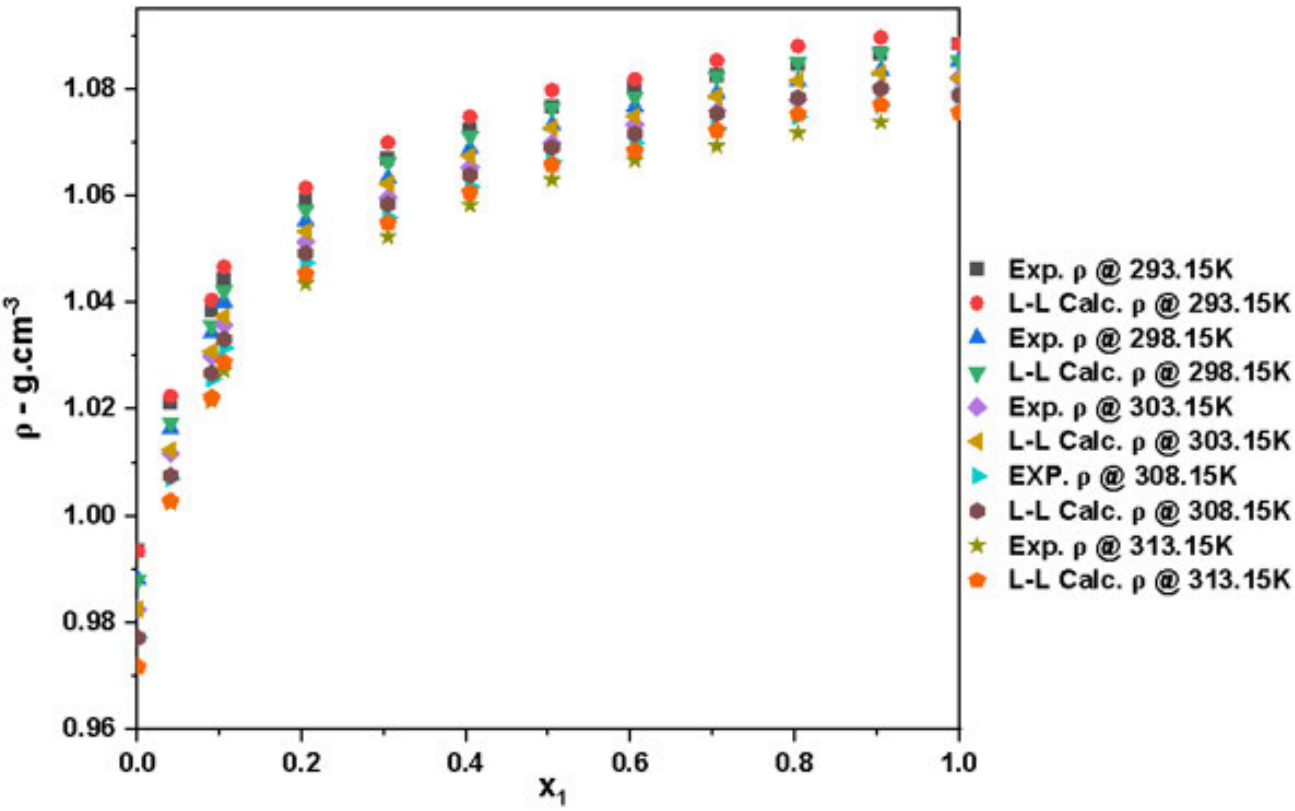

Figure 5.38: Graph of L-L density approximation of {[BDMIM]Cl: EG + propanoic acid} binary mixtures against mole fraction, x_1, at different temperatures (293.15 – 313.15) K and at atmospheric pressure.

Figure 5.39 is the graph of L-L refractive indices approximation of {[BDMIM]Cl: EG + acetic acid} binary mixtures against mole fraction, x_1, at different temperatures (293.15 – 313.15) K and at atmospheric pressure.

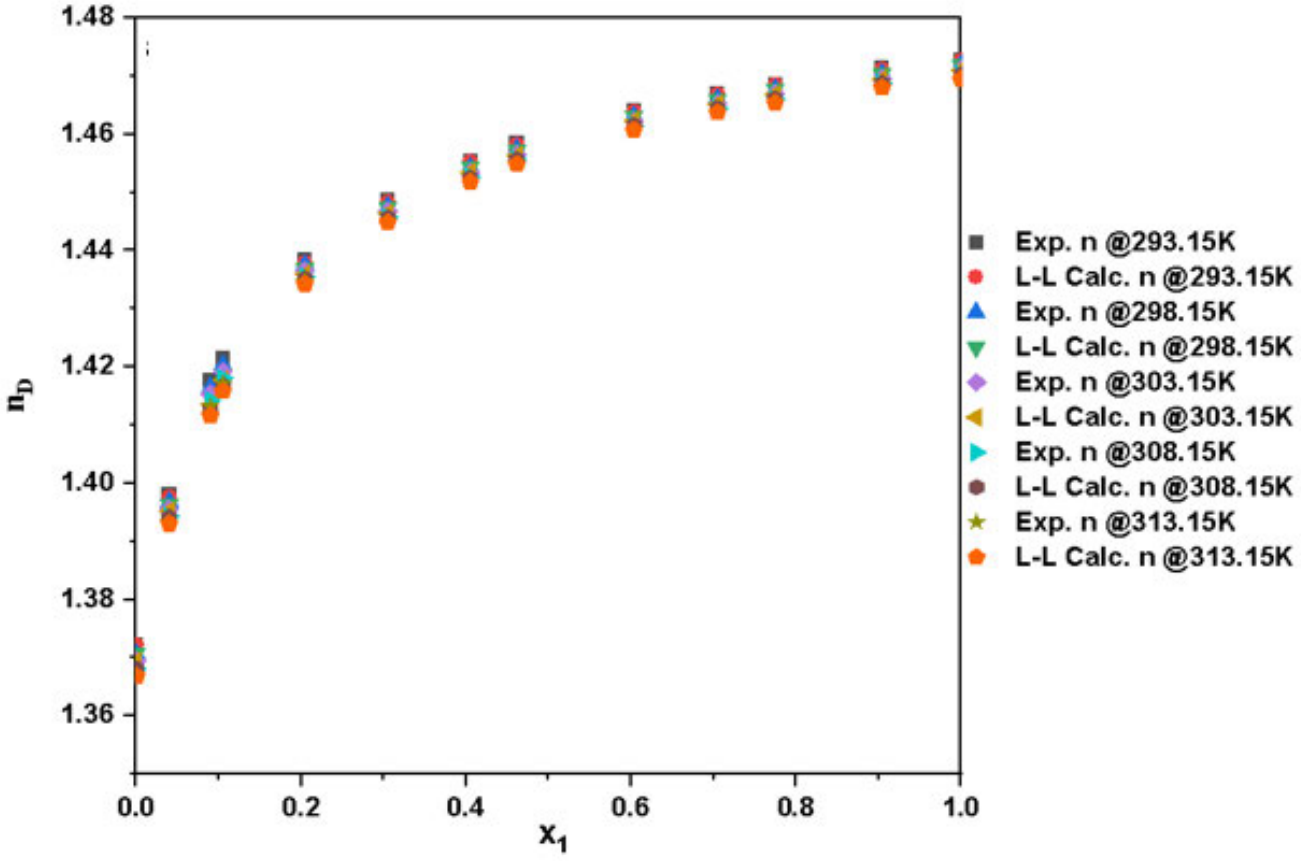

Figure 5.39: Graph of L-L refractive indices approximation of {[BDMIM]Cl: EG + acetic acid} binary mixtures against mole fraction, x_1, at different temperatures (293.15 – 313.15) K and at atmospheric pressure.

The graph of L-L refractive indices approximation of {[BDMIM]Cl: EG + propanoic acid} binary mixtures against mole fraction, x_1, at different temperatures (293.15 – 313.15) K and at atmospheric pressure is given in Figure 5.40.

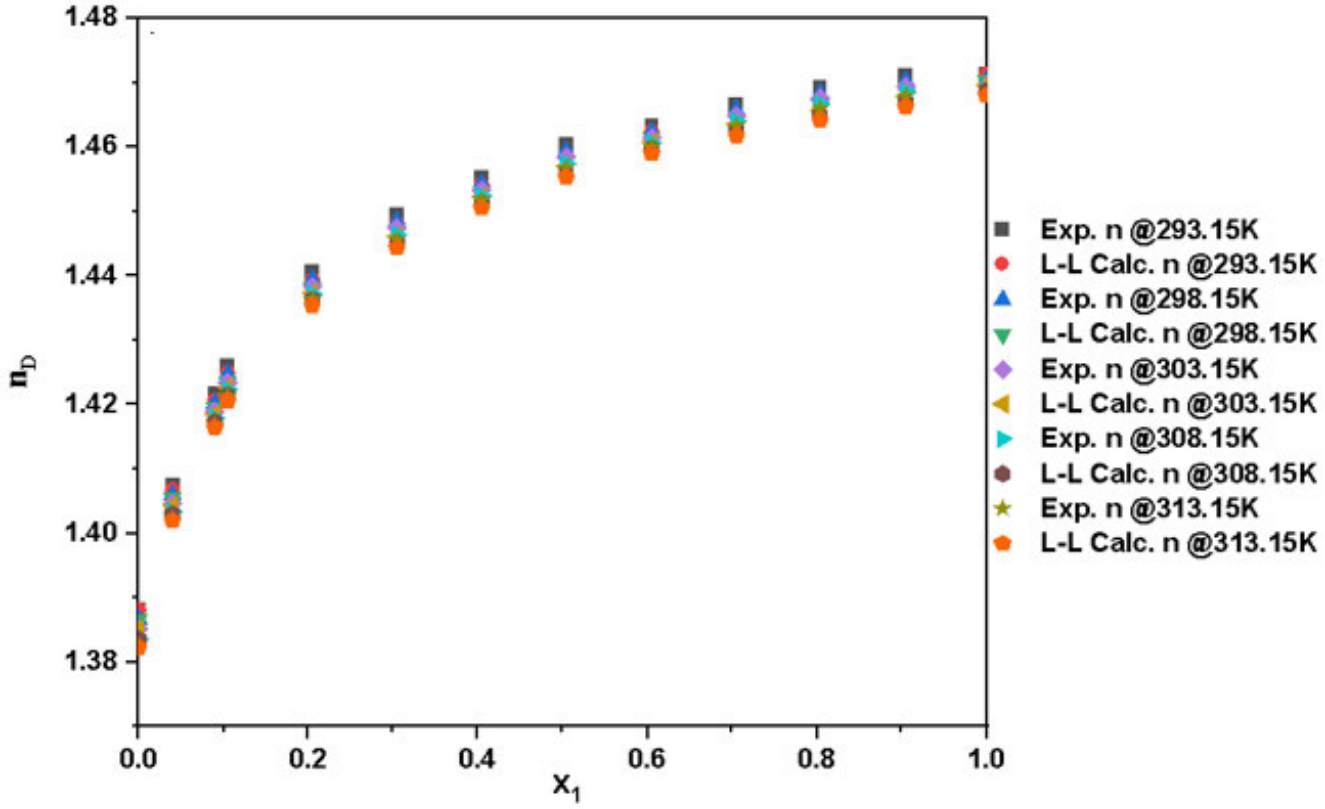

Figure 5.40: Graph of L-L refractive indices approximation of {[BDMIM]Cl: EG + propanoic acid} binary mixtures against mole fraction, x_1, at different temperatures (293.15 – 313.15) K and at atmospheric pressure.

The results for the root mean square, σ, obtained from the Lorentz-Lorenz correlation for V_m^E, ρ, and Δn_D for {[BDMIM]Cl: EG + acetic acid, or propanoic acid} binary mixtures at T = (293.15, 298.15, 303.15, 308.15 and 313.15) K is given in Table 5.10.

Table 5-10: Root mean square deviation, $\boldsymbol{\sigma}$, obtained from the Lorentz-Lorenz correlation for $\boldsymbol{V_m^E}$, $\boldsymbol{\rho}$, and n for binary mixtures at $\boldsymbol{T}$ = (293.15, 298.15, 303.15, 308.15, and 303.15) K.

σ					
Properties	[BDMIM]Cl: EG + acetic acid				
	T/K				
	293.15	**298.15**	**303.15**	**308.15**	**313.15**
V_m^E/ cm^3.mol^{-1}	0.706	0.682	0.661	0.635	0.608
ρ/ g.cm^{-3}	0.0018	0.00172	0.00157	0.0143	0.00137
n_D	0.00874	0.00814	0.00763	0.00728	0.00712
[BDMIM]Cl: EG + propanoic acid					
V_m^E/ cm^3.mol^{-1}	0.679	0.659	0.660	0.650	0.641
ρ/ g.cm^{-3}	0.00247	0.00244	0.00220	0.00218	0.00229
n_D	0.00121	0.00120	0.00109	0.00108	0.00114

The results for the experimental densities and speed of sound of pure compounds used in this work and those found in literature is given in Table 5.11.

Table 5-11: is the experimental densities and speed of sound of the pure compounds used in this work and those found in the literature.

Component	T/K	ρ/(g·cm^{-3})		u/(m·s^{-1})		n_D	
		Exp.	Lit.	Exp.	Lit.	Exp.	Lit.
DES [BMIM] Cl: EG	293.15	1.0893	--	1752.9	--	1.4681	--
	298.15	1.0862	--	1741.2	--	1.4668	--
	303.15	1.0829	--	1729.2	--	1.4655	--
	308.15	1.0798	--	1717.3	--	1.4641	--
	313.15	1.0766	--	1705.3	--	1.4627	--
DES [BMIM] Cl: EG	293.15	1.0884	--	1788.4	--	1.4727	--
	298.15	1.0853	--	1776.0	--	1.4719	--
	303.15	1.0821	--	1763.5	--	1.4710	--
	308.15	1.0789	--	1750.8	--	1.4702	--
	313.15	1.0757	--	1738.2	--	1.4695	--
Methanol	293.15	0.7924	0.7912[a]	1120.4	1119.0[a]	1.3298	1.3284[a]
			0.7910[b]		1119.6[b]		1.3290[b]
			0.7920[m]		1120.6[c]		
	298.15	0.7872	0.7866[a]	1104.6	1102.0[a]	1.3279	1.3270[c]
			0.7870[c]		1103.9[c]		1.3265[a]
	303.15	0.7843	0.7818[a]	1088.6	1086.0[a]	1.3261	1.3241[a]
			0.7820[c]		1087.6[c]		1.3250[c]
	308.15	0.7819	--	1072.6	--	1.3259	--
	313.15	0.7794	0.7726[a]	1057.3	1054.0[a]	1.3249	1.3205[a]
			0.7730[c]		1055.1[c]		1.3210[c]
Ethanol	293.15	0.7954	0.7893[a]	1173.4	1160.0[a]	1.3599	1.3613[a]
			0.7900[c]		1162.5[c]		1.3620[c]
	298.15	0.7910	0.7850[a]	1156.6	1142.0[a]	1.3579	1.3592[a]
			0.7860[c]		1144.9[c]		1.3610[c]
	303.15	0.7867	0.7807[a]	1139.7	1126.0[a]	1.559	1.3568[a]

			0.7810[c]		1127.9[c]		1.4580[c]
	308.15	0.7823	--	1122.9	--	1.3539	--
	313.15	0.7779	0.7721[a]	1106.2	1093.0[a]	1.3540	1.3530[a]
			0.7720[c]		1094.3[c]		1.3540[c]
Component	T/K	ρ/(g·cm^{-3})		u/(m·s^{-1})		n_D	
		Exp.	Lit.	Exp.	Lit.	Exp.	Lit.
Acetic acid	293.15	1.0495	1.0495[a]	1151.2	1152.7[d]	1.3722	1.3720[a]
			1.0498[d]		1150.0[h]		1.3710[h]
	298.15	1.0438	1.0437[e]	1134.3	1132.0[f]	1.3707	1.3700[g]
			1.0441[d]		1149.0[d]		1.3713[i]
	303.15	1.0382	1.0385[d]	1117.2	1118.4[d]	1.3694	--
			1.0380[e]		1115.0[e]		
	308.15	1.0325	1.0328[d]	1100.1	1101.2[d]	1.3681	--
	313.15	1.0269	1.0272[d]	1082.9	1084.0[d]	1.3668	--
Propanoic acid	293.15	0.9935	0.9925[a]	1165.6	1165.6[f]	1.3881	1.3811[a]
			0.9934[f]		1162.0[b]		1.3868[c]
	298.15	0.9881	0.9889[f]	1150.1	1146.7[f]	1.3866	1.3860[d]
			0.9885[f]		--		1.3847[f]
	303.15	0.9826	0.9831[f]	1131.6	1127.7[f]	1.3851	1.3826[f]
			0.7810[j]		--		1.3830[k]
	308.15	0.9772	0.9777[f]	1113.27	1108.9[f]	1.3836	1.3804[f]
			0.9776[b]		--		1.3813[k]
	313.15	0.9718	0.9723[f]	1095.4	1090.2[f]	1.3823	1.3783[f]
			0.9721[l]		--		1.3790[k]

(Kiran Kumar and Kabanda, 2022)[a], (Sannamed and González-Salgado, 2012)[b], (Wypch and Matsumoto, 2019)[c], (Singh and Bahadur, 2014)[d], (Gonza´lez and Dominguez, 2004)[e], (Bahadur and Deenadayalu, 2013)[f], (Smallwood et al., 1996)[g], (Demirel and Çehreli, 2013)[h], (Ince and Lalikoglu, 2014)[i], (Arez and Ramero, 2011)[j], (Gabriela and Mercedes,1990)[k], (Vong and Tsai, 1997.)[l]. (Grossman and Daramola, 2021)[m].

Figure 5.41 is the graph of comparison of density values between experimental results and the literature data of pure acetic acid, test system.

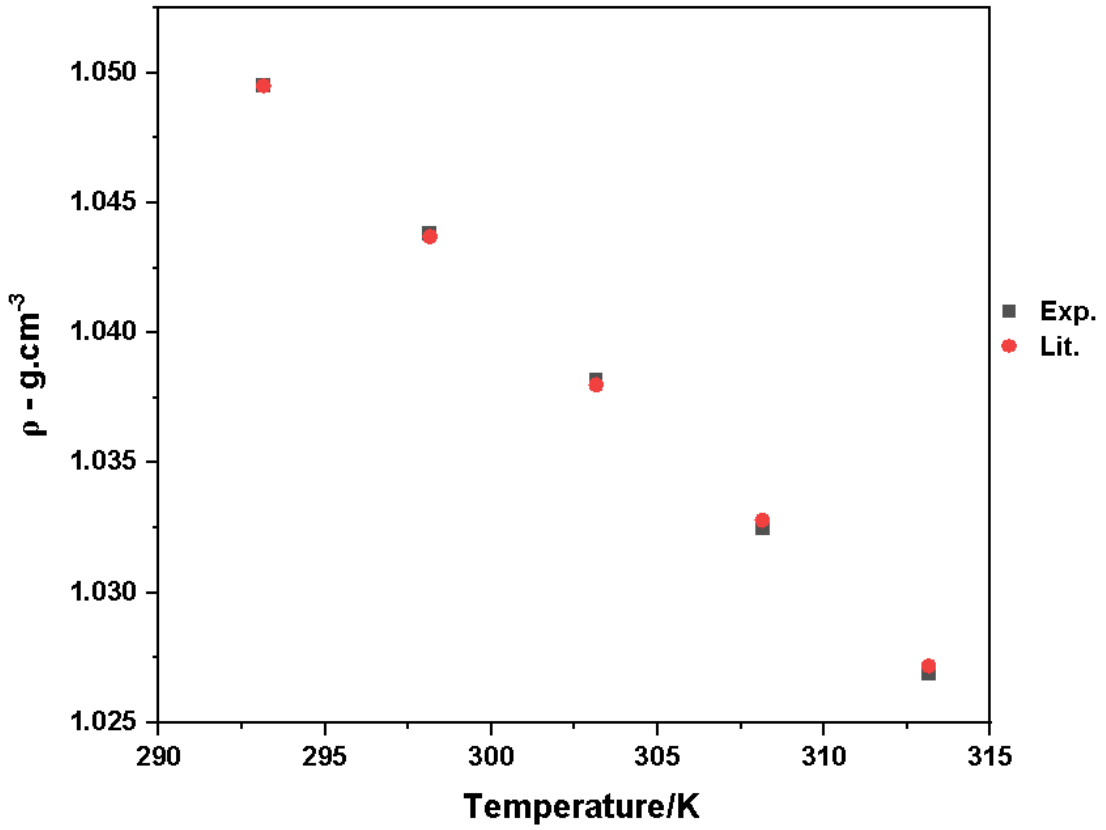

Figure 5.41: Graph of comparison of density values between experimental results and the literature data of pure acetic acid, test system.

The graph of comparison of speed of sound values between experimental results and literature data of pure propanoic acid, test system is given in Figure 5.42.

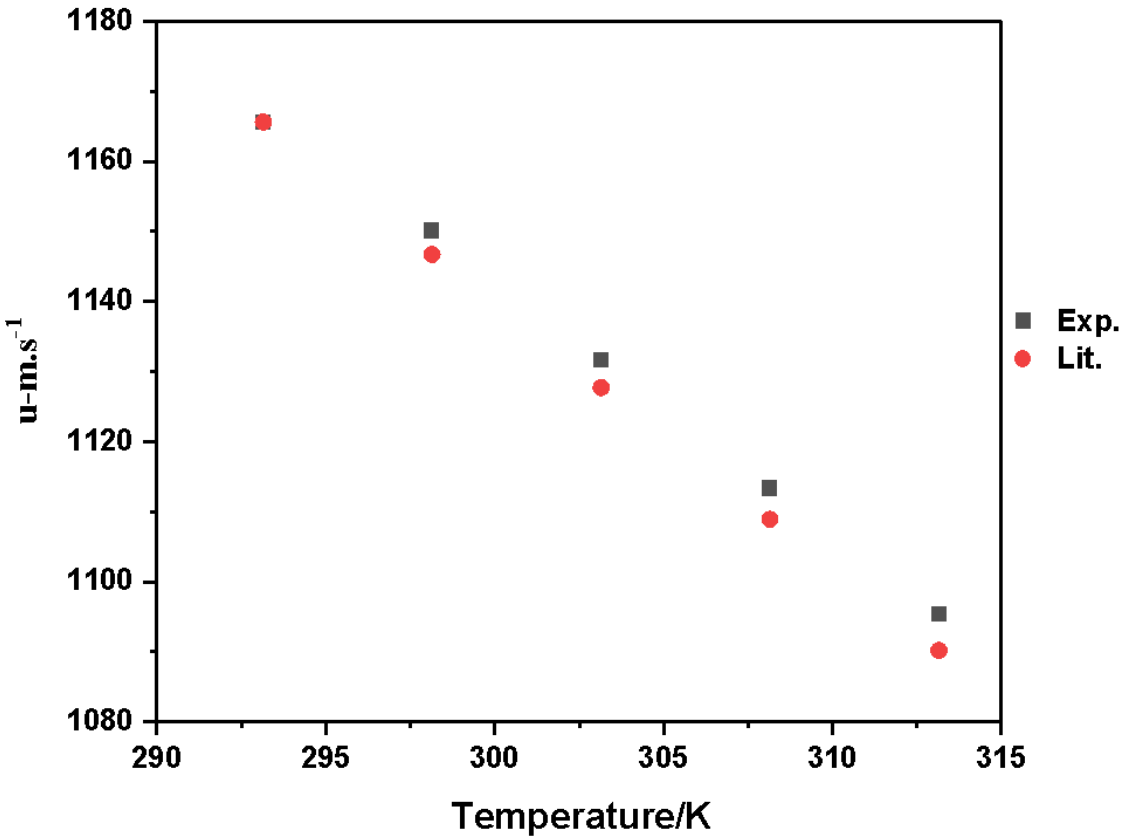

Figure 5.42: Graph of comparison of speed of sound values between experimental results and literature data of pure propanoic acid, test system.

Computational analysis

5.2 1-Butyl-2,3-dimethylimidazolium chloride + acetic acid or propanoic acid

The results for the thermodynamic parameters of ethylene glycol, 1-butyl-2,3-dimethylaimidazolium chloride, ethylene glycol, DES, acetic acid, propanoic acid, DES + acetic acid and DES + propanoic acid calculated from DFT is given in Table 5.12.

Table 5-12: Thermodynamic parameters of ethylene glycol, 1-butyl-2,3-dimethylimidazolium chloride, ethylene glycol, DES, acetic acid, propanoic acid, DES + acetic acid and DES + propanoic acid calculated from DFT.

System	**Optimization energy (Hartree)**	**Dipole moment (Debye)**	**Change in Electronic energy ($\Delta E_{O.E.}$) (Hartree)**
[BDMIM]Cl	-922.96	24.89	
Ethylene glycol	-230.282	0	-
DES	-1613.72	29.86	-0.086
Acetic acid	-229.113	2.342	-
Propanoic acid	-268.429	2.486	-
DES + acetic acid	-1843.36	27.22	-0.527
DES + propanoic acid	-1882.14	28.15	-0.009

The results of physicochemical descriptors of ethylene glycol, [BDMIM]Cl, DES, acetic acid, propanoic acid, DES + acetic acid, DES + propanoic acid is given in Table 5.13.

Table 5-13: Physicochemical descriptors of ethylene glycol, [BDMIM]Cl, DES, acetic acid, propanoic acid, DES + acetic acid, DES + propanoic acid.

Compound Name	E_H (Hartree)	E_L (Hartree)	$\lvert E_H - E_L \rvert$ (Hartree)	η (Hartree)	χ (Hartree)	S $(\text{Hartree})^{-1}$	μ (Hartree)	Ω (Hartree)
[BDMIM]Cl	-0.032	-0.247	0.215	0.107	0.140	9.281	-0.140	0.091
Ethylene glycol	-0.288	0.002	0.291	0.145	0.143	3.434	-0.143	0.070
DES	-0.028	-0.245	0.217	0.108	0.137	9.201	-0.137	0.086
Acetic acid	-0.297	-0.012	0.285	0.142	0.154	3.507	-0.154	0.084
Propanoic acid	-0.293	-0.016	0.277	0.138	0.154	3.607	-0.154	0.086
DES + acetic acid	-0.170	-0.253	0.083	0.041	0.212	24.052	-0.212	0.541
DES+ propanoic acid	-0.033	-0.254	0.220	0.110	0.143	9.056	-0.143	0.093

The results for the natural bonding orbital of [BDMIM]Cl: EG DES + acetic acid or propanoic acid is given in Table 5.14.

Table 5-14**:** Natural bonding orbital analysis of [BDMIM]Cl: EG DES + acetic acid or propanoic acid.

System	Donor NBO	Acceptor NBO	E(2) (kcal/mol)
DES + Acetic Acid	BD C 1 - N 2	BD* (2) C 3 - C 4	4.92
	BD C 1 - N 5	BD* (1) N 2 - C 6	2.72
	BD N 2 - C 3	BD* (1) C 1 - C 7	2.93
	BD C 3 - C 4	BD* C 1 - N 2	4.02
	BD C 7 - H 18	BD* C 1 - N 5	2.80
	LP N 5	BD* C 1 - N 2	14.85
	LP N 5	BD* C 3 - C 4	7.42
	BD* C 1 - N 2	BD* C 3 - C 4	6.21
	LP O 38	BD* C 33 - H 34	2.84
	LP O 38	BD* C 33 - H 35	2.97
	LP O 46	BD* C 40 - H 41	2.91
	LP O 46	BD* C 40 - H 42	2.92
	LP O 48	BD* C 43 - H 44	2.92
	LP O 48	BD* C 43 - H 45	2.91
	LP O 58	BD* C 53 - H 54	2.91
	LP O 58	BD* C 53 - H 55	2.89
	BD C 60 - C 64	LP* O 68	8.28
	BD C 64 - H 65	LP* O 68	12.36
	LP O 66	BD* C 64 - H 65	2.62
	LP O 66	BD* C 64 - O 68	3.74
	LP O 68	BD* C 64 - O 66	16.70
DES + Propanoic acid	BD C 1 - N 2	BD* N 5 - C 8	4.23
	BD C 1 - N 5	BD* N 2 - C 6	4.26
	BD C 1 - N 5	BD* C 3 - C 4	16.41
	BD C 1 - N 5	BD* C 8 - C 9	3.20
	BD C 1 - C 7	BD* N 2 - C 3	2.81
	BD C 1 - C 7	BD* C 4 - N 5	2.73
	BD N 2 - C 3	BD* C 1 - C 7	4.31
	BD N 2 - C 3	BD* C 4 - H 13	3.03
	BD C 3 - C 4	BD* N 2 - C 6	4.63
	BD C 3 - C 4	BD* N 5 - C 8	4.50
	BD C 3 - C 4	BD* C 1 - N 5	13.15

	BD C 3 - H 12	BD* C 1 - N 2	3.72
	BD C 4 - N 5	BD* C 1 - C 7	4.40
	BD C 4 - N 5	BD* C 3 - H 12	3.11
	BD C 4 - H 13	BD* C 1 - N 5	3.78
	BD C 6 - H 14	BD* C 1 - N 2	5.25
	BD C 7 - H 17	BD* C 1 - N 5	7.65
	BD C 7 - H 18	BD* C 1 - N 5	6.19
	BD C 7 - H 19	BD* C 1 - N 2	5.62
	BD C 8 - H 20	BD* C 1 - N 5	4.21
	BD C 8 - H 21	BD* C 4 - N 5	3.89
	BD C 9 - C 10	BD* N 5 - C 8	3.09
	BD C 11 - H 26	BD* C 9 - C 10	3.21
	LP N 2	BD* C 1 - N 5	80.50
	LP N 2	BD* C 3 - C 4	27.86
	BD* C 1 - N 5	BD* C 3 - C 4	14.48
	LP Cl 29	BD* O 48 - H 49	15.43
	LP O 38	BD* C 33 - H 34	4.45
	LP O 38	BD* C 33 - H 35	5.93
	LP O 48	BD* C 4 - H 13	5.67
	LP O 46	BD* C 40 - H 41	5.29
	LP O 46	BD* C 40 - H 42	5.53
	LP O 48	BD* C 43 - H 45	6.75
	LP O 56	BD* C 50 - H 51	5.60
	LP O 56	BD* C 50 - H 52	4.59
	LP O 58	BD* C 53 - H 54	5.82
	LP O 58	BD* C 53 - H 55	5.37
	LP O 70	BD* O 38 - H 39	9.66
	BD C 60 - H 63	BD* C 64 - C 67	3.47
	BD C 60 - C 64	BD* C 67 - O 70	4.45
	BD C 64 - H 65	BD* C 67 - O 70	4.99
	BD C 64 - H 66	BD* C 67 - O 68	5.11
	CR O 70	RY* C 67	6.54
	LP O 68	BD* C 67 - O 70	6.70
	LP O 68	BD* C 67 - O 70	51.30
	LP O 70	RY* C 67	14.77
	LP O 70	BD* C 64 - C 67	13.92
	LP O 70	BD* C 67 - O 68	30.77

The optimized geometry and contours of frontier orbitals (HOMO and LUMO) of [BDMIM]Cl, ethylene glycol, DES, acetic acid, propanoic acid, acetic acid-DES and propanoic acid-DES is given in Figure 5.43.

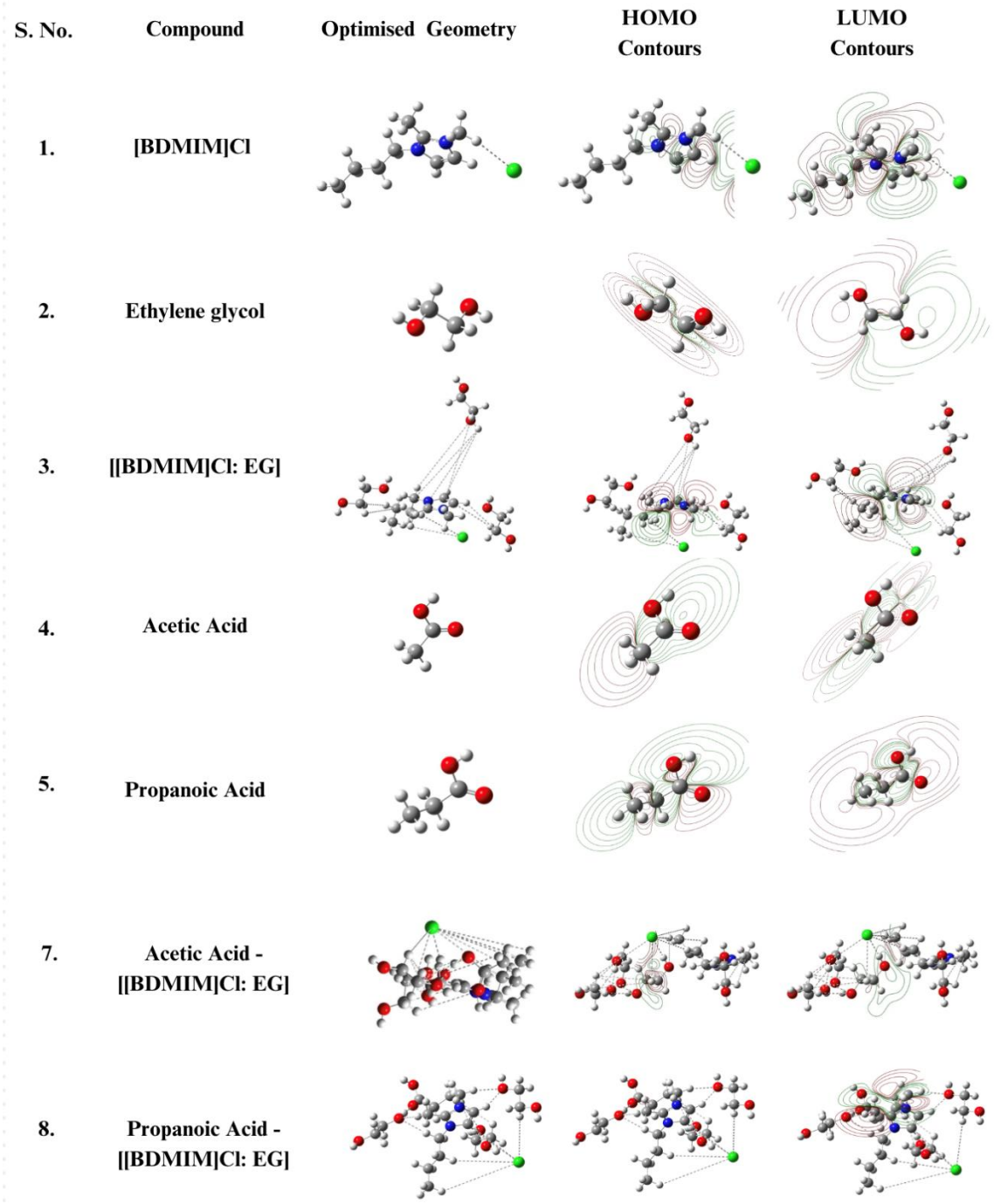

Figure 5.43: Optimized geometry and contours of frontier orbitals (HOMO and LUMO) of [BDMIM]Cl, ethylene glycol, DES, acetic acid, propanoic acid, acetic acid-DES and propanoic acid-DES.

Figure 5.44 is the numbered structure of a) acetic acid-DES and b) propanoic acid-DES.

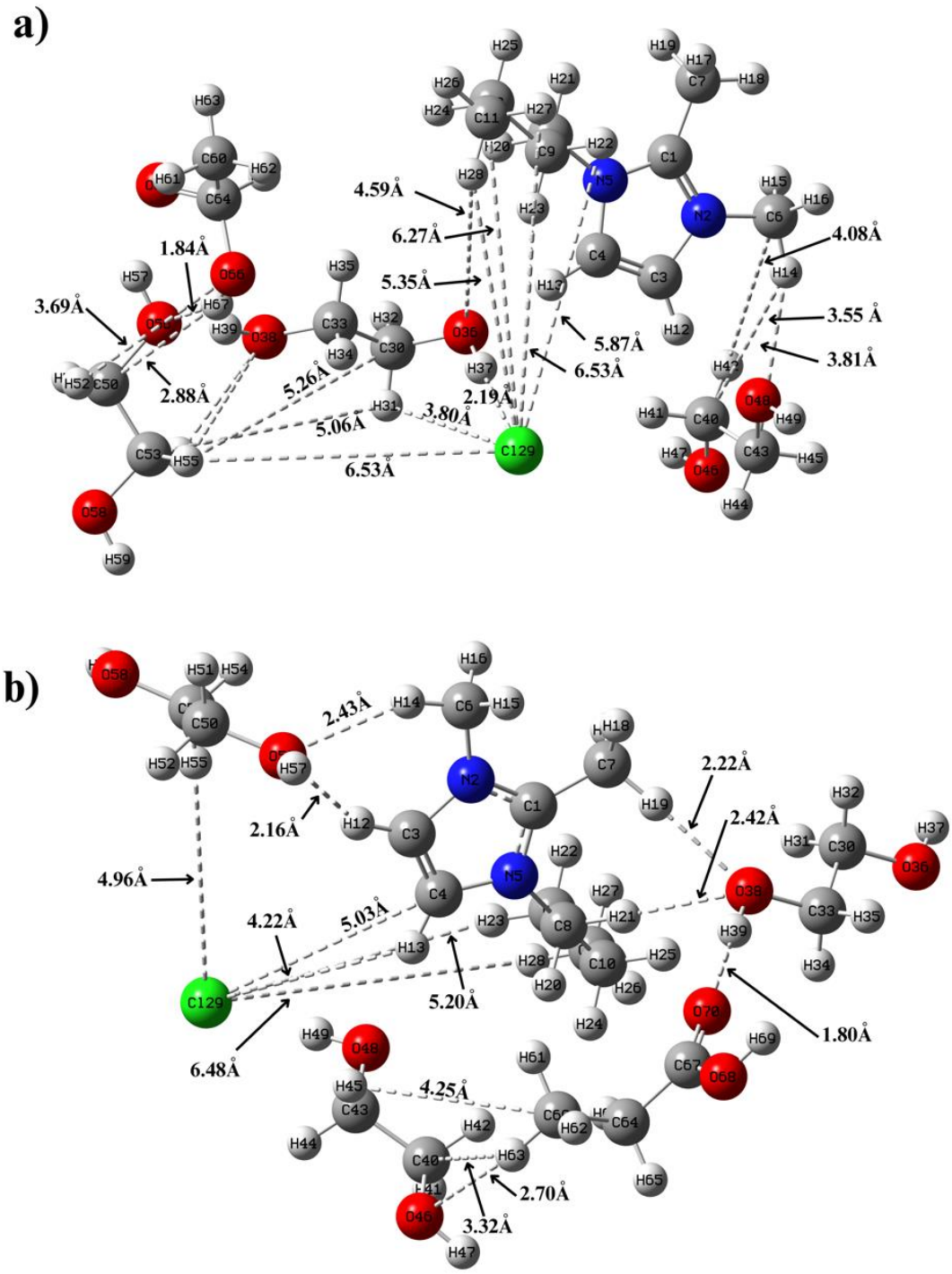

Figure 5.44: Numbered structure of a) acetic acid-DES and b) propanoic acid-DES.

The 2D scatter plot of a) DES, b) acetic acid-DES, c) propanoic acid-DES obtained from DFT calculations for NCI analysis with RDG against electron density multiplied by the sign of the second Hessian eigenvalue (sign(λ_2)ρ) is given in Figure 5.45.

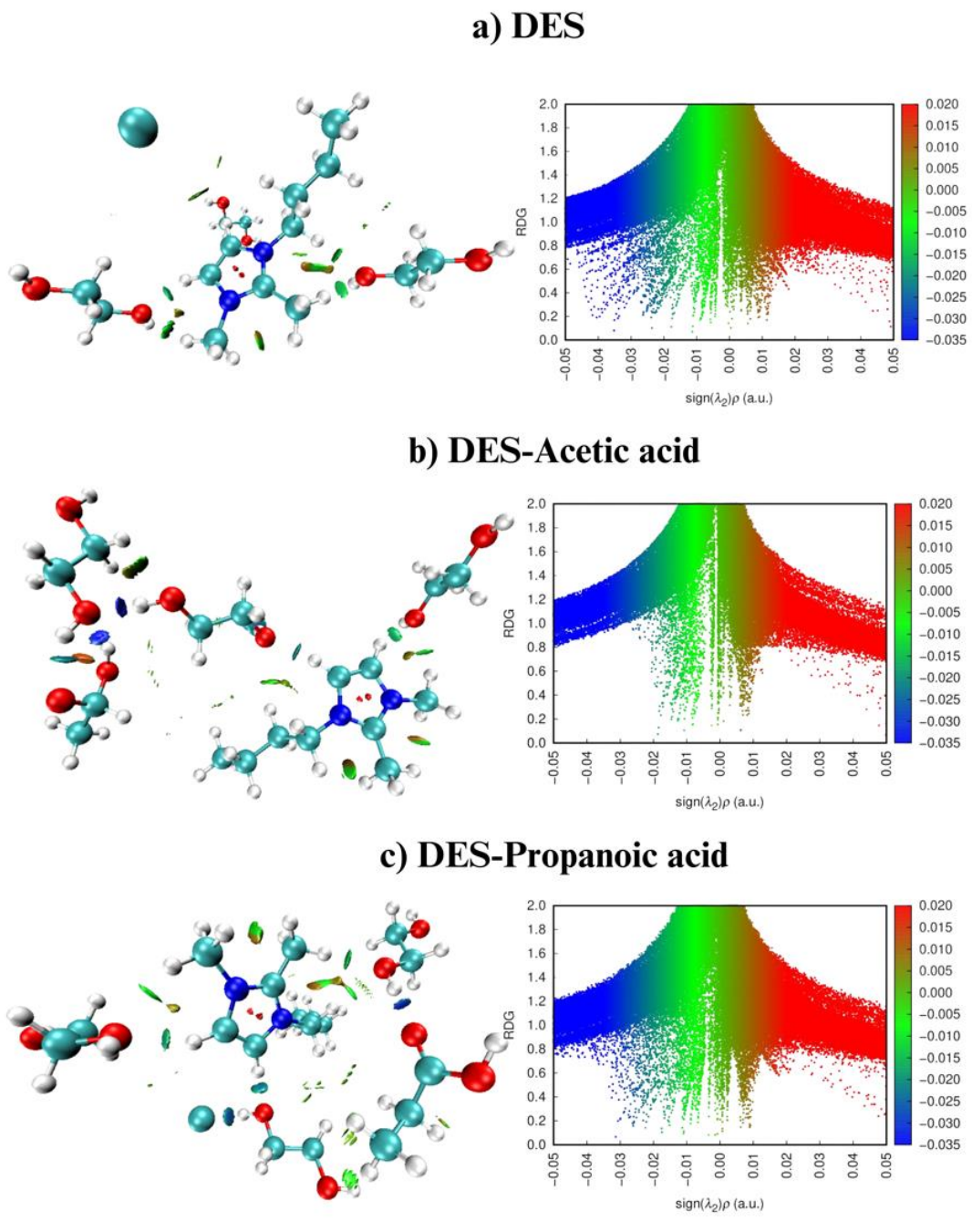

Figure 5.45: 2D scatter plot of a) DES, b) acetic acid-DES, c) propanoic acid-DES obtained from DFT calculations for NCI analysis with RDG against electron density multiplied by the sign of the second Hessian eigenvalue (sign(λ_2)ρ)

Figure 5.46 is the 3D map of electron localization function (ELF) of a) DES, b) acetic acid-DES, c) propanoic acid-DES.

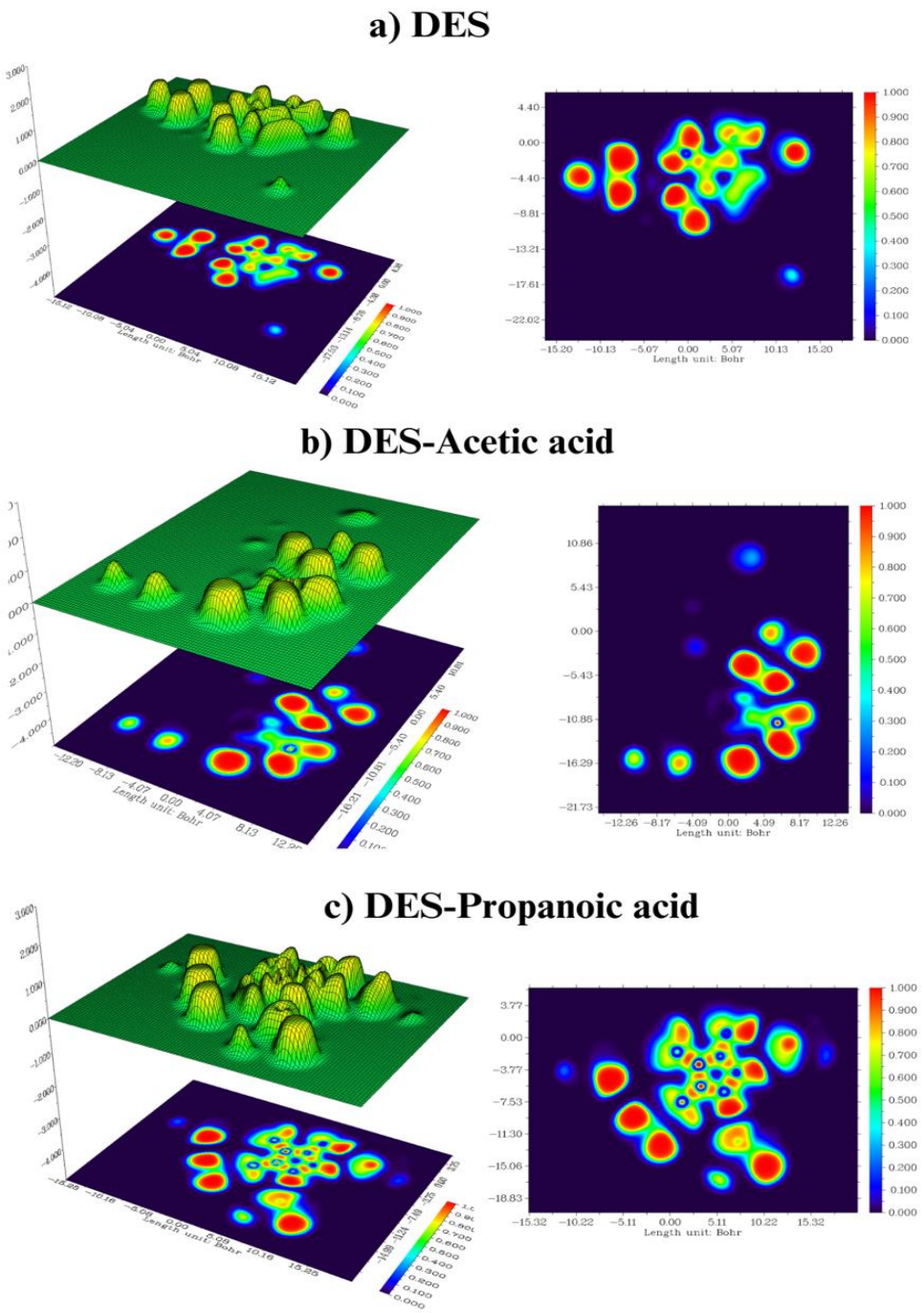

Figure 5.46: 3D map of electron localization function (ELF) of a) DES, b) acetic acid-DES, c) propanoic acid-DES.

5.3 1-Butyl-3-dimethylimidazolium chloride with methanol or ethanol

The energy level diagram for the optimisation of the 6 molecular configurations is given in Figure 5.47.

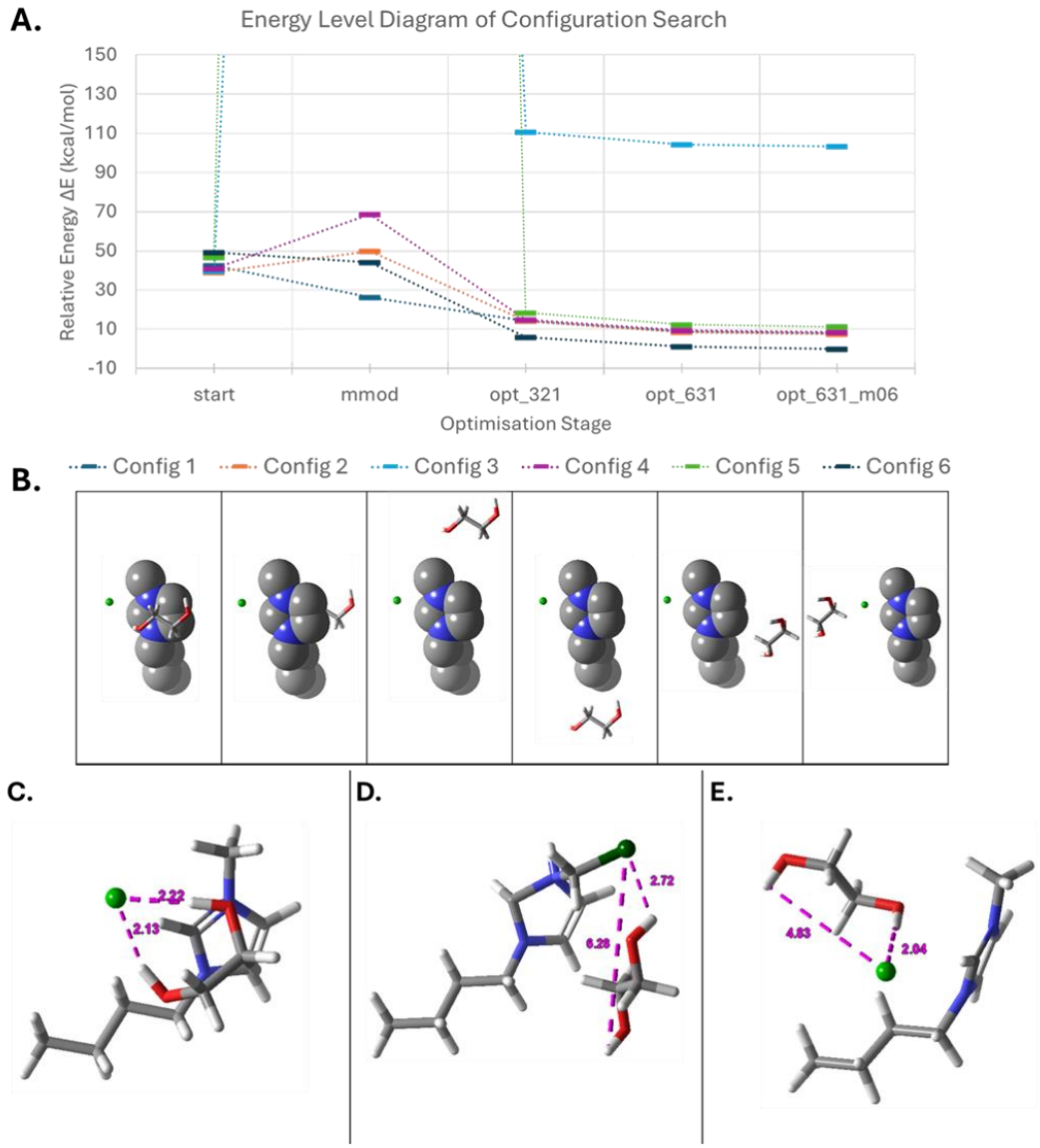

Figure 5.47: Energy level diagram for the optimisation of the 6 molecular configurations.

A. The relative energies of the initial conformations (start), optimisation from MacroModel (mmod), optimisation using 3-21 G++* in B3LYP-D3 (opt_321), optimisation using 6-31 G++** in B3LYP-D3 (opt_631), and optimisation using 6-31 G++** M06-2X-D3 systems. B. The legend showing the position of the EG molecule relative to the [BMIM]Cl complex in the starting conformation for each configuration. The atoms of the EG molecules are indicated by thick tube representations, the chloride ion as ball-and-stick representation and [BMIM] as CPK representation with H atoms hidden for simplicity. C. The optimized Config 6 conformation displayed as thick tube representation with bond lengths (magenta) between hydroxyl H atoms of EG. D. The optimized Config 3 conformation. E. The optimized Config 4 conformation.

The results of the interaction energies of the ethylene glycol co-solvent with the [BMIM]Cl complex is given in Table 5.15.

Table 5-15: Interaction energies (kcal) of the EG co-solvent with the [BMIM]Cl complex.

	Vacuum		**Ethanol**		**Methanol**	
	Gas phase	**Solution phase**	Gas phase	**Solution phase**	Gas phase	**Solution phase**
	Kcal					
$E_{complex}$		-698776.85		-698799.83		-698800.80
$E_{solute(comp)}$		-554318.07		-554352.84		-554352.54
$E_{solvent(comp)}$		-144424.01		-144437.62		-144438.15
$E_{inter(uncorr)}$		**-34.77**		**-9.37**		**-10.11**
$E_{complex(cp-uncorr)}$	-698776.85		-698771.51		-698771.13	
$E_{complex(cp-corr)}$	-698776.87		-698776.88		-698776.87	
$\Delta E_{cp-corr} \approx$ BSSE		0.02		5.37		5.75
$E_{inter(corr)}$		**-34.79**		**-14.73**		**-15.86**

The results of the HOMO-LUMO energies of ethylene glycol co-solvent with the [BMIM]Cl complex is given in Table 5.16.

Table 5-16: HOMO-LUMO energies (kcal.mol^{-1}) of the EG co-solvent with the [BMIM]Cl complex.

System	**Surface**	**Energy (kcal.mol^{-1})**	**∆ Energy (kcal.mol^{-1})**
A (Vacuum)	LUMO	-178.681	
	HOMO	-12.908	
			-165.77
B (Ethanol)	HOMO	-206.240	
	LUMO	-1.977	
			-204.26
C(Methanol)	HOMO	-206.705	
	LUMO	-1.970	
			-204.73

The results of XYZ coordinated of optical configuration (config 6) is given in Table 5.17.

Table 5-17: XYZ coordinates of optical configuration (config 6) displayed atoms.

Atom	X	Y	Z
C	-0.1578	-6.138	2.375
N	-1.367	-5.527	2.614
C	0.4118	-5.484	1.325
C	-1.538	-4.541	1.735
N	-0.4644	-4.489	0.9451
C	-0.3148	-3.599	-0.2202
C	-1.025	-2.268	-0.02320
C	-0.9618	-1.426	-1.297
C	-1.697	-0.09820	-1.130
C	-2.366	-5.915	3.611

H	0.1912	-6.969	2.967
H	1.353	-5.636	0.8219
H	-2.447	-3.936	1.668
H	-0.7454	-4.120	-1.079
H	-0.7599	-3.456	-0.3665
H	-0.5734	-1.726	0.8178
H	-2.079	-2.440	0.2241
H	-1.416	-1.998	-2.114
H	0.0850	-1.243	-1.573
H	-1.252	0.4996	-0.3283
H	-1.662	0.4919	-2.050
H	-2.747	-0.2702	-0.8767
H	-3.193	-5.206	3.546
H	-1.913	-5.885	4.602
H	-2.742	-6.907	3.364
Cl	-4.596	-3.474	1.475
O	-3.777	-6.522	1.109
C	-3.175	-6.733	-0.1508
C	-3.604	-5.744	-1.223
O	-3.078	-4.449	-1.003
H	-4.199	-5.639	1.159
H	-2.075	-6.674	-0.05250
H	-3.425	-7.751	-0.4781
H	-3.225	-6.089	-2.192
H	-4.701	-5.713	-1.277
H	-3.667	-3.980	-0.3726

The select distances (Å) between interacting species in the optimized [BMIM]Cl EG complexes is given in Table 5.48.

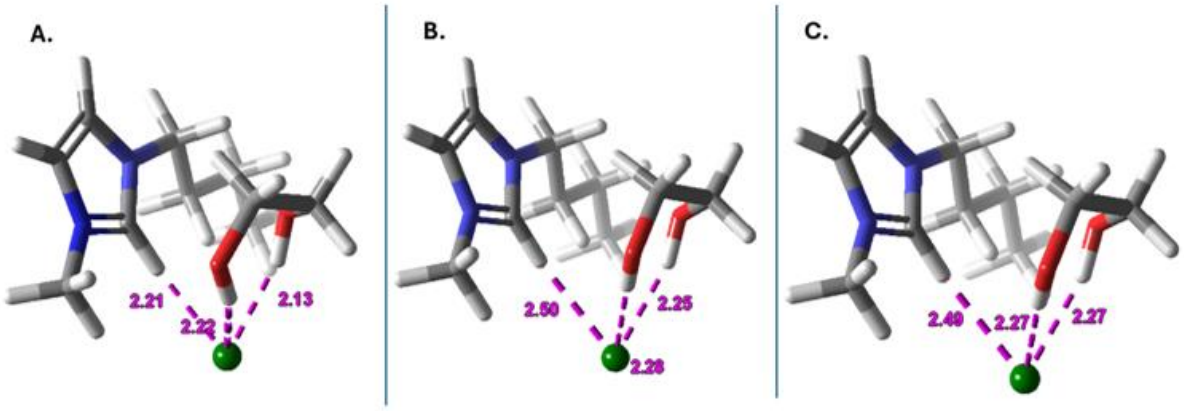

Figure 5.48: Select distances (Å) between interacting species in the optimized [BMIM]Cl EG complexes.

The atoms are coloured according to the following: carbons (grey), hydrogens (white), nitrogen (blue), oxygen (red), and chlorine (green).

Figure 5.49 is the electron density plot.

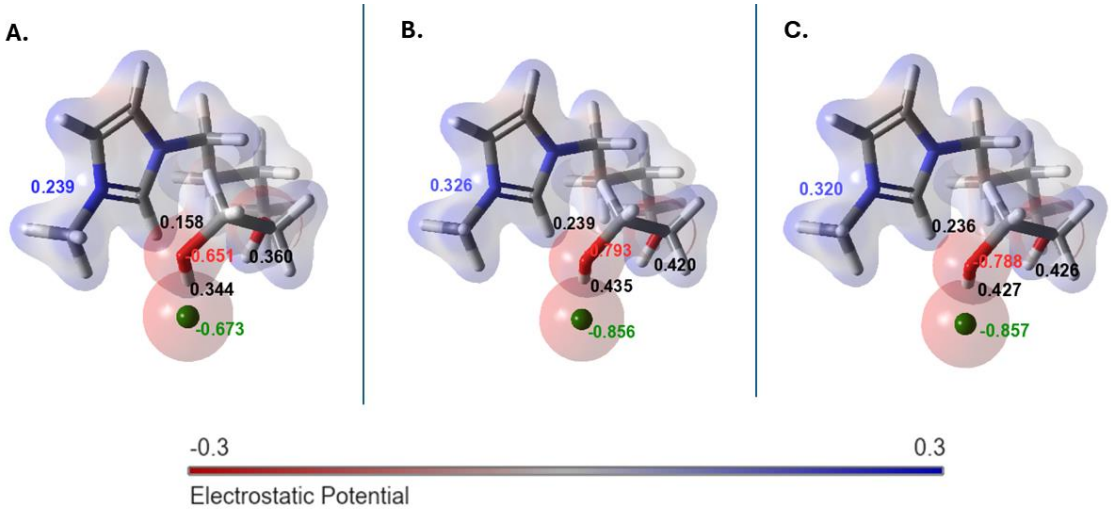

Figure 5.49: Electron density plot.

A. vacuum optimized system. B. ethanol optimized system. C. methanol optimized system. The bond distances are measured between the Cl^- ion with the following atoms: H atom of the imidazolium ring, and the H atoms of the hydroxyl groups of the EG co-solvent and displayed in magenta. Electron density plots coloured by the electrostatic potential of the optimised molecular systems with the region of positive electrostatic potential indicated in blue, while the region of negative electrostatic potential indicated by red. The atoms of the molecules are indicated by thick tube representations, where carbons (grey), hydrogens (white), nitrogen (blue), oxygen (red), and chlorine (green). The Mulliken charges computed are displayed over the following selected set of atoms: the methylated N atom of the imidazolium ring (blue), the H atom of the imidazolium ring (black), the H atoms of the hydroxyl groups of the EG co-solvent (black), the bulk solvent exposed O atom of EG co-solvent (red), the Cl^- atom (green). A) vacuum optimized system. B. ethanol optimized system. C. methanol optimized system.

Figure 5.50 is the HOMO (A, B, and C) LUMO (A, B, and C) surface plots of the optimised molecular systems.

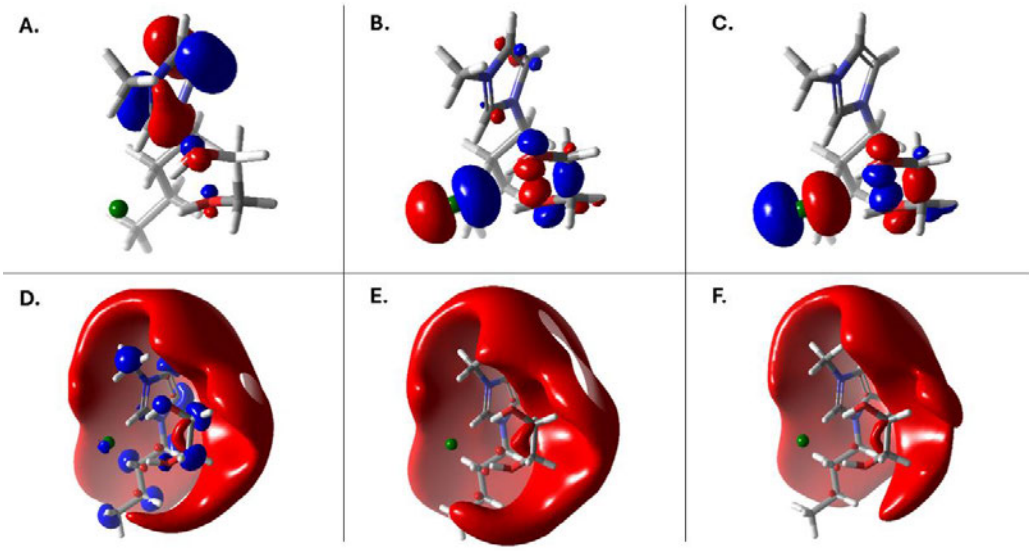

Figure 5.50: HOMO (A, B, and C) LUMO (A, B, and C) surface plots of the optimised molecular systems.

The HOMO orbitals are displayed with surfaces visible at iso-values of -0.05 while the LUMO orbitals are adjusted to iso-values of 0.012 (vacuum), -0.011 (ethanol) and -0.013 (methanol). A., D. vacuum optimized systems. B., E. ethanol optimized systems. C., F. methanol optimized computed.

Characterization analysis

5.3.1 Thermogravimetric analysis of Tetrabutylammonium acetate with ethylene glycol or diethylene glycol

The TGA profiles of [TBN] AcO + EG are shown in Figure 5.51 and 5.52

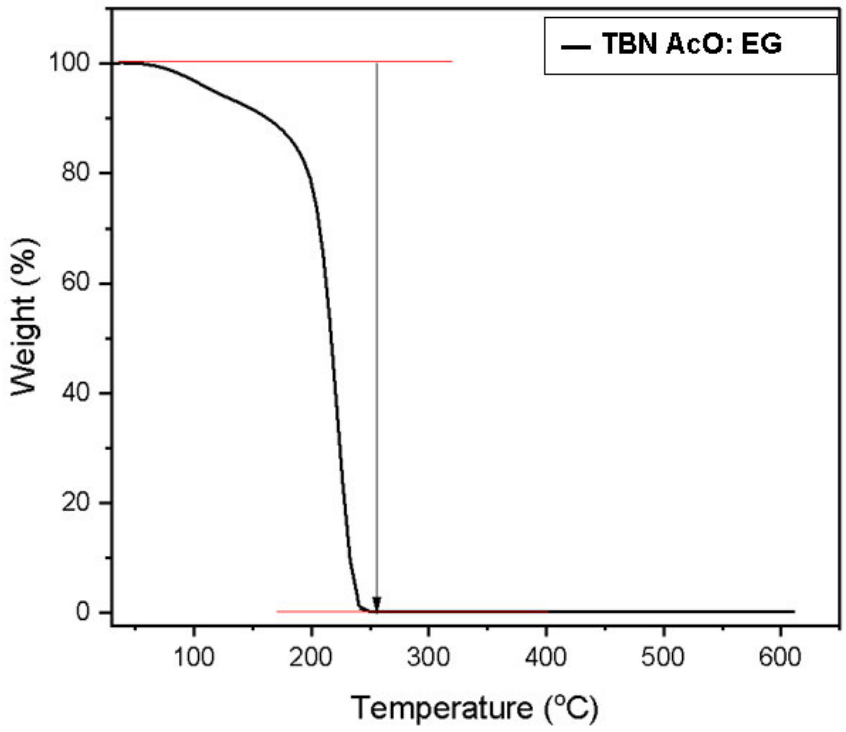

Figure 5.51: Thermogravimetric weight % of [TBN] AcO: EG.

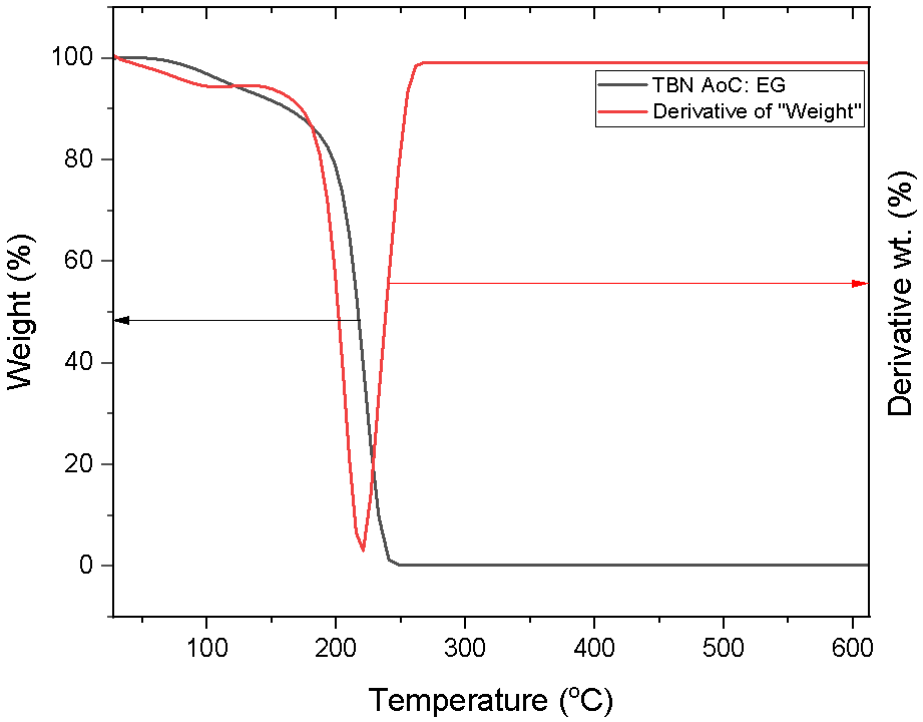

Figure 5.52: Thermogravimetric derivative weight % of [TBN] AcO: EG.

The TGA profiles for [TBN] AcO: DEG are shown in Figures 5.53 and 5.54.

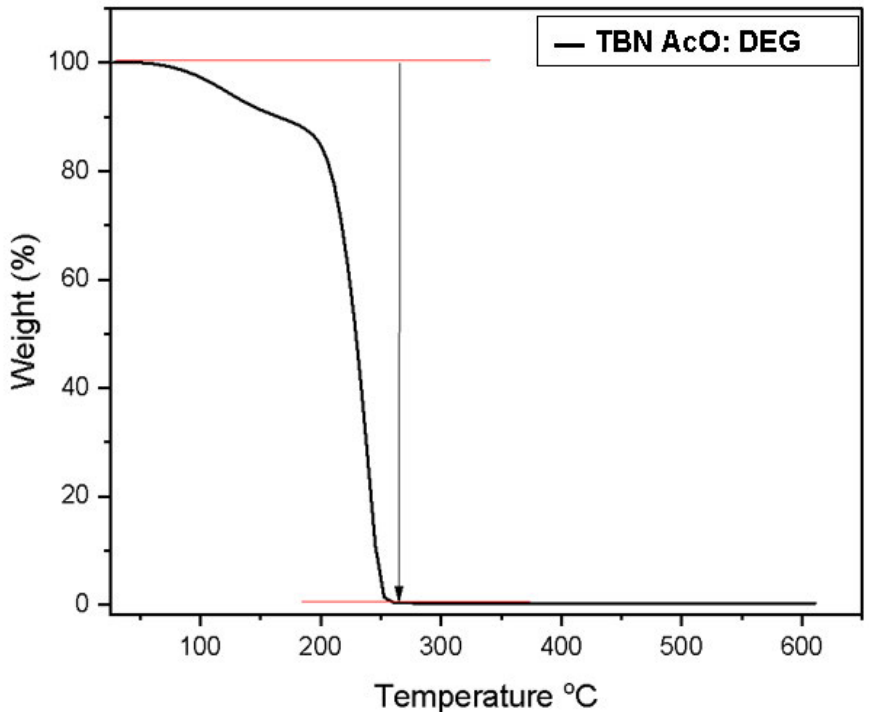

Figure 5.53: Thermogravimetric weight % of [TBN] AcO: DEG

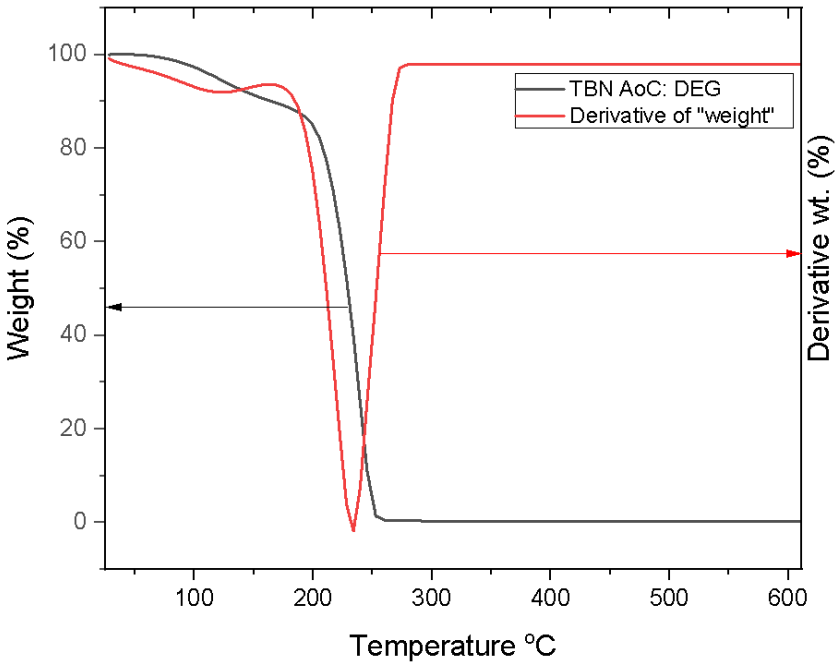

Figure 5.54: Thermogravimetric derivative weight % of [TBN] AcO: DEG

5.3.2 Fourier transformation infrared analysis of Tetrabutylammonium acetate with ethylene glycol and diethylene glycol

The FTIR profiles of ethylene glycol, [TBN] AcO and DES ([TBN] AcO + EG) are shown in Figure 5.55 and 5.56.

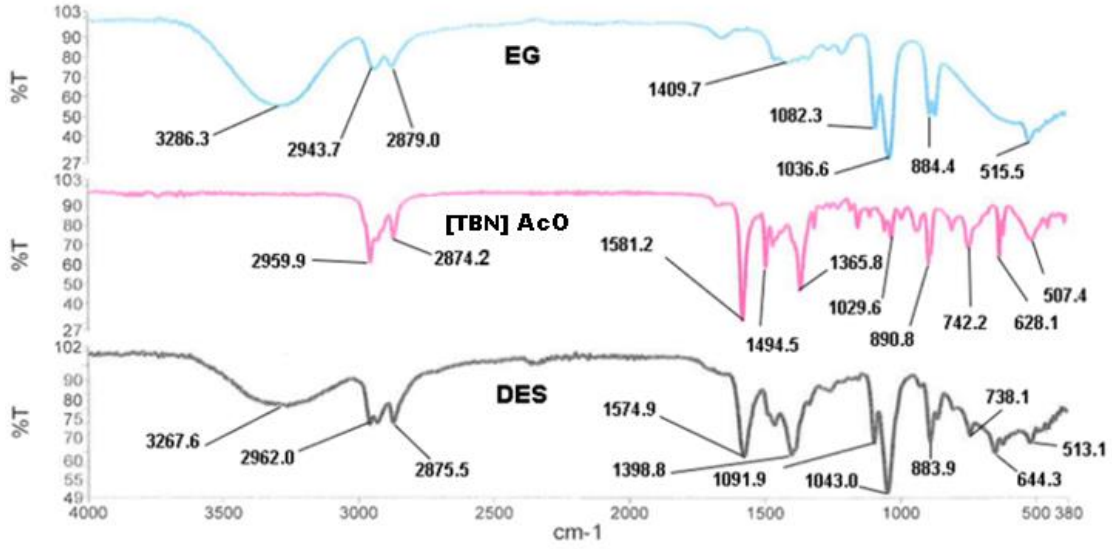

Figure 5.55: FTIR spectra of ethylene glycol, [TBN] AcO and DES ([TBN] AcO: EG).

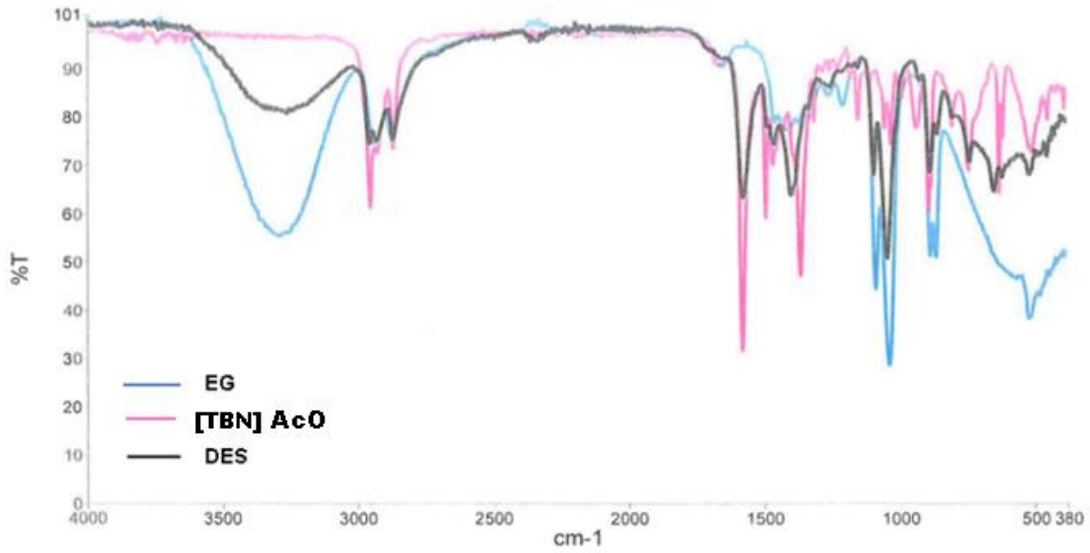

Figure 5.56: FTIR superimpose spectra of ethylene glycol, [TBN] AcO, and DES ([TBN] AcO: EG).

The FTIR profiles of diethylene glycol, [TBN] AcO and DES ([TBN] AcO + EG) are shown in Figure 5.57 and 5.58.

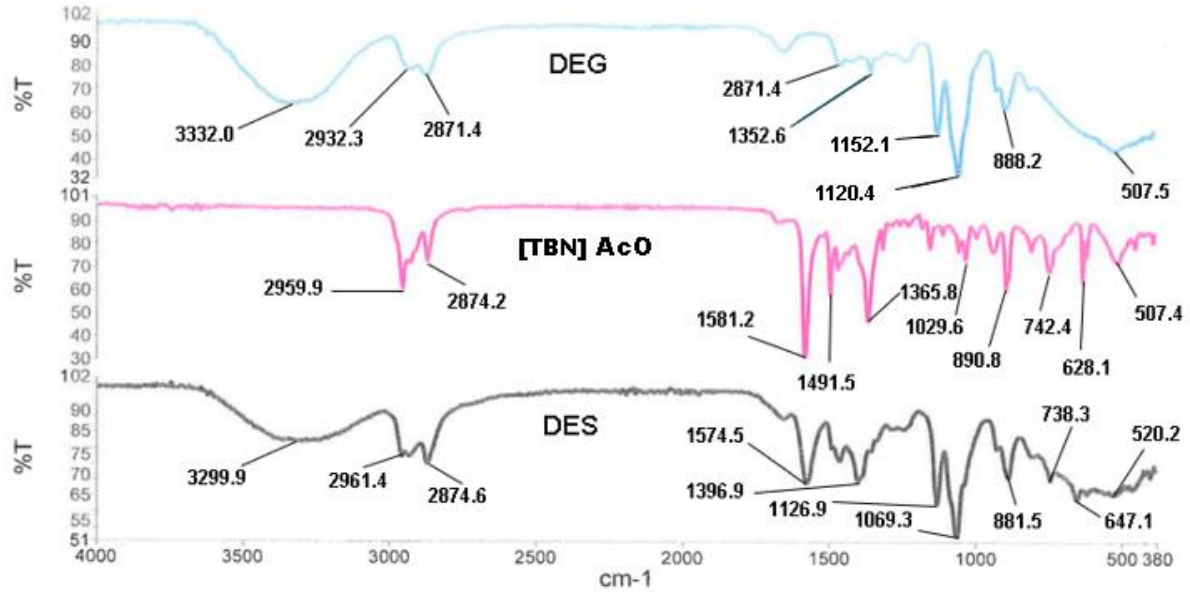

Figure 5.57: FTIR spectra of diethylene glycol, [TBN] AcO and DES ([TBN] AcO: DEG).

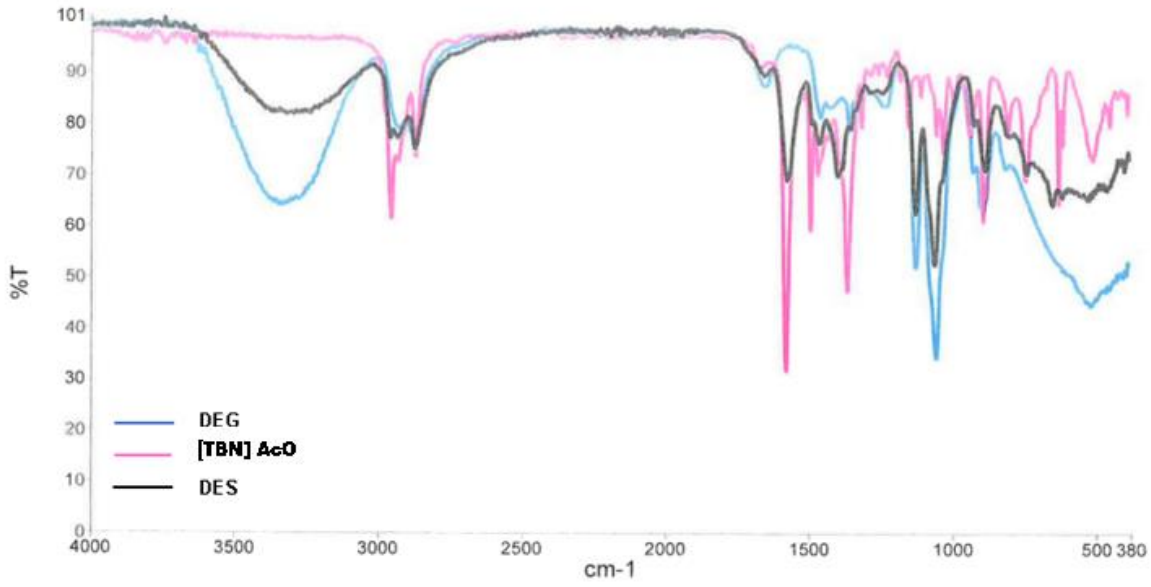

Figure 5.58: FTIR superimpose spectra of diethylene glycol, [TBN] AcO, and DES ([TBN AcO, DEG).

5.3.3 ^{1}H-NMR and ^{13}C-NMR spectroscopic analysis

The deep eutectic solvent prepared by tetrabutylammonium acetate with ethylene glycol, ([TBN] AcO: EG) and tetrabutylammonium acetate with diethylene glycol, ([TBN] AcO: DEG), were characterized by ^{1}H-NMR as well as ^{13}C-NMR.

The ^{1}H-NMR and ^{13}C-NMR spectroscopic profiles of DES ([TBN] AcO + EG) are shown in Figure 5.59 and 5.60.

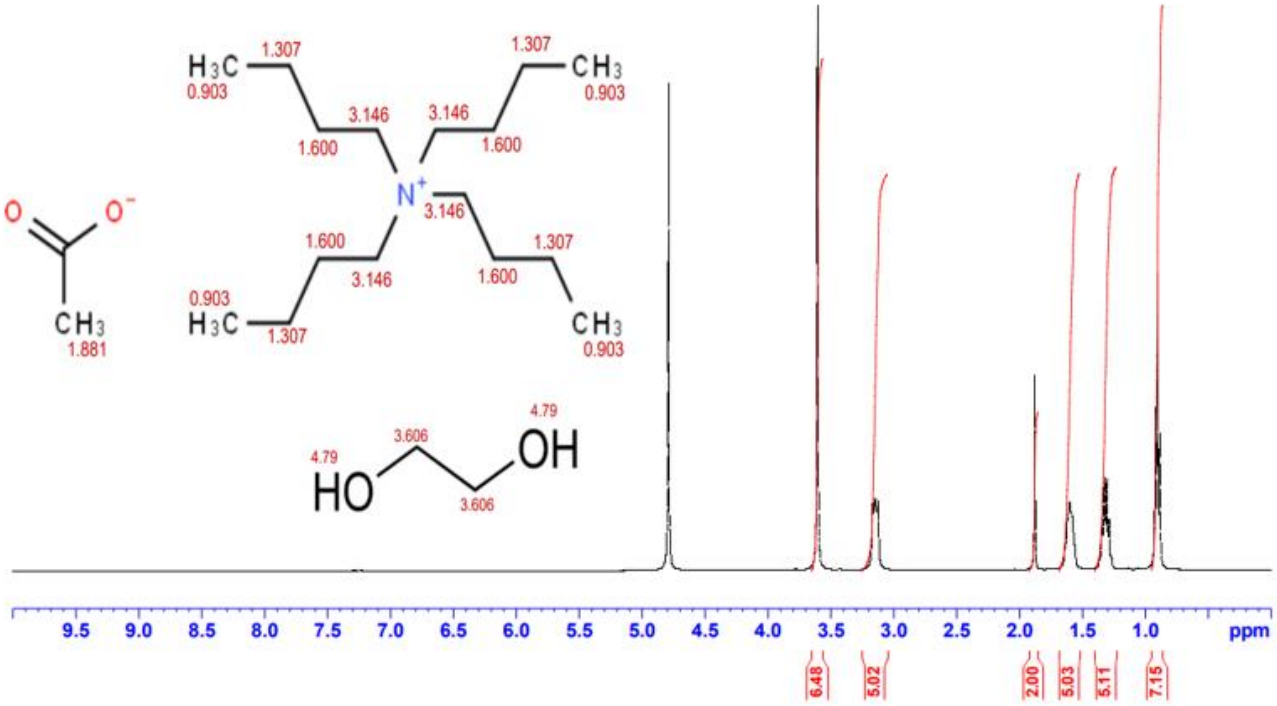

Figure 5.59: Proton ^{1}H-NMR spectra for deep eutectic solvent [TBN] AcO: EG.

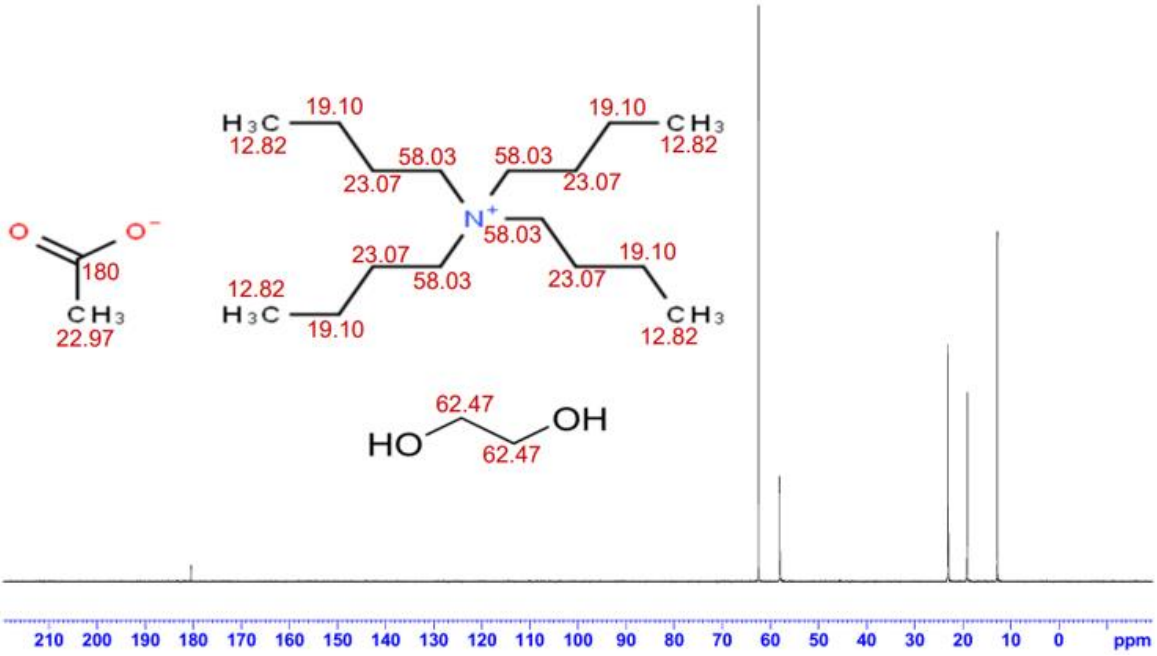

Figure 5.60: Carbon ^{13}C-NMR spectra for deep eutectic solvent [TBN] AcO: EG

The ^{1}H-NMR and ^{13}C-NMR spectroscopic profiles of DES ([TBN] AcO + DEG) are shown in Figure 5.61 and 5.62

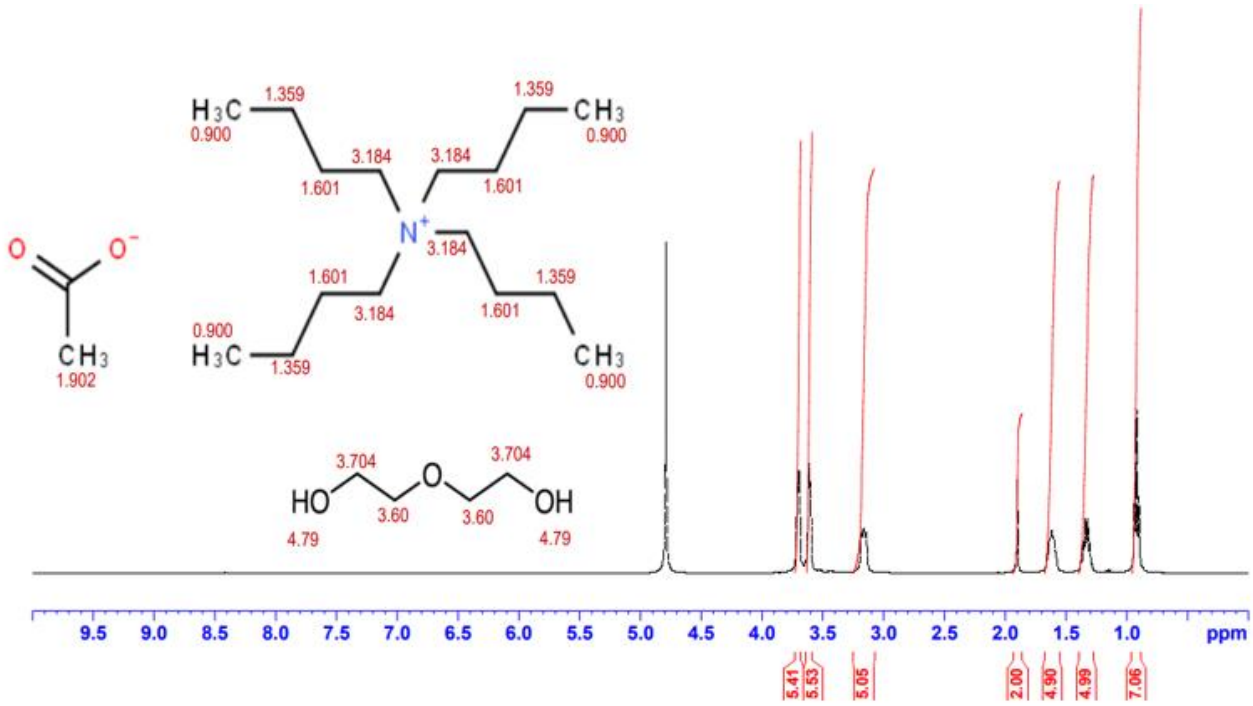

Figure 5.61: Proton ^{1}H-NMR spectra for deep eutectic solvent [TBN] AcO: DEG)

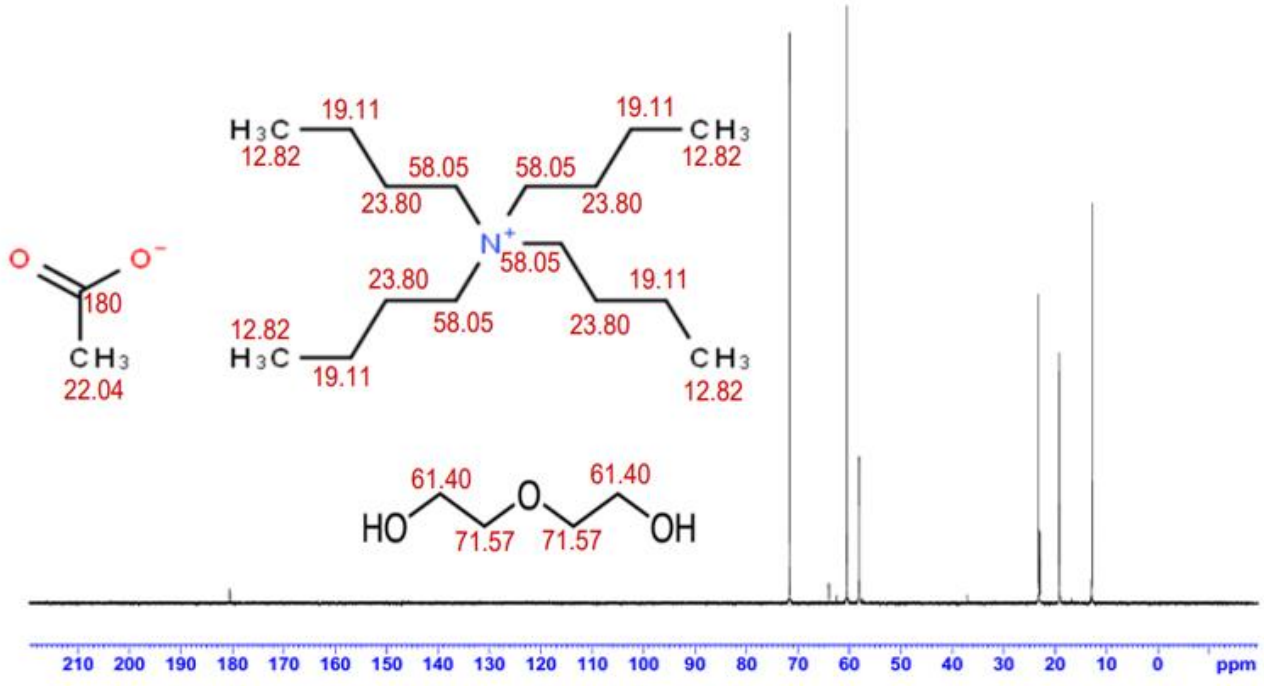

Figure 5.62: Carbon ^{13}C-NMR spectra for deep eutectic solvent [TBN] AcO: DEG

Activity coefficient at infinite dilution

5.4 Tetrabutylammonium acetate with ethylene glycol (TBN] AcO: EG)

The results of critical data for the solutes (acentric factor (ω) calculated from saturated vapour pressure and critical pressure solutes) is given in Table 5.18.

Table 5-18: Critical data for the solutes (acentric factor (ω) calculated from saturated vapor pressure and critical pressure of solutes).

Solutes	Tc (K)	Pc (Pa)	Vc (cm^3.mol^{-1})	ω
Helium	5.1900	227000	57.3000	-0.390
2,2-Dimethylbutane	489.0000	3102000	358.0000	0.2330
Pentane	469.7000	3370000	311.0000	0.2520
Hexane	507.6000	3020000	369.0000	0.2990
Heptane	540.2000	2740000	429.0000	0.3500

n-Nonane	594.6000	2290000	555.0000	0.4450
n-Decane	617.7000	2110000	624.0000	0.4900
1-Pentene	464.8000	3560000	298.4000	0.2370
1-Hexene	504.0000	3143000	355.1000	0.2810
1-Heptene	537.3000	2920000	409.0000	0.3430
1-Nonene	594.0000	23300000	526.0000	0.4110
1-Decene	617.0000	2220000	584.0000	0.4910
Cyclohexene	560.4000	4075000	296.0000	0.2040
Cyclohexane	553.5000	4073000	308.0000	0.2110
Cyclooctane	647.2000	3570000	410.0000	0.2540
1-Pentyne	487.3000	4162330	278.0000	0.3940
1-Hexyne	501.8800	3690970	334.0000	0.2490
1-Heptyne	559.6400	3295000	389.5000	0.4430
Benzene	562.0500	4895000	256.0000	0.2200
Toluene	591.7000	4108000	316.0000	0.2640
Ethylbenzene	617.0000	3640000	374.0000	0.3040
m-Xylene	617.0000	3541000	375.0000	0.3270
p-Xylene	616.2000	3511000	378.0000	0.3220
o-Xylene	630.3000	3732000	370.0000	0.3120
Methanol	512.6400	8097000	118.0000	0.5650
Ethanol	513.6400	6148000	167.0000	0.6490
Propanol	536.7800	5175000	219.0000	0.6290
Butanol	563.0500	4423000	275.0000	0.5900
THF	540.2000	5190000	224.0000	0.3640
Acetonitrile	574.9000	4830000	173.0000	0.3270
Thiophene	580.0000	5660000	219.0000	0.1960
Acetone	508.1000	4700000	209.0000	0.3070
2-butanone	535.0000	4220000	267.0000	0.3220
Octane	568.7000	2490000	409.0000	0.3990

The results of Virial Coefficients of solutes are shown in Table 5.19.

Table 5-19: Virial Coefficients of solutes.

B_{11} ($m^3 \cdot mol^{-1}$)					
Solutes	**313.15 K**	**323.15 K**	**333.15 K**	**343.15 K**	**353.15 K**
2,2-dimethylbutane	-0.001446	-0.001328	-0.001224	-0.0006406	-0.001052
Pentane	-0.001054	-0.0009738	-0.0009026	-0.0004338	-0.0007829
Hexane	-0.001648	-0.001511	-0.001390	-0.0007533	-0.001191
Heptane	-0.002474	-0.002252	-0.002060	-0.001221	-0.001743
n-Nonane	-0.005066	-0.004559	-0.004123	-0.002766	-0.003417
n-Decane	-0.006985	-0.006258	-0.005635	-0.003942	-0.004631
1-Pentene	-0.0009850	-0.0009102	-0.0008440	-0.0004013	-0.0007325
1-Hexene	-0.001559	-0.001429	-0.001316	-0.0007084	-0.001128
1-Heptene	-0.002326	-0.002118	-0.001938	-0.001144	-0.001641
1-Nonene	-0.004785	-0.004306	-0.003895	-0.002611	-0.003229
1-Decene	-0.006511	-0.005823	-0.005253	-0.003673	-0.004318
Cyclohexene	-0.001761	-0.001606	-0.001471	-0.000868	-0.001249
Cyclohexane	-0.001767	-0.001613	-0001478	-0.0008633	-0.001257
Cyclooctane	-0.004613	-0.004143	-0.003740	-0.002588	-0.003089
1-Pentyne	-0.0009872	-0.0009112	-0.0008440	-0.0004130	-0.0007313
1-Hexyne	-0.001449	-0.001329	-0.001224	-0.0006563	-0.001050
1-Heptyne	-0.002508	-0.002278	-0.002079	-0.001269	-0.001754
Benzene	-0.001537	-0.001401	-0.001283	-0.0007590	-0.001089
Toluene	-0.002423	-0.002194	-0.001997	-0.001270	-0.001675
Ethylbenzene	-0.003577	-0003221	-0.002915	-0.001959	-0.002420
m-Xylene	-0.003586	-0.003230	-0.002923	-0.001964	-0.002426
p-Xylene	-0.003599	-0.003241	-0.002934	-0.001970	-0.002435
o-Xylene	-0.003803	-0.003420	-0.003092	-0.002106	-0.002561
Methanol	-0.0003399	-0.0003212	-0.0003040	-0.0001156	-0.0002736
Ethanol	-0.0005414	-0.0005071	-0.0004763	-0.0002032	-0.0004228
Propanol	-0.0008707	-0.0008087	-0.0007525	-0.0003644	-0.0006600
Butanol	-0.001370	-0.001262	-0.001167	-0.0006292	-0.001008

THF	-0.001002	-0.0009244	-0.0008560	-0.0004451	-0.0007416
Acetonitrile	-0.0007115	-0.0006650	-0.0006232	-0.0002927	-0.0005514
Thiophene	-0.001181	-0.001086	-0.001003	-0.0005546	-0.0008642
Acetone	-0.0007308	-0.0006800	-0.0006347	-0.0002918	-0.0005574
2-butanone	-0.001175	-0.001084	-0.001004	-0.0005193	-0.0008706
Octane	-0.003599	-0.003257	-0.002960	-0.001881	-0.002478

B_{12} ($m^3 \cdot mol^{-1}$)					
Solutes	**313.15 K**	**323.15 K**	**333.15 K**	**343.15 K**	**353.15 K**
2,2-dimethylbutane	5.317E-05	5.375E-05	5.430E-05	5.481E-05	5.529E-05
Pentane	4.808E-05	4.863E-05	4.915E-05	4.963E-05	5.008E-05
Hexane	5.423E-05	5.446E-05	5.503E-05	5.556E-05	5.606E-05
Heptane	6.031E-05	6.055E-05	6.116E-05	6.174E-05	6.227E-05
n-Nonane	7.289E-05	7.316E-05	7.385E-05	7.450E-05	7.511E-05
n-Decane	7.963E-05	7.991E-05	8.064E-05	8.132E-05	8.196E-05
1-Pentene	4.738E-05	4.758E-05	4.807E-05	4.854E-05	4.897E-05
1-Hexene	5.315E-05	5.337E-05	5.391E-05	5.443E-05	5.491E-05
1-Heptene	5.854E-05	5.877E-05	5.637E-05	5.992E-05	6.044E-05
1-Nonene	7.001E-05	7.028E-05	7.096E-05	7.159E-05	7.218E-05
1-Decene	7.564E-05	7.592E-05	7.663E-05	7.729E-05	7.791E-05
Cyclohexene	4.570E-05	4.591E-05	4.646E-05	4.696E-05	4.744E-05
Cyclohexane	4.676E-05	4.669E-05	4.755E-05	4.807E-05	4.857E-05
Cyclooctane	5.648E-05	5.675E-05	5.742E-05	5.801E-05	5.863E-05
1-Pentyne	4.454E-05	4.474E-05	4.524E-05	4.571E-05	4.615E-05
1-Hexyne	5.055E-05	5.077E-05	5.131E-05	5.182E-05	5.230E-05
1-Heptyne	5.568E-05	5.593E-05	5.653E-05	5.710E-05	5.764E-05
Benzene	4.091E-05	4.113E-05	4.165E-05	4.214E-05	4.260E-05
Toluene	4.752E-05	4.775E-05	4.832E-05	4.885E-05	4.935E-05
Ethylbenzene	5.359E-05	5.384E-05	5.446E-05	5.503E-05	5.557E-05
m-Xylene	5.382E-05	5.407E-05	5.467E-05	5.525E-05	5.578E-05
p-Xylene	5.423E-05	5.448E-05	5.509E-05	5.566E-05	5.619E-05
o-Xylene	5.305E-05	5.330E-05	5.392E-05	5.449E-05	5.503E-05

Methanol	2.432E-05	2.449E-05	2.487E-05	2.523E-05	2.557E-05
Ethanol	3.057E-05	3.075E-05	3.119E-05	3.160E-05	3.199E-05
Propanol	3.659E-05	3.680E-05	3.729E-05	3.775E-05	3.819E-05
Butanol	4.284E-05	4.307E-05	4.361E-05	4.412E-05	4.460E-05
THF	3.743E-05	3.764E-05	3.812E-05	3.858E-05	3.901E-05
Acetonitrile	2.995E-05	3.016E-05	3.065E-05	3.111E-05	3.154E-05
Thiophene	3.646E-05	3.667E-05	3.717E-05	3.764E-05	3.808E-05
Acetone	3.602E-05	3.621E-05	3.667E-05	3.711E-05	3.752E-05
2-butanone	4.248E-05	4.270E-05	4.322E-05	4.370E-05	4.416E-05
Octane	6.431E-05	6.461E-05	6.534E-05	6.060E-05	6.667E-05

The results of the average activity coefficient at infinite dilution of organic solutes at 1.00:300 molar ration of (Tetrabutylammonium acetate: ethylene glycol) at different temperatures at atmospheric pressure is given in Table 5.20.

Table 5-20: is the average activity coefficients at infinite dilution of organic solutes at 1.00:3.00 molar ratio of (Tetrabutylammonium acetate: ethylene glycol) with the standard uncertainty of molar ratio (DES molar ratio) = 0.005, at different temperatures, $\boldsymbol{T}$ = (313.15, 323.15, 333.15, 343.15 and 363.15) K. The standard state of solutes is hypothetical liquid at zero pressure.

Average of infinite dilution activity coefficients (γ_{13}^{∞})					
	Temperature				
Organic Solutes	**313.15 K**	**323.15 K**	**333.15 K**	**343.15 K**	**353.15 K**
2,2-Dimethylbutane	22.98	20.59	18.9	17.07	15.78
Pentane	17.79	16.08	14.7	13.28	12.29
Hexane	36.58	31.35	28.4	25.46	22.95
Heptane	62.31	53.94	46.4	43.03	37.86
Octane	89.56	78.27	69.7	65.19	56.93
n-Nonane	129.75	115.82	101.2	91.97	81.79
n-Decane	194.60	174.21	157.1	138.54	124.95
1-Pentene	16.33	14.32	12.97	12.07	11.20

1-Hexene	29.48	26.10	23.30	20.75	18.73
1-Heptene	47.67	43.53	38.36	34.50	31.37
1-Nonene	108.30	96.15	84.80	75.40	66.42
1-Decene	188.36	160.92	143.3	122.13	105.73
Cyclohexene	21.25	19.88	17.86	15.92	14.48
Cyclohexane	26.89	23.80	21.7	19.37	17.37
Cyclooctane	48.48	41.03	34.7	32.26	29.00
1-Pentyne	13.42	12.57	11.9	11.24	10.73
1-Hexyne	19.11	18.29	17.5	16.72	16.24
1-Heptyne	26.39	24.72	23.8	22.44	21.36
Benzene	12.76	12.23	11.5	10.98	10.47
Toluene	21.23	19.04	17.8	16.73	15.71
Ethylbenzene	27.20	26.01	25.0	24.09	23.39
m-Xylene	28.80	27.78	26.8	26.23	25.44
p-Xylene	28.05	26.92	26.4	25.72	24.85
o-Xylene	26.85	25.68	24.2	23.66	23.20
Methanol	2.26	1.98	1.79	1.66	1.55
Ethanol	3.63	3.10	2.75	2.54	2.25
1-Propanol	9.01	7.76	6.86	6.36	5.82
1-Butanol	11.47	9.92	8.94	8.10	7.33
THF	10.09	8.98	8.12	7.40	6.79
Acetonitrile	11.68	10.64	9.74	8.97	8.34
Thiophene	7.58	7.80	7.93	8.12	8.39
Acetone	7.01	6.94	6.81	6.74	6.61
2-Butanone	7.95	7.81	7.66	7.52	7.38

***Standard uncertainty u is $u_T(\gamma_{13}^{\infty}) = 0.06$, u(T) = 0.02 K, u ([TBN AoC: EG) = 0.007.**

The results of partial molar excess properties , enthalpies ($\Delta \boldsymbol{H}_{\mathbf{1}}^{\mathbf{E},\infty}$), Gibbs free energies ($\Delta \boldsymbol{G}_{\mathbf{1}}^{\mathbf{E},\infty}$), and entropies $\left(\boldsymbol{T}_{\boldsymbol{ref}}\Delta \boldsymbol{S}_{\mathbf{1}}^{\mathbf{E},\infty}\right)$ for the various organic solutes in tetrabutylammonium acetate to ethylene glycol at $\boldsymbol{T}_{\boldsymbol{ref}}$ = 323.15 K is given in Table 5.21.

Table 5-21: is the partial molar excess properties, enthalpies ($\Delta \boldsymbol{H}_{\mathbf{1}}^{\mathbf{E},\infty}$), Gibbs free energies ($\Delta \boldsymbol{G}_{\mathbf{1}}^{\mathbf{E},\infty}$), and entropies $\left(\boldsymbol{T}_{\boldsymbol{ref}}\Delta \boldsymbol{S}_{\mathbf{1}}^{\mathbf{E},\infty}\right)$ for the various organic solutes in tetrabutylammonium acetate to ethylene glycol at $\boldsymbol{T}_{\boldsymbol{ref}}$ = 323.15 K.

Organic solutes	$\Delta \boldsymbol{H}_{\mathbf{1}}^{\mathbf{E},\infty}$/kJ.mol^{-1}	$\Delta \boldsymbol{G}_{\mathbf{1}}^{\mathbf{E},\infty}$/kJ.mol^{-1}	$\boldsymbol{T}_{\boldsymbol{ref}}\Delta \boldsymbol{S}_{\mathbf{1}}^{\mathbf{E},\infty}$/kJ.mol^{-1}
2,2-Dimethylbutane	8.480	8.130	0.360
Pentane	8.560	7.460	1.100
Hexane	10.51	9.260	1.250
Heptane	11.27	10.71	0.5600
Octane	10.03	11.71	-1.690
n-Nonane	10.62	12.77	-2.150
n-Decane	10.25	13.86	-3.610
1-Pentene	8.520	7.150	1.370
1-Hexene	10.47	8.760	1.710
1-Heptene	9.840	10.14	-0.3000
1-Nonene	11.23	12.27	-1.040
1-Decene	13.21	13.67	-0.1000
Cyclohexene	9.080	8.030	1.050
Cyclohexane	8.580	8.520	0.0700
Cyclooctane	11.72	9.980	1.740
1-Pentyne	5.160	6.800	-1.640
1-Hexyne	3.830	7.810	-3.980
1-Heptyne	4.780	8.620	-3.840
Benzene	4.620	6.730	-2.110
Toluene	6.740	7.920	-1.170
Ethylbenzene	3.490	8.760	-5.270
m-Xylene	2.820	8.930	-6.120

o-Xylene	3.460	8.720	-5.260
Methanol	8.650	1.710	6.940
Ethanol	10.67	2.970	7.700
1-Propanol	9.920	5.650	4.270
1-Butanol	10.12	6.430	3.680
THF	9.090	5.900	3.190
Acetonitrile	7.770	6.350	1.410
Thiophene	-2.230	5.520	-7.750
Acetone	1.350	5.200	-3.850
2-Butanone	1.690	5.520	-3.830

***Standard uncertainty u is $u_T(\gamma_{13}^{\infty})$ = 0.06, u(T) = 0.02 K, u (TBN AoC: EG) = 0.007.**

The graph of $\ln\gamma_{13}^{\infty}$ against 1000/T(K^{-1}) for alkanes in DES – ([TBN] AcO]: EG) at $\boldsymbol{T}$ = (313.15 – 343.15) K is given in Figure 5.63.

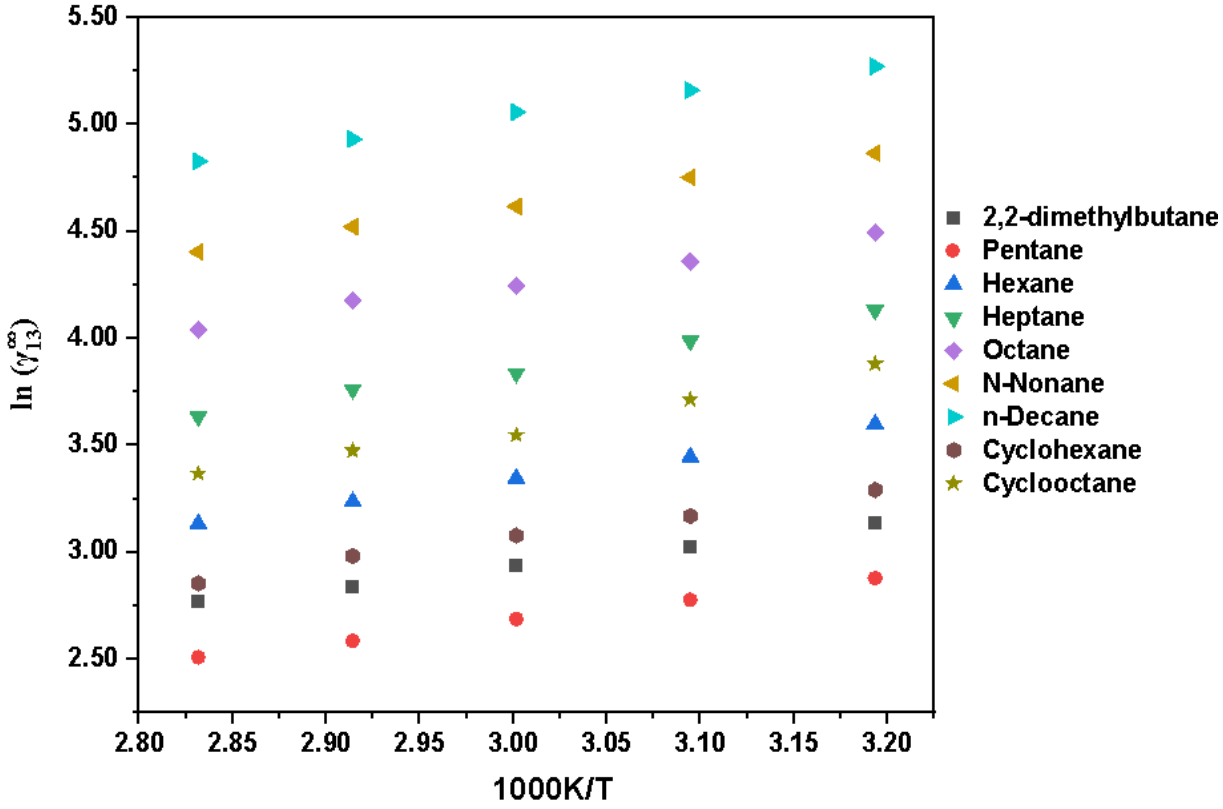

Figure 5.63: Graph of $\ln\gamma_{13}^{\infty}$ against 1000/T(K^{-1}) for alkanes in DES – ([TBN] AcO]: EG) at $\boldsymbol{T}$ = (313.15 – 343.15) K.

Figure 5.64 is the graph of $\ln\gamma_{13}^{\infty}$ against 1000/T (K^{-1}) for alkenes in DES - ([TBN] AcO: EG) at $\boldsymbol{T}$ = (313.15 – 343.15) K.

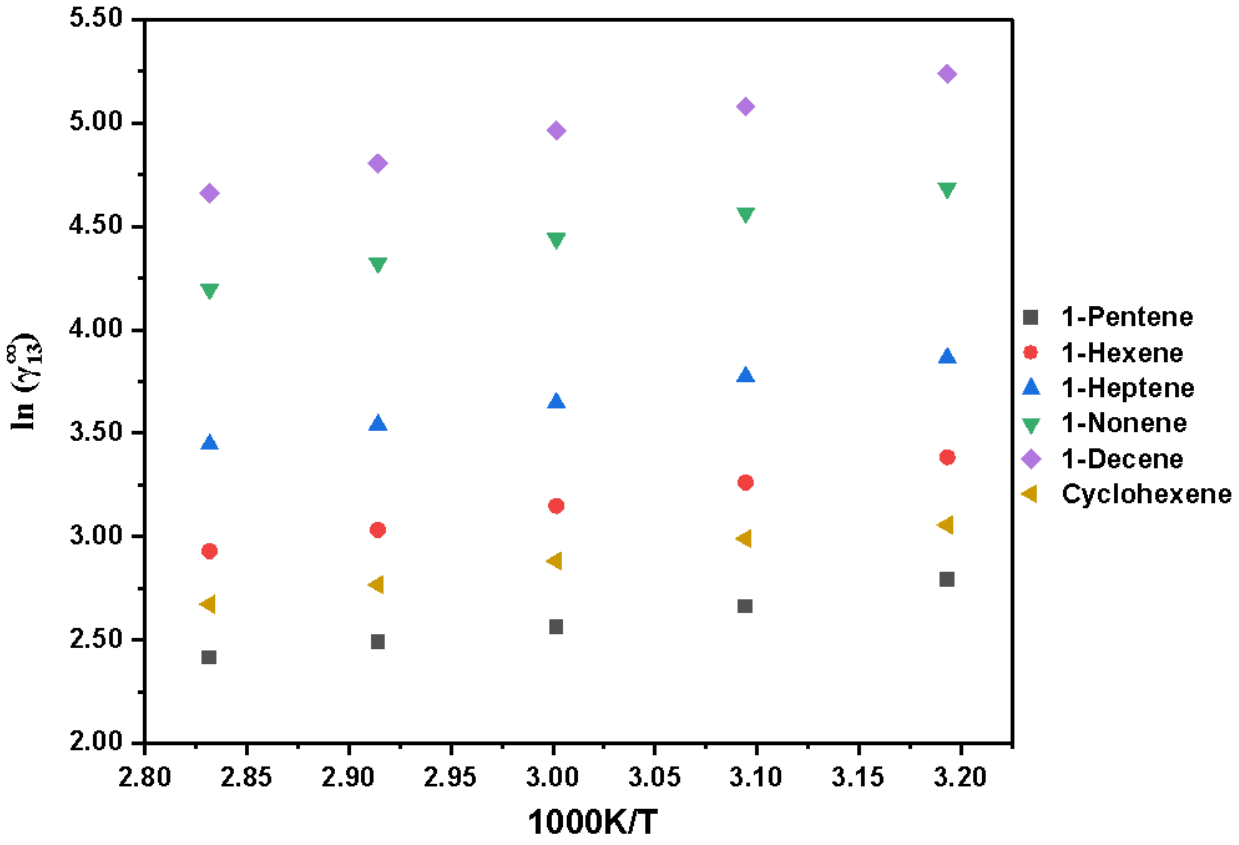

Figure 5.64: Graph of $\ln\gamma_{13}^{\infty}$ against 1000/T (K^{-1}) for alkenes in DES - ([TBN] AcO: EG) at $\boldsymbol{T}$ = (313.15 – 343.15) K.

The graph of $\ln\gamma_{13}^{\infty}$ against 1000/T (K^{-1}) for alkynes in DES – ([TBN] AcO: EG) at $\boldsymbol{T}$ = (313.15 – 343.15) K is given in Figure 5.65.

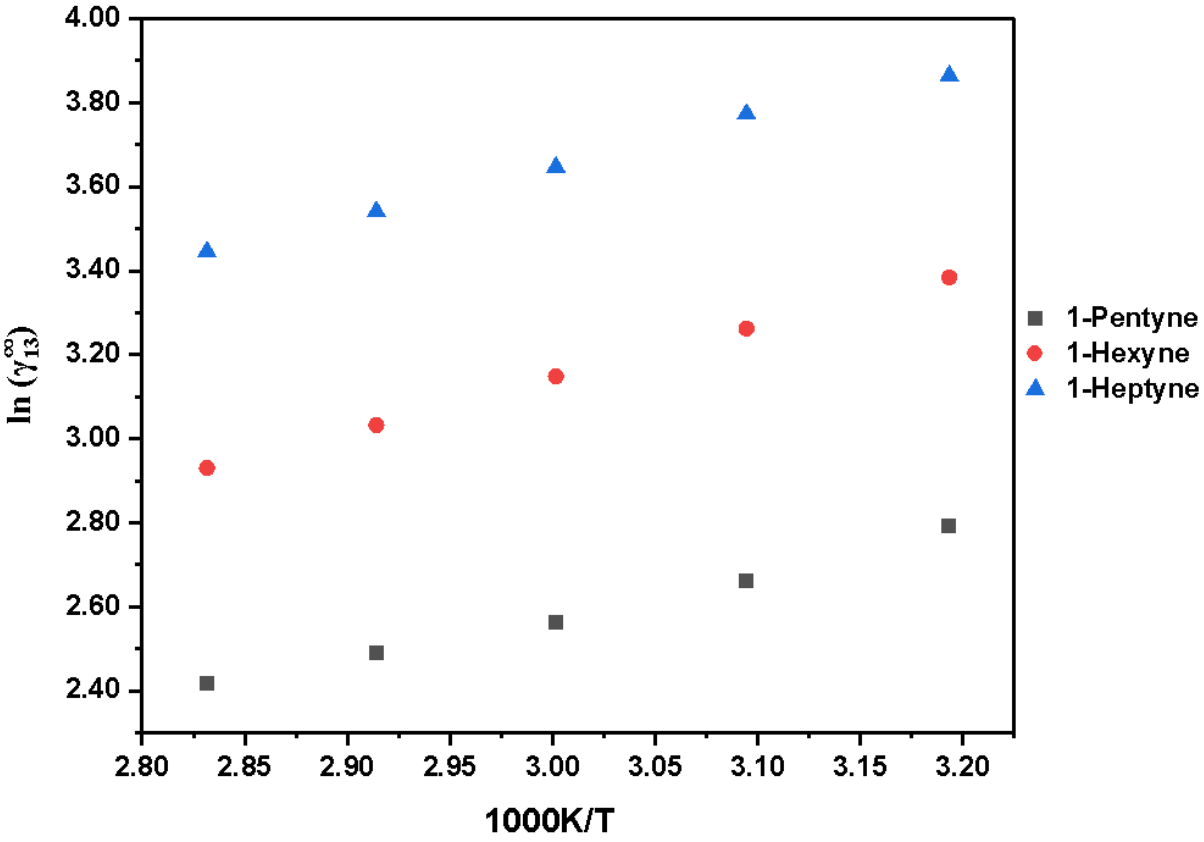

Figure 5.65: Graph of $\ln\gamma_{13}^{\infty}$ against 1000/T (K^{-1}) for alkynes in DES – ([TBN] AcO: EG) at $\boldsymbol{T}$ = (313.15 – 343.15) K.

Figure 5.66 is the graph of $\ln\gamma_{13}^{\infty}$ against 1000/T (K^{-1}) for aromatic hydrocarbons in DES – ([TBN] AcO: EG) at $\boldsymbol{T}$ = (313.15 – 343.15) K.

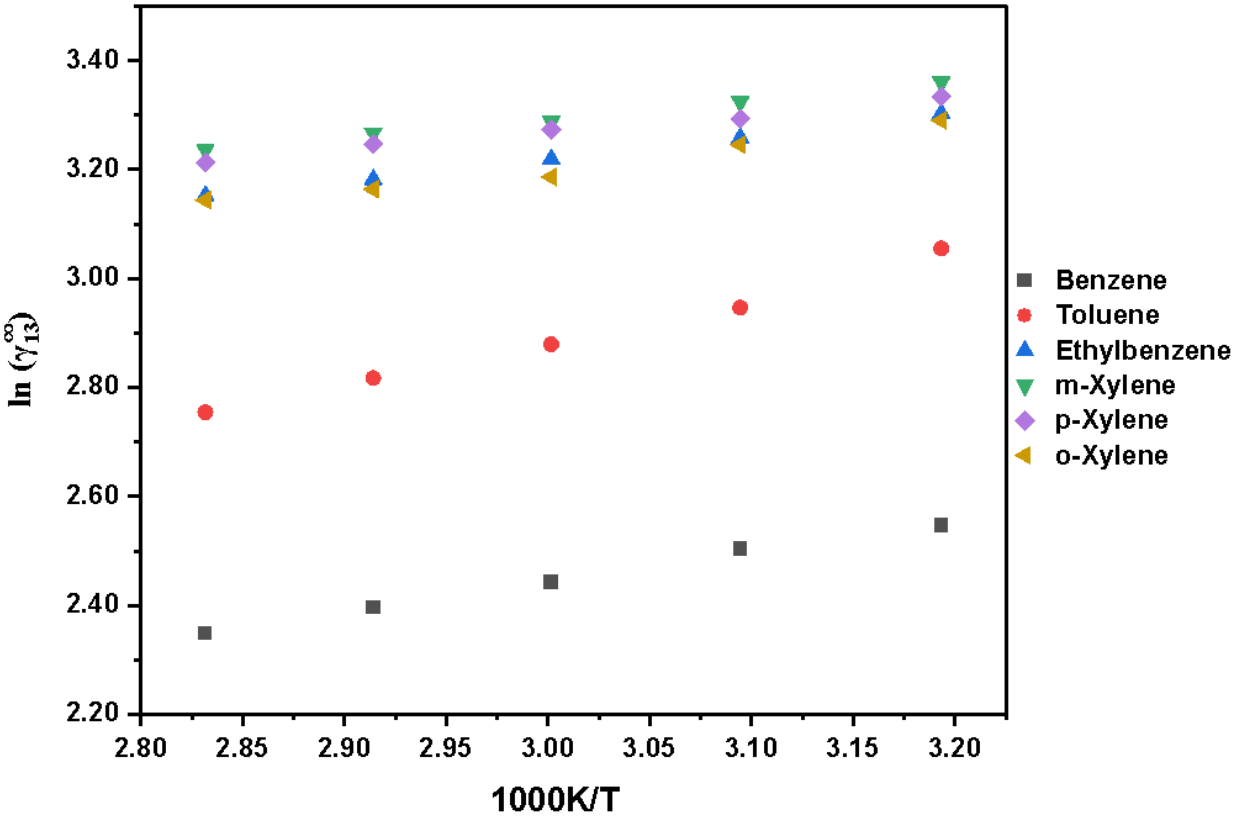

Figure 5.66: Graph of $\ln\gamma_{13}^{\infty}$ against 1000/T (K^{-1}) for aromatic hydrocarbons in DES – ([TBN] AcO: EG) at $\boldsymbol{T}$ = (313.15 – 343.15) K.

The graph of $\ln\gamma_{13}^{\infty}$ against 1000/T (K^{-1}) for alcohols in DES – ([TBN] AcO: EG) at $\boldsymbol{T}$ = (313.15 – 343.15) K is given in Figure 5.67.

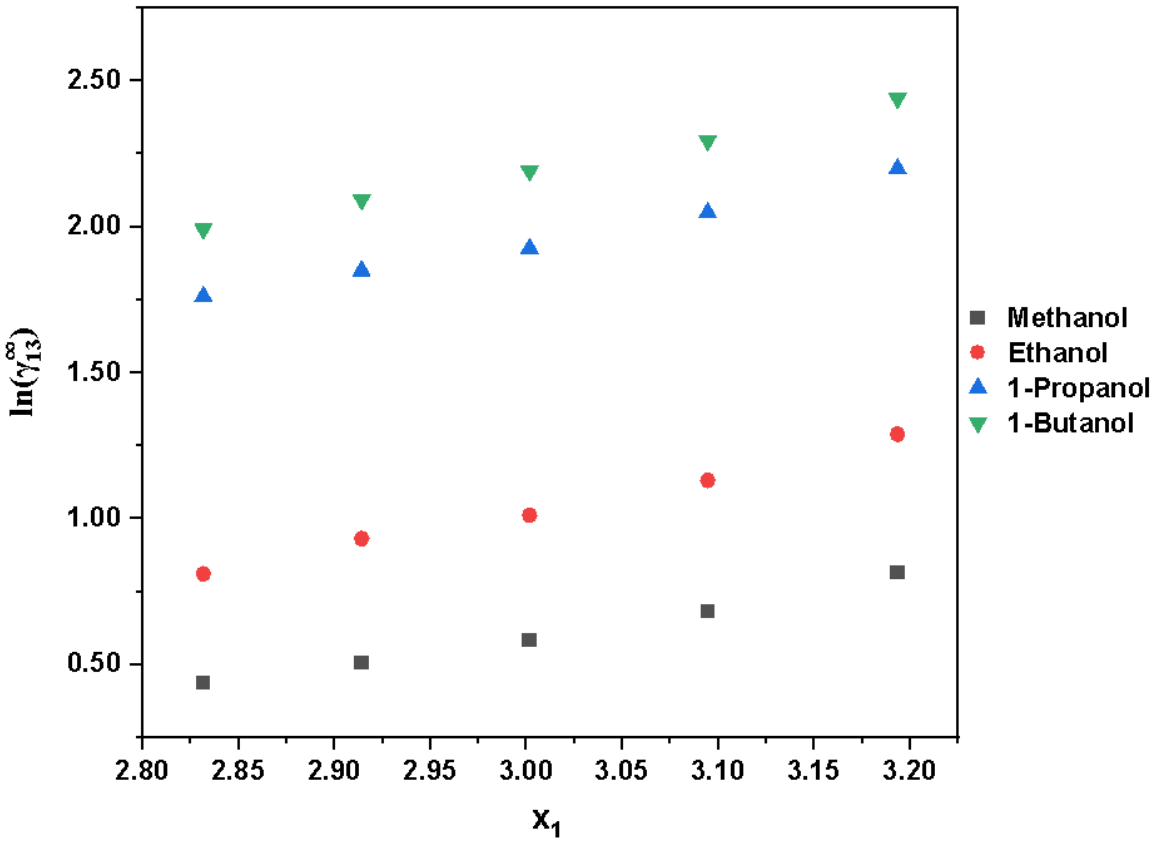

Figure 5.67: Graph of $\ln\gamma_{13}^{\infty}$ against 1000/T (K^{-1}) for alcohols in DES – ([TBN] AcO: EG) at $\boldsymbol{T}$ = (313.15 – 343.15) K.

Figure 5.68 is the graph of $\ln\gamma_{13}^{\infty}$ against 1000/T (K^{-1}) for ketones in DES – ([TBN] AcO: EG) at $\boldsymbol{T}$ = (313.15 – 343.15) K.

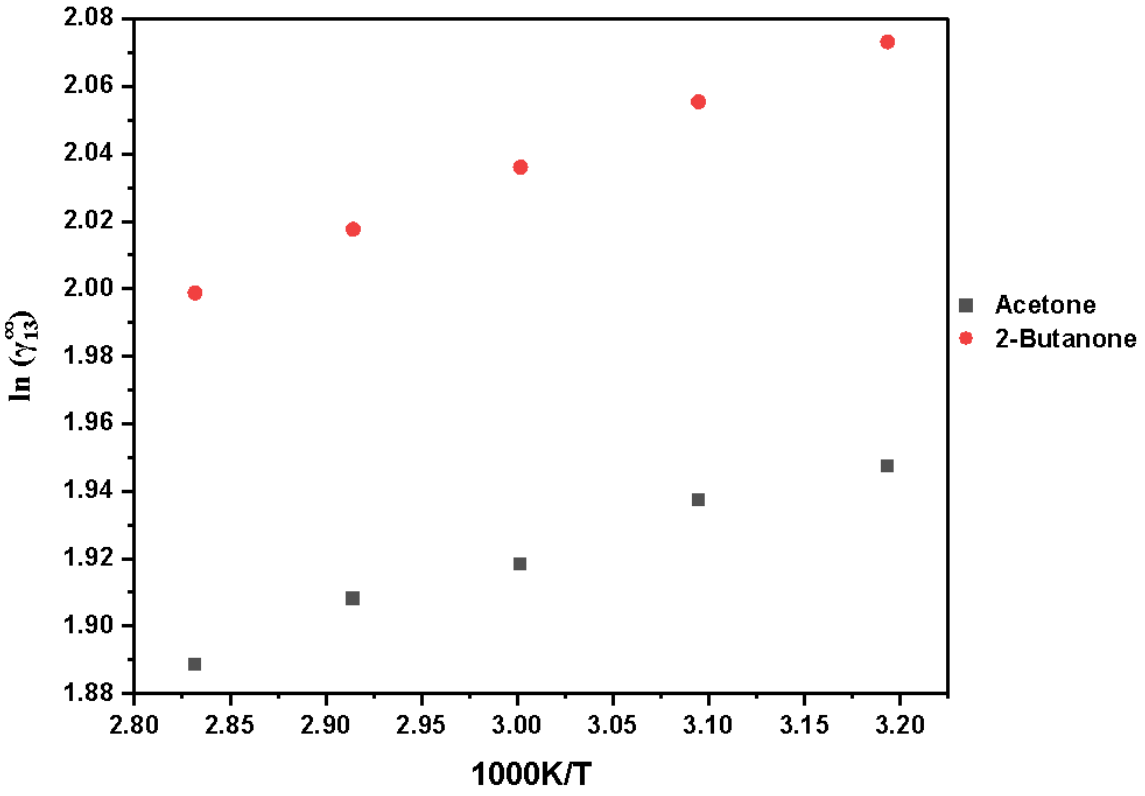

Figure 5.68: Graph of $\ln\gamma_{13}^{\infty}$ against 1000/T (K^{-1}) for ketones in DES – ([TBN] AcO: EG) at $\boldsymbol{T}$ = (313.15 – 343.15) K.

The graph of $\ln\gamma_{13}^{\infty}$ against 1000/T (K^{-1}) for THF, acetonitrile and thiophene in DES – ([TBN] AcO: EG) at T = (313.15 – 343.15) K is given in Figure 5.69.

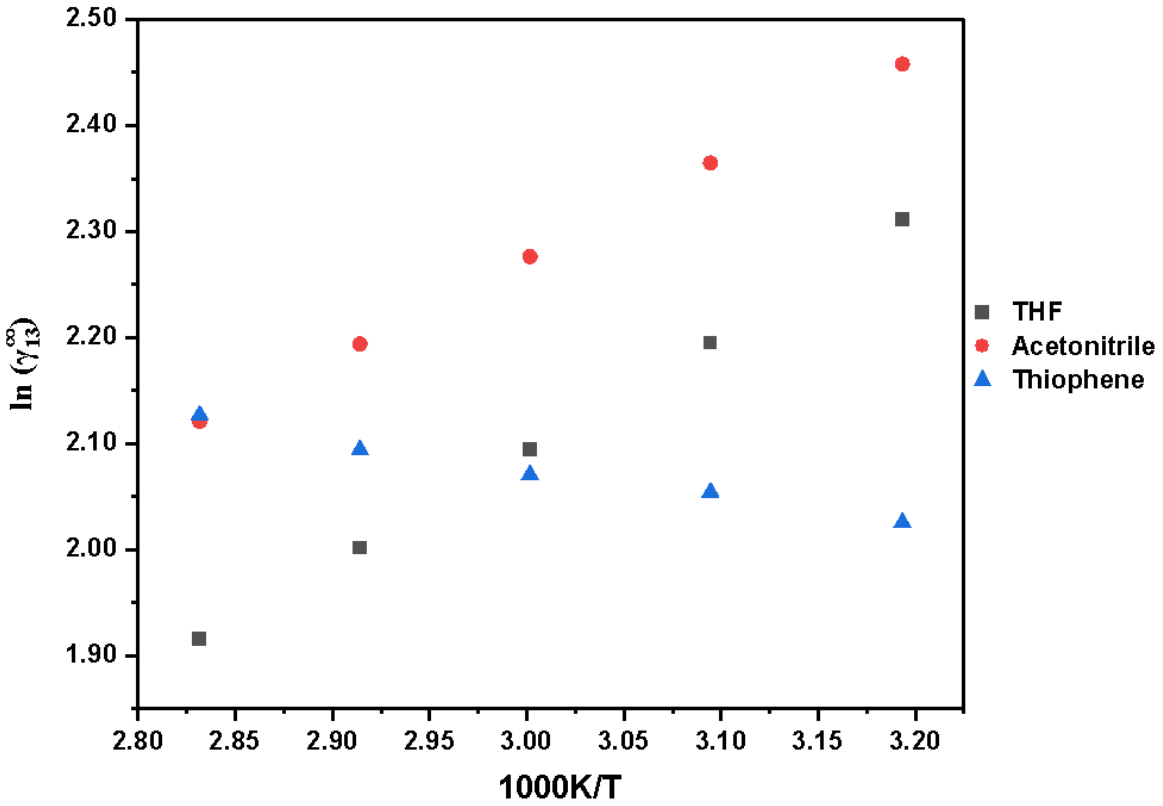

Figure 5.69: Graph of $\ln\gamma_{13}^{\infty}$ against 1000/T (K^{-1}) for THF, acetonitrile and thiophene in DES – ([TBN] AcO: EG) at T = (313.15 – 343.15) K.

5.5 Tetrabutylammonium acetate with diethylene glycol (TBN AoC: DEG)

The results of the average activity coefficient at infinite dilution of organic solutes at 1.00:300 molar ration of (Tetrabutylammonium acetate: diethylene glycol) at different temperatures at atmospheric pressure is given in Table 5.22.

Table 5-22: is the average activity coefficients at infinite dilution of organic solutes in 1.00:3.00 molar ratio of (Tetrabutylammonium acetate : ethylene glycol) with the standard uncertainty of molar ratio (DES molar ratio) = 0.005, at different temperatures, $\boldsymbol{T}$ = (313.15, 323.15, 333.15, 343.15 and 363.15) K. The standard state of solutes is hypothetical liquid at zero pressure.

Average activity coefficients at infinite dilution (γ_{13}^{∞})					
	Temperature				
Organic Solutes	**313.15 K**	**323.15 K**	**333.15 K**	**343.15 K**	**353.15 K**
2,2-Dimethylbutane	22.25	19.83	17.74	16.21	15.11
Pentane	16.47	15.46	13.87	12.32	11.95
Hexane	33.95	30.25	26.97	24.55	22.14
Heptane	58.26	51.52	44.81	40.01	36.47
Octane	75.94	70.45	63.41	58.22	52.25
n-Nonane	116.4	106.3	99.32	86.96	78.77
n-Decane	169.8	156.3	143.92	132.2	122.1
1-Pentene	12.17	11.16	9.80	9.210	8.42
1-Hexene	28.02	25.05	22.52	20.14	18.21
1-Heptene	46.02	41.84	37.91	33.62	30.72
1-Nonene	104.4	93.78	83.18	73.58	65.30
1-Decene	149.9	135.8	127.7	114.8	102.5
Cyclohexene	17.09	15.08	13.80	12.64	11.40
Cyclohexane	24.29	22.34	20.40	18.18	16.25
Cyclooctane	44.54	39.73	33.52	30.55	26.69
1-Pentyne	6.90	6.530	6.10	5.750	5.410
1-Hexyne	13.04	12.63	12.20	11.66	11.17
1-Heptyne	18.35	17.65	16.80	16.13	15.13
Benzene	8.010	7.720	7.40	7.160	6.820

Toluene	11.79	11.43	11.00	10.68	10.20
Ethylbenzene	16.62	16.10	16.00	15.56	15.05
m-Xylene	18.11	17.65	17.50	16.91	16.51
p-Xylene	17.68	17.36	16.90	16.53	16.26
o-Xylene	15.99	15.70	15.40	14.96	14.65
Methanol	1.190	1.130	1.060	1.020	0.980
Ethanol	1.790	1.670	1.580	1.490	1.380
1-Propanol	4.790	4.540	4.310	4.030	3.800
1-Butanol	6.920	6.470	6.190	5.790	5.480
THF	6.930	6.610	6.320	6.050	5.830
Acetonitrile	7.770	7.440	7.180	6.900	6.690
Thiophene	5.180	5.370	5.540	5.700	5.940
Acetone	5.840	5.570	5.310	5.080	4.850
2-Butanone	7.910	7.790	7.410	7.090	6.750

***Standard uncertainties are $u_T(\gamma_{13}^{\infty})$ = 0.06, u(T) = 0.02 K, u ([TBA]Ac: EG) = 0.007.**

The results of partial molar excess properties , enthalpies ($\Delta \boldsymbol{H}_{\mathbf{1}}^{\mathbf{E},\infty}$), Gibbs free energies ($\Delta \boldsymbol{G}_{\mathbf{1}}^{\mathbf{E},\infty}$), and entropies $\left(\boldsymbol{T}_{\boldsymbol{ref}} \Delta \boldsymbol{S}_{\mathbf{1}}^{\mathbf{E},\infty}\right)$ for the various organic solutes in tetrabutylammonium acetate to diethylene glycol at $\boldsymbol{T}_{\boldsymbol{ref}}$ = 323.15 K is given in Table 5.23.

Table 5-23: Partial molar excess properties, enthalpies $\left(\Delta \boldsymbol{H}_{\mathbf{1}}^{\mathbf{E},\infty}\right)$, Gibbs free energies $\left(\Delta \boldsymbol{G}_{\mathbf{1}}^{\mathbf{E},\infty}\right)$, and entropies $\left(\boldsymbol{T}_{\boldsymbol{ref}} \Delta \boldsymbol{S}_{\mathbf{1}}^{\mathbf{E},\infty}\right)$ for the various organic solutes in ([TBN] AcO: DEG) at $\boldsymbol{T}_{\boldsymbol{ref}}$ = 323.15 K.

Organic solutes	$\Delta \boldsymbol{H}_{\mathbf{1}}^{\mathbf{E},\infty}$**/kJ.mol^{-1}**	$\Delta \boldsymbol{G}_{\mathbf{1}}^{E,\infty}$**/kJ·mol^{-1}**	$\boldsymbol{T}_{\boldsymbol{ref}} \Delta \boldsymbol{S}_{\mathbf{1}}^{\mathbf{E},\infty}$**/kJ·mol^{-1}**
2,2-Dimethylbutane	9.000	8.030	0.9700
Pentane	8.000	7.360	0.6400
Hexane	9.790	9.160	0.6300
Heptane	10.96	10.59	0.3600
Octane	8.620	11.74	-2.810
n-Nonane	9.030	12.54	-3.510

n-Decane	7.640	13.58	-5.940
1-Pentene	8.560	6.480	2.080
1-Hexene	9.930	8.650	1.280
1-Heptene	9.460	10.03	-0.5700
1-Nonene	10.36	12.27	-1.830
1-Decene	8.520	13.20	-4.670
Cyclohexene	9.080	7.290	1.790
Cyclohexane	9.270	8.350	0.930
Cyclooctane	11.84	9.890	1.950
1-Pentyne	5.620	4.700	0.9200
1-Hexyne	3.590	6.600	-3.050
1-Heptyne	4.340	7.470	-3.130
Benzene	3.650	5.290	-1.640
Toluene	3.280	6.360	-3.090
Ethylbenzene	2.130	7.370	-5.240
m-Xylene	2.090	7.600	-5.510
p-Xylene	1.990	7.540	-5.550
o-Xylene	2.090	7.270	-5.210
Methanol	4.600	0.1800	4.420
Ethanol	5.910	1.340	4.570
1-Propanol	5.340	4.290	1.050
1-Butanol	5.320	5.350	-0.030
THF	4.000	5.520	-1.080
Acetonitrile	3.510	5.390	-1.890
Thiophene	-3.070	4.510	-7.580
Acetone	4.270	4.610	-0.340
2-Butanone	4.340	5.520	-1.180

***Standard uncertainties are $u_T(\gamma_{13}^{\infty})$ = 0.06, u(T) = 0.02 K, u ([TBA]Ac: EG) = 0.007.**

The graph of $\ln\gamma_{13}^{\infty}$ against 1000/T (K^{-1}) for alkanes in deep eutectic solvent ([TBN] AcO: DEG) at $\boldsymbol{T}$ = (313.15 – 343.15) K is given in Figure 5.70.

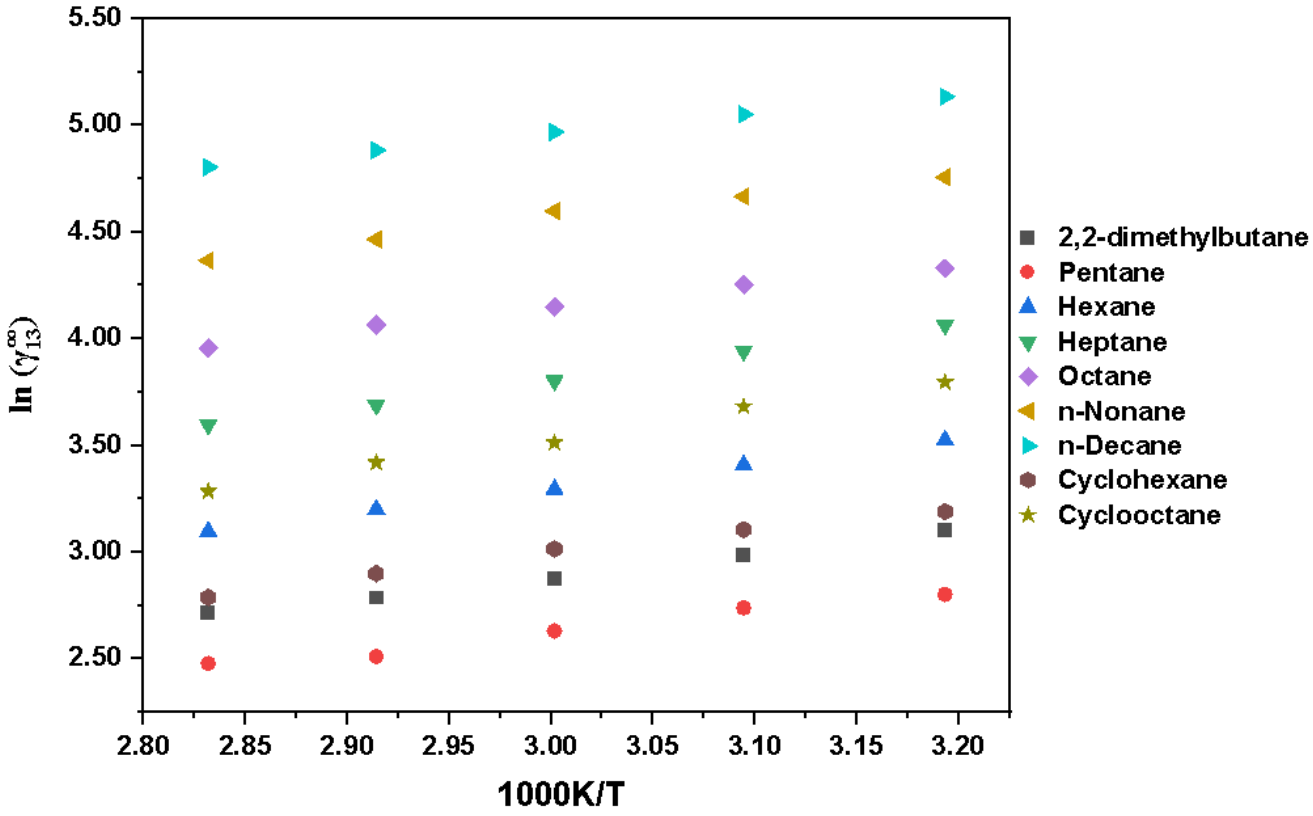

Figure 5.70: Graph of $\ln\gamma_{13}^{\infty}$ against 1000/T (K^{-1}) for alkanes in deep eutectic solvent ([TBN] AcO: DEG) at $\boldsymbol{T}$ = (313.15 – 343.15) K.

Figure 5.71 is the graph of $\ln\gamma_{13}^{\infty}$ against 1000/T (K^{-1}) for alkenes in deep eutectic solvent ([TBN] AcO: DEG) at $\boldsymbol{T}$ = (313.15 – 343.15) K.

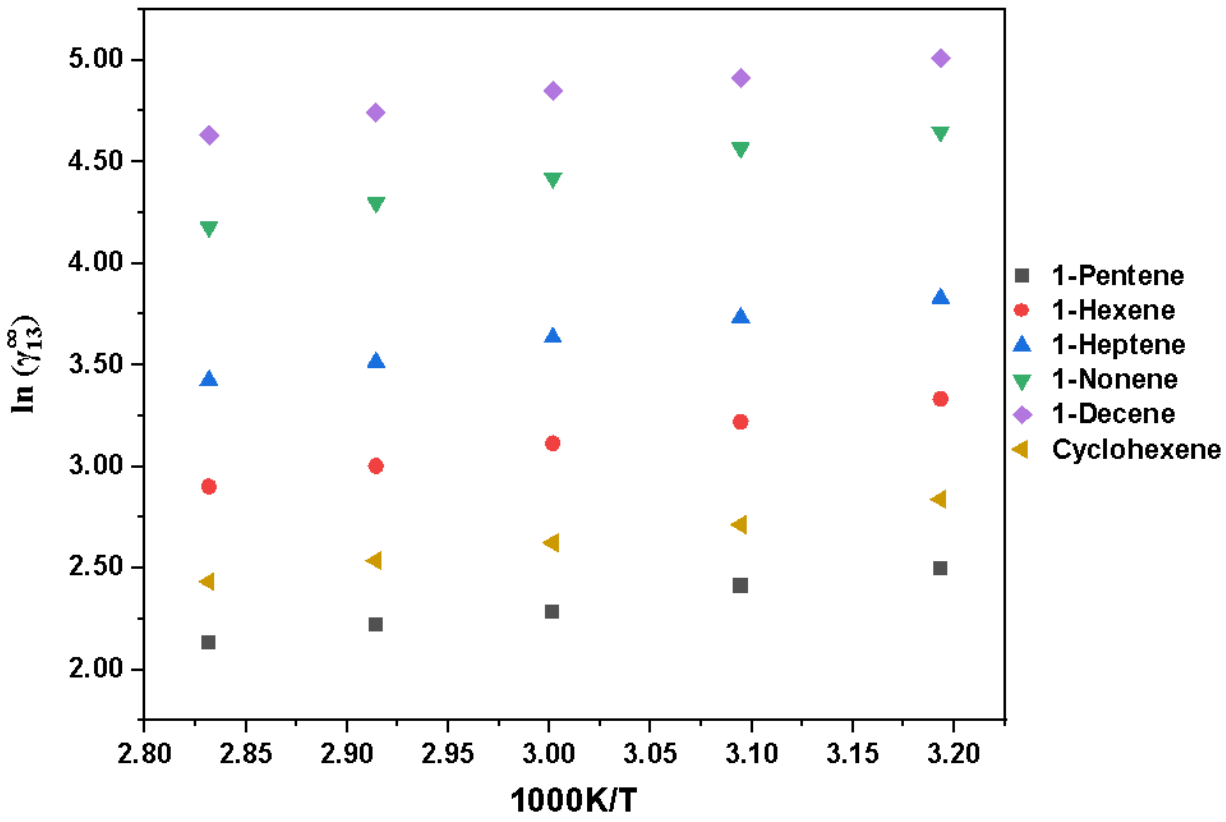

Figure 5.71: Graph of $\ln\gamma_{13}^{\infty}$ against 1000/T (K^{-1}) for alkenes in deep eutectic solvent ([TBN] AcO: DEG) at $\boldsymbol{T}$ = (313.15 – 343.15) K.

The graph of $\ln\gamma_{13}^{\infty}$ against 1000/T (K^{-1}) for alkynes in deep eutectic solvent ([TBN] AcO: DEG) at $\boldsymbol{T}$ = (313.15 – 343.15) K is given in Figure 5.72.

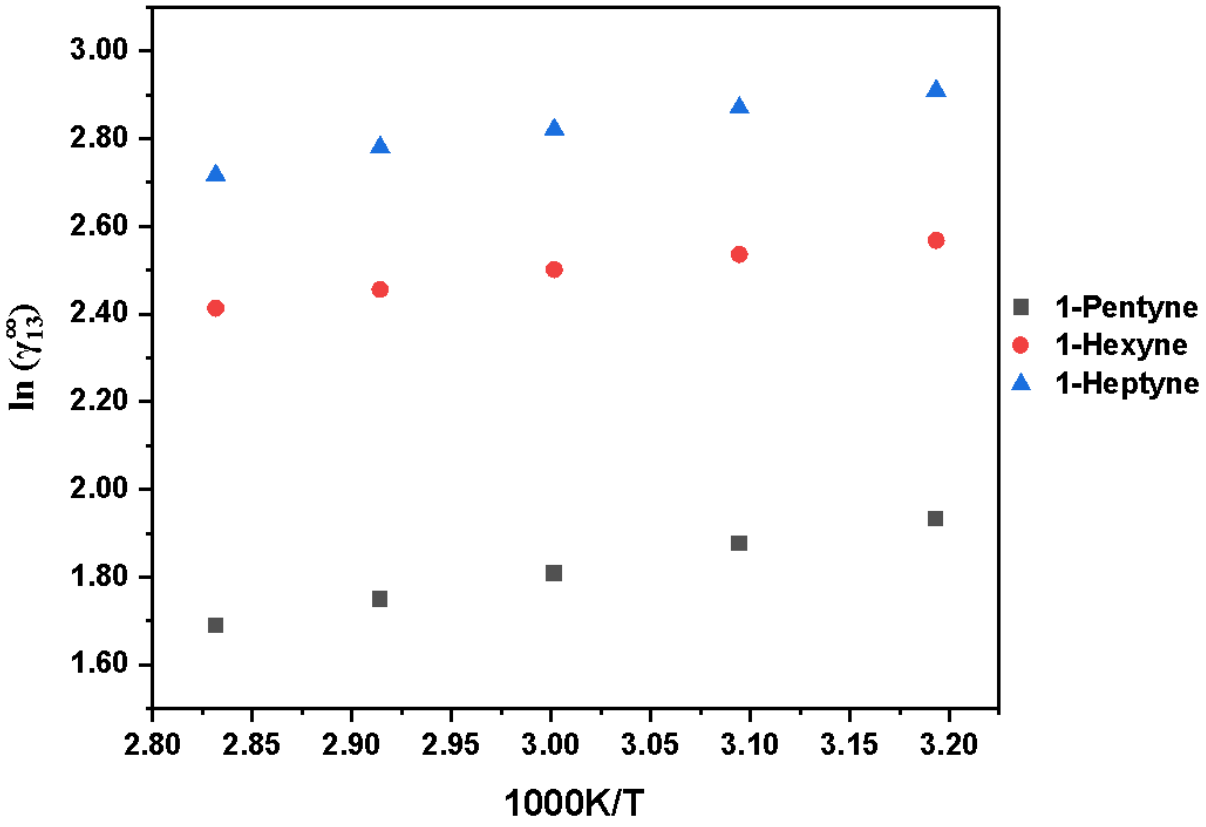

Figure 5.72: Graph of $\ln\gamma_{13}^{\infty}$ against 1000/T (K^{-1}) for alkynes in deep eutectic solvent ([TBN] AcO: DEG) at $\boldsymbol{T}$ = (313.15 – 343.15) K.

Figure 5.73 is the graph of $\ln\gamma_{13}^{\infty}$ against 1000/T (K^{-1}) for aromatic hydrocarbons in deep eutectic solvent ([TBN] AcO: DEG) at $\boldsymbol{T}$ = (313.15 – 343.15) K.

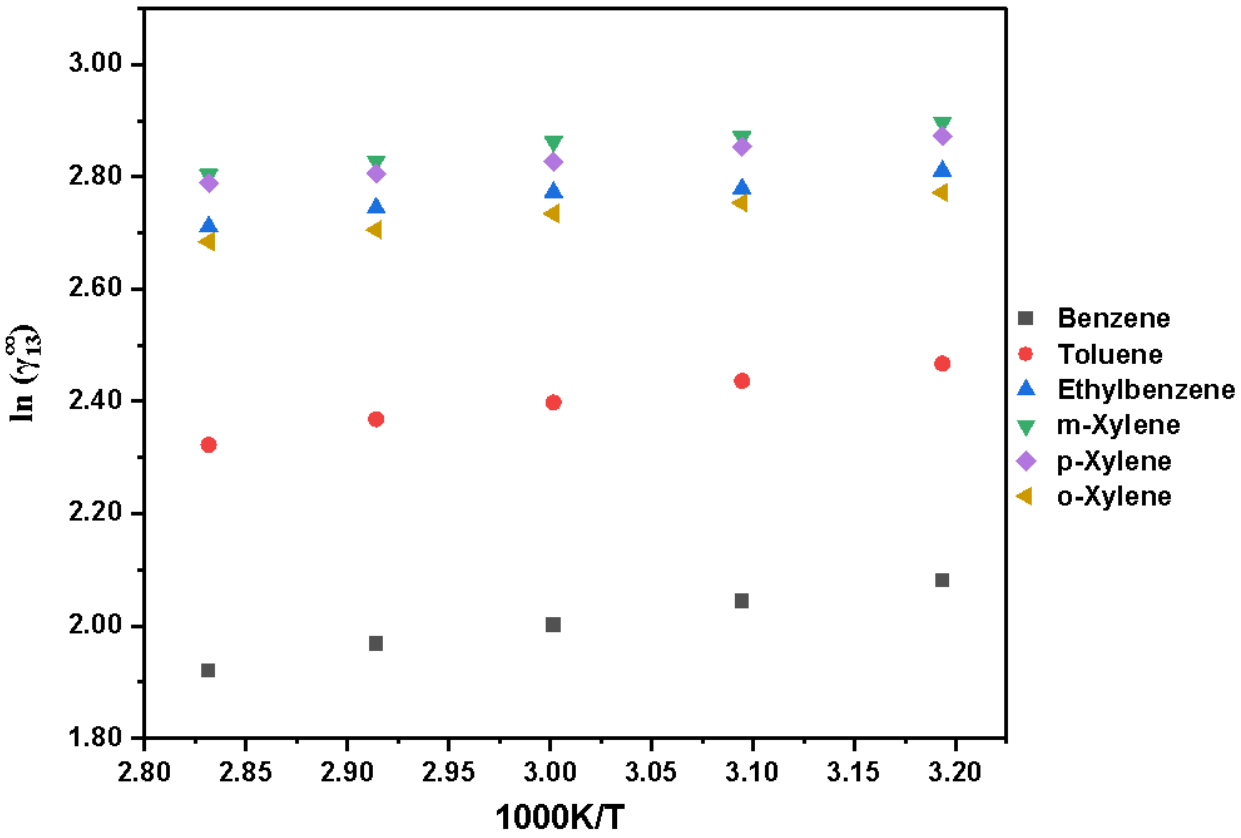

Figure 5.73: Graph of $\ln\gamma_{13}^{\infty}$ against 1000/T (K^{-1}) for aromatic hydrocarbons in deep eutectic solvent ([TBN] AcO: DEG) at $\boldsymbol{T}$ = (313.15 – 343.15) K.

The graph of $\ln\gamma_{13}^{\infty}$ against 1000/T (K^{-1}) for alcohols in deep eutectic solvent ([TBN] AcO: DEG) at $\boldsymbol{T}$ = (313.15 – 343.15) K is given in Figure 5.74.

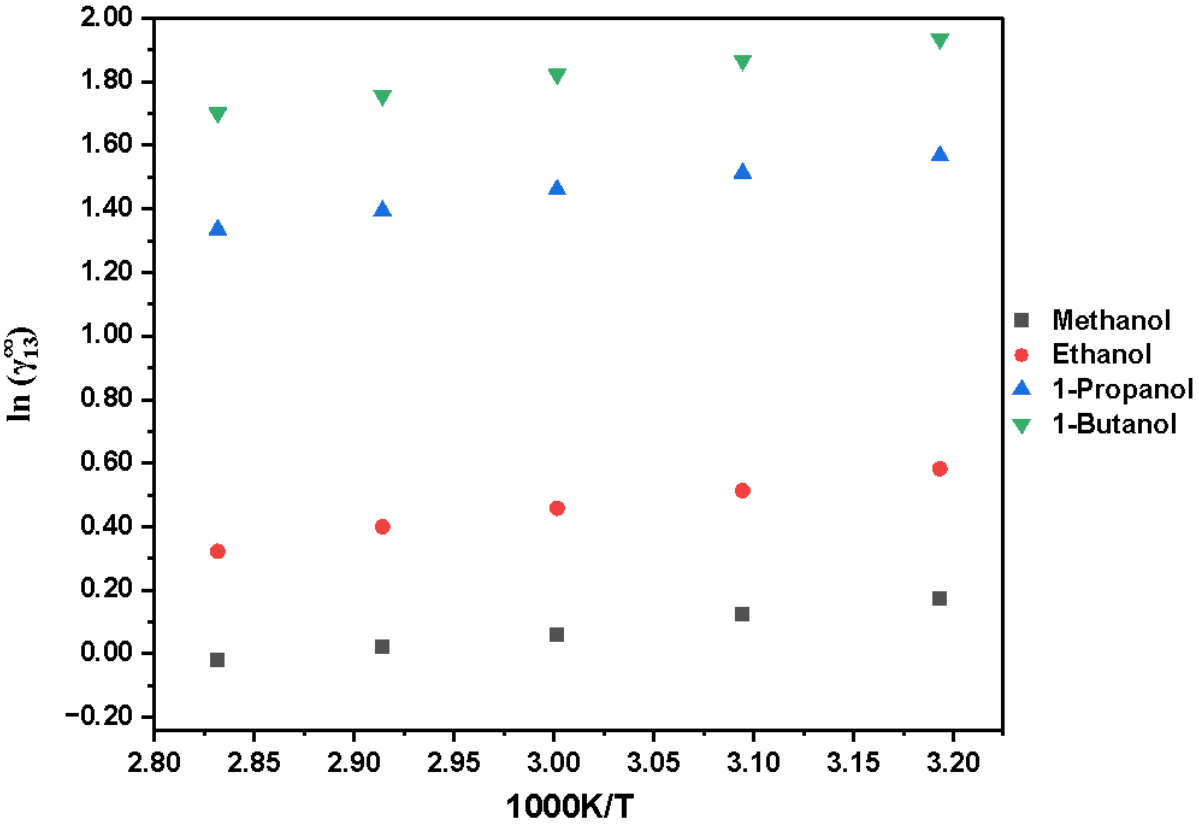

Figure 5.74: Graph of $\ln\gamma_{13}^{\infty}$ against 1000/T (K^{-1}) for alcohols in deep eutectic solvent ([TBN] AcO: DEG) at $\boldsymbol{T}$ = (313.15 – 343.15) K.

The graph of $\ln\gamma_{13}^{\infty}$ against 1000/T (K^{-1}) for ketones in deep eutectic solvent ([TBN] AcO: DEG) at $\boldsymbol{T}$ = (313.15 – 343.15) K is given in Figure 5.75.

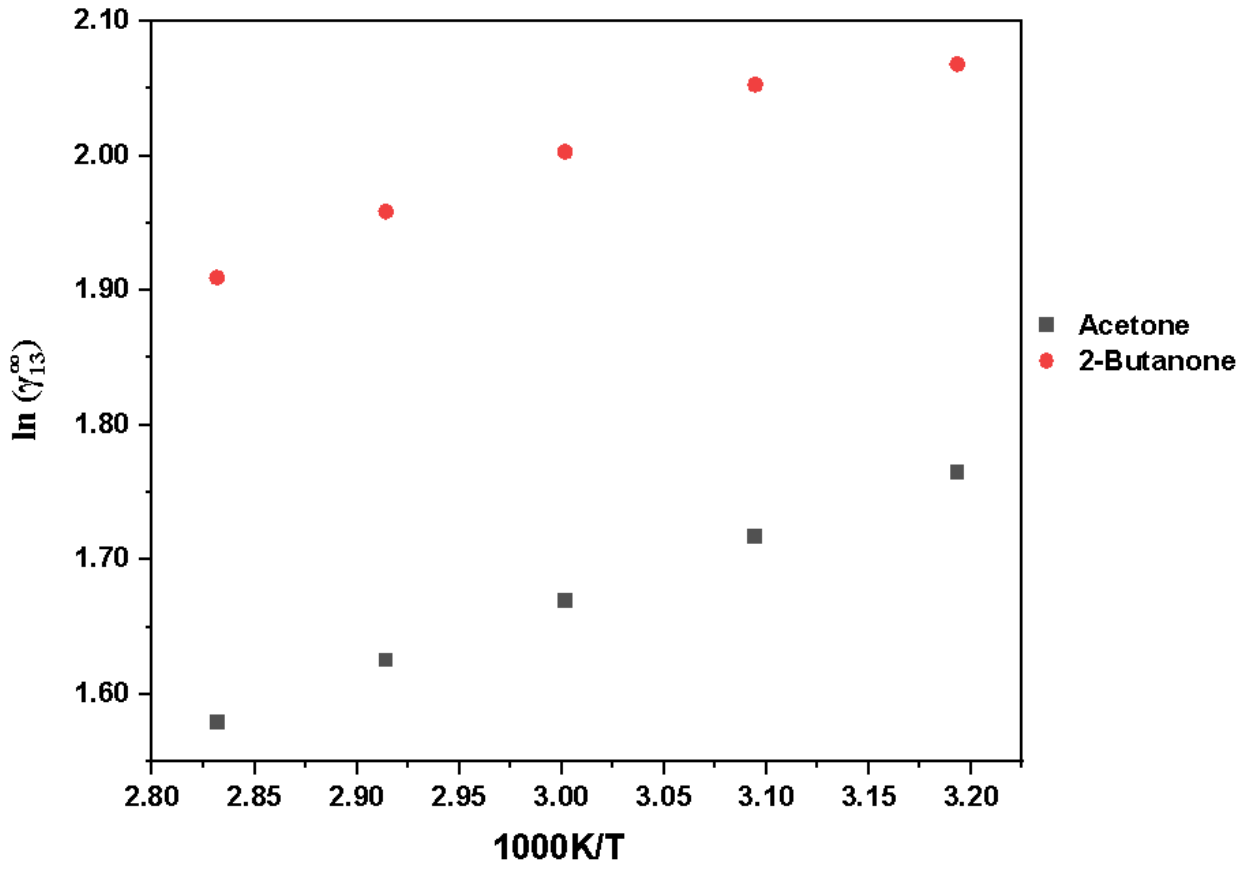

Figure 5.75: Graph of $\ln\gamma_{13}^{\infty}$ against 1000/T (K^{-1}) for ketones in deep eutectic solvent ([TBN] AcO: DEG) at $\boldsymbol{T}$ = (313.15 – 343.15) K.

Figure 5.76 is the graph of $\ln\gamma_{13}^{\infty}$ against 1000/T (K^{-1}) for THF, acetonitrile and thiophene in deep eutectic solvent ([TBN] AcO: DEG) at T = (313.15 – 343.15) K.

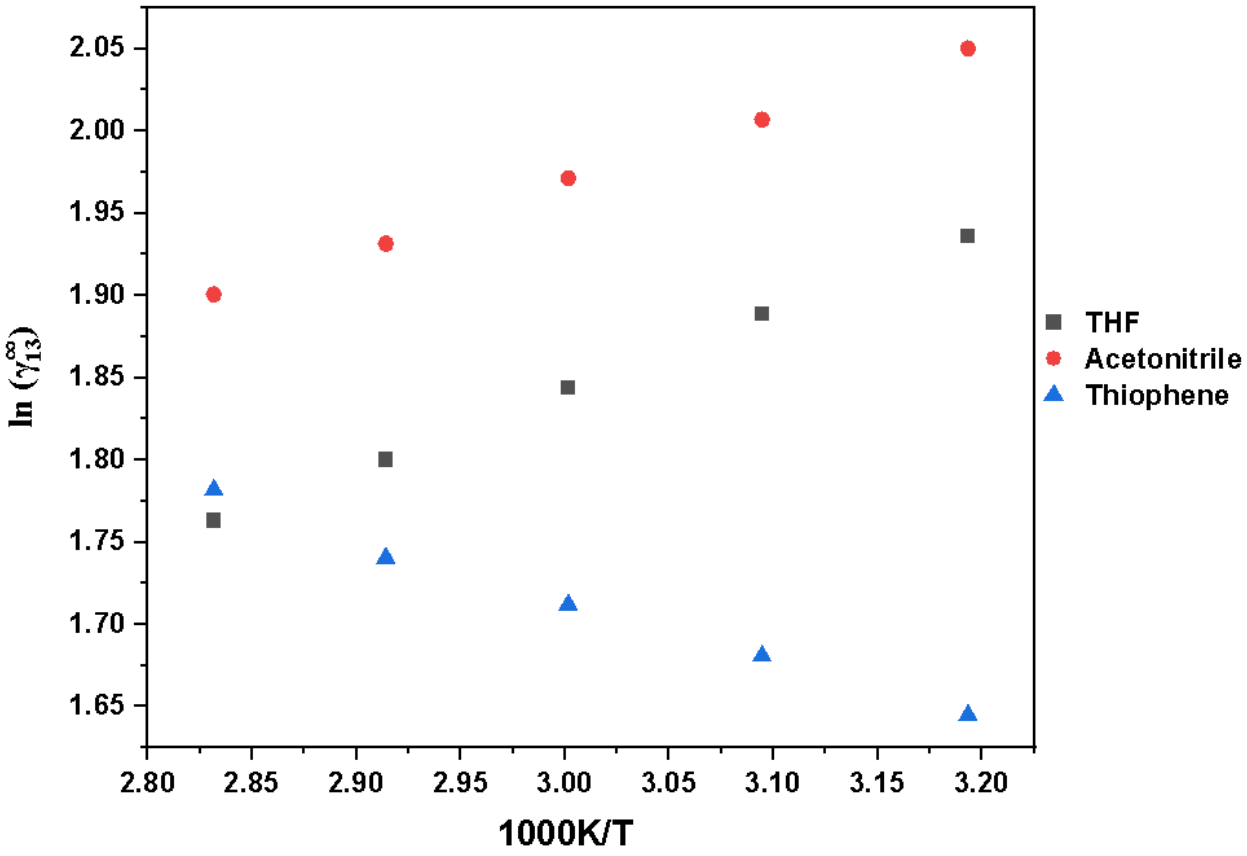

Figure 5.76: Graph of $\ln\gamma_{13}^{\infty}$ against 1000/T (K^{-1}) for THF, acetonitrile and thiophene in deep eutectic solvent ([TBN] AcO: DEG) at T = (313.15 – 343.15) K.

The results of comparison of selectivities (S_{ij}^{∞}) and capacities (k_j^{∞}) at infinite dilution for the investigated entrainers with other solvents for various separation problems at T = 313.15K is given in Table 5.24.

Table 5-24: Comparison of selectivities (S_{ij}^{∞}) and capacities (k_j^{∞}) at infinite dilution for the investigated entrainers with other solvents for various separation problems at T = 313.15K

Solvent	S_{ij}^{∞}				k_j^{∞}		**Ref.**
	heptane/ ethanol	**hexane/ ethanol**	**acetone/ ethanol**	**THF/ methanol**	**ethanol**	**methanol**	
[TBA] AcO: EG–1:3	17.70	10.08	1.930	4.460	0.280	0.440	This work
[TBA] AcO: DEG -1:3	42.22	26.31	4.230	5.820	0.720	1.020	This work
[EMIM Cl_4Al] [DEG] 1.000:4.001	219.4	125.5	4.410	8.640	3.740	5.180	*m*
[$ZnCl_2$ + acetic acid] 1:4	265.2	177.5	5.562	0.145	1.560	1.820	*n*
[$ZnCl_2$ + Phosphoric acid] 1:2.5	449.2	335.3	48.09	24.10	3.960	5.000	*n*
[4C_3N Br + Hdiol]	67.93	69.36	3.320	--	0.310	--	*o*
[HMIM][Cl]	372.3	332.2	8.614	27.10	3.680	6.850	*p*
[BMPYR][DCA]	148.4	--	1.701	3.980	1.870	2.980	*q*
[Choline chloride +1,5-pentanediol 1:3.998	154.7	121.7	4.770	93.80	0.4500	0.8300	*r*
[C_3MPYR][SLC]	1024.9	663.9	21.62	54.90	4.150	5.180	*s*

(de P Soares *et al.* 2023)[m], (Mgxadeni *et al.* 2022)[n],(Nkosi *et al.* 2018)[o], (Iwai and Seki, 2019)[p], (Durski *et al.* 2018)[q], (Li and wang, 2022)[r], Arumugam *et al.* 2022)[s].

CHAPTER 6

DISCUSSION

6.1 Physicochemical properties

Physicochemical properties measured in this study including density, (ρ), speed of sound, (u), and refractive indices, (n), and the computed thermodynamic properties such as excess molar volume, (V_m^{E}), isentropic compressibility, (k_s) deviation isentropic compressibility, (Δk_s) deviation refractive indices, (Δn), and intermolecular free length, (L_f), can be interpreted in terms of the intermolecular interactions occurring in the binary mixtures. The imidazolium based binary mixtures studied are as follows:

- ([1-butyl-3-methylimidazolium chloride: ethylene glycol] + methanol), ([BMIM]Cl: EG + methanol).
- ([1-butyl-3-methylimidazolium chloride: ethylene glycol] + ethanol), ([BMIM]Cl: EG + ethanol).
- ([1-butyl-2,3-dimethylimidazolium chloride: ethylene glycol] + acetic acid), ([BDMIM]Cl: EG + acetic acid).
- ([1-butyl-2,3-dimethylimidazolium chloride: ethylene glycol] + propanoic acid), ([BDMIM]Cl: EG + propanoic acid).

The temperature conditions for measured physicochemical properties for binary mixtures were over the range temperature of T = (293.15, 298.15, 303.15, 308.15, and 313.15) K and the mole fraction range x_1 = (0 – 1) for all systems in this study. The physical properties are not isolated, they co-vary in ways that reflect the underlying strength, nature, and geometry of intermolecular forces.

6.1.1 Density

The measured densities of the binary mixtures, ([BMIM]Cl: EG + methanol), ([BMIM]Cl: EG + ethanol]), ([BDMIM]Cl: EG + acetic acid), and ([BDMIM]Cl: EG + propanoic acid) given in Tables (5.1 and 5.6), and Figures (5.1, 5.2, 5.21, and 5.22) indicates the density being directly proportional with mole fraction of the DES in the binary mixtures and inversely proportional with temperature, at elevated temperatures,

density decreases as a result weakened intermolecular interaction. Additionally, molecular rearrangements occur due to the vibrations of anionic and cationic components of the DES. High density of the mixtures affects the speed of sound due to thickness of the medium. The latter effect is more paramount for the {[BDMIM]Cl: EG + acetic acid or propanoic acid binary mixture. Tables (5.1 and 5.6) shows low density values of ([BMIM]Cl: EG) + methanol or ethanol compared to ([BDMIM]Cl: EG) + acetic acid or propanoic acid across the temperature range. This can be attributed to variations in hydrogen bond strength, van der Waals interactions, and the molecular size and shape of the solvents.

The binary mixtures comprising ([BDMIM]Cl: EG) with either acetic acid or propanoic acid demonstrate enhanced hydrogen bonding and superior packing efficiency, as evidenced by their elevated density values.

Density measurements across mixtures such as ([BMIM]Cl: EG + methanol), ([BMIM]Cl: EG + ethanol), ([BDMIM]Cl: EG + acetic acid), and ([BDMIM]Cl: EG + propanoic acid) reveal consistent trends with respect to both composition and temperature. These patterns reflect the underlying molecular interactions and structural ordering within the systems, and they interplay with other properties including speed of sound, excess molar volume, isentropic compressibility, and intermolecular free length.

Increasing density correlates positively with speed of sound, indicating that denser media propagate sound more efficiently due to tighter molecular packing.

Higher density corresponds to lower isentropic compressibility, showing a negative correlation that signifies stronger intermolecular cohesion and reduced volumetric responsiveness.

As density increases, excess molar volume decreases, revealing a negative correlation that reflects non-ideal mixing and improved packing efficiency.

Temperature elevation leads to reduced density, consistent with a negative correlation that suggests thermal agitation disrupts molecular interactions and lowers packing efficiency.

These interlinked trends reinforce the role of density as a central descriptor of molecular organization, influencing both acoustic and volumetric behaviour.

Understanding the co-variation between density and compressibility is valuable when designing solvent systems for applications that require specific mechanical or acoustic properties. Mixtures exhibiting high density and low compressibility are particularly suited for separation and reaction media where molecular rigidity enhances performance and selectivity.

The observed correlations lend support to predictive frameworks such as Redlich-Kister formulations and validate assumptions concerning non-ideal behaviour and molecular association within complex solvent systems.

6.1.2 Speed of sound

The speed of sound is a useful parameter to determine intermolecular interactions between liquid mixtures which include the solvent-solvent, solvent-solute, and solute-solute interactions. The results are presented in Tables (5.1 and 5.6), and Figures (5.3, 5.4, 5.23, and 5.24). The speed of sound decreases with increasing temperature and increase with increasing mole fraction of the DES in the binary mixture. The speed of sound for ([BMIM]Cl: EG + methanol) is less than ([BMIM]Cl: EG + ethanol) mixture at the same temperatures. Due to the stronger hydrogen bonding and smaller molecular size of methanol, with -3% - 4.7% deviation at 0.000 mole fraction this attribute to the solution becoming more compact and less compressible, which results in lower speed of sound compared to the ([BMIM]Cl: EG) + ethanol. At intermediate mole fractions ($x_1 \approx 0.1050–0.3050$), methanol systems show higher sound velocities, with deviations peaking around +6.25% at 303.15 K. This suggests that the DES-methanol interactions dominate, enhancing molecular rigidity.

An increase in the speed of sound is associated with a decrease in isentropic compressibility, reflecting a negative correlation that signifies stronger molecular cohesion. Similarly, higher sound velocity corresponds to shorter intermolecular free length, indicating tighter molecular packing. These relationships underscore the utility of speed of sound as an indirect measure of molecular rigidity and interaction scale. Systems characterized by high density and low compressibility typically exhibit

elevated sound velocities, pointing to more structured and cohesive molecular arrangements.

Speed of sound metrics offer valuable guidance for selecting solvents in applications that demand specific acoustic or mechanical properties. Systems with higher sound velocity may be particularly advantageous for ultrasonic-assisted separations or reaction media where enhanced rigidity improves selectivity.

The observed trends lend support to theoretical models such as Nomoto's relation, acoustic impedance equations, and Free Length Theory, while also validating core assumptions related to non-ideal behaviour and molecular association in complex solvent systems.

6.1.3 Refractive index

This refractive index parameter is important as it relates to the speed of and light travelling within the liquid system. Tables (5.1 and 5.6), and Figures (5.5, 5.6, 5.25, and 5.26) shows influence of temperature and mole fraction of DES in the binary system. It is evident that the values decrease with increasing temperature. This shown that at elevated temperatures the molecules acquire enough energy and the light travels freely within the medium. ([BMIM]Cl: EG) + methanol or ethanol has high refractive indices compared to ([BDMIM]Cl: EG) + acetic acid or propanoic acid through the entire range of temperature. The stronger hydrogen bonding, higher van der Waals forces, smaller molecular size, and higher polarizability of methanol and ethanol contribute to the higher refractive indices of ([BMIM]Cl: EG) + methanol or ethanol solutions compared to ([BDMIM]Cl: EG) + acetic acid or propanoic acid.

In liquid systems, the refractive index is governed by molecular polarizability, density, and intermolecular interactions. Denser media typically exhibit higher refractive indices due to tighter molecular packing and enhanced polarizability, demonstrating a positive correlation between refractive index and density. Likewise, increasingly negative excess molar volume values indicate more efficient packing, which also aligns with higher refractive indices, reinforcing the positive relationship. These trends suggest that refractive index serves as a valuable proxy for evaluating molecular cohesion and structural compactness within solvents.

High refractive index systems are particularly relevant for applications involving optical sensing, photonic technologies, and formulations where light matter interactions are critical. Understanding how refractive index co-varies with properties such as density and isentropic compressibility supports solvent selection for separation processes, reaction media, and formulation strategies in process optimization. These correlations further validate the applicability of theoretical mixing models such as the Lorentz–Lorenz and Weiner approaches and justify foundational assumptions in predictive frameworks for both optical and thermodynamic behaviour.

6.2 Thermodynamic excess properties

6.2.1 Excess molar volumes

For excess molar volumes, Tables (5.2 and 5.7) was calculated using Equation (3.4) (Walas 1985, McGlashan 1979 and Letcher 1975). The values for the excess molar volumes, V_m^{E} are for the pure and the binary systems calculated over the temperature range of T = (293.15-313.15) K with the mole fraction range ($x_1 = 0$ - 1). The V_m^{E} data in Tables (5.2 and 5.7) indicates that the studied DESs ([BMIM]Cl: EG and ([BDMIM]Cl: EG]) have a strong ability to interact with methanol or ethanol and acetic acid and or propanoic acid respectively, which results from the hydrogen bonding and dipolar interactions (Singh and Bahadur, 2015).

The negative values of computed V_m^{E} values of the binary systems ([BMIM]Cl: EG + methanol), ([BMIM]Cl: EG + ethanol), ([BDMIM]Cl: EG + acetic acid) and ([BDMIM]Cl: EG + propanoic acid) indicates a stronger packing and attractive interaction between ($[BMIM]^+$ $[Cl]^-$ + methanol), ($[BMIM]^+$ $[Cl]^-$ + ethanol), ($[BDMIM]^+[Cl]^-$ + acetic acid), and ($[BDMIM]^+[Cl]^-$ + propanoic acid) leading to a reduction in volume. Other contributing factors to the negative values of V_m^{E} results from the unlike molecular interactions due to van de Waals or dispersion forces. Methanol, ethanol, acetic acid and propanoic acid are polar solvents, and the molecules are held together by hydrogen bonds. The anions (Cl^-) of [BMIM]Cl and [BDMIM]Cl exhibit close packing around the cation $[BMIM]^+$ and $[BDMIM]^+$ at all mole fractions, the molecule of methanol, ethanol, acetic acid or propanoic acid can form hydrogen bonds with the cations. Stronger interactions occurred between the DESs + methanol compared to ethanol as well as in DES + acetic acid compared to propanoic acid. This is due to the fact that the degree of

polarity changes with the number of carbons which results in weak intermolecular interactions and or packing effects.

The influence of temperature is also observed as the excess molar volumes decreases with increase in temperature revealing that at higher temperatures, the molecules of DES form H bond with the molecules of methanol, or ethanol, or acetic acid, or propanoic acid in voids. Figures (5.7, 5.8, 5.27, and 5.28), illustrates that across the entire range of mole fraction in this study, the V_m^{E}, minimum is observed from (-1.7423 to -2.0376) $cm^3 \cdot mol^{-1}$ for ([BMIM]Cl: EG + methanol), (-1.1696 to -1.3493) $cm^3 \cdot mol^{-1}$ for ([BDMIM]Cl: EG + ethanol), (-1.2714 to -1.4643) $cm^3 \cdot mol^{-1}$ for ([BDMIM]Cl: EG + acetic acid), (-1.7301 to 1.9720) $cm^3 \cdot mol^{-1}$ for ([BDMIM]Cl: EG + propanoic acid) and observed at x_1 = (0.2034 or 0.244) for ([BMIM]Cl: EG + methanol), and ([BDMIM]Cl: EG + ethanol) respectively and (0.2045 and 2.047) for ([BMIM]Cl: EG + acetic acid) and ([BDMIM]Cl: EG + propanoic acid, respectively.

As the excess molar volume provides a direct measure of deviation from ideal mixing behaviour, reflecting the net effect of intermolecular forces, molecular size, and packing efficiency. Shorter interactions reduce compressibility, leading to more negative excess molar volume. The larger excess molar volume aligns with greater free length, indicating nonideal mixing and weaker interactions showing the positive correlation of intermolecular free length and excess molar volume. These correlations suggest that excess molar volume serves as a central integrative parameter, linking volumetric, and optical behaviour to molecular-level interactions.

Excess molar volume trends assist in identifying mixtures with optimal packing and interaction profiles for separation, extraction, or reaction media. The systems with high negative excess molar volume may offer enhanced selectivity and stability under varying thermal conditions. These support the use of Redlich-Kister and other excess property models, and justify assumptions about non-ideality and molecular association

6.2.2 Isentropic and deviation isentropic compressibilities

Isentropic compressibilities was determined by Newton-Laplace Equation (3.6). Tables (5.2 and 5.6) data shows that the isentropic compressibilities increase with temperature and decreases with mole fraction of the binary mixtures. The values of

isentropic compressibilities are positive due to the stronger interaction between ([BMIM]Cl: EG) + methanol or ethanol and ([BDMIM]Cl: EG) + acetic acid or propanoic acid making the binary mixture more compressible than the ideal mixture. The deviation isentropic compressibilities was calculated using Equation (3.7) showing the negative values of Δk_s in Tables (5.2 and 5.7). This indicates that the binary mixtures are less compressible than pure components.

Isentropic compressibility describes a liquid's resistance to volume changes under adiabatic conditions and is strongly influenced by intermolecular interactions, packing efficiency, and structural rigidity. Higher compressibility values indicate longer intermolecular free lengths, suggesting a more loosely packed molecular arrangement. This positive correlation underscores isentropic compressibility as a key indicator of interaction strength and molecular rigidity.

Systems exhibiting low isentropic compressibility are well-suited for applications requiring structurally rigid media, such as ultrasonic-assisted separation or high-pressure reaction environments. Mapping compressibility trends supports solvent selection for processes sensitive to mechanical and thermal perturbations.

These findings offer validation for predictive models, including the Newton-Laplace and Redlich-Kister formulations, and reinforce assumptions related to mixture non-ideality and molecular association.

6.2.3 Intermolecular free length

Intermolecular free length was computed using Equation (3.7) and the intermolecular free length calculated for binary systems ([BMIM]Cl: EG + methanol or ethanol) and ([BDMIM]Cl: EG + acetic acid or propanoic acid) are shown in Tables (5.2 and 5.7) over the temperature range and the entire mole fraction range. The plots are given in Figures (5.9, 5.10, 5.29, and 5.30). The attractive forces between the molecules are dependent on the on the distance between their centres whereas the distance between the surface of the molecules is reflective of repulsive forces. Speed of sound variations in the liquids plays a critical role in examining the intermolecular free length. There’s clear evidence that the speed of sound and intermolecular free length are inversely related from Tables (5.1 and 5.2) and Figures (5.3, 5.4, 5.9, and 5.10) for

([BMIM]Cl: EG + methanol and or ethanol) and Tables (5.6 and 5.7) and Figures (5.23,5.24, 5.29, and 5.30) for ([BDMIM]CL:EG + acetic acid or propanoic acid). Intermolecular free length decreases with increasing mole fraction and increases with increasing temperature. Elevated temperatures increase the intermolecular free length by weakening the intermolecular interactions leading to a decrease of hydrogen bonds and van der Waals forces. This implies that the distance between the surface increases with temperature.

Intermolecular free length represents the average spatial separation between the surfaces of neighbouring molecules within a liquid system. It is influenced by both attractive forces such as hydrogen bonding and dipolar interactions and repulsive forces, including steric hindrance and thermal agitation. In the binary mixtures examined, this parameter serves as a sensitive indicator of molecular packing density, interaction strength, and thermal responsiveness.

The observed correlations underscore the importance of intermolecular free length as a key structural descriptor that connects molecular-level interactions to bulk acoustic, volumetric, and thermodynamic behaviour. Its trends enable the identification of mixtures with optimal packing efficiency and rigidity, relevant to separation processes, extraction methods, and reactive media design. Systems exhibiting lower intermolecular free length may demonstrate superior selectivity and thermal stability.

These findings lend support to predictive frameworks such as Jacobson’s free length theory and Schaaff’s collision factor model and help justify assumptions regarding mixture non-ideality and molecular association.

6.2.4 Deviation in refractive indices

The change in refractive indices are positive for all the binary mixtures under investigation ([BMIM]Cl: EG + methanol or ethanol) and ([BDMIM]Cl: EG + acetic acid or propanoic acid) at all temperature range are shown in Tables (5.2 and 5.7) and Figures (5.15, 5.16, 5.35, and 5.36). This shows the strong molecular interactions on the binary mixtures such as hydrogen bonding and the formation of dipole-dipole interaction between the dissimilar components. The refractive indices are inversely proportional to the temperature, this shows that at higher temperatures, the molecules

are able to move faster and become less dense and viscous causing the light to travel faster in the system. Negative deviation simply indicates weak interactions between the components.

6.3 Lorentz-Lorenz correlations

6.3.1 Correlation of excess molar volume by Lorentz-Lorenz equation

The Lorentz-Lorenz approximation was used for correlation of the excess molar volume, V_m^{E}, for all the binary mixtures under investigation using Equations (3.12, 3.13, 3.14, 3.15, and 3.16). Tables (5.3 and 5.8), shows the experimental and the computed data not in good agreement, that is observed in the (root mean square deviation, σ, obtained for the Lorentz-Lorenz approximation for the excess molar volumes at a temperature range T = (293.15 to 313.15) K computed in Tables (5.5 and 5.10) for ([BMIM]Cl: EG + methanol or ethanol) and ([BDMIM]Cl: EG + acetic acid or propanoic acid) is too high meaning that it is not accurate, the values predicated are too far from the experimental values.

These findings indicate that while the Lorentz–Lorenz approximation is effective for estimating optical properties, it falls short in capturing the intricate volumetric behaviour of deep eutectic solvent (DES)–based mixtures. The poor correlation arises from multiple factors that disrupt the model's assumptions of ideality: (i) the presumption of linear molar fraction additivity fails in systems dominated by strong specific interactions, such as hydrogen bonding and ion–dipole forces; (ii) structural heterogeneity manifested as microphase domains and dynamic hydrogen-bond networks introduces nonlinear volumetric contributions not addressed by the model; and (iii) temperature-dependent variations in molecular packing and interaction strength further confound predictions, yet are not incorporated. These limitations underscore the necessity of more robust frameworks, such as the Redlich–Kister approach, which accommodates both non-ideal mixing and thermal effects. Accurate estimation of excess molar volume is pivotal for solvent screening, formulation optimization, and process design in DES-centric applications. Ultimately, the observed mismatch emphasizes the importance of experimental validation and cautions against the uncritical application of simplified theoretical models in structurally complex systems.

6.4 Predictions of densities and refractive indices.

The Lorentz-Lorenz equation was also used for predicting the densities, ρ, which are related to the refractive indices, n_D, using Equations (3.17 and 3.18) respectively. Table (5.4 and 5.9) for computed results shows the low root mean square deviation meaning that the predicted densities and refractive indices values are in good agreement with the experimental values for all the systems under the study and it is observed in Figures (5.17, 5.18, 5.37, and 5.38) for densities and Figures (5.19, 5.20, 5.39, and 5.40) for refractive indices. This also suggest that Lorentz-Lorenz is precise and definite for the prediction of densities and refractive indices.

The strong concordance observed affirms the robustness and reliability of the Lorentz–Lorenz model in systems where molecular interactions minimally disrupt the linear correlation between molar volume and polarizability. Its proven accuracy in predicting density and refractive index endorses its application in process monitoring, sensor calibration, and formulation development. Reliable estimation of these parameters facilitates precise control over optical clarity, rheological behaviour, and solvent compatibility in industrial contexts. These outcomes align with complementary findings such as excess molar volume, compressibility, and intermolecular free length and collectively reinforce a unified framework linking molecular architecture to macroscopic physical properties.

6.5 Simulation of binary interactions using DFT

6.5.1 Analysis of thermodynamic parameters

Using Gaussian DFT software and optimized structures from ChemDraw Table 5.12 results were obtained and Table 5.12 shows the optimization energy of the molecules. The DFT analysis of the DES formed from [BDMIM]Cl: EG at 1:3 mole ratio revealed significant stabilization, with an optimized energy of -1613.75 Hartree and dipole moment of 29.86 Debye. There is an indication of strong interactions between the components as indicated by the negative values in Table 5.12. Interaction of the DES with acetic acid resulted in a further decrease in energy to -1843.36 Hartree and a reduced dipole of 27.22 Debye, suggesting significant bonding that redistributed charge density. Similarly, the DES-propanoic acid interaction showed an optimization

energy of -1882.14 Hartree with a dipole moment of 28.15 Debye. While both acids interacted strongly with DES, acetic acid led to a more substantial change in electronic energy ($\Delta E_{O.E.}$ of -0.527 Hartree) compared to propanoic acid ($\Delta E_{O.E.}$ of -0.009 Hartree), indicating a slightly stronger interaction with propanoic acid. The changes in dipole moment suggest that the interactions were driven by hydrogen bonding, leading to a decrease in system polarity.

The larger shift in electronic energy observed for acetic acid suggests more substantial electronic reorganization, even though propanoic acid exhibits marginally greater overall stabilization.

The optimized geometries and electronic properties of the compounds were analyzed, focusing on the HOMO and LUMO contours (Figure 5.43). The HOMO of [BDMIM]Cl was primarily localized around the imidazolium ring, while LUMO, solutes are dispersed around the ring except the chloride ion. For ethylene glycol, the HOMO was spread across the molecule, and the LUMO was localized around the oxygen atoms. In acetic acid-DES the HOMO was concentrated around the imidazolium ring and acetate group, with the LUMO dispersed around the acetate group. Acetic acid and propanoic acid showed HOMO localization around the carboxyl group and LUMO dispersion around the molecules. The interactions of the DES with acetic acid and propanoic acid revealed significant changes in electronic properties, with the HOMO becoming more localized and the LUMO concentrated around the DES, indicating strong electron-donating interactions from the DES to the acids.

The orbital distributions confirm the role of the DES as an electron donor and the acids as electron acceptors, contributing to the formation of stable hydrogen-bonded complexes.

A decrease in dipole moment accompanied by a lower refractive index reveals a positive correlation, suggesting that reduced polarity is associated with diminished optical density.

A decline in optimization energy alongside reduced excess molar volume implies stronger intermolecular interactions that promote denser molecular packing.

A narrowing HOMO–LUMO gap correlated with decreased compressibility suggests enhanced electron delocalization contributes to increased structural rigidity.

Charge redistribution aligned with shortened intermolecular free length indicates a negative correlation, where stronger bonding interactions minimize molecular separation.

These correlations reinforce a unified interpretation: systems with intensified electronic interactions tend to be more compact, less compressible, and optically less polar mirroring observed trends in density, refractive index, and compressibility.

From a solvent design perspective, DFT insights enable rational selection of DES–acid combinations with tailored electronic and structural attributes for targeted applications. A deeper understanding of charge transfer dynamics and dipole modulation informs decisions across separation technologies, catalytic processes, and formulation strategies. The close agreement between DFT-based predictions and experimental results further strengthens confidence in quantum chemical methodologies as reliable tools for predictive modelling and solvent screening.

6.5.2 Physicochemical Descriptors analysis

The physicochemical descriptors for the DES-acetic acid and DES-propanoic acid systems were also calculated and analyzed (Table 5.13). The chemical potential (μ) values for DES- acetic acid (-0.170 Hartree) and DES-propanoic acid (-0.033 Hartree) indicated that these systems tend to donate electrons, similar to the individual DES. The electronegativity (χ) values for the DES-acetic acid (0.212 Hartree) and DES-propanoic acid (0.143 Hartree) were higher than those of the individual DES, suggesting an increased electro-accepting ability when the DES interacts with the acids. The hardness (η) values for DES-acetic (0.083 Hartree) and DES-propanoic acid (0.220 Hartree) were lower than those of the individual acids, indicating higher reactivity in the combined systems. The global electrophilicity index (ω) values for DES-acetic acid (24.052 Hartree) and DES-propanoic acid (9.056 Hartree) were significantly higher, suggesting that these systems behave as strong electrophiles.

The observed trends indicate that the DES–acetic acid system exhibits heightened reactivity and electronic polarization, consistent with experimentally verified stronger hydrogen bonding and more efficient molecular packing.

A decline in chemical potential and compressibility reveals a positive correlation, suggesting that electron-donating systems exhibit lower compressibility due to increased cohesive forces.

An increase in electronegativity paired with higher refractive index demonstrates a positive correlation, linking stronger electronegative character to enhanced polarization and greater optical density.

A reduction in hardness alongside decreased excess molar volume reflects a positive correlation, indicating that softer molecular environments facilitate denser packing and minimize volumetric expansion.

An elevated global electrophilicity index with shortened intermolecular free length reveals a negative correlation, implying that pronounced electrophilic character enhances packing density by reducing molecular spacing.

These correlations underscore the predictive power of electronic descriptors in interpreting macroscopic behaviour, strengthening the conceptual foundation of the study. Descriptor analysis facilitates the rational selection of DES acid systems based on tailored reactivity and interaction profiles crucial for solvent design and optimization. Systems characterized by high electrophilicity and low hardness may offer superior selectivity in catalytic processes, separation technologies, or advanced formulations.

The agreement between DFT-derived descriptors and experimental observations affirms the reliability of quantum chemical methodologies in predictive modelling and strategic solvent screening.

6.5.3 Natural Bonding Orbital analysis

Natural Bonding Orbital (NBO) analysis includes the breakdown of molecular orbitals into isolated orbitals corresponding to specific bonds, lone pairs, and other chemical groups. The E(2) energy, a vital parameter in NBO analysis, measures the second-order perturbation energy linked to the interactions between the donor and acceptor.

The calculation is performed using second-order perturbation theory within the NBO framework. Density Functional Theory is the fundamental computational approach for NBO computations. Higher E(2) values suggest a more robust connection between electrons from donors and acceptors. This indicates an increased movement of electrons from donors to acceptors, which enhances the level of conjugation within the system. The presence of a greater spread in electron density between occupied Lewis-type NBO orbital, such as bonds or Rydberg orbitals, indicates the strengthened donor-acceptor interaction (Briceño-Vargas and Quesadas-Rojas, 2023). Table 5.14 contains the E (2) values, donor NBO and acceptor NBO of a few significant interactions occurring in acetic acid-DES and propanoic acid-DES system.

The NBO analysis for both the DES-acetic acid and DES-propanoic acid systems revealed significant interactions, highlighting the electron donation from the lone pairs on oxygen and nitrogen atoms to the antibonding orbitals of the DES. Figure 5.44 shows various interactions occurring between the molecules along the bond distance. In the DES-acetic acid system, Figure 5.44 notable interactions LP (O46) donating BD* (C40 – H41) with an E2 value of 2.91 kcal·mol^{-1}, LP (O48) donating to BD* (C43 – H44) with an E2 value of 2.92 kcal·mol^{-1}, LP (O58) donating to BD* (C53 – H54) with an E2 value of 2.91 kcal·mol^{-1}, LP (O66) donating to BD* (C64 – H65) with an E2 of 2.62 kcal·mol^{-1}, and LP (O68) donating to BD* (C64 – O66) with an E2 value of 16.70 kcal·mol^{-1}.

In the DES-propanoic acid system, significant interactions included BD C1 – N5 donating to BD* N2 - C6 with an E2 value of 4.26 kcal·mol^{-1}, kcal·mol^{-1}, BD C1 – N5 donating to BD* C3 – C4 with an E2 value of 16.41 kcal·mol^{-1}, LP N2 donating to BD* C1 – N5 with an E2 value of 80.50 kcal·mol^{-1}, LP O38 donating BD* C33 – H34 with

an E2 value of 4.45 kcal·mol^{-1}, LP O46 donating to BD* C40 – H41 with an E2 value of 5.29 kcal·mol^{-1}, and LP O68 donating to BD* C67 – O70 with an E2 value of

51.30 kcal·mol^{-1}. These interactions indicated strong stabilization due to electron donation, with the highest stabilization energy observed for the interaction between LP N2 and BD* C1 – N5, suggesting the strongest interaction.

The second-order perturbation energy E(2) values derived from NBO analysis quantify the stabilization achieved through donor–acceptor interactions, particularly those involving lone pair LP to antibonding orbital BD* transitions. These electronic interactions manifest as electron delocalization, hydrogen bonding, and charge redistribution factors that critically influence the structural rigidity, molecular packing, and reactivity within DES acid systems.

Correlative trends between E(2) values and physicochemical properties reveal the following insights:

Elevated E(2) values and reduced excess molar volume exhibit a negative correlation, suggesting that stronger donor–acceptor interactions facilitate denser molecular packing.

Higher E(2) values paired with lower isentropic compressibility reflect enhanced electron delocalization, which reinforces structural rigidity and diminishes compressibility.

Increasing E(2) and declining intermolecular free length support a negative relationship, indicating that pronounced bonding interactions narrow molecular separation.

Elevated E(2) values and rising refractive index reveal a positive correlation, implying that orbital mixing boosts polarizability, thereby enhancing optical density.

Systems characterized by strong second-order perturbation energies tend to exhibit superior selectivity, robustness, and stability key attributes for applications in separation processes, catalytic frameworks, and advanced formulation strategies. Insight into donor–acceptor dynamics further enables informed decisions in ultrasonic-

assisted reactions, solvent compatibility screening, and molecular recognition design. The alignment between NBO-derived parameters and experimental behaviour underscores the utility of quantum chemical methods in predictive modelling and solvent optimization.

6.5.4 Non-Covalent Interactions analysis

The Non-Covalent Interactions (NCI) analysis for the DES, DES - acetic acid, and DES-propanoic acid systems provide a detailed insight into the nature of attractive and repulsive forces within these systems, as visualized through Reduced Density Gradient (RDG) scatter plot (Figure 5.45). In the DES system, The RDG scatter plot revealed several regions of non-covalent interactions, with peaks indicating both attractive forces, such as hydrogen bonds and van der Waals interactions (negative λ2 values), and repulsive forces, such as steric hindrance (positive λ2 values). For the DES-acetic acid system, the RDG scatter plot showed significant peaks corresponding to strong non-covalent interactions between the DES and acetic acid molecules, with attractive interactions enhancing the stability and reactivity of the complex. Similarly, the DES-propanoic acid system exhibited notable non-covalent interactions, with strong hydrogen and van der Waal forces contributing to its stability and reactivity.

The Reduced Density Gradient (RDG) scatter plots generated for the DES, DES–acetic acid, and DES–propanoic acid systems offer a nuanced visualization of non-covalent interaction (NCI) regions, clearly differentiating between attractive forces (e.g., hydrogen bonding, van der Waals interactions) and repulsive forces (e.g., steric hindrance). These interactions are determined by the sign of the second eigenvalue (λ_2) of the electron density Hessian matrix:

Negative λ_2 values denote attractive interactions, including dipole–dipole alignments and hydrogen bonding.

Positive λ_2 values indicate repulsive regions, often stemming from steric interference or overlapping electron clouds.

The following correlations were observed between RDG-derived interaction patterns and physicochemical properties:

Higher attractive RDG features with reduced excess molar volume reveal a negative correlation, suggesting stronger non-covalent interactions promote tighter molecular packing and decreased volumetric expansion.

Elevated steric repulsion coupled with increased isentropic compressibility shows a positive correlation, indicating that repulsive forces enhance molecular flexibility and compressibility.

Enhanced hydrogen bonding aligned with a rise in refractive index reflects a positive correlation, interpreting that stronger polar interactions improve polarizability and raise optical density.

Amplified dispersion forces linked to extended intermolecular free length present a positive correlation, implying weaker interactions allow greater molecular separation.

These correlations highlight how NCI profiles derived from RDG plots translate into quantifiable physicochemical behaviours, offering a coherent framework for assessing solvent performance. Such insights inform strategic decisions in solvent design, formulation, and functionality especially in contexts prioritizing tunable intermolecular forces and targeted molecular interactions.

6.5.5 Electron Localization Function analysis

The Electron Localization Function (ELF) analysis for the DES, DES-acetic acid, and DES-propanoic acid systems provided a detailed insight into the electron distribution and bonding characteristics within these systems. In the DES system, the ELF plots revealed regions of high electron localization around the nitrogen and oxygen atoms of the 1-butyl-2,3-dimethylimidazolium chloride and ethylene glycol components, indicating strong covalent bonding and areas of electron pairing, particularly around the imidazolium ring and the hydroxyl groups of ethylene glycol (Figure 5.46). For the DES-acetic acid system, the ELF analysis showed significant changes in electron localization due to the interaction with acetic acid. The ELF plots highlighted increased electron localization around the carboxyl group of acetic acid and the chloride ion of the DES, suggesting the formation of strong hydrogen bonds. Additionally, there was notable electron localization around the nitrogen atoms of the imidazolium ring,

indicating interactions that contributed to the overall stability of the complex. Similarly, the DES-propanoic acid system exhibited notable changes in electron localization, with high electron localization observed around the carboxyl group of propanoic acid and the chloride ion of the DES, indicating strong hydrogen bonding. Significant electron localization around the nitrogen atoms of the imidazolium ring and the hydroxyl groups of ethylene glycol suggested robust interactions that enhanced the stability and reactivity of the DES-propanoic acid complex.

The Electron Localization Function (ELF) profiles observed align closely with earlier findings derived from NBO analysis, DFT calculations, and physicochemical descriptors. These results reaffirm that acetic acid facilitates the formation of a more compact and electronically favourable complex, whereas propanoic acid introduces enhanced steric flexibility.

Elevated ELF intensity near donor atoms, coupled with a decline in excess molar volume, exhibits a negative correlation indicating that strong bonding interactions encourage tighter molecular packing and reduced volumetric expansion.

Increased ELF localization around Cl^- coincides with diminished isentropic compressibility, implying that electron-rich domains reinforce rigidity and suppress compressibility.

Enhanced electron density near carboxyl groups shows a positive correlation with refractive index, suggesting that localized electrons contribute to greater optical density.

ELF overlap with decreasing intermolecular free length reflects a negative correlation, pointing to the role of strong localized interactions in minimizing molecular separation.

These associations highlight how electron localization patterns govern physicochemical behaviour, presenting a unified framework for interpreting solvent structure–function relationships. ELF analysis thus emerges as a powerful tool for identifying molecular systems with favourable electron distribution profiles, supporting targeted reactivity, enhanced structural stability, and improved optical properties. The strong agreement between ELF-based bonding patterns and experimental trends

underscores the predictive utility of DFT methodologies in solvent screening and molecular design workflows.

6.5.6 Computational interrogation of interactions

6.5.6.1 Ideal conformation analysis

The ideal conformation to use for the interrogation of the DES [BMIM]Cl: EG complex, was chosen by searching for the lowest configuration from an optimisation workflow that evaluated the 6 configurations. The lowest energy conformation was further optimized in the presence of solvent and analysed in the presence and absence of implicit ethanol or methanol solvent where necessary. The energies of the conformations obtained from optimization of each of the 6 configurations were obtained and their energies relative to the lowest energy conformation were plotted, (Figure 5.47). The lowest energy configuration was from Config 6 (Table 5.17) which was the configuration that enabled coordination of the EG co-solvent with the Cl^- ion reporting distances of 2.13 and 2.22 Å between the EG hydroxyl H atoms and the Cl atom (Figure 5.47 C). After the MacroModel conformational search stage the conformations of Config 3 and Config 5 accessed unstable conformations with relative energies of 1,834 and 3,504 kcal/mol respectively and after the geometry optimisation stages they accessed final confirmations within 100 kcal/mol of Config 6. When interrogated further the least stable configuration, Config 3, maintained a distance of less than 1.9 Å between the Cl atom and the C atom of methyl group on the imidazolium ring while a distance of 2.72 and 6.28 Å were maintained between the EG hydroxyl H atoms (Figure 5.47 D). Although the position of the EG in the Config 4 starting conformation had the furthest distance from the Cl atom, after optimisation the hydroxyl H atoms had distances of 2.04 and 4.83 Å (Figure 5.47 E). The distance measurements, position, and conformation of EG in the lowest energy conformation of Config 6 satisfied the criteria for selection as the conformation for study in the absence of an experimental structure.

These geometries suggest that shorter EG–Cl^- distances and balanced hydroxyl positioning are critical for electrostatic stabilization and hydrogen bonding, which in turn influence macroscopic properties such as density, compressibility, and refractive index.

Increase EG–Cl^- Coordination and the decrease in excess molar volume shows a negative relationship interpretation of strong interactions reduce free volume. Increase in EG–Cl^- Coordination with decrease in isentropic compressibility shows a negative relationship interpreting tighter packing enhances rigidity. Increased in EG–Cl^- Coordination and increased refractive index shows a positive relationship interpreting the Increased polarizability from electron-rich zones. Increased EG–Cl^- Coordination and a decrease in intermolecular free length shows a negative relationship interpreting Strong bonding reduces intermolecular separation. These correlations reinforce the idea that ideal conformations are not merely energetically favourable, but also structurally predictive of solvent behaviour in real-world applications.

Config 6 offers a molecular blueprint for designing DESs with optimal coordination and packing efficiency. Understanding how conformational geometry influences interaction strength aids in selecting solvents for separation, catalysis, and formulation. The consistency between conformational energetics and experimental trends supports the use of MacroModel and DFT-based workflows in predictive modelling.

The geometries indicate that shorter EG–Cl^- distances and well-positioned hydroxyl groups play a crucial role in stabilizing electrostatic interactions and facilitating hydrogen bonding, thereby influencing bulk properties such as density, compressibility, and refractive index.

Increased EG–Cl^- coordination correlating with reduced excess molar volume suggests that stronger interactions result in diminished free volume.

A corresponding decline in isentropic compressibility points to enhanced molecular rigidity driven by tighter packing.

A rise in refractive index alongside EG–Cl^- coordination implies heightened polarizability, attributable to dense electron-rich regions.

Additionally, reduced intermolecular free length reflects compact structural organization due to stronger bonding.

These relationships underscore the structural relevance of ideal conformations, not just in terms of energetic favourability but also as predictors of solvent performance in applied contexts. Configuration 6, in particular, serves as a molecular blueprint for designing DESs with optimal coordination and efficient packing. Understanding how geometric features govern interaction strength provides a strategic basis for selecting solvents suited to separation, catalysis, and formulation workflows. The alignment between conformational attributes and experimental observables affirms the value of MacroModel and DFT-based methodologies in predictive solvent design.

6.5.6.2 Select distance analysis between the atoms

The select distances measured between the interacting species in the optimized [BMIM]Cl: EG complexes of the lowest energy conformation of Config 6 further optimized in the presence of solvent show a trend in the presence of solvent (Figure 5.48). The distance between the imidazolium ring H atom and the Cl^- ion of the system optimized in vacuum (2.21 Å) is shorter than in the ethanol (2.50 Å) or methanol (2.49 Å) solvent optimized systems. The distances between the EG hydroxyl H atoms and the Cl^- ion in the vacuum system (2.22 and 2.13 Å), the ethanol system (2.28 and 2.25 Å) and the methanol system (both 2.27 Å) follow the trend that the solvent optimized systems are stabilized further from the Cl^- ion. These observations show that the inclusion of the solvent field introduces dispersive forces on the Cl^- ion that affect the optimized structures as expected.

Selective distance analysis of the optimized [BMIM]Cl: EG complex (Configuration 6) reveals the impact of solvent environments—specifically ethanol and methanol—on spatial arrangements and interaction strengths between key atomic centres. The elongation of interatomic distances observed in solvent-optimized systems relative to vacuum optimization underscores the influence of dispersive and dielectric forces introduced by the solvent field.

A positive correlation between increased H–Cl^- distance and higher isentropic compressibility suggests that weakened electrostatic interactions lead to more compressible systems.

The same distance increase, paired with a less negative excess molar volume, indicates reduced packing efficiency due to solvent-driven separation.

A rise in intermolecular free length alongside increased H–Cl^- separation reflects looser structural organization and expanded molecular spacing.

Conversely, a negative correlation between H–Cl^- distance and refractive index implies diminished polarizability stemming from reduced electron density overlap.

These interrelations highlight how solvent-induced shifts in atomic distances can directly modulate bulk properties, offering molecular-level explanations for trends in density, compressibility, and optical behaviour. Understanding such modulations enables strategic design of DES systems with tailored interaction profiles. Notably, systems exhibiting shorter H–Cl^- distances may exhibit superior selectivity, rigidity, and thermal stability for separation and catalytic applications. The strong agreement between distance metrics and experimental data affirms the utility of implicit solvent models and geometry optimization frameworks in predictive solvent engineering.

6.5.6.3 Charge distribution analysis

The charge distribution calculations of the 3 optimized systems are complementary to the distance measurements observed in (Figure 5.49) and shed light on the influence of the Cl^- ion as well as the solvent effects in the interactions of the binary complexes. The partial charges show that the H atom of the imidazolium ring in the vacuo optimized system (Figure 5.49) is less charged (0.158 $e^-/\text{Å}^3$) than the corresponding atom in the ethanol and methanol solvent optimized systems (0.239 $e^-/\text{Å}^3$ and 0.236 $e^-/\text{Å}^3$) (Figure 5.48, B and C), while the Cl^- ion (-0.673 $e^-/\text{Å}^3$) is less charged than in the more stable solvent optimized systems (-0.856 $e^-/\text{Å}^3$and -0.857$e^-/\text{Å}^3$). Based on the inductive effect the partial charge of the H atom closest to the Cl^- ion (vacuo) is expected to be more positive than that which is further (solvent optimized), but this is not the case in our systems as the solvated systems with the Cl^- ions is more charged, exert a greater withdrawing effect reflected in the more positive partial charge on this H atom in the solvated systems. The partial charges of the Cl^- ion in the solvated systems experience a further stabilisation effect absent in the vacuo system which reduces their charge increasing their influence on the electron density of the

imidazolium ring. The partial charge on the N atom of the methylated imidazolium ring in the vacuo optimized system (0.239 $e^{-}/\text{Å}^{3}$) is thus lower than that of the corresponding atom in the ethanol (0.326 $e^{-}/\text{Å}^{3}$) and methanol (0.320 $e^{-}/\text{Å}^{3}$) optimized solvent system, even though the Cl^{-} is closer, consistent with the observations from the H atom of the ring closest to the Cl^{-} ion. The inductive effective on the imidazolium ring of these solvated systems is increased and thus the electron density on the N atom increased more than in the vacuo systems. The inclusion of solvent into the system serves to dissociate the Cl^{-} ion from the complex as observed from the distance measurements and is expected to reduce the impact of the electronegative group on the imidazolium ring ensuring that more of the charge is delocalized on the $[BMIM]^{+}$ cation. The polar solvents however are shown to stabilize the Cl^{-} ion affecting the charge distribution of the imidazolium ring that would be expected to dissociate the system. The partial charges of the oxygen atoms of EG in the vacuo system (-0.651$e^{-}/\text{Å}^{3}$) are less negative than those from the ethanol (-0.793 $e^{-}/\text{Å}^{3}$) and methanol (-0.788 $e^{-}/\text{Å}^{3}$) systems as the solvated systems are expected to have larger solvent shells which would contribute to a stabilizing of the bonding interaction reducing the impact of the negative Cl^{-} ion. The solvated systems are thus stabilized by more species than the unsolvated systems and these observations confirm the significance of electrostatic forces in mediating the interactions of DESs (Liu *et al.* 2008, Nkuku *et al.* 2007, Wypych *et al.* 2019).

Partial charge analysis of the [BMIM]Cl: EG complex, optimized across vacuum, ethanol, and methanol environments, highlights the role of solvent polarity and dielectric properties in modulating electrostatic interactions and electron density distribution. These variations are interconnected with changes in interatomic distances, bonding strength, and bulk thermophysical properties, including compressibility, refractive index, and excess molar volume.

An increase in Cl^{-} charge accompanied by reduced isentropic compressibility suggests a negative correlation, indicating that stronger electrostatic interactions decrease compressibility.

Enhanced H/N charge and elevated refractive index show a positive relationship, further supporting the notion that intensified electrostatics influence optical properties and compressibility.

A rise in O(EG) charge coupled with lower excess molar volume implies stronger bonding facilitates molecular packing and volume contraction.

Increased Cl^- cation separation and larger intermolecular free length reveal a positive trend, suggesting solvent-driven dissociation contributes to expanded molecular spacing.

Collectively, these correlations underscore charge distribution as a predictive descriptor for solvent behaviour, bridging molecular-scale interactions with macroscopic properties. This analysis aids in identifying systems with favourable electrostatic profiles for applications such as extraction and catalysis. Moreover, the alignment between charge variation trends and experimental data supports the use of DFT-based charge mapping as a robust tool in predictive modelling and solvent design.

6.5.6.4 Computed energy estimation of deep eutectic solvent

The computed $E_{inter(corr)}$ of the systems show a dependence on the solvent polarity for the stability of the DES complex and results are shown in Table 5.12. The vacuum optimised systems have a larger negative $E_{inter(corr)}$ (-34.79 kcal/mol) as expected due to the proximity of the Cl^- ion than the ethanol (-14.73 kcal/mol) and methanol (-15.86 kcal/mol) solvent optimized systems. As seen in the literature, the E_{inter} computed in vacuo is larger than those observed in the presence of solvent while those in the DES remain negative highlighting the thermodynamic favourability of this interaction, (Kabanda *et al.* 2022). Overall, the interactions between the EG co-solvent and the [BMIM]Cl are shown to be influenced largely by the polarity of the solvents and are likely due to by the anionic Cl^- ion. A combination of methanol's higher polarity, dielectric constant, smaller size which enables it to form more numerous hydrogen bonds, and a more stable solvent shell contribute to the stronger interactions and thus

improved solubility profile of the DES in methanol than in ethanol (Kiran Kumar *et al.* 2022). This treatment allows us to isolate the impact of the co-solvent in the DES ionic liquid as the methanol solvent interacting more strongly with the co-solvent as shown, stabilizes the E_{inter} observed in the treatments presented.

When the electronic properties of the complexes are considered by interrogating the HOMO/LUMO surfaces the ethanol and methanol solvated systems (-204.26 and 204.73 kcal/mol) have respectively negative smaller band gaps than the vacuo system (-165.77 kcal/mol) from Table 5.16. The electronic properties of the complexes are changed due to the presence of the solvent which leads to differential stabilization of the molecular orbitals and the high dielectric constant of the solvent results in polarisation of the complexes which result in the reduction of the band gap. From Figure 5.48 A, C, E, the HOMO surface of the complexes in the presence of solvent shows a shift to the Cl^- ion while in the vacuum system this is located largely on the ring. The stability of HOMO levels is largely driven by the stabilisation of the electronic states in the complex by the polar solvent. Further stabilisation of the band gap can be seen from the HOMO energy levels that experience a stabilising influence in the vacuum (-12.908 kcal/mol) which is less negative in the ethanol (-1.977 kcal/mol) and methanol systems (-1.970 kcal/mol). Although the LUMO surfaces of the solvent systems have nearly identical energies and iso-surface plots, the HOMO orbital in methanol experiences more stabilisation (-206.705 kcal/mol) than that in ethanol (-206.240 kcal/mol) and further to this its iso-surface on the ring appears more diffuse than in the ethanol system (Figure 5.48 B and C). By investigating the electronic properties of the complexes in the solvent it is possible to infer an additional influence on the stability of the complex in the different solvents. The stability of the complex in the solvent is not only driven by the Cl^- but as can be seen from the HOMO/LUMO interrogations, the impact of the polar solvent on the electronic distribution over the imidazolium ring contributes to the stability observed (Kiran Kumar *et al.* 2022). As expected, the methanol solvent polarises both the HOMO and LUMO surfaces decreasing the energy gap and together these changes contribute towards an increase in the band gap of the methanol systems when compared to the ethanol systems. These observations confirm the significance of electrostatic forces in mediating the interactions between the systems.

The trends observed from the computational studies are consistent with those observed from the experimental studies, showing that the stronger interactions between the DES and bulk solvent are observed with methanol owing to the influence of the degree of polarity of the solvent on the anionic Cl^- ion and the imidazolium ring. The EG co-solvent is shown to stabilize the complex and the formation of a co-ordination complex with Cl^- influenced the stability of the complex as shown from the configuration search experiments.

6.6 Characterization of deep eutectic solvents with binary mixtures

6.6.1 Thermogravimetric analysis

For ([TBN] AcO: EG), Figure 5.51 shows the drying phase to encounter weight changes due to volatile substances with a weight loss 0.085% at approximately 58.82 ℃. It eliminates interferences to get precise data on the actual decomposition and thermal properties of the sample. Figure 5.53 shows the drying phase weight loss of 0.29% at approximately 63.5 ºC for ([TBN] AcO: DEG). Both the DESs ([TBN] AcO: EG) and ([TBN] AcO: DEG) show the onset temperature at approximately 99 ºC which is the initial degradation stage. For DES ([TBN] AcO: EG), a significant weight loss is evident at 240.7 ℃ where there is a significant weight loss of 99.07% and the residue of 0.25%. For DES ([TBN] AcO: DEG) a significant weight loss is seen at 260.1 ℃ where there is a significant weight loss at 98.5% with the residue of 0.35%. The maximum weight loss temperature can be obtained by using the peak in the differential thermogravimetric analysis curve Figure 5.52 for ([TBN] AcO: EG) at T = 220.8 ℃ with maximum weight loss of 39.57% and Figure 5.54 for ([TBN] AcO: DEG) at T = 233.8 ℃ with maximum weight loss of 39.78%. tetrabutylammonium acetate with diethylene glycol shows more stability than tetrabutylammonium acetate with ethylene glycol when comparing Figure (5.51 and 5.53).

6.6.2 FTIR analysis

Figure 5.55 shows the FTIR spectra of tetrabutylammonium acetate, Ethylene glycol and DES ([TBN] AcO: EG). Spectra of $[TBN]^+[AcO]^-$ does not have stretching bands of $[N\text{-}H]^+$ observed around (3300 – 3000) cm^{-1}. (C=O) from acetate ion $[CH_3COO]^-$ should show strong absorption band at around 1700 cm^{-1} due to (C=O) stretching but

when interacting with tetrabutylammonium cation this band shifts to lower frequencies at around (1660 – 1550) cm^{-1} due to the ionic interaction. For $[TBN]^+$ and $[AcO]^-$, (C=O) is present at 1581.2 cm^{-1}, peaks at 2874.2 cm^{-1} for (C-H) stretching, 2959.9 cm^{-1} for (O-H) acid stretching, 1029.6 cm^{-1} for (N-C) stretching, 1365.8 cm^{-1} for (C-H) bending, 1226.5 cm^{-1} for (C-C) stretching, (N-O) there is no bonding, there is only the ionic interaction between $[TBN]^+$ and $[AcO]^-$ (Yahya and Arof, 2002, Wang and Golden, 2013) , 1314.77 cm^{-1} for (C-O) stretching. FTIR spectra for ethylene glycol, 3286.3 cm^{-1} for (O-H) stretching, 1208.0 cm^{-1} for (C-C) stretching, 1082.3 cm^{-1} for (C-O) stretching, 2943.7 cm^{-1} stretching (C-H), and 1409.7 cm^{-1} (C-H) bending. FTIR spectra for DES ([TBN] AcO: EG), shows 3286.3 cm^{-1} for (O-H) stretching, 2962.0 cm^{-1} for (O-H) acid stretching, 2875.5 cm^{-1} for (C-H) stretching, 1574.9 cm^{-1} for (C=O) stretching, 1398.8 cm^{-1} (C-H) bending, 1043.0 cm^{-1} (C-N) stretching, 1091.9 cm^{-1} for (C-O) stretching for both [Ac] + ethylene glycol . Figure 5.56 is a plot of superimposed spectra of tetrabutylammonium acetate, ethylene glycol and (DES [TBN] AcO: EG). The spectrum shows the significant change in intensities or positions of certain bands indicating the interactions or complex formation between [TBN] AcO and ethylene glycol. The changes are observed between (3500 – 3000) cm^{-1} due to O-H stretching, between (2950 – 28.50) for (C-H), between (1600 – 1000) cm^{-1} due to (C=O), (C-H), (C-O), (N-C) and (C-C).

Figure 5.57 shows the spectra of tetrabutylammonium acetate, diethylene glycol and DES ([TBN] AcO: DEG). Tetrabutylammonium acetate is discussed in Figure 5.55. FTIR spectra for diethylene glycol, 3332.0 cm^{-1} for (O-H), 2932.3 cm^{-1} for (C-H) stretching 1352.6 cm^{-1} for (C-H) bending, 1152.1cm^{-1} for (C-O) stretching, 1120.4 cm^{-1} for (C-O-C) and FTIR for DES ([TBN] AcO: DEG), FTIR spectra shows similar behavior as DES in Figure 5.56 and with the superimposed spectra in Figure 5.58. Changes are observed between (3500-3000) cm^{-1} due to (O-H), (3000-2700) cm^{-1}(C-H), (1600-1200) cm^{-1} due to N-O, C-O, C=O, and C-C. These changes show interactions and the formation of the deep eutectic solvent.

6.6.3 NMR analysis

For the prepared DES ([TBN] AcO: EG) and ([TBN] AcO: DEG), Figures (5.59 and 5.61) – show the ^{1}H-NMR spectra peaks corresponding to terminal methyl (-CH_3) of butyl chain at 0.903 ppm and at 0.900 ppm, (-CH_2-) at 1.307 ppm and at 1.359 ppm

bonded to terminal methyl, (-CH_2-) at 1.600 ppm and 1.601 ppm which is in the middle of the butyl chain, (-CH_2-) at 3.146 ppm and 3.184 ppm bonded to nitrogen. Spectral peak signals of ethyl acetate as for (-CH_3) at 1.881 ppm and 1.902 ppm for both the DESs and ethylene glycol, spectral peaks show (-OH) at 4.79 ppm and (-CH_2OH) at 3.606 ppm adjacent to (-OH) and diethylene glycol spectral peaks show (-OH) at 4.79 ppm (-CH_2-O-CH_2-) at 3.60 ppm adjacent to either oxygen, and or (-CH_2OH) at 3.704 ppm.

^{13}C-NMR for prepared DES ([TBN] AcO: EG) and DES ([TBN] AcO: DEG) are shown in Figures (5.60 and 5.62). These figures show signals tetrabutylammonium acetate ion which shows the (-CH_3) methyl terminal of the butyl chain at 12.82 ppm for both the DESs, (-CH_2-) bonded to the terminal methyl signal is at 19.10 ppm and 19.11 ppm, (-CH_2-) in the middle of the butyl chain shows signal at 23.07 ppm and 23.80 ppm, (-CH_2-) bonded to nitrogen shows a signal at 58.03 ppm and 58.05 ppm respectively. Peak signals for ethyl acetate ion show (-CH_3) at 22.97 ppm and 22.04 ppm, and (-C=O) signal is at 180 ppm for both the DESs respectively and for ethylene glycol signals are showing at 62.47 ppm. Diethylene glycol signals of (-CH_2) bonded to OH are at 61.4 ppm and signal for (-CH_2) bonded to oxygen, signal is at 71.57 ppm. The NMR spectra has confirmed that tetrabutylammonium acetate and ethylene glycol and or diethylene glycol are the composite of two DESs, ([TBN] AcO: EG) and ([TBN] AcO: DEG).

6.7 Activity coefficient at infinite dilution

The results of the activity coefficients for 33 solutes partitioning between the carrier gas (helium) and ([TBN] AcO): ethylene glycol or diethylene glycol as an extracting solvent were determined based on the obtained retention data acquired by gas liquid chromatography at temperatures T = (313.15, 323.15, 333.15, 343.15, and 353.15) K. The γ_{13}^{∞} values are displayed in Tables (5.20 and 5.22) at their corresponding temperatures. Natural logarithms ($\ln\gamma_{13}^{\infty}$) are plotted as a function of inverse absolute temperature (1000K/T) for all the studied solutes in ([TBN] AcO: EG) and ([TBN] AcO: DEG) based on their functional groups shown in Figures (5.63 – 5.69) for ([TBN] AcO: EG) and Figures (5.70 – 5.76), respectively

Low intermolecular interactions of solutes (tetrabutylammonium acetate: diethylene glycol) resulting to high (γ_{13}^{∞}) values when compared to (tetrabutylammonium acetate: ethylene glycol). To give an example at T = 313.15 K, γ_{13}^{∞} = 89.56 and 75.94 for octane, γ_{13}^{∞} = 129.75 and 116.44 for n-nonane, and γ_{13}^{∞} = 29.48 and 28.02 in (tetrabutylammonium acetate: ethylene glycol) and (tetrabutylammonium acetate: diethylene glycol), respectively. The negative (γ_{13}^{∞}) indicates strong intermolecular interactions. For acetone at T = 333.15 K, γ_{13}^{∞} = 6.81 and 5.31 in (tetrabutylammonium acetate: ethylene glycol) and (tetrabutylammonium acetate: diethylene glycol), respectively. The calculated activity coefficients at infinite dilution decreased as the temperature increased in both DESs, except for thiophene and alcohols only in DES (tetrabutylammonium acetate: diethylene glycol). Diethylene glycol, due to the four-carbon dimer there's an easy accessibility of the hydroxyl hydrogen atom when compared to ethylene glycol. In thiophene, relatively low γ_{13}^{∞} values, (γ_{13}^{∞} = 7.80) were observed in tetrabutylammonium acetate: ethylene glycol solvent, and (γ_{13}^{∞} = 5.37) observed in (tetrabutylammonium acetate: diethylene glycol) at T = 323.15 K. This signifies an increase in intermolecular interactions and an increase in solubility for thiophene in (tetrabutylammonium acetate: diethylene glycol), thiophene due to π-hydrogen bonding interacts with polar active sites of the DES.

Figures (5.63 - 5.65) for ([TBN] AcO: EG) DES and Figures (5.70 - 5.72) for ([TBN] AcO: DEG), alkanes, alkenes, alkynes and cycloalkanes show that there is an indirect proportional relationship between the temperature and the activity coefficients. This is due to the intermolecular attractive forces between the solute and solvent at relatively higher temperatures, although individually weak, become cumulatively more significant as the number of atoms and electrons in the molecule increases. The activity coefficients increase as the number of carbon atoms increases which shows that the number of extended alkyl group (-CH_2) have an impact on the interactions, this is as the larger the molecules, there is reduced interaction with the solvent. This reveals that the lipophilicity increases with -CH_2 addition to the solutes that lead to reduced attraction between the solvent and solutes. Additionally, the polarity of the solute can be affected by the addition of carbon atoms, the less polar a molecule is, can contribute towards less interactions with the solvent on to the column. The double bonds in alkenes and triple bonds found in alkynes are readily available to interact with the hydroxyl hydrogen atom in ethylene glycol or diethylene glycol resulting to lower

(γ_{13}^{∞}) values when compared to straight chain alkanes. For the cyclic hydrocarbons, the activity coefficients at infinite dilution values were found to be lower when compared to the alkanes. In the aromatic compounds the presence of six-hydrogen atom electron cloud both above and below the ring structure, promoting delocalized π-electrons in the benzene and toluene structures resulting in stronger interactions. Lower values were observed in the DES (tetrabutylammonium acetate: diethylene glycol) compared to DES composed of ethylene glycol, this is influenced by the lone pairs contained in the diethylene glycol resulting to high energy of attractive interactions. The temperature dependency of the prepared solvents with the aromatic hydrocarbons is shown in Figures (5.66 and 5.73). For the ketones, lower activity coefficients are resulting from the dipole-dipole forces between the solute molecules, leading to a decreased interaction between the solute and the solvent. The temperature dependency of the solutes (alcohols and ketones) is shown in Figures (5.67, 5.68, 5.74 and 5.75), (γ_{13}^{∞}) decreased with increase in temperature.

Excess thermodynamic functions serve as crucial criteria in selecting DESs tailored to specific solute categories, enabling the optimization of selectivity, solubility, and system stability. Insights into the co-variation of excess enthalpy $\Delta H_1^{\mathrm{E},\infty}$, and $\Delta S_1^{\mathrm{E},\infty}$ provide strategic direction for controlling temperature, enhancing solvent recovery, and improving energy efficiency in separation applications. These relationships lend robust support to predictive models such as COSMO-RS and UNIFAC and underpin assumptions regarding molecular association and deviations from ideal behavior.

6.8 Excess thermodynamic functions at infinite dilution

The excess thermodynamic properties at infinite dilution including enthalpies ($\Delta H_1^{\mathrm{E},\infty}$), entropies ($\Delta S_1^{\mathrm{E},\infty}$) and Gibbs free energies ($\Delta G_i^{\mathrm{E},\infty}$) were calculated from the activity coefficients at infinite dilution values. The excess properties were computed to interpret the intermolecular interactions and to evaluate the behaviour of the system (solutes and DESs). The Vant Hoff's equations (John *et al.* 2000) were used to calculate the values of entropies and enthalpies at infinite dilution.

The calculated values for the excess thermodynamic properties are shown in Tables (5.21 and 5.23). ($\Delta H_1^{E,\infty}$), is also associated with the solubility and dissolution of solutes in the solvent, including the attraction among the solutes and solvents and the endothermic breaking bonds. The breaking of hydrogen bonds (solvent-solvent) is endothermic, and the exothermic process results from the solvent-solutes interactions. The calculated enthalpy ($\Delta H_1^{E,\infty}$), values are all positive except for thiophene in (tetrabutylammonium acetate: ethylene glycol). Thiophene exhibit a relative degree of hydrophilicity when interacting with the DES as it contains ethylene glycol or diethylene glycol and due to the potential for hydrogen bonding between the sulphur atom contained in thiophene and the hydroxyl groups. In (tetrabutylammonium acetate: diethylene glycol), the enthalpy is positive for the alkanes, alkenes and ketones and negative for the thiophene. The negative values imply the hydrophilic character of the investigated deep eutectic solvents towards the solutes while positive values reveal hydrophobic properties of the solvent. The negative values also imply that high energy would be required to break the bonds between the investigated solvents and the solutes with negative values. Entropy and enthalpy are closely connected. The entropy data shows how orderly solutes are packed in the voids of the solvent including the randomness. The negative entropy calculated values imply strong interactions of the solutes and easy packing of the solutes in the voids of the deep eutectic solvents. The positive entropy calculated values indicate the repulsive forces with random arrangements of the solutes in the voids of the investigated solvents. The calculated Gibbs free energies are positive for all the investigated solutes in the solvents. The change in Gibbs free energies relates to the spontaneity or the driving forces of the process. These positive values indicate that the process is non-spontaneous and requires an input of energy to occur. In addition, these values are due to poor miscibility between the solvent and solutes.

Excess enthalpies, excess Gibbs free energy, and excess entropies are presented Table 5.21, DES ([TBN] AcO: EG), with positive excess enthalpies except for thiophene with a negative value of $\Delta H_1^{E,\infty}$ = -2.23 kJ·mol^{-1}, implying the energy released when the solute dissolves in the solvent (exothermic dissolution). All other solutes presented positive enthalpies indicate endothermic dissolution process, where it shows that solute-solvent interaction is weaker than solute-solute and solvent-

solvent interactions meaning strong attractive forces including van der Waals forces, dipole-dipole interactions and hydrogen bonds between solute and the solvent. For DES ([TBN] AcO: DEG), enthalpy is positive for alkanes, alkenes, cycloalkenes, cycloalkanes, acetonitrile, and ketones and enthalpy are negative for other solutes. Gibbs energy is positive for all investigated solutes and solvents ([TBN] AcO: EG) and ([TBA] AcO: DEG), the Gibbs energy relates to the spontaneity of the process. The positive Gibbs energy is an indication that the process is non-spontaneous due to strong solute-solute bonds that require significant energy to break. The entropies are positive and negative for the solutes interacting with ([TBN] AcO: EG) DES. Table 5.21, the ([TBN] AcO: EG) negative entropy is observed for alkanes which are octane, n-nonane and n-decane, for alkenes only 1-decene, all alkynes, aromatic hydrocarbons, thiophene and ketones. This shows strong intermolecular forces that lead to more structured system whereas the positive entropy is observed for alkanes 2.2-dimethylbutane, pentane, hexane, all alkenes except for 1-decene, cycloalkanes, cycloalkenes, alcohols, THF and acetonitrile, molecules mix and disperse and weak molecular forces allowing the increase in entropy. For ([TBN] AcO: DEG), Table 5.23 positive entropy is observed 1-pentene, 1-Hexene and cyclohexene and all other solvents have the negative entropy. DES ([TBN] AcO: DEG) has strong intermolecular forces that leads to more structured systems between the solutes and solvent compared to ([TBN] AcO: EG).

Excess thermodynamic parameters are pivotal in customizing DESs for specific solute classes, aiding in the optimization of selectivity, solubility, and system stability. Examining the co-variation between excess enthalpy $\Delta H_1^{\mathrm{E},\infty}$ and entropy $\Delta S_1^{\mathrm{E},\infty}$ provides actionable insight into temperature regulation, solvent recovery strategies, and energy-efficient separation design. These trends substantiate predictive frameworks like COSMO-RS and UNIFAC and validate core assumptions regarding molecular association and deviations from ideality.

6.8.1 Selectivity and capacity

The pre-screening of extracting solvents for a particular binary system are based on the separation parameter (capacity and selectivity) values. These parameters are useful as they give a clear understanding regarding the amount of solvent that would

be required for a specific extraction including the selectivity of the entrainer towards a specific solute. High selectivity values imply high solubility and selectiveness of the solvent, while low-capacity values reveal that large amounts of the solvent would be required. Selectivity and capacity are important when considering the design and optimizing the separation processes. The selectivities and capacities were calculated using Equations (3.46 and 3.47).

Selectivity and capacity were calculated to determine the feasibility of the solvents in separating alcohols from alkanes. From all the investigated volatile organic solvent, alcohols were observed to have high solubility in the solvent. The separation parameters were calculated for the separation of (THF/methanol; heptane/ethanol; hexane/ethanol and acetone/ethanol). The separation technique that is based on the liquid-liquid extraction can be utilized to separate these selected azeotropes comprising alcohols. The separation parameters were calculated at a temperature of T = 313.15 K and results are shown in Table 5.24 in comparison with those in literature.

Tetrabutylammonium acetate: diethylene glycol and in tetrabutylammonium acetate: ethylene glycol, the mixture of heptane or hexane – ethanol, the capacity values observed were k_j^{∞} = (0.72 and 1.02). Even though these values are relatively small, higher selectivity values shows that the deep eutectic solvents can highly interact with ethanol. Calculated selectivity values for hexane/ethanol S_{ij}^{∞} = 26.31 and for heptane/ethanol S_{ij}^{∞} = 42.22 in tetrabutylammonium acetate to diethylene glycol. In tetrabutylammonium acetate to ethylene glycol, selectivity values observed S_{ij}^{∞} = (10.08 and 17.17) for hexane/ethanol and heptane/ethanol, respectively. These values were found to be relatively lower when compared to some investigated deep eutectic solvents (Kabane et al. 2023, Mgxadeni *et al.* 2022, Nkosi *et al.* 2018, Iwai *et al.* 2019, Durski *et al.* 2018, Li *et al.* 2022 and Kabane *et al.* 2022). The selectivity and capacity values for the mixture of acetone/ethanol that normally leads to hemiacetal are shown in Table 5.24. The calculated values are relatively lower revealing high solubility of the compounds forming this mixture. For the separation of tetrahydrofuran/methanol, high solubility was observed in both investigated solvents.

The benefit of utilizing the activity coefficient of solutes at infinite dilution γ_{13}^{∞} was to acquire the potential performance of the DES tetrabutylammonium acetate with

ethylene glycol ([TBN] AcO: EG) and or diethylene glycol ([TBN] AcO: DEG) as solvents for separation of close boiling mixtures. Selectivity and capacity were calculated using Equations (3.46 and 3.47) at temperature T = 313.15 K respectively and the results are tabulated in Table 5.24. The results tabulated include the Ionic and DES solvents from literature to be compared with the investigated DESs.

Both the DESs under investigation are very low comparing selectivity and capacity values with ionic solvents and DES solvents from literature. These results indicate that relatively high amounts of solvent would be required to achieve desired separations, however for ([TBN] AcO: DEG).

Selectivity and capacity metrics inform the targeted design of DESs for separating specific azeotropes, particularly within alcohol–alkane systems. Evaluating how these properties co-vary with temperature and solute structure offers valuable insight for optimizing solvent dosage, minimizing energy consumption, and improving recyclability. These observations reinforce the predictive accuracy of models such as COSMO-RS and UNIFAC, while substantiating assumptions related to non-ideal behaviour and molecular interactions.

6.8.2 Evaluating the impact of increased length of the HBD

Tables 5.20 and 5.22 illustrate that the activity coefficients computed data for organic solutes using the solvents under investigation ([TBN] AcO: DEG) are lower than those obtained when using the solvent ([TBN] AcO: EG), this is because of the different length of diethylene glycol from ethylene glycol. This is evident in ([TBN] AcO: EG), n-decane γ_{13}^{∞} is 194.60 and for ([TBN] AcO: DEG) – n-decane γ_{13}^{∞} is 167.43. For both DESs the computed activity coefficient at infinite dilution decreases as the temperature increases, as for thiophene and alcohols they are increasing with increasing temperature only with DES ([TBN] AcO: DEG) in the temperature range of *T* = 315.15 – 353.15) K at atmospheric pressure. This reveals the influence of ethylene glycol on alcohols as this impact is due to the four carbons of diethylene glycol and the availability of the hydroxyl hydrogen atom in diethylene glycol compared to ethylene glycol. Thiophene activity coefficient values at infinite dilution were observed to be low in ([TBN] AcO: DEG indicating intermolecular interactions and relatively high solubility

between the solvent and the thiophene due to polar active sites of the DES π-hydrogen of the thiophene.

Increasing the hydrogen bond donor (HBD) chain length improves solvation capacity, molecular selectivity, and conformational flexibility, thereby enhancing the suitability of DEG-based DESs for solubilizing aromatic and polar compounds. Insights into how HBD architecture impacts activity coefficients at infinite dilution $\gamma_{13}^{\infty}$and related thermodynamic behavior provide guidance for optimizing temperature profiles, solvent dosage, and energy efficiency in separation processes. These correlations reinforce the validity of predictive models such as COSMO-RS and UNIFAC, while also substantiating assumptions concerning non-ideal behavior and molecular association.

CHAPTER 7

CONCLUSION

The imidazolium based deep eutectic solvents binary systems, (1-butyl-3-methylimidazolium chloride: ethylene glycol) + methanol and or ethanol, and (1-butyl-2,3-dimethylimidazolium chloride: ethylene glycol) + acetic acid or propanoic acid, was investigated. The binary systems were investigated at T = (293.15 – 313.15) K and at atmospheric pressure by measuring densities, speed of sound using a DSA 5000M. Refractive indices were also measured at corresponding temperatures and pressure using refractometer. The excess thermodynamic properties such as V_m^{E}, and Δk_s are negative, Δn_D, is positive values over the entire molar composition range. The measured negative values for the derived properties indicates the presence of ion-dipole interactions and high packing effect between methanol or ethanol + DES ([BMIM]Cl: EG) and acetic acid or propanoic acid + DES ([BDMIM]Cl: EG). V_m^{E} and Δk_s indicates the strongest intermolecular interaction at ≈0.20 mole fraction for all investigated systems ([BMIM]Cl: EG + methanol and or ethanol), ([BDMIM]Cl: EG + acetic acid or propanoic acid) binary mixtures.

Lorentz -Lorenz equation was used to predict the experimental density as well as the refractive indices and to correlate the excess molar volume. Lorentz-Lorenz gave good prediction results for the densities and refractive indices and poor correlation for the excess molar volume.

Computational simulation for the binary systems were also investigated, interactions of thermodynamic parameters showed the significant stability of the DES [BDMIM]Cl + ethylene glycol at (1:3 mole ratio). It was observed that the dipole moment indicated that the interactions were driven by hydrogen bonding leading to a decreased systems polarity between the DES and acetic acid. The analysis of the optimized geometries and electron properties provided insight into the electron properties and reactivity of the DES and the interactions with acetic acid and propanoic acid.

Chemical potential and electronegativity demonstrated collectively that the DES ([BDMIM]Cl: EG), when interacting with acetic acid or propanoic acid, exhibited enhanced reactivity and electron-accepting ability, facilitating the formation and

reactivity of these systems. This analysis provided deeper a insight into the electronic properties and interactions of the DES ([BDMIM]Cl: EG) + carboxylic acids.

The natural bond orbital analysis implies that the interactions on the physicochemical properties of the DES-acetic acid and DES-propanoic acid systems were significant. The strong electron donation and resulting stabilization enhanced the reactivity and stability of both systems. The high E2 values indicated that both DES-acetic acid and DES-propanoic acid complexes were likely to exhibit increased chemical potential and electrophilicity, making them strong electrophiles. This enhanced reactivity could facilitate various chemical reactions, making these DES systems promising candidates for applications requiring high reactivity and stability. The detailed understanding of these interactions provided valuable insights into the design and optimization of DES-based systems for specific chemical processes.

The non-covalent interaction analysis detailed the analysis of reduced density gradient (RDG) scatter plots for DES-acetic acid and DES-propanoic acid systems provided comprehensive understanding of the balance between attractive and repulsive forces, influencing properties such as solubility, viscosity, and thermal stability. These findings underscored the importance of non-covalent interactions in determining the physicochemical properties of DES-based systems, offering valuable insight for their design and optimization in various chemical processes.

The electron localization detailed analysis that provides valuable insight into the electronic structure and bonding properties of the DES systems, which were crucial to understanding their stability, reactivity and potential applications in various chemical processes.

The trends observed from the computational studies are consistent with those observed from the experimental studies, showing that the stronger interactions between the DES and bulk solvent are observed with methanol owing to the influence of the degree of polarity of the solvent on the anionic Cl^- ion and the imidazolium ring. The EG co-solvent is shown to stabilize the complex and the formation of a co-ordination complex with Cl^- influenced the stability of the complex as shown from the configuration search experiments.

Computational studies examined the interactions between solute and co-solvents, the trends of the impact of methanol or ethanol on the stability of the systems was shown to corelate with the experimental data. The polarity of the solvent influences the interactions between the co-solvent and [BMIM]Cl showing that interactions are largely mediated by the anionic Cl^- ion with coordination complexes with the EG co-solvent significant in stabilizing the complex. The electronic distribution, the geometric optimizations, HOMO-LUMO inspections and the interaction energies show stronger interactions between the DES and methanol bulk solvent highlighting the influence of the degree of polarity of the solvent.

Thermal stability for the deep eutectic solvents ([TBN] AcO: EG) and ([TBN] AcO: DEG) was determined using thermogravimetric analysis and characterization of these

investigated DESs ([TBN] AcO: EG) and ([TBN] AcO: DEG) were confirmed by using FTIR and NMR techniques.

Furthermore, the extent of the molecular interactions reported was based on the activity coefficients at infinite dilution of the volatile organic solvents, the solutes were tested in the deep eutectic solvents tetrabutylammonium acetate with ethylene glycol and or diethylene glycol. The values were calculated from the retention data acquired by gas liquid chromatography operated at different temperatures, T = (313.15 - 353.15) K and at atmospheric pressure. Excess thermodynamic parameters (enthalpies, entropies and Gibbs energies) at infinite dilution were calculated to further investigate and detail the intermolecular forces between the solvent and the solute. The influence of the hydrogen bond donor was investigated and discussed as it was evident that from the activity coefficients at infinite dilution values. The separation parameters (selectivity and capacity) for the azeotropes comprising of alcohols and alkanes in the investigated entrainers were calculated. The DESs investigated ([TBN] AcO: EG) and ([TBN] AcO: DEG) showed relatively greater affinity for alcohols with higher packing effect and high solubility especially in DES ([TBN] AcO: DEG) at 1:3 mole ratio. This reflects that diethylene glycol is prepared by the combination of two ethylene glycol molecules which increases the affinity of alcohols. The selection of the deep eutectic solvents as the entrainers can be impacted by several factors including the ratio of hydrogen bond acceptor to hydrogen bond donor as well as temperature which affect the yield.

REFERENCES

Abbott, A. P., 2022. Deep eutectic solvents and their application in electrochemistry. Current Opinion in Green and Sustainable Chemistry, 36: 100649.

Abbott, A. P., Capper, G., Davies, D. L., Rasheed, R. K. and Tambyrajah, V. 2003. Novel solvent properties of choline chloride/urea mixtures. The Journal of Chemical Communications, 1: 70-71.

Abbort, A. P., Boothby, D., Capper, G., Davies, D. L and Rasheed, R. K. 2004. Deep eutectic solvents formed between choline chloride and carboxylic acids: versatile alternatives to ionic liquids. Journal of American Chemical Society, 126: 9142-9147.

Abbott, A. P., Capper, G. and Gray. 2006. Design of improved Deep Eutectic Solvents using Hole theory. Chem Phys Chem., 7 (4): 803-806.

Abbott, A. P., Barron, J.C., Ryder, K. S. and Wilson, D. 2007. Eutectic-based ionic liquids with metal-containing anions and cations. Chemistry: A European Journal, 13 (22): 6495 – 6501

Abbott, A.P., Smith E. L. and Ryder, K. S. 2014. Deep eutectic solvents (DESs) and their applications. Chemical reviews, 114 (114): 11060-11082.

Al-Murshedi. 2019. Thermophysical properties in deep eutectic solvents with/without water. Journal of Physics: Conference series, 1294: 052041.

Albuquerque, B. R., Heleno, S. A., Oliveira, M. B. P., Barros, L. and Ferreira, I. C. 2021. Phenolic compounds: current industrial applications, limitations and future challenges. Food and Function, 12 (1): 14-29.

Arez, M. A. and Romero, C. M. 2011. Apparent Molar Volume and Surface Tension of Dilute Aqueous Solutions of carboxylic Acids, Journal of Chemical Engineering Data, 56 (5): 1778-1786.

Aslam, M., Pandey, G., Deshwal, N., Kumar, A., Kumari K., Bahadur, I., Sing, P., Mohammad, F., and Soleiman, A. 2024. Study the solubility of pharmaceutical ingredients and their eutectic mixtures: An in-depth density functional theory and

molecular dynamics simulations approaches. Journal of Molecular Liquids, 397: 124070.

Aslam, M., Singh, M.B., Sing, P., Pandey, G., Kuma, A., Singh, S., Tumba K., Chopra, H., Kumar, D. and Kumari K. 2023. Impact of functional group positioning in the anion of ionic liquids on aqueous solubility: a study through DFT calculations. Ionics (Kiel), 30: 875-887.

Arriaga, S. and Aizpuru, A. 2019. Chapter 9 – Innovative none-aqueous phases and partitioning bioreactor configurations. Advances in Chemical Engineering, 54: 299-348.

Armenta, S., Garrigues, S., Esteve-Turrillas, F. A. and de la Guardia, M. 2019. Green extraction techniques in green analytical chemistry. Trends in Analytical Chemistry, 116: 248-253.

Azadeh, A. M., Heydar, K. T. and Amini, M. H. 2025. Investigation and characterization of deep eutectic solvent (DES) based stationary phase in gas chromatography. Journal of Chromatography, 1739: 465511.

Bahadur, I., Govender, B. B., Osmans, K., Williams-Wynn, M. D., Nelson, W. M. and Ramjugernath, D. 2014. Measurement of activity coefficient at infinite dilution of organic solutes in the ionic liquid 1-ethyl-3-methylimidazolium, 2-(2-methoxyethoxy) ethylsulfate at T = (308.15, 313.15, 323.15 and 333.15) K. The Journal of Chemical Thermodynamics, 70: 245-252.

Bahadur, I., Deenadayalu, N., Naidoo and P., Ramjugerna. Density, speed of sound, and refractive index measurements for the binary systems (butonic acid + propanoic acid, or 2-methyl-propanoic acid) at T = (293.15 to 313.15) K. The Journal of Chemical Thermodynamics, 57: 203 – 211.

Banks, J. L. Beard, H. S. Cao, Y. Cho, A. E. Damm, W. Farid, R. Felts, Halgren, T. A. Mainz, D. T. Maple, J. R. Murphy, R. Philip, D. M. Repasky, M. P. Zhang, L. Y. Berne, B. J. Friesner, R. A. Gallicchio, E. and Levy, R. M. 2005. Integrated Modelling Program, Applied Chemical Theory (IMPACT). Journal of Computational Chemistry, 26: 1752-1780.

Boublia, A., Guezzout, Z., Haddaoui, N., Badawi, M., Darwish, T., Lemaoui, T., Lebiuachera, S. E. I., Yadav, K. K., Alreshidi, M. A., Algethami, J.S., Abbas, M., Banat, Alnashef, A., Jeon, B. and Benguerba, Y. 2023. The curious case of polyaniline – graphene nanocomposites: A review of their applications as exceptionally conductive and gas sensitive materials. Critical Reviews in Solid State Materials Science, 45 (5): 973-997.

Bonab, P. J., Esrafili, M. D., Ebrahimzadeh, A. R. and Sardroodi, J. J. 2021. Molecular dynamics simulations of choline chloride and phenyl propanoic acid deep eutectic solvents: Investigation of structural and dynamics properties. Journal of Molecular Graphics and Modelling, 106: 107908.

Briceño-Vargas, F. M., Quesadas-Rojas, M., Mirón-López, G., Cáceres-Castillo, D., Carballo, R. M., Mena-Rejón, G. J. and Quijano-Quiñones, R. F. 2023. Molecular orbital and topological electron density study of n $\rightarrow \pi^*$ interactions: amides and thioamides cases. Royal Society of Chemistry Advances, 13: 31321.

Brocos, P., Piñeiro, Á., Bravo, R. and Amigo, A. 2003. Refractive indices, molar volumes and molar refractions of binary liquid mixtures: concepts and correlations. Physical Chemistry Chemical Physics, 5 (3): 550-557.

Castro, V.M.J., Cordeiro, C.C.J., Baceti, J.M.F., Blanco, R.C., Olivieri, V.G., Cella, R., Morgon, H.N. and Torres, R.B. 2024. Molecular interactions between 2-methyltetrahdrofuran and alcohols: a combination of quantum chemistry studies. Journal of Molecular Liquids, 394: 123755.

Celebi, A. T., Vlugt, T. J. H. and Moultos, O. A. 2019. Structural, Thermodynamic, and Transport propertiesof aqueous reline and ethaline solutions from molecular dynamics simulations. The Journal of Physical chemistry B, 123: 11014-11025.

Chem, B. Lei, Z. and Zhongwei D. 2005. Second Edition Special Distillation Processes Book. Elsevier, Books.google.com.

Choi, Y. H. and Verpoorte, R. 2019. Green solvents for the extraction of bioactive compounds from natural products using ionic liquids and deep eutectic solvents. Current Opinion in Food Science, 26: 87-93.

Chokkareddy, R. Kabane, K. and Redhi, G. G. 2019. Separation of (water/butan-1-ol) binary systems based on activity coefficient at infinite dilution with phosphonium ionic liquid. Journal of Chemical Thermodynamics, 137: 7-12.

Countinho, J. A. P. and Pinto, S. P. 2017. Special issue on deep eutectic solvents: a foreword. Fluid Phase Equillibria. 448: 1.

Cousins, K. R. 2005. ChemDraw Ultra 9.0. CambridgeSoft, 100 CambridgePark Drive, Cambridge, MA 02140. www.cambridgesoft.com. See Web site for pricing options. Journal of the American Chemical Society, 127 (11): 4115-4116.

Cruickshank, A., Gainey, B., Hicks, C., Letcher, T., Moody, R. and Young, C. 1969. Gas liquid chromatographic determination of cross-term second virial coefficients using glycerol. Benzene + nitrogen and benzene + carbon dioxide at 50^{o}C. Transactions of the Faraday Society, 65: 1014-1031.

Cseri, L., Razali, M., Pogany, P. and Szekely, G. 2018. Organic solvents in sustainable synthesis and engineering. Green Chemistry an Inclusive Approach, Elsevier, Book Chapter 3.15.: 513-553.

Cvetanovic, A. 2019. Extractions without organic solvents: advantages and disadvantages. Chemistry Africa, 2 (3): 343-349.

Demirel, Ç. and Çehreli, S. 2013. Phase equilibrium of (water + formic acid + ethyl heptanoate) ternary liquid system at different temperatures. Fluid Phase Equilibria, 356: 71-77.

Domańska, U. and Marciniak, A. 2008. Measurements of activity coefficients at infinite dilution of aromatic and aliphatic hydrocarbons, alcohols, and water in the new ionic liquid [EMIM][SCN] using GLC. The Journal of Chemical Thermodynamics, 40 (5): 860-866.

Durski, M., Naidoo, P., Ramjugernath, D. and Damańska, U. 2018. Thermodynamics and activity coefficients at infinite dilution for organic solutes in the ionic liquid 1-butyl-1-methylpyrolidinium dicyanamide. Fluid Phase Equilibria, 473: 175-182.

Everett, D. 1965. Effect of gas imperfection on GLC measurements: a refined method for determining activity coefficients, Transactions of the Faraday Society. 61: 1637-1645.

Francisco, M., van den Bruinhorst, A. and Kroon, M. C. 2013. Low-transition-temperature mixtures (LTTMs): A new generation of designer solvents. Angewandte chemie International Edition, 52 (11): 3074-3085.

Gabriela, B. G., Mercedes, E. and Albertina, R. 1990. Densities and refractive indices of pure organic acids as a function of temperature. Journal of Chemical. Engineering Data, 35 (2): 202-204.

Golgoun, S., Mokhtarpour, M. and Shekaari, H. 2020.Solubility Enhancement of Betamethasone, Meloxicam and Piroxicam by Use of Choline-Based Deep Eutectic Solvents. Pharmaceutical Science. 27, 86–10.

Gonza´lez, B., Dominguez, A. and Tojo, J. 2004. Dynamic viscosities, densities, and speed of sound and derived properties of the binary systems acetic acid with water, methanol, ethanol, ethyl acetate, and methyl acetate at *T* = (293.15, 298.15 and 303.15) K at atmospheric pressure. Journal of Chemical Engineering Data. 49: 1590 – 1696.

González-Campos, L. B., Pérez-Nava, A., Valle-Sánchez, M. and Delgado-Rangel, L. H. 2024. Deep eutectic solvents applications aligned to 2030 United Nations Agenda for sustainable development. Chemical Engineering and Processing – Process Intensification, Elsevier, 199: 109751.

Gullón, P., Gullón, B., Romaní, A., Rocchetti, G. and Lorenzo, J. M. 2020. Smart advanced solvents for bioactive compounds recovery from agri-food by-products: A review. Trends in Food Science & Technology, 101: 182-197.

Grundtvig, I. P. R., Heintz, S., Krühne, U., Gernaey, K. V., Adlercreutz, P., Hayler, J. D., Wells, A. S. and Woodley, J. M. 2018. Screening of organic solvents for bioprocesses using aqueous-organic two-phase systems. Biotechnology Advances, 36 (7): 1801-1814

Habila, M.A.; Alabdullkarem, E. A. ALOthman, Z. A. Yilmaz, E. and Soylak, M. 2020. Thiomalic acid/ferric chloride-based deep eutectic solvent microextracion of chromium natural water prior to FAAS analysis. International Journal of Environmental Analytical Chemistry. 102: 1825-1833

Hansen, B. B., Spittle, S., Chen, B., Poe, D., Zhang, Y., Klein, J. M., Horton, A., Adhikari, L., Zelovich, T. and Doherty, B. W. 2020. Deep eutectic solvents: A review of fundamentals and applications. Chemical Reviews, 121 (3): 1232-1285.

Halder, A. K., Haghbakhsh, R., Voroshylova, L. V., Duarte, A. C. and Cordeiro, M. N, D, S. 2021. Density of deep eutectic solvents: Th path forward cheminformatics-driven reliable predictions for mixtures. Molecules, 26 (19): 5779.

Hao, L., Wang, M., Shan, W., Deng, C, Ren, W., Shi, Z. and Lü, H. 2017. L-proline-based deep eutectic solvent (DESs) for deep eutectic catalytic oxidative desulphurization (ODS) for diesel. Journal of Hazardous materials, 339: 216 – 222.

Hartley, J. M. 2014. EXAFS study into the speciation of metal salts dissolved in ionic liquids and deep eutectic solvents. Inorganic Chemistry, 53 (12): 6280-6288.

Hevia, F. Alonso, V. Cobos, A. González, J. A. Sanz, and L. F. Fuente, I. G. 2022. Density, speed of sound, refractive index, and relative permittivity of methanol, propan-1-ol or pentan-1-ol + benzylamine liquid mixtures. Application of the Kirkwood-Fröhlich model. The Journal of Chemical Thermodynamics, 168: 106737.

Hu, D., Wang, Q., Li, J., Chen, Y., Muhammad, F., Zhang, Y., Yalikun, N. and Huang. 2024. Thermodynamic propertied of TPAC-EG deep eutectic solvents: A study based on IGC method with molecular simulations. Journal of molecular liquids, 407: 125120.

IJardar, S. P., Singh V. and Gardas. R. L. 2022. Revisiting the physicochemical properties and application of Deep eutectic solvents. Journal of Molecular Liquids, 27 (4): 1368.

Ince, E., Lalikoglu, M. and Constantinescu, D. 2014. Liquid phase equilibria of water + dimethyl carbonate ternary system at several temperatures. Journal of Chemical and Engineering Data. 2781-2787.

Iwai, Y., Seki, R and Tanaka, Y. 2019. Correlation of phase equilibria by new activity coefficient model. Fluid Phase Equilibria, 488: 62-71.

Jalili, V., Barkhordari, A. and Ghiasvand, A. 2020. New a media in microextraction techniques. A review of reviews. Microchemical Journal, 153: 104386

Johanbaksh-Bonab, P., Khoshnazar, Z., Sardroodi, J. J. and Heidaryan, E. 2024 A computational probe into the physicochemical properties of deep eutectic solvents for extraction processes. Carbohydrate Polymer Technologies and Applications,8: 100596.

Jakobsen, H. A., Lindborg, H. and Dorao, C. A. 2005. Modeling of bubble column reactors: Progress and limitations. Industrial and Engineering Chemistry Research, 44 (14): 5107-5151.

John, D. M. and Weeks, K. M. 2000. Van't Hoff enthalpies without baseline. Protein Science, 9 (7): 1415-1419.

Joshi, D. R. and Adhikari, N. 2019. An overview on common organic solvents and their toxicity. Journal of Pharmaceutical Research International, 28 (3): 1-18.

Kabane, B. and Redhi. G. G. 2020. Thermodynamic properties and activity coefficients at infinite dilution for different solutes in deep eutectic solvent: 1-butyl-3-methylimidazolium chloride+ glycerol. Journal of Molecular Liquids, 311: 113216.

Kabane, B., Arumugam, V. and Redhi, G. G. 2022. Application of synthesized ionic liquid for possible use in industrial separation problems: A useful tool for solvent selection tool. Journal of Molecular Liquids, 346: 117854

Kabane, B., de P Soares, P., Deenadayalu, N. and Bahadur, I. 2023. Pre-screening of 1-ethylene-3methylimidazolium tetra chloroaluminate and influence of diethylene glycol on the ionic liquid in separation of molecular solutes: Activity coefficients at infinite dilution ans COSMO-SAC modelling. Fluid Phase equilibria, 571: 113808.

Kabanda, M. M., & Bahadur, I. 2022. Hydrogen bonding between 1-ethyl-3-methylimidazolium dicyanamide ionic liquid and selected co-solvents with varying polarity: A DFT study. Journal of Molecular Liquids, 360: 119418.

Kaya, S. and Putz, V. 2022. Atoms-In-molecules' faces of chemical hardness by conceptual Density Functional Theory, Molecules 27 (24): 8825.

Khirade, P. W. Chaudhari, J. B, Shinde, S. N, Helambe, S. N. and Mehrotra, S. C. 1999. Static Dielectrical Constant and Relaxation Time Measurements on Binary Mixtures of Dimethyl Sulfoxide with Ethanol, 2-Ethoxyethanol, and Propan-1-ol at 293, 303, 313, and 323 K. Journal of Chemical Engineering Data, 44: 879-881.

Kiran Kumar, P., Kabanda, M. M., Bahadur, I., Venkatesu, P., Ebenso, E. E. 2022. Influence of temperatureand concentration on the molecular interactions of pyrrolidinium-based ionic liquid with water and alcohols: an experimental and DFT studies. Journal of Molecular liquids. 360: 119554.

Kurtulbaş, E.; Pekel, A.G.; Toprakçı, İ.; Özçelik, G.; Bilgin, M. and Şahin, S. 2020. Hydrophobic carboxylic acid based deep eutectic solvent for the removal of dichlofenac. Biomass Convers and Biorefinery,12: 2219-2227.

Laroche, L. Andersen, H. W. Morari, M. and Bekiaris, N. 1991. Homogeneous azeotropic distillation: comparing entrainers. Canadian Journal of Chemical Engineering, 69 (6): 1302-1319.

Lee, A. K., Lewis, D. M. and Ashman, P. J. 2012. Disruption of microalgal cells for the extraction of lipids for biofuels: Processes and specific energy requirements. Biomass and Bioenergy, 46: 89-101.

Lei, Z. Li, C. and Chen, B. 2003. Extractive distillation: A Review. Separation and Purification. A Review, 32 (2): 121-213.

Lei, Z. Dai, C. Zhu, J. and Chen, B. 2014. Extractive distillation with ionic liquids: a review. AIChE Journal, 60 (9): 3312-3329.

Lee, J., Kim, H., Kang, S., Baik, N., Hwang, I. and Chung, D. S. 2020. Applications of deep eutectic solvents to quantitative analyses of pharmaceuticals and pesticides in various matrices: a brief review. Archives of pharmacal research: 43: 900-919.

Letcher, T. M. and Whitehead, P. G. 1996. The determination of activity coefficients of alkenes, alkynes, and cycloalkanes at infinite dilution with polar solvent

tetrahydrothiophene-1,1-dioxide (Sulpholane) using a glc technique at T = 303.15 K and T = 313.15 K. Journal of Chemical Thermodynamics, 28 (8): 843-849.

Li, Y., Wang, W., Qiang, W., Nuerbiya, Y. and Jun, T. 2022. Thermodynamic parameters at infinite dilution activity coefficients for organic solutes in deep eutectic solvent: Choline Chloride + 1,5-Pentanediol. Journal of Chemical Thermodynamics, 170: 106784.

Li, G. and Row, K. H. 2019. Utilization of deep eutectic solvents in dispersive liquid-liquid micro-extraction. TrAc – Trends Analytical Chemistry, 120: 115651.

Li, K., Zong, K., Wang, X., Cui, G. and Deng, D. 2023. Ionic liquids and deep eutectic solvents for NH_3 absorption and separation: a review. New Journal of Chemistry. 46.

Lin, Z., Zhang, Y., Zhao, Q., Chen, A. and Jiao, B. 2021. Ultrasound - assisted dispersive liquid-phase microextraction by solidifying L-menthol – decanoic acid hydrophobic deep eutectic solvents for detection of five fungicides in fruit juices and tea drinks. Journal of Separation Science, 44 (20): 3870-3882.

Liu, W., Li, T., Yu, G., Wang, J., Zhou, Z. and Ren, Z. 2020. One-pot oxidative desulfurization of fuels using dual-acidic deep eutectic solvents. Fuel, 265: 116967.

Liu, Y., Friesen, J.B., McAlpine, J.B., Lankin, D.C., Chen, S.-N. and Pauli, G.F. 2018. Natural Deep Eutectic Solvents: Properties, Applications, and Perspectives. Journal of Natural Products, 81 (3): 679–690.

Liu, L., Kong, Y., Xu, H., Li, P. J., Dong, J. X., and Lin, Z. 2008. Ionothermal synthesis of a three-dimensional zinc phosphate with DFT topology using unstable deep eutectic solvent as a template-delivery agent, Microporous and Mesoporous Materials, 115 (3): 624-628.

Long, G. Yang, C. Yang, X. Zhao, T. and Xu, M. 2020. Deep eutectic solvents consisting of 1-ethyl-3methylimidazolium chloride and glycerol derivatives for highly efficient and reversible SO2 capture. Journal Molecular Liquids, 302: 112538.

Lorentz, H. A. 1953. The theory of electrons and its application to the phenomena of light and radiant heat. Dover Publications, New York. 2nd edition Book.

Lorentz, L., 1818. “*Ueber die refraktionsconstante”* Wied. Annalen der Physik.1; 247 (9): 70-103.

Lu, C., Wu, C. Ghoreishi, D. Chen, W. Wang, L. Damm, W. Ross, G. A. Dahlgren, E. Russel, E. Von Bargen, C. D. Abel, R. Friesner, R. A. and Harder, E. D. 2021. Improving force field accuracy on challenging regimes of chemical space. Journal of Chemical Theory and Computation, 17 (7): 4291-4300.

Mahdi, T. Ahmad, A. Nasef, M. M. and Ripin, A. 2015. State-of-the-art technologies for separation of azeotropic mixtures. Separation and Purification Reviews, 44 (4): 308-330.

Makos, P., Słupek, E. and Gebicki, J. 2020. Hydrophobic deep eutectic solvents in microextraction techniques-A review. Microchemical journal, 152: 104384.

Manyoni, L., Kabane, B. and Redhi, G. 2022. Excess thermodynamics functions of phosphonium-based deep eutectic solvent for various organic solutes at different temperatures. Journal of the Taiwan Institute of Chemical Engineers, 138: 104463.

Manyoni, L., Redhi, G. 2023. Separation potential of 1,5-pantanediol-based deep eutectic solvent: infinite dilution activity coefficients and excess thermodynamic data. Heliyon, 9 (3): e21516.

Martins, P. L. G., Braga, A. R. and de Rosso, V. V. 2017. Can ionic liquid solvents be applied in the food industry? Trends in Food Science and Technology, 66: 117-124.

Mgxadeni, N. Mmelesi, O., Kabane, B. and Bahadur, I. 2022. Influence of hydrogen bond donor on zinc chloride in separation of binary mixtures: Activity coefficients at infinite dilution. Journal of Molecular Liquids, 351: 118596.

Mgxadeni, N. Kabane, B. Bahadur, I. Paredes, M. L. L. Soares, R. P. Singh, K. F. and Soleiman, A. A. 2023. Thermodynamic properties, activity coefficients at infinite dilution and Cosmo-Sac Modelling of deep eutectic solvents at different temperatures. Chemistry Select, 8 (30): e202204192.

Mgxadeni, N. Kabane, B. Bahadur, I. Varma, Rajendar. S. Singh, Shailendra. K. 2023. Deep eutectic solvents as a sustainable solvent for industrial separation problems: A recent update. Journal of Ionic Liquids, 3 (2): 100065.

Miranda-Quintana, R. A., Heidar-Zadeh, F., Fias, S., Champman, A. E. A., Liu, S., Morell, C., Gómez, T., Cárdenas, C. and Ayers, P. W. 2022. Molecular interactions from the density functional theory for chemical reactivity: Interaction chemical potential, hardness, and reactivity principles. Frontier in Chemical, 10: 929464.

Mohamadi, F. Richards, N. G. J. Guida, W. C. Liskamp, R. Lipton, M. Caufield, C. Chang, G. Hendrickson, T. and Clark Stil, W. 1990. Macromodel-an integrated software system for modelling organic and bioorganic molecules using molecular mechanics. Journal of Computational Chemistry, 11 (4): 440-467.

Moollan, W. C. and Letcher, T. M., 1995. The determination of activity coefficient of hydrocarbons at infinite dilution using a g.l.c. techniques with the popular solvent tetrahydrothiophene-1,1-dioxide, *c*-$(CH_2)_4SO_2$, (sulfonate) at temperature 303.15 K. Journal of Chemical Thermodynamics, 27 (8): 867-872.

Mullins, O. C, and Sheu (Eds.) E. Y. 1998. Structure and Dynamic of Asphaltenes., Springer, US, Boston, MA. Book.

Mullins, O. C., Sheu, E. Y., Hammami, A. and Marshall, A. G. 2007. Asphaltenes, Heavy oils, and Petroleomics. Springer Science Business Media book, 5-89.

Mulliken, R. S. 1955, Electronic population analysis on LCAO-MO molecular wave functions. II. Overlap populations, bond orders, and covalent bond energies. Journal of Chemical Physics, 23: 1833-1840.

Murador, D. C., de Souza Mesquita, L. M., Vannuchi, N., Braga, A. R. C. and de Rosso, V. V. 2019. Bioavailability and biological effects of bioactive compounds extracted with natural deep eutectic solvents and ionic liquids: Advantages over conventional organic solvents. Current Opinion in Food Science, 26: 25-34.

Mustafa, N.R., Spelbos, V.S., Witkamp, G.-J., Verpoorte, R. and Choi, Y.H. 2021. Solubility and Stability of Some Pharmaceuticals in Natural Deep Eutectic Solvents-Based Formulations. Molecules, 26, 2645.

Nakhle, L., Kfoury, M., Mallard, I., Landy, D. and Greige-Gerges, H. 2021.Microextraction of bioactive compounds using deep eutectic solvents. A Review. Environmental Chemistry Letter, 19: 3747–3759.

Neni, A., Boublia, A., Bouras, M., Bentoumi, K., Albrahim, M., Elboughdiri, N. and Benguerba, Y. 2024. Evaluating Asphaltene dispersion with choline chloride or menthol based deep eutectic solvents: A Cosmo-RS analysis. Journal of Molecular liquids. 407: 125272.

Neubauer, M. Wallek, T. and Lux, Sasanne. 2022. Deep eutectic solvents as entrainers in extractive distillation – A review. 184: 402-418.

Nkosi, N., Tumba, K. and Ramsuroop, S. 2018a. Activity coefficients at infinite dilution of various solutes in tetrapropylammonium bromide+ 1, 6-hexanediol deep eutectic solvent. Journal of Chemical & Engineering Data, 63 (12): 4502-4512.

Nkosi, N., Tumba, K. and Ramsuroop, S. 2018b. Measurements of activity coefficient at infinite dilution for organic solutes in tetramethylammonium chloride+ ethylene glycol deep eutectic solvent using gas-liquid chromatography. Fluid Phase Equilibria, 462: 31-37

Nkosi, N., Tumba, S., and Ramsuroop, S. 2018. Tetramethylammonium chloride + glycerol deep eutectic solvents as separations agent for organic mixtures: Assessment from experimental limiting activity coefficients. Fluid Phase Equilibria, 473: 98-105.

Nkuku, C. A. and LeSuer, R. J. 2007. Electrochemistry in deep eutectic solvents, Journal of Physical Chemstry B, 111 (46): 13271-13277.

Paiva, A., Carveiro, I., Aroso, M., Martins, R. L., Reis, and Duarte, A. R. C. 2014. Natural deep eutectic solvents – Solvents for 21st century. ACS Sustainable chemistry & Engineering, 2: 1063-1071.

Paucar, N. E., Kiggins, P., Blad, B., De Jesus, K., Afrin, F., Pashikanti, S. and Sharma, K. 2021. Ionic liquids for the removal of sulfur and nitrogen compounds in fuels: a review. Environmental Chemistry Letters: 1-24.

Pacheco-Fernández, I. and Pino, V. 2019. Green solvents in analytical chemistry. Current Opinion in Green and Sustainable Chemistry, 18: 42-50.

Patyar, P., Ali, A. and Malek, N. I. 2021. Experimental and theoretical excess molar properties of aqueous choline chloride based deep eutectic solvents. Journal of Molecular Liquids, 324: 114340.

Parr, R. and Yang, W. 1984. Density Functional Approach to the Frontier-Electron Theory of Chemical Reactivity. Journal of American Chemical Society, 106 (14): 4049-4050.

Pena-Pereira, F., Kloskowski, A. and Namiesnik, J. 2015. Perspectives on the replacement of harmful organic solvents in analytical methodologies: a framework toward the implementation of a generation of eco-friendly alternatives. Green Chemistry, 17 (7): 3687-3705.

Poling, B. E., Prausnitz, J. M. and O'connel, J. P. 2001. Properties of gases and liquids. McGraw-Hill Education, 5th Edition. Journal of American Chemical Society, 123 (27): 6745.

Raman, A. P. S., Singh, P., Vishvakarma, V. K., Jain, P., Kumar A., Sachdeva, S., Kumari, K. and Singh, P. 2023. An investigation for the interaction of gamma oryzanol with Mpro of SATR-CoV-2 to combat COVID-19: DFT, molecular docking, ADME and molecular dynamic simulations, Journal of Biomolecular Structure and Dynamics, 41 (5): 1919-1929.

Ramon, D. J. and Guillena, G. 2020. Deep Eutectic Solvents: Synthesis, Properties, and Applications. Green Chemistry, 22 (12): 3668-3692

Reeves, C. J., Kasar, A. K. and Menezes, P. L. 2021. Tribological performance of environmentally friendly ionic liquids for high-temperature applications. Journal of Cleaner Production, 279: 123666.

Riley, K. E.M and Merz, M. K. 2007. Assessment of density functional methods for computation of heats of formation and ionization potentials of systems containing third row transition metals. The Journal of Physical Chemistry A, 111 (27): 6044-6053.

Ríos-Gutiérrez, M., Saz Siosa, A. and Domingo, L. R. 2023. Electrophilicity and nucleophilicity scales at different DFT computational levels. Journal of Physical Organic Chemistry, 36 (7): e4503.

Rodríguez, N. R. Gonzalez, A. S. B. Tijssen, P. M. A. and Kroon, M. C. 2015. Low transition temperature mixtures (LTTMs) as novel entrainers in extractive distillation. Fluid Phase Equilibria. 385: 72-78.

Rozas, S. and Benito, C. 2021. Insight on the water effect on deep eutectic solvents properties and structuring: The archetypical case of choline chloride + ethylene glycol. Journal of Molecular Liquids, 344: 117717.

Ruesgas-Ramón, M., Figueroa – Espinoza, M. C. and Durand, E. 2017. Application of Deep Eutectic Solvents (DES) for Phenolic compounds Extraction: Overview, Challenges, and Opportunities. Journal of Agricultural and Food Chemistry, 65 (18): 3591-3601.

Sanmamed, Y. A., González-Salgado, D., Troncoso, J., Cerdeirina, C. A. and Romani, L. 2013. Viscosity induced error in the density determination of room temperature ionic liquids using vibrating densitometry. Fluid phase equilibria. 252: 96.

Scelsi, E., Angelini, A. and Pastore., C. 2021. Deep eutectic solvents for the lignocellulosic Biomasses towards fine chemicals. Biomass, 1: 26 – 59.

Shekaari, H., Zafarani-Moattar, M. T. and Mohammadi, B. 2020a. Liquid-liquid equilibria and thermophysical properties of ternary mixtures {(benzene/thiophene) + hexane+ deep eutectic solvents}. Fluid Phase Equilibria, 509: 112455.

Shekaari, H., Zafarani-Moattar, M. T. and Mohammadi, B. 2020b. Thermophysical properties of choline chloride/urea deep eutectic solvent in aqueous solution at infinite dilution at T= 293.15–323.15 K. Journal of Thermal Analysis and Calorimetry, 139 (6): 3603-3612.

Shekaari, H., Zafarani-Moattar, M. T., Mokhtarpour, M. and Faraji, S. 2020c. Compatibility of sustainable solvents ionic liquid, 1-ethyl-3-methylimidazolium ethyl sulfate in some choline chloride based deep eutectic solvents: thermodynamics study. The Journal of Chemical Thermodynamics, 141: 105961.

Shekaari, H., Zafarani-Moattar, M. T., Mokhtarpour, M. and Faraji, S. 2021. Deep eutectic solvents for antiepileptic drug phenytoin solubilization: Thermodynamic Study. Scientific Reports, 11 (1): 1-14.

Sheu, E. Y. 2002. Petroleum Asphaltene properties, characterization, and issues. Energy fuels. 16: 74-82.

Shishov, A., Pochivalov, A., Nugbienyo, L., Andruch, V. and Bulatov, A. 2020. Deep eutectic solvents are not only effective extractants. Trends in Analytical Chemistry, 129: 115956.

Singh, M. B., Jain, P., Tomar, J., Kumar, V., Arya, D. K. and Singh, P. 2022. An in Silico investigation for acyclovir and its derivatives to fight the COVID-19: Molecular docking, DFT calculations, ADME and td-Molecular dynamics simulations. Journal of the Indian Chemical Society, 99: 100433.

Singh, S. K. and Savoy, A. W. 2020. Ionic liquids synthesis and applications: An overview. Journal of Molecular Liquids, 297: 112038.

Singh, S., Bahadur, I., Redhi, G. G., Ebenso, E. E. and Ramjugernath, D. 2014.Density and speed of sound of 1-ethyl-3-methylimidazolium ethyl sulphate with acetic acid or propionic acid at different temperatures. Journal of Molecular Liquid, 199: 518-523.

Smallwood, I. 1996. Consultant, in Handbook of organic solvent properties.

Smink, D., Kersten, S. R. and Schuur, B. 2020. Recovery of lignin from deep eutectic solvents by liquid-liquid extraction. Separation and purification technology, 235: 116127.

Tobiszewski, M. and Namiesnik, J. 2017. Greener organic solvents in analytical chemistry. Current Opinion in Green and Sustainable Chemistry, 5: 1-4.

Thompson, M. W., Matsumoto, R., Sacci, R. L., Sanders, N. C. and Cummings, P. T. 2019. Scalable screening of soft matter: A case study of mixtures of ionic liquids and organic solvents. The Journal of Physical Chemistry B, 123 (6): 1340-1347.

Troter, D.Z., Todorović, Z.B., Dokić-Stojanović, D.R., Stamenković, O.S. and Veljković, V.B. 2016. Application of ionic liquids and deep eutectic solvents in biodiesel production: A review. Renewable and Sustainable Energy Reviews, 6 1: 473–500.

Uddin, M. N., Basak, D., Hopefl, R. and Minofar, B. 2020. Potential application of ionic liquids in pharmaceutical dosage forms for small molecule drug and vaccine delivery system. Journal of Pharmacy and Pharmaceutical Sciences, 23: 158-176.

Umar, A., Manur, M., Murtaza, M., Sultana, R., Riaz, M. A., Srinivasan, G. R., Firdous, A. and Saeed, M. 2020. Egyptian Journal of Chemistry, 63: 59-69.

Verma, C., Alrefaee, S. H., Quraishi, M., Ebenso, E. E. and Hussain, C. M. 2020. Recent developments in sustainable corrosion inhibitors using ionic liquids: A review. Journal of Molecular Liquids: 114484.

Wang, A. Q. and Golden, T. D. 2013. Electrode position of oriented cerium oxide films. International Journal of Electrochemistry, 2013: 10. ID 482187.

Wasserscheid, P. and Welton, T. 2008. Ionic Liquids in synthesis. John Wiley & Sons.

Wypych, G., Matsomoto, M., Isken, S., de Bont, J. A. M., Botzenhart, K., Hahn, T., Schweinberg, F., Yamane, T., Hasenclever, K. D., Wakelyn, P. J., Wan, P. J., Volland, G., Bauer, M., Barthélémy, C., Serageldin, M. and Reeves, D. 2019. Solvents used in industries, Handbook of solvents, Volume 2: Use Health, and Environment. 901-1124.

Yadav, S., Sewariya, S., Chandra, R., Singh, P., Kumar, A., Jain, A. Sachdeva, S. and Kumari, K. 2023. An investigation to understand the correlation between the experimental and density functional theory calculations of noscapine. Journal of Physics Organic Chemistry, 36 (7): e4502.

Yahya, M. Z. A. and Arof, A. K., 2002. Effect of oleic acid placticizer on chirosan-lithium acetate solid polymer electrolytes. European Polymer Journal 39: 897-902.

Yang, Z. 2018. Natural Deep Eutectic Solvents and Their Applications in Biotechnology. Advances in Biochemical Engineering/Biotechnology, 168: 31–59.

Zante, G., Braun, A., Masmoudi, A., Barillon, R., Trebouet, D. and Boltoeva, M. 2020. Solvent extraction fractionation of manganese, cobalt, nickel and lithium using ionic liquids and deep eutectic solvents. Minerals Engineering, 156: 106512.

Zhang, M., Zhang, X., Liu, Y., Wu, K., Zhu, Y., Lu, H. 2021. Insights into the relationships between physicochemical properties, solvents performance, and applications of deep eutectic solvents. Environmental Science and Pollution Research, 28: 35537-63.

Zang, Q. 2012. Deep eutectic solvents: synthesis, properties and applications. Chemical Society Review, 41 (21): 7108-7146.